Characterisation and Nanobody Targeting of Essential Cytoskeletal Proteins of Trypanosoma brucei

Christine Broster

université de BORDEAUX

n°93905

A thesis submitted in fulfilment of the requirements for the degree of
Doctor of Philosophy *of*

THE UNIVERSITY OF BORDEAUX

in the department of

Life and Health Sciences

Characterisation and Nanobody Targeting of Essential Cytoskeletal Proteins of *Trypanosoma brucei*

Author: **Christine Elizabeth BROSTER REIX**

Supervisor: Dr Derrick R. ROBINSON

President: Prof Martin Teichmann, University of Bordeaux, France
Rapporteur: Prof Sue Vaughan, Oxford Brookes University, U.K.
Rapporteur: Dr Helen Price, Keele University, U.K.
Examiner: Dr Isabelle Sagot, University of Bordeaux, France
Examiner: Dr Philippe Bastin, Institut Pasteur, Paris, France

Date: Thursday, September 26th 2019

"By hook or by crook this peril too shall be something that we remember."

Homer

Abstract

Kinetoplastid parasites, including trypanosomes and *Leishmania*, are responsible for several diseases of socio-economic and public health importance worldwide. These include the Neglected Tropical Diseases: Sleeping Sickness, Chagas disease and Leishmaniasis, as classified by the World Health Organisation (WHO) and the global wasting disease of animals, Surra, as reported by the Food and Agricultural Organisation of the United Nations (FAO). Animal African Trypanosomiais (AAT) causes the death of 3 million cattle per year in sub-Saharan Africa, with an annual loss of 4.5 billion US dollars to the African economy. Cutaneous leishmaniasis is a zoonotic disease, with 1.5 million new cases reported globally each year.

Trypanosoma brucei is an ancient, early diverging eukaryote, used as a model organism in the laboratory for studying eukaryotic cilia and flagella. Remodelling of the trypanosome cytoskeleton is essential for cell morphology, organelle positioning and division. Study of essential proteins of the cytoskeleton provides insight into intracellular processes and could provide potential targets for therapeutic interventions. Trypanosomes evade the host immune system by periodically changing their external surface coat, which is endocytosed, along with any attached host antibodies, *via* a structure called the flagellar pocket. *Tb*BILBO1 is a structural protein of the flagellar pocket collar (FPC) that is essential for FPC biogenesis and parasite survival. Due to the importance of *Tb*BILBO1 for survival of the parasite, protein partners were investigated.

In my thesis, I describe, firstly, the characterisation of a novel and essential trypanosome-specific cytoskeletal protein, FPC6, of the FPC/hook complex (HC) of *T. brucei*; FPC6 is a partner of *Tb*BILBO1. Knock-down of FPC6 protein, by RNA interference (RNAi), leads to rapid cell death in the bloodstream form of the parasite accompanied with a block in endocytosis. Secondly, I describe the purification and intracellular expression of a nanobody (Nb48), raised against *Tb*BILBO1. The purified Nb is able to identify *Tb*BILBO1 in fixed trypanosomes by immunofluorescence and denatured protein from trypanosome whole cells samples. Surface Plasmon Resonance analysis confirmed a high affinity of Nb48 to *Tb*BILBO1: K_D=8.8nM. Expression of Nb48 as an intrabody in *T. brucei*, reveals that it binds precisely to its target, *Tb*BILBO1, and leads to rapid cell death. Further exploration of the potential uses of this trypanocidal nanobody is warranted.

Keywords: *Trypanosoma brucei*, cytoskeleton, flagellar pocket, Neglected Tropical Diseases, nanobody, RNAi.

Résumé

Caractérisation et Ciblage de Protéines Essentielles via l'utilisation de Nanobodies chez *Trypanosoma brucei*

Les parasites de la classe des Kinetoplastidae, comprenant notamment les trypanosomes et les leishmanies, sont responsables pour plusieurs maladies d'importance socio-économique et de santé publique. La maladie du sommeil, la maladie de Chagas et la leishmaniose, classées comme maladies tropicales négligées (NTD) par l'Organisation mondiale de la santé (OMS) et la Surra, reportée par l'Organisation pour l'alimentation et l'agriculture, des Nations Unies (FAO). La Trypanosomiase Animale Africain sub-saharienne entraîne la mort de 3 millions bovins par an accompagné d'une perte annuelle de l'économie de 4,5 milliards de dollars américains. La leishmaniose cutanée, une maladie zoonose, présente 1,5 millions de nouveaux cas chaque année.

Trypanosoma brucei (*T. brucei*) est un ancien eucaryote, utilisé comme organisme modèle dans le laboratoire pour l'étude des cils et des flagelles. Le remodelage du cytosquelette des trypanosomes est essentiel pour la morphologie cellulaire, le positionnement et la division des organites. L'étude des protéines essentielles du cytosquelette permet de mieux comprendre les processus cellulaires. Ces protéines pourraient également constituer des cibles potentielles pour des traitements thérapeutiques. Les trypanosomes échappent au système immunitaire de l'hôte en modifiant périodiquement les antigènes de présent à leur surface. En effet ces antigènes de surface sont endocytés, ainsi que les anticorps de l'hôte qui y sont attachés, au niveau d'une structure appelée la poche flagellaire (FP). *Tb*BILBO1 est une protéine structurelle du collier de la poche flagellaire (FPC), essentielle à la biogenèse du FPC et à la survie du parasite. En raison du rôle majeur de la protéine *Tb*BILBO1 dans le parasite, des partenaires de *Tb*BILBO1 ont été recherchés.

Dans ce travail, j'ai pu caractériser une nouvelle protéine essentielle du cytoskelette, la protéine FPC6, partenaire de *Tb*BILBO1, qui se situe au niveau du complexe FPC/Complexe du hook de *T. brucei*. L'ARN interférence de FPC6 conduit à une mort rapide des formes sanguines des trypanosomes, accompagnée d'un blocage de l'endocytose. Ensuite, j'ai produit un nanobody (Nb48), dirigé contre *Tb*BILBO1, dans le système d'expression bactérien. Je l'ai également exprimé dans les lignées de trypanosomes. Le Nb48 reconnait TbBILBO1 sur les trypanosomes fixés par immunofluorescence et dans les extraits totaux de protéines dénaturées. L'analyse par résonance plasmonique de surface a confirmé une haute affinité du Nb48 pour

*Tb*BILBO1. L'expression de Nb48 dans le parasite *T. brucei* en tant qu'intrabody demontrant que ce nanobody pouvait être exprimé de manière fonctionnelle, capable de reconnaitre spécifiquement sa cible protéique, *Tb*BILBO1, intra-cellulaire et de bloquer sa fonction conduit à un effet trypanocide rapide. Ces études ouvrant ainsi la voie pour de nouvelles utilisations potentielles thérapeutiques dans le traitement des trypanosomiases.

Mot clés: *Trypanosoma brucei*, cytoskelette, poche flagellaire, Maladies Tropicales Négligées, nanobody, ARNi.

Acknowledgements

This thesis would not have been possible but for the support of those around me both in the laboratory and at home, not only in recent years but throughout the course of my career. My thanks goes to the French Ministry of National Education (Ministère de l'Éducation Nationale) for the financial scholarship to support my doctoral studies. I thank ParaFrap, the French Parasitology Alliance For Health Care programme, for my inclusion in a number of their workshops.

I wish to thank the members of my thesis committee: Prof Martin Teichmann, president of the jury, Prof Sue Vaughan and Dr Helen Price who kindly accepted to review my thesis and together with Dr Isabelle Sagot and Dr Philippe Bastin for their participation in my oral examination.

My sincere thanks to my supervisor, Dr Derrick Robinson, who, from our very first meeting, had faith in my ability to complete this study and welcomed me wholeheartedly into his laboratory. Thank you for your unwavering support and guidance during my PhD studies. Thank you to Dr Mélanie Bonhivers, who helped me, in particularly, get to grips with certain aspects of molecular biology and the ability to manipulate my genes of interest.

I express my extreme gratitude to Dr Denis Dacheux, whose boundless enthusiasm, infectious energy and careful guidance, helped me through my early days in the laboratory and gave me the skills and knowledge to develop my studies independently and with confidence. Many thanks to Nicolas Landrein, for his unending patience with my questions on various techniques throughout the course of my PhD. Thank you, to my fellow lab members, post-doc and doctoral students, past and present: Dr Doranda Perdomo, Dr Anna Albisetti, Anne Cayrel, Charlotte Isch and Rijatiana Miharisoa Ramanantslama who lightened the days with music and jokes, and to all members of the Microbiologie Fondamentale et Pathogénicité group, UMR 5234, for their help and support. A special thank you to two students that worked with me on the FPC6 experiments: Amélie Mailhé and Corentin Agnero-Rigot.

My thoughts go back to numerous mentors who have inspired me throughout my undergraduate veterinary studies, my early veterinary and later research career: Lord Sandy Trees, Prof Eduardo Berriatua, Prof Ron Jones, Prof Lorin Warnik, Dr Ellen Singer, Prof Barrie Edwards, Prof Derek Knottenbelt, Prof Becky Whay and all of the vets working for The Brooke that I had the honour to meet and work with in Egypt, India, Pakistan and Kenya. Words of wisdom, support and motivation given by these, and others, still continue to inspire me.

A heartfelt thank you to, my parents, John and Iris Broster who have always encouraged me to achieve my best. Finally, none of this would have been possible without the continued support of my husband, Fabrice Reix, for your unwavering encouragement and support throughout this journey and, of course, my children Thomas and Raphael, who always bring me back to the important things in life.

Contents

List of Figures

List of Tables

List of Abbreviations

aa	**a**mino **a**cid
BSA	**B**ovine **S**erum **A**lbumin
BSF	**B**lood**s**tream **F**orm
DNA	**D**eoxyribo**n**ucleic **A**cid
EGTA	**E**thylene **G**lycol **T**etraacetic **a**cid
FAO	**F**ood and **A**griculture **O**rganisation of the United Nations
FAZ	**F**lagellar **A**ttachment **Z**one
FBS	**F**oetal **B**ovine **S**erum
FITC	**F**luorescein **I**so**t**hio**c**yanate
FPS	**F**lagellar **P**ocket **C**ollar
GFP	**G**reen **F**luorescent **P**rotein
HC	**H**ook **C**omplex
ICZN	**I**nternational **C**ommission on **Z**oological **N**omenclature
IFA	**I**mmuno **F**luorescence **A**ssay
Ig	**I**mmuno**g**lobulin
IMDM	**I**scove's **M**odified **D**ulbecco's **M**edium
LB	**L**uria-Bertani **B**roth
mAb	**m**onoclonal **A**nti**b**odies
mybp	**m**illion **y**ears **b**efore **p**resent
Nb	**N**ano**b**ody
NTD	**N**eglected **T**ropical **D**isease
PBS	**P**hosphate **B**uffered **S**aline
PCF	**P**rocyclic **C**ulture **F**orm
PFA	**P**ara**f**orm**a**ldehyde
PFR	**P**ara**f**lagellar **R**od
PIPES	**Pi**perazine-N, N'-bis **E**thane**s**ulfonic acid
PVDF	**P**oly**v**inylidene **D**i**f**luoride membrane
RNA	**R**ibo**n**ucleic **A**cid
RNAi	**RNA i**nterference
SAXO	**S**tabiliser of **Ax**o**o**nemal microtubules
SDM	**S**emi **D**efined **M**edium
SDS-PAGE	**S**odium **D**odecyl **S**ulfate **P**oly**a**crylamide **G**el **E**lectrophoresis
RT	**R**oom **T**emperature
SmOx	**S**ingle **M**arker **Ox**ford strain
SSUrRNA	**S**mall **S**ub **U**nit **R**ibo**n**ucleic **A**cid
WHO	**W**orld **H**ealth **O**rganisation
WT	**W**ild **T**ype

This thesis is dedicated to all the animals and people suffering the consequences of trypanosomiasis.

Chapter 1

Introduction

1.1 Trypanosomes

1.1.1 Evolution

Trypanosomes are single-celled flagellated protists which have been evolving separately from other eukaryotes for over 500 million years ago, according to phylogenetic trees based on host species fossil records (Hafner and Nadler, 1988, Lukeš et al., 2014). The Cambrian explosion appeared in the fossil record as a time just over 500 million years ago when an evolutionary burst gave rise to a huge array of animals, which flourished in the seas, many of which exist today, including annelids,the ancestors of leeches (a vector of trypanosomes) present since the Cambrian period, 541-495 million years before present (mybp) (Budd, 2013). Variation in the nucleotide sequence of the small unit ribosomal RNA (SSU rRNA) has been explored to add accuracy to the molecular clock model, leading to very similar estimates for the divergence of salivarian trypanosomes between 260 and 500 mybp (Haag et al., 1998). Stevens and Gibson, 1999 calculated that parasitism itself evolved around 300 million years ago when the first salivarian trypanosomes are likely to have diverged from other trypanosomatids.

Modern pathogenic trypanosomes are likely to have evolved from free-living species, similar to *Bodo caudatus*, see Figure 1.1. Simpson et al., 2006 propose that parasitism by trypanosomes and hence a move from a monoxenous to a dixenous life is likely to have occurred at least four times over the course of evolution and in the case of *T. evansi* and *T. equiperdum*, a reversal from the dixenous back to the monoxenous life-cycle (Sánchez et al., 2015). Acquisition of a parasitic lifestyle necessitates a vector, either arthropod or leech in the case of aquatic species such as marine fish as described by Hayes et al., 2014.

In opposition to the vertebrate-first evolutionary point-of-view, another school of thought gaining momentum, is that trypanosomes were primarily parasites of insects i.e. invertebrate first and vertebrates were parasitised subsequent to their appearance on earth. Evidence for this theory, as discussed earlier by Vickerman, 1969 is given by Hamilton et al., 2004. Although these theories do not wholely explain aquatic leech vectors of trypanosomes and those that parasitise flowering plants.

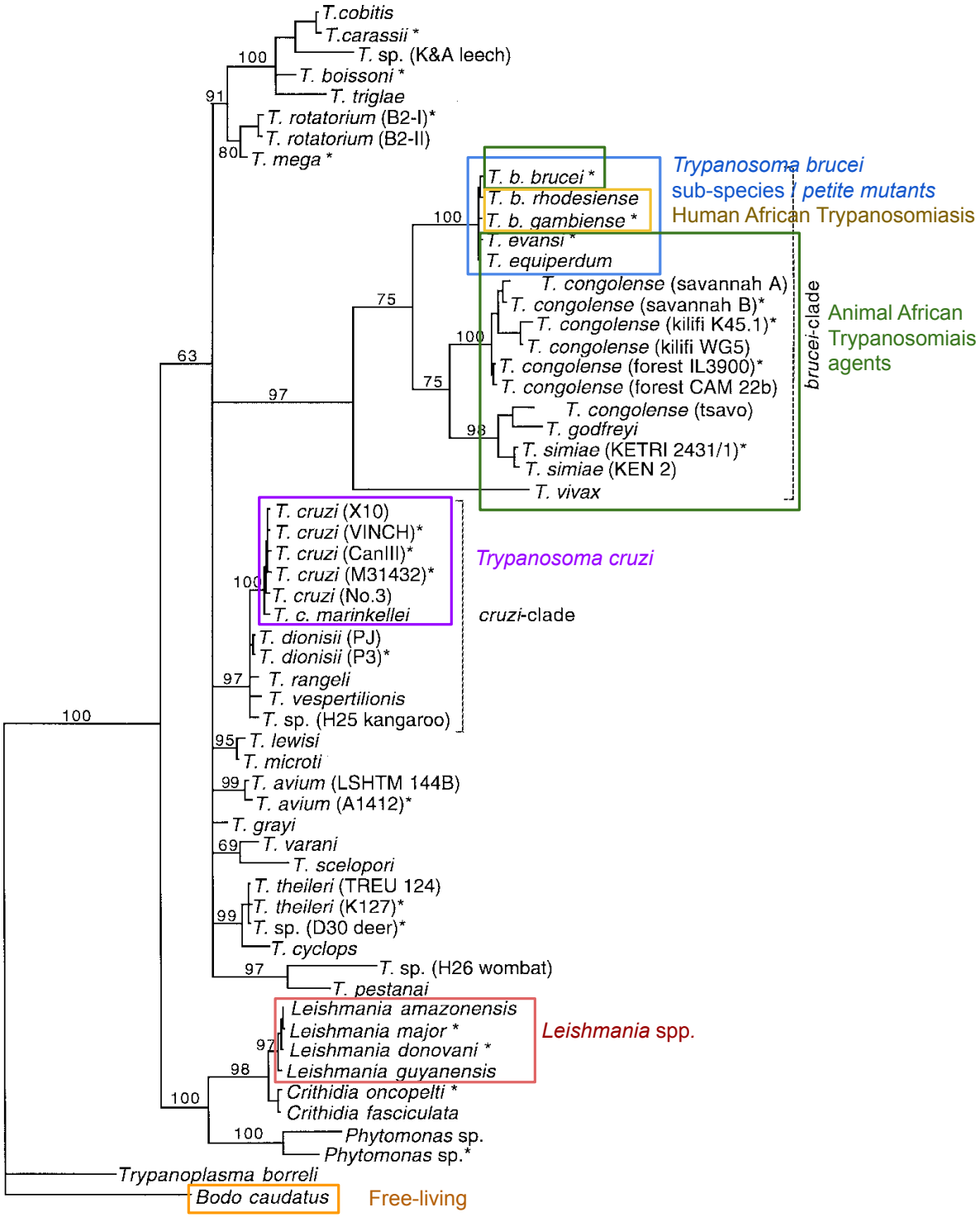

FIGURE 1.1: **Phylogenetic tree of the major kinetoplastid pathogens of Humans and Domestic Animals** based on 18S ssu rRNA nucleotide sequence analysis, rooted on *Bodo caudatus*; bootstrap values are given; main groups are highlighted in boxes; adapted from Stevens et al., 1998.

A single fossil record exists of kinetoplastid-like organisms preserved in a piece of amber from Burma dating from 100 mybp, in the Early Cretaceous period (Poinar, 2007). These kinetoplastids were present in the mid-gut of sand fly larvae; the authors propose that these flagellates would have passed on transstadially to adult flies and then over time and due to feeding habits of insects, transmitted to vertebrates who adapted as hosts and thus supports the view that trypanosomes were primarily parasites of flies and later were transmitted to vertebrate hosts.

Not only have trypanosomes evolved with land vertebrates but so too have the host species evolved over thousands and millions of years with trypanosomes (Stevens et al., 1998). Examples of this co-evolution are given here, one in cattle and the other in humans. Trypanotolerant cattle from West Africa, such as the indigenous N'dama, were first observed to be resistant to the disease by Chandler, 1952, a veterinary research officer working in Northern Nigeria; these animals show tolerance to trypanosome infection possibly due to a long co-evolution. A more recent study by Berthier et al., 2015 has shown two further cattle breeds: the Shorthorn Taurine Lagune and Baoulé, to be trypanotolerant. Cape buffalo (*Syncerus caffer*) are able to limit and control parasitaemia due to trypanosomes, but the exact mechanisms involved are unknown (Black et al., 2001). In the case of humans, an association was made by Genovese et al., 2010 between the high incidence of kidney disease in African-Americans and a variant of the *APOL1* gene. It was shown by Rifkin, 1978, that normal human serum contained a high density lipoprotein trypanosome lytic factor (TLF), later to be extended to two TLFs, of which TFL1 was shown by Raper et al., 1999 to contain apolipoprotein L1 (ApoL1) capable of neutralising infection to *T. b. brucei*, but not to *T. b. gambiense* or *T. b. rhodesiense*. These latter two trypanosome species are able to resist these trypanolytic factors of normal human serum. *T. b. rhodesiense* expresses a serum resistance-associated (*SRA*) gene, first identified by Van Xong et al., 1998, derived from a truncated variant surface glycoprotein (VSG). *T. b. gambiense* has a different specific glycoprotein gene, *TgsGP*, located in the telomere of chromosome 2, identified by Berberof et al., 2001. These findings gives evidence that a chance mutation could have led to resistance in the case of human or trypanosome and therefore survival.

1.1.2 Historical descriptions

Early recordings of trypanosome infection in animals, can be seen in ancient Egyptian hieroglyphic inscriptions on papyrus, taken from "Hieratic papyri from Kahun and Gurob (principally of the Middle Kingdom)" prepared by Francis Llewellyn Griffiths, 1898. The section highlighted by the box in Figure 1.2 describes symptoms of a disease of cattle fitting with Nagana.

Disease caused by trypanosomes has hindered livestock production since early times of intensification of farming and also in the case of introduced species. The first modern scientific documentation of a *T. brucei* subspecies was published in 1880 by Griffith Evans, a Welsh veterinarian (and medical doctor) investigating an equine

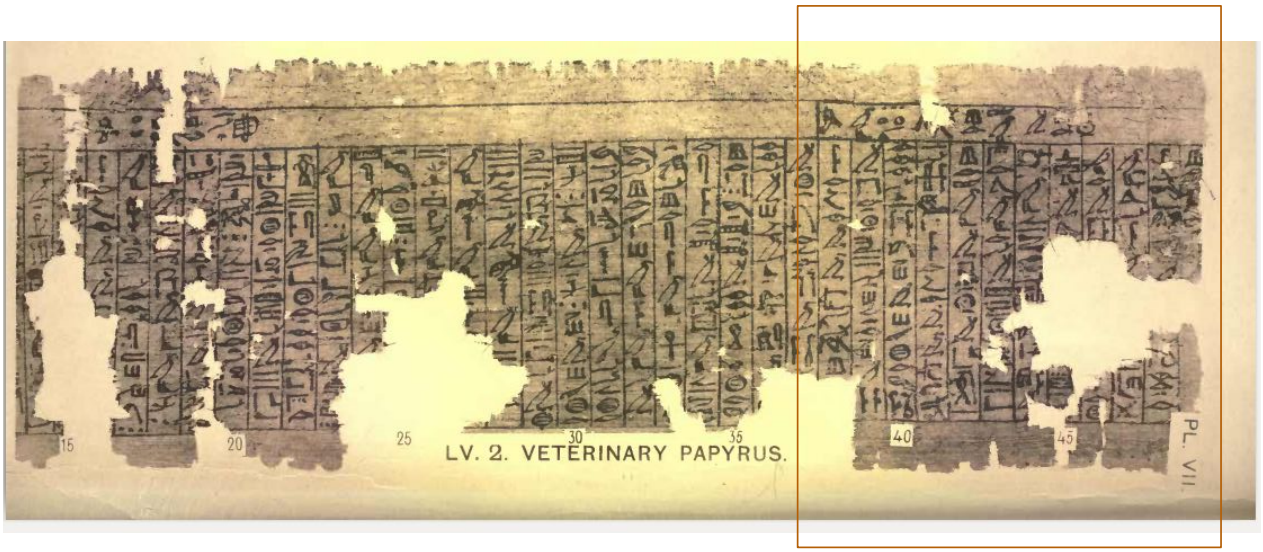

FIGURE 1.2: **Veterinary text on papyrus from Ancient Egypt** describing symptoms of Nagana in cattle in the Nile delta in the period 2000 - 1300 BC; taken from plates prepared by Griffiths, 1898, The Petrie Papyri: Hieratic Papyri from Kahun and Gurob (Principally of the Middle Kingdom).

wasting disease called Surra, in India; the parasite was subsequently named *T. evansi* after him. *T. b. brucei*, was first described by Sir David Bruce (in 1895) a Scottish physician, pathologist and microbiologist, in the blood of animals in Uganda, as the causative agent of Nagana. He named the parasite *Trypanosoma ingens* (Bruce et al., 1909), but it was later renamed *T. brucei* after him. *T. b. gambiense* was first identified in 1902, by the English physician Joseph Everett Dutton, and *T. b. rhodesiense* was first described by John William Watson Stephens and Harold Benjamin Fantham in 1910 (**Steverding2008TheTrypanosomiasis.**).

1.1.3 Taxonomy

The study of taxonomy aims to group organisms according to certain characteristics, be it morphology, life cycle or genetic markers. Classification of animals, including protists, comes under the code of the International Commission on Zoological Nomenclature (ICZN London, UK). Nomenclature of species is subject to change over the years and historically inaccurate names persist over time to become the mainstay with reluctance to change even with advancing modalities of classification (Molinari and Moreno, 2018).

The term "trypanosome" was first coined in 1843 by Gruby, 1843 looking at haemoflagellates of frogs and was taken up over the following decades, leading to the classification of pathogenic African trypanosomes by Sir David Bruce in 1914, and others. Initial classification of organisms was by morphology (e.g. shape and position of kinetoplast), mode of development (either in the tsetse fly or vertebrate host) and indeed host range and pathogenicity (Hoare, 1964).

Trypanosomes belong to the order Kinetoplastida, possessing a concentrated mass of mitochondrial DNA, termed the kinetoplast (kDNA). In the case of the subgenus *Trypanozoon*, two views have been proposed: firstly, by Carnes et al., 2015, that *T. evansi* and *T. equiperdum* should be reclassified as *T. brucei evansi* and *T. brucei equiperdum* due to extreme similarities between these organisms and, in fact, *T. evansi* and *T. equiperdum* are petite mutants of *T. brucei* with either partial (dyskinetoplasia) or complete loss of the kDNA (akinetoplasia) (Lai et al., 2008). *T. evansi* has also been described as a phenotypic variant of *T. brucei* by Takeet et al., 2016. Indeed, no molecular test exists that is able to discriminate between *T. equiperdum* and *T. brucei*, diagnosis (as described later) taken by epidemiological indications, host presenting symptoms and morphology of trypanosome species (Büscher et al., 2019).

An opposing view places the emphasis on the fact that *T. evansi* was historically classified first and therefore *T. brucei* and sub-species, should be notated as *T. evansi evansi*, *T. evansi rhodesiense* and *T. evansi gambiense*; with adjoining notes to stipulate which disease they cause, be it nagana, surra or dourine (Molinari and Moreno,

Superfamily	Eukaryota
Kingdom	Protista
Phyllum	Euglenozoa
Class	Kinetoplastea
Order	Kinetoplastida
Family	Trypanosomatidae
Genus	*Trypanosoma*

TABLE 1.1: **Classification of Trypanosomes.** Details are given for the genus *Trypanosoma*, taken from Gruby, 1843, Cavalier-Smith, 1993, Stevens and Gibson, 1999, D'avila-Levy et al., 2015 and Ruggiero et al., 2015.

2018). A concensus view by Stevens and Gibson, 1999 and Carnes et al., 2015 stipulates that *Trypanosoma equiperdum* belongs to the subgenus *Trypanozoon* together with *T. brucei* and *T. evansi*.

A Table of flagellated kinetoplastid classification is shown in Table 1.1, as supported by Gruby, 1843, Cavalier-Smith, 1993, D'avila-Levy et al., 2015, Ruggiero et al., 2015 and Stevens and Gibson, 1999.

1.2 Disease

1.2.1 Epidemiology

Kinetoplastids are present globally, comprising both pathogenic and non-pathogenic, infecting both animals and plants, and free living species, such as *Bodo* spp.

A number of trypanosome species cause disease, most notably in mammals, but also in reptiles, fish and plants. In humans, two subspecies *T. brucei rhodesiense* and *T. brucei gambiense* are the cause of the acute and chronic forms of sleeping sickness in sub-Saharan Africa. A further subspecies, *T. brucei brucei*, contributes along with *T. vivax* and *T. congolense*, to the disease Nagana in cattle in sub-Saharan Africa, with a huge loss to the African economy, in fact Kristjanson et al., 1999 calculated the annual cost of the disease through loss of animals (cattle, goats, sheep and horses), loss of meat, milk, manure and traction, to be $1.34 billion.

T. b. rhodesiense has been shown to infect and cause a fatal CNS disease in cattle experimentally (Wellde et al., 2016) and movement of infected cattle to restock new areas in Eastern Uganda, has been purported as the cause of spread of the disease into the human population (Fèvre et al., 2001). Closely related to *T. brucei* are two species that have lost the ability to differentiate inside an insect host: *T. evansi* and *T. equiperdum*. *T. evansi* has the largest geographical spread, causing a wasting disease in horses, camels, donkeys and other mammals such as dogs; the disease is known as surra, derrengadera, murrina or mal de cadeiras (Sánchez et al., 2015). This disease affects animals of traction leading to suffering and economic losses for some of the world's poorest communities reliant on these animals of traction for their main energy source; in fact up to half the world's population is reliant on animals of traction for their main energy source (Ramaswami, 1994). With estimates of over 100 million working equids worldwide FAO, 2017 this potentially affects a considerable number of income-providing animals and their communities.

Dourine is a disease caused by *T. equiperdum*, and unlike the other trypanosome diseases, it is transmitted by coitus. In Europe and North America, Dourine is notifiable

Disease	Transmission	Subgenus	Species	Host	Vector	Distribution
Animal Trypanosomosis	Salivaria	*Duttonella*	*Trypanosoma vivax*	Cow, Goat, Horse, Sheep	*Glossina* spp, *Tabanus* spp, *Stomoxys* spp	Sub-Saharan Africa, South America*
Nagana (African Animal Trypanosomosis - AAT)		*Nannomonas*	*T. congolense,* *T. simiae*	Cow, Dog, Horse, Goat, Pig, Sheep Pig	Tsetse: *Glossina* spp	Sub-Saharan Africa
		Pycnomonas	*T. suis*	Pig		
		Trypanozoon	*T. brucei brucei*	Cow, Goat, Horse, Sheep		
Human African Trypanosomiasis (HAT) Sleeping Sickness		*Trypanozoon*	*T. b. gambiense*	Human		West and Central Africa
			T. b. rhodesiense	Human (Cow)		East, Central and South Africa
Surra	Mechanical, oral route, coitus?	*Trypanozoon*	*T. evansi*	Cow, Camel, Dog, Donkey, Horse	*Tabanus* spp, *Stomoxys* spp, Vampire bats	Africa, Asia, South and Central America; occasionally in Europe
Dourine	Venereal	*Trypanozoon*	*T. equiperdum*	Donkey, horse	*n/a*	
Chagas, American Trypanosomiasis	Stercoraria	*Schizotrypanum*	*T. cruzi*	Cat, Dog, (Horse), Human, Pig	*Triatoma* spp, *Rhodnius* spp	South and Central America, southern USA, Europe**

TABLE 1.2: **Pathogenic Trypanosomes of Humans and Domestic Animals.** Note that many of these trypanosomes can infect a wider range of mammals than stated, including wildlife. * Spreading outside the tsetse belt due to mechanical transmission by biting flies. ** Cases in Europe and southern states of USA initially due to travel of infected people, but autochthonous transmission has been reported in Louisiana (Dorn et al., 2007, Hutchinson and Gibson, 2015, Radwanska et al., 2018, Büscher et al., 2019).

as laid out by the OIE, with strict rules on movement and control of the disease in horses.

In South America, *T. cruzi* is the cause of Chagas disease, transmitted by the biting *Triatoma* insects. Cases of Chagas disease has also been noted in Spain due to travel of already infected patients from South America (Navarro et al., 2012). Three out of the seventeen Neglected Tropical Diseases, as classified by the World Health Organisation (WHO), are caused by Kinetoplastid parasites: Sleeping sickness in Sub-saharan Africa caused by *T. b. rhodesiense* and *T. b. gambiense*, Chagas disease in South-America caused by *T. cruzi*, and Leishmaniasis caused by *Leishmania* spp. Of these, *T. b. rhodesiense* and *Leishmania* are zoonotic. Trypanosomosis in cattle is classified as a list B disease by the Food and Agriculture Organization of the United Nations (FAO), L'Office International des Epizooties (OIE; World Organisation for Animal Health) and the Institute for Animal Health, UK. List B diseases are defined as "Transmissible diseases which are considered to be of socio-economic and/or public health importance within countries and which are significant in the international trade of animals and animal products." *T. evansi*, the cause of the equine disease Surra is also in the FAO's B list, as is leishmaniosis which affects dogs and cats (OIE, 2019). A summary of the main pathogenic trypanosomes of humans and domestic animals/livestock are included in Table 1.2.

Within Africa alone, a third of the land mass is affected by trypanosome-related disease leading to 3 million cattle deaths *per annum* contributing to increased hunger and poverty (Steverding, 2008). In fact the disease is so wide-spread that one survey in Uganda showed that over 85% of cattle herds and 57% of the working donkey population were seropositive for *trypanosoma* spp. (Muhanguzi et al., 2017). In an economic study carried out by Okello et al., 2015 showed that parasitic diseases of livestock, such as trypanosomiasis, can reduce household incomes by over 30%. Donkeys are proven to ease the burden of life and this is particularly true for women who do much of the water carrying in developing countries (Upjohn and Valette, 2014). Another epidemiological study in West Africa sampled pigs at abattoirs and markets, found almost a third of all animals tested to be infected with a species of trypanosomes (Omeke, 1994), only to be surpassed by a study in Ghana showing up to 84% prevalence in pig herds sampled (Bauer et al., 2011). Trypanosomiosis also afflicts domestic animals and has been stated as a major cause of death of dogs in Nigeria (Anene et al., 2006). For a summary of pathogenic trypanosomes of humans and domestic animals, see Table 1.2

Zoonotic Trypanosomiasis

It has been reported that animals can serve as a reservoir of human infective species, such as *T. b. rhodesiense*. In Uganda, large intervention studies were carried out by Hamill et al., 2017 and Fyfe et al., 2017 where over a combined total of 60,000 cattle were administered with a single dose of trypanocide (either diminazene aceturate

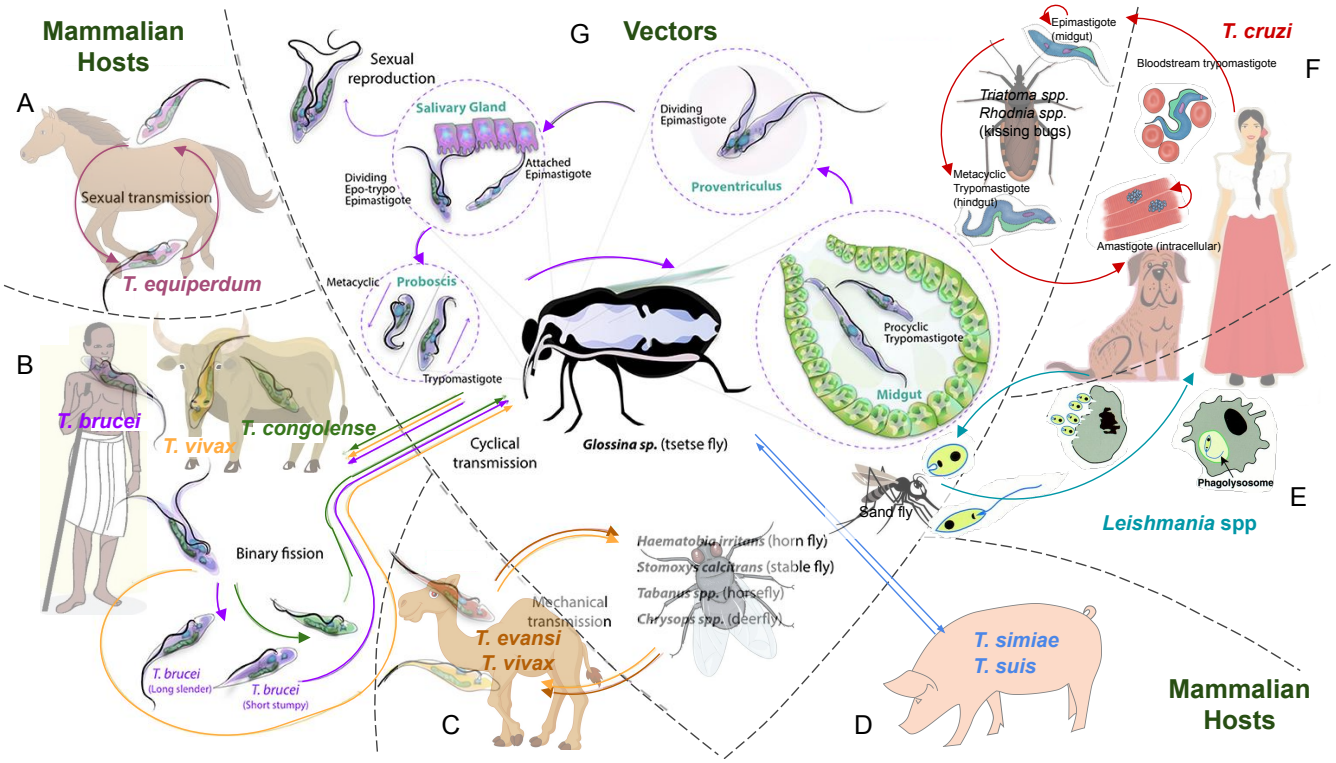

FIGURE 1.3: **Life cycle of Pathogenic Kinetoplastids of Humans and Domestic Animals.** Host range often larger than depicted. Adapted from Handman, 2001, The Chagas Disease Foundation, 2019, Radwanska et al., 2018 and Büscher et al., 2019.

or isometamidium chloride) resulting in a significant reduction in human infective *T. b. rhodesiense* and a reduction in human clinical cases. Evidence has also been reported by Hamill et al., 2013 of pigs in Tanzania, where half of the *T. brucei* species isolated were in fact *T. b. rhodesiense*. Regarding *T. evansi*, a couple of cases have been reported: the first was a farmer in India in 2005 (Joshi et al., 2005) who contracted *T. evansi* most likely from an infected animal. A more recent case in 2016, was the report of a women in Vietnam who was diagnosed with *T. evansi* infection; sampling of bovine animals in her location revealed 47% positive by PCR for *T. evansi* on blood sampling (Van Vinh Chau et al., 2016); both cases made a full recovery with treatment using suramin.

1.2.2 Symptoms

Humans

Human infective subspecies *T. b. gambiense* and *T. b. rhodesiense* cause the chronic and acute forms, respectively, of the Neglected Tropical Disease, Human African Trypanosomiasis (HAT) known as Sleeping sickness (Nussbaum et al., 2010). *T. b. gambiense* is present throughout West and Central Africa, whilst *T. b. rhodesiense* is present in East Africa and has been shown to be zoonotic, with a migratory spread of the infection seen within Uganda due to re-stocking of cattle in areas previously unaffected by the disease (Fèvre et al., 2001). Following a tsetse fly bite and subsequent infection, a trypanosomal skin chancre is seen (mostly with *T. b. rhodesiense*) at the bite site, around 48 hours post-bite, followed by symptoms of headache, fever, pruritus and lymphadenopathy; these signs constitute stage one of the disease, when the parasite is present in the haemolymphatic system, and bodily tissues (Brun et al., 2010). Stage two occurs when the parasite crosses the blood-brain barrier and leads to neurological symptoms including disturbance of the circadian rhythm (Rijo-Ferreira et al., 2018) and hence symptoms of sleep disturbance, which gives the disease its common name.

Throughout the 20th century deadly epidemics of HAT have flared up, notably in the 1960's and concerted efforts over the past decade or so have enabled control of the disease to the current status of around 1447 new cases (reported in 2014), leading the World Health Organisation to declare the goal of eliminating sleeping sickness as a public health problem by 2020 (WHO, 2018).

T. b. brucei is a subspecies which is not infective to humans and old world monkeys due to variants of *APOL1* gene which code for a serum trypanolytic factor (TLF) called APOL1. Two high density lipoprotein complexes containing apolioprotein L1 exist: TFL1 and TFL2 (Thomson et al., 2014). TFL1 contains APOL1 and a haptoglobin-related protein and this complex is taken up by the parasite by the haptoglobulin-haemoglobin receptor (HpHbR). A pH change in the lysosome triggers ApoL1 to create pores in the endosomal-lysosomal membranes (including mitochondrial) leading to death of the parasites (Hager et al., 1994). TFL2 is a complex

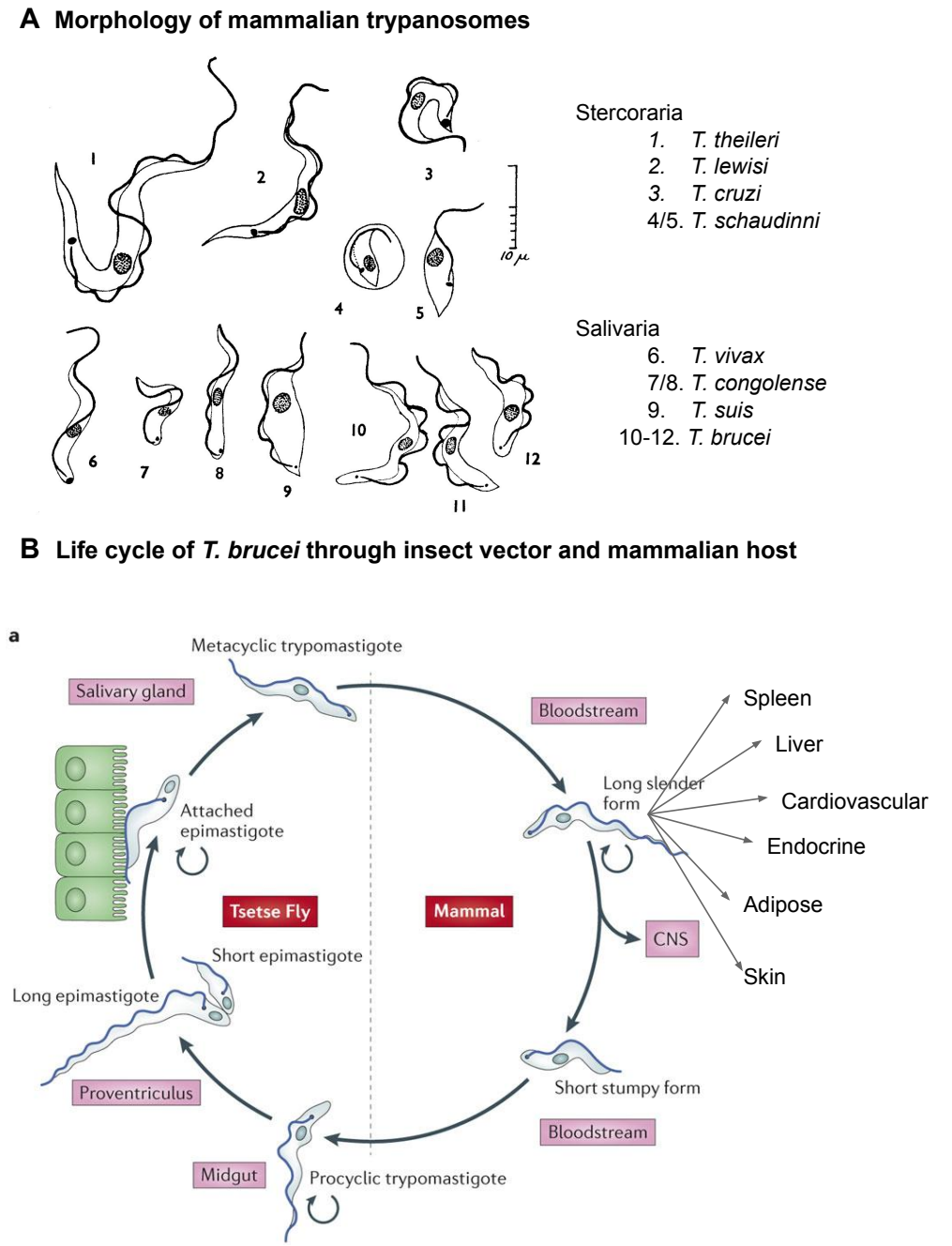

FIGURE 1.4: **Morphology of Mammalian Trypanosomes and Life Cycle of *T. brucei*.** **A** Different species of trypanosome exhibit different morphological characteristics as observed by Hoare, 1964. **B** life cycle in the insect, *Glossina* vector and mammalian host, adapted from Langousis and Hill, 2014.

with IgM. *T. b. brucei* can, however, infect animals and contributes to Nagana. *T. b. gambiense* and *T. b. rhodesiense* posses a serum resistant-associated protein (SRA) that binds to ApoL1 thereby inhibiting its lethal function and rendering these subspecies of trypanosome resistance to normal human serum (Oli et al., 2006).

Animals

Animal Trypanosomosis is caused by a plethora of trypanosome species, namely *T. vivax, T. congolense, T. evansi, T. equiperdum, T. simiae, T. suis, T. brucei* and *T. cruzi*, depending on the geographical location and host species. The disease itself, also has numerous terms depending on the country, host and symptoms. Due to the fact that *T. vivax, T. evansi* and *T. equiperdum* are not dependent on the tsetse fly, they can circulate in a much greater geographical range outside of the tsetse fly belt (Muhanguzi et al., 2017). *T. evansi* can be transmitted, not only by tsetse flies but by haematophagous, biting flies such as *tabanid* and *stomoxys* spp., by vampire bats, by the oral route after eating contaminated meat (Raina et al., 1985) and even by the venereal route.

Clinical signs in animals are not pathognomonic, often with a general wasting condition, fever, anaemia (Luckins, 1992), oedema (especially on the ventrum in cattle and horses), lacrimation, enlarged lymph nodes, abortion and decreased fertility, anorexia and eventual death in chronic cases, with or without neurological signs. This list of general symptoms can also be seen with other diseases such as babesiosis, anaplasmosis, theileriosis, anthrax, chronic helminth infection and chronic malnutrition, therefore a definitive diagnosis can be challenging. "The cardinal sign of African trypanosomiasis in the bovine is anemia" stated Murray, 1979 although much of its development was unexplained. Szempruch et al., 2016 cited the description of extracellular vesicles (EV) produced from *T. brucei* nanotubes that could fuse to mammalian red blood cells inciting their rapid clearance; the authors also alleged that these EV could carry serum resistance-associated protein (SRA) from one sub-species to another, indicative of a communication between parasites *in vivo*.

1.2.3 Life cycle and transmission

Uniquely, African trypanosomes, *T. brucei* spp., are transmitted by the bite of an infected tsetse fly *Glossina spp.* and a complex life cycle ensues over 15-21 days (Matthews, 2009) with multiple forms within the insect vector and the mammalian host (Figures 1.3 and 1.4.B).

Certain pathogenic trypanosomes have escaped the tsetse fly and now circulate by the mechanical biting of a fly, *Stomoxys* spp. and tabanids (*T. evansi* and *T. vivax*), or by coitus (*T. equiperdum*), enabling their distribution globally to be greatly enhanced. In South America, *T. cruzi* is spread via the bite of a *Triatoma* spp. insect, otherwise known as the "kissing bug" (Teixeira et al., 2011).

Trypanosomes are principally extracellular parasites: *T. vivax* and *T. congolense* are primarily blood parasites, whilst the others have tissue tropism, with *T. equiperdum* primarily a tissue parasite. *T. brucei* species have been overlooked as tissue parasites for many years. It has long been known that *T. b. gambiense* and *T. b. rhodesiense* cross the blood brain barrier and inhabit the CNS, as observed by clinical symptoms (Kennedy, 2004), but also the spleen, liver, skin, eyes, cardiovascular and endocrine systems. Wolbach and L Binger, 1912 reported *T. b. gambiense* in skin sections, but this knowledge was overlooked for many years until recent interest brought about a number of publications including Capewell et al., 2016) reporting the skin as the main reservoir for infections. In the same year, Trindade et al., 2016 reported the adaptation of *T. brucei* to adipose tissue. By contrast, *T. cruzi* and *Leishmania* spp. are obligate intracellular parasites. *T. cruzi* replicates in the blood but invades non-phagocytic cells and has a tropism for muscle, including heart smooth muscle, leading to symptoms of the disease (Teixeira et al., 2011). *Leishmania* reside in macrophages in the mammalian host and clinical symptoms are related to the immune system response of the host, either giving a localised disease, or more generalised of the skin or visceral organs (Torres-Guerrero et al., 2017).

Morphology

Trypanosomes exhibit a generalised cell shape, however, within this there is a great variation on detail of length and positioning of the kinetoplast and length of flagellum, in particular. A range of early sketches by Hoare, 1964 of the morphology of a range of mammalian trypanosomes can be seen in Figure 1.4.A. This variation in morphology is maintained by the cytoskeleton, as described in section 1.4.

Life cycle of *T. brucei*, VSGs and SIF

In the laboratory, I have been working with *T. b. brucei*, therefore I shall give a description of the life cycle of this parasite. I shall begin the cycle with the bite of an infected tsetse fly. Within the tsetse fly salivary gland are non-replicative metacyclics, which are pre-adapted for transmission into the mammalian host, displaying a VSG coat on their surface (Matthews, 2005). It has long been described that the tsetse fly is a "pool-feeder" (Laviopierre, 1965), but the intricate details of this have more recently been highlighted by Gibson et al., 2017 revealing high resolution images of the proboscis with which the tsetse fly pierces the skin and then uses rasp-like teeth structures to tear away at the skin structure; the fly then feeds on the resultant blood pool, depositing saliva and metacyclics into the host. Once in the the host bloodstream, the metacyclics differentiate into a proliferative trypomastigote form, dividing by binary fission, otherwise known as the long slender bloodstream form (Matthews, 2005). This form is able to be transported around the body due to the blood circulatory system and may even pass the blood brain barrier to the CNS (see Figure 1.4.B.).

A Parasitaemia profile of an infected patient

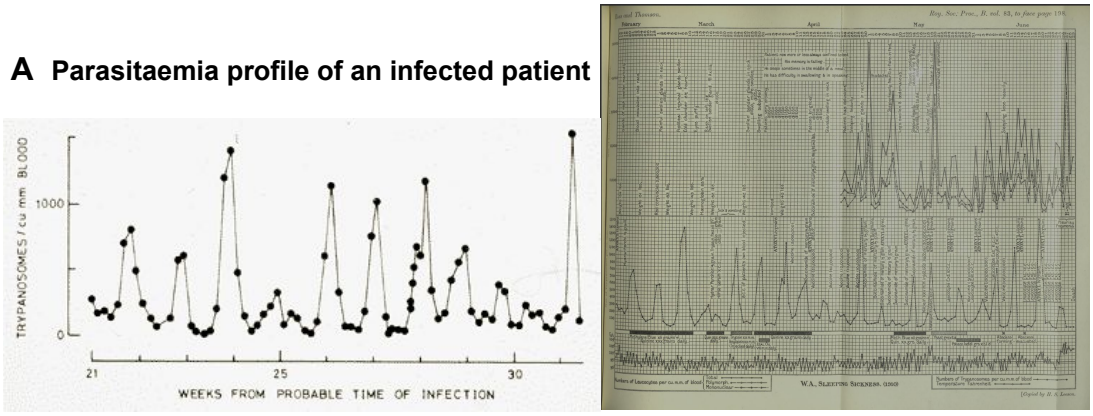

B Waves of parasitaemia comprise of populations expressing single VSG

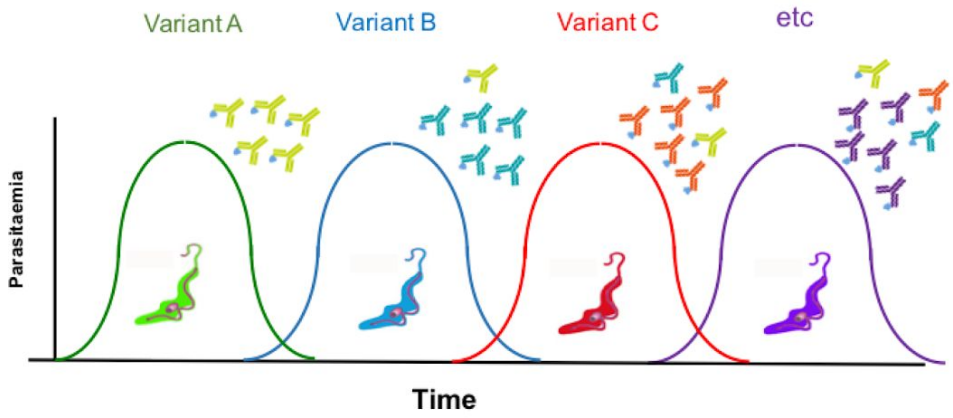

C Sub-telomeric location of VSG expression sites in *T. brucei*

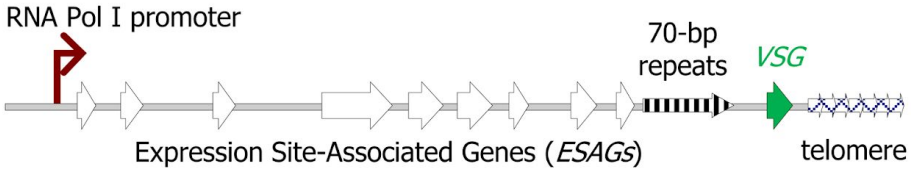

FIGURE 1.5: **Parasitaemia and VSG expression in *T. brucei*. A** Undulating waves of trypanosome parasitaemia are observed in mammalian hosts, such as recorded with *T. b. gambiense* by Ross and Thomson, 1910. **B** waves of parasitaemia coincide with variation in the VSG coat of *T. brucei*. **C** VSG expression site located sub-telomerically on the chromosomes, taken from McCulloch et al., 2017.

During an infection the parasite has a number of mechanisms of control: periodic changing of the main surface protein exposed to the host immune system, the variant surface glycoprotein (VSG) first identified and purified by Cross, 1975 and a density-dependant, quorum sensing mechanism to prepare for transmission to a new host, first described by Vassella et al., 1997.

The trypanosome surface coat is composed of around 10^7 glycosyl-phosphatidylinositol (GPI) anchored glycoproteins of ~60kDa, the entire surface coat can be recycled in 7 minutes due to the extremely high rate of endocytosis (see Section 1.4.6). An individual parasite expresses just one VSG at a time, but is able to switch to a distinct antigenic VSG, taking 4.5 days to fully make the change (Pinger et al., 2017). The initial infecting population of trypanosomes are cleared by host IgM, but some parasites in the population exhibiting a different VSG, survive and multiply to form the new dominant population (McCulloch et al., 2017). This gives rise to peaks of parasitaemia as observed in a sailor in Liverpool by Ross and Thomson, 1910, see Figure 1.5.A. Consecutive waves of trypanosome populations can be seen in Figure 1.5.B. At any one time the population of trypanosomes in a host expresses a dominant VSG coat, however *T. brucei* possesses a repertoire of around 2000 VSG genes, located mainly in sub-telomeric locations of chromosomes (Figure 1.5.C).

To continue on its life cycle and to adapt to be taken up by a tsetse fly, it has long been held that *T. brucei* must differentiate from a long slender form to a short stumpy form (see Figure 1.5.B.). However, new data from Schuster et al., 2019 might challenge this paradigm by showing that long slender blood stream form trypanosomes were able to infect the tsetse fly. Control of this change is determined by a density-sensing mechanism, or quorum-sensing ability of *T. brucei* triggered by the release of a Stumpy Induction Factor (SIF) (MacGregor et al., 2012). Rojas et al., 2019 recently identified an essential surface protein, *Tb*GPR89, which transports oligopeptides that in turn drives stumpy formation *in vivo* with a paracrine signalling pathway. Furthermore, Cayla et al., 2019 describe an atypical DYRK-family kinase of *T. brucei* playing a major role in development of stumpy forms from slender in the quorum-sensing pathway.

The stumpy form trypomastigotes reside in the skin and tissues, are essentially quiescent, non-proliferative forms and are pre-adapted for uptake by tsetse flies when feeding. In the tsetse fly mid-gut, the parasites differentiate into the proliferative procyclic form which now express a single surface coat protein composed of EP and GPEET procyclins (Matthews, 2005). The kinetoplast is now positioned sub-terminal as apposed to the terminal position in the bloodstream forms (Figure 1.4.B). From the mid-gut, trypanosomes arrest from division and migrate to the proventriculus where they differentiate again, into an epimastigote form, where the kinetoplast is now positioned anterior to the nucleus, continuing on their migration towards the salivary gland. This epimastigote form is proliferative, but divides into one long and one short daughter cells; the long cells are attached to the epithelium of

the salivary gland. The tsetse fly is the definitive host and Peacock et al., 2014 documented that meiosis/sexual reproduction can occur in the salivary glands. The trypanosomes migrate to the proboscis where they differentiate into metacyclic forms, to be re-injected into a new host, thereby completing the life cycle (Radwanska et al., 2018) see Figure 1.3 and 1.4.B.

Metabolism

As the parasite progresses through its life cycle, differentiation also brings about changes in metabolism, based on available nutrients. The BSF have a preference for glucose and the main pathway for ATP production is glycolysis performed in peroxisome-like organelles called glycosomes. The procyclic, insect form, performs primarily oxidative phosphorylation, using proline as the main nutrient source, with an elaborate single mitochondrion (Smith et al., 2017).

1.2.4 Diagnosis, prevention and treatment

Diagnosis

Diagnosis can be based on clinical symptoms, parasitological and/or molecular methods. In the field, clinical signs are the first indication of disease, however, they are not pathognomonic and positive confirmation of trypanosomiasis involves a combination of identification of the parasite (or its antigens) and/or antibodies raised against the parasite after exposure during infection.

A blood or lymph node expirate can be examined under the microscope for live trypanosomes, however, due to fluctuating parasitaemias, parasites are not always observed; therefore a concentration method might be employed. A number of methods are available including m-AECT (miniature anion-exchange centrifugation technique), buffy coat test (BCT) and indeed cerebrospinal fluid (CSF) sampling by lumbar puncture for second stage HAT. The gold standard for detection of parasites in blood is concentration by anion exchanger DEAE cellulose column, first developed by Sheila Lanham, 1968, over 50 years ago for detection of *T. congolense* and now with recent improvements (Courtois et al., 2019). Sensitivity of parasitological tests vary from less than 30% for blood smears, to over 90% for anion-exchangers.

Serological screening can be carried out to detect antibodies to trypanosome species in the blood. The CARD Agglutination test (CATT) is a standard field test for HAT diagnosis, requiring a simple finger prick and is used to detect antigens against *T. b. gambiense*; however, false negative and false positive results can occur (Bonnet et al., 2015). A CATT also exists for *T. evansi* (Songa and Hamers, 1988) but cross-reacts with *T. vivax*. The OIE recommends using Immunofluorescence antibody test (IFT) or ELISA for diagnosis of *T. evansi* and the complement fixation test (CFT) for *T.*

equiperdum (Büscher et al., 2019). Boulangé et al., 2017 developed a rapid point-of-care diagnostic test for *T. congolense* and *T. vivax* antigens.

In the field, molecular diagnostics may not be possible due to the specialised equipment and electrical power necessary for PCR reactions. Sensitivity is excellent with PCR, however some species may not be detectable with current primers and in the case of *T. brucei*, *T. equiperdum* and possibly *T. evansi*, it is not possible to distinguish between them making definitive diagnosis difficult (Büscher et al., 2019).

Prevention

Control of the tsetse fly vector has played a part in control of the disease. Improvements have been reported in West Africa using blue-coloured pheromone bated traps and topical repellents (synthetic pyrethroids) on the ventrum of cattle, transmission has been greatly controlled. One success story was seen in the protection of pig herds in Ghana using deltamethrin impregnated fences, where prevalence of trypanosomes fell from 72 to 16% with a reduction in tsetse fly densities of over 95% (Bauer et al., 2011). The release of sterile male tsetse flies could be advantageous as the female only mates once in her lifespan but proves expensive to develop. Naturally Trypanotolerant cattle, such as N'Dama and West African Shorthorn, have been considered in breeding programmes, but these breeds are small and less productive, so cross-breeding is a possibility (Berthier et al., 2015). Control of *T. b. rhodesiense* in the human population has been aided by treatment of cattle in the area, resulting in a seven-fold decrease in HAT cases in a study in Eastern Uganda (Fyfe et al., 2017). Chemoprophylaxis is possible with isometamidium chloride for prevention of infection with *T. congolense* and *T. vivax* in livestock.

Vaccination

Due to constant periodic replacement of the whole variant surface glycoprotein (VSG) coat in the mammalian forms, it has so far proved impossible to produce an effective vaccine against trypanosome pathogens. It was noted as far back as the turn of the 20th century that wild animals within the tsetse belt had the ability to thrive, as do trypanotolerant cattle (see below). The phenomenon seen in wildlife may in fact be due to premunition, i.e. continuous labile infection that no longer results in disease, as reported by Schilling, 1935. Attempts have been made to immunise cattle using live and dead trypanosomes, however, Hornby, 1941 reported that at that time, no effective vaccine had yet been produced. Fast forward 54 years, Mkunza et al., 1995 interestingly did show a partial protection against trypanosome infection in cattle after vaccinating with a flagellar pocket antigen preparation from *T. b. rhodesiense*.

Treatment of Human Trypanosomiasis			
Drug (reference)	*Trypanosoma* spp.	Disease / stage / species	Mechanism / target
Eflornithine (Van Nieuwenhove, 1985; approved 1990)	*T. b .gambiense*	Sleeping sickness (HAT) stage 2	Inhibit ornithine decarboxylase
Fexinidazole (Mesu *et al.,* 2018)	*T. b .gambiense*	HAT; both stage 1 and 2	Mitochondrial disruption
Melarsoprol (Friedheim, 1949)	*T. b .gambiense* *T. b. rhodesiense*	HAT both stages; used for *T. b. rhodesiense* stage 2	Disrupt redox metabolism and glycolysis
NECT: Nifutimox-eflornithine (Priotto *et al*., 2009)	*T. b .gambiense*	HAT both stages; used for stage 2	Nifurtimox induces oxidative stress and mitochondrial disruption
Nifutimox (Bock *et al*., 1969) / Benznidazole (Richle, 1973)	*T. cruzi*	Chagas	Bz oxidizes nucleotides, leading to lethal DNA breaks
Pentamidine (Yorke, 1940)	*T. b .gambiense*	HAT stage 1	Mitochondrial disruption
Suramin (Haedel & Joetlen, 1920)	*T. b. rhodesiense*	HAT stage 1	Glycolysis disruption
Treatment of Animal Trypanosomosis			
Diminazene aceturate (Jensch, 1955)	*T. congolense, T. vivax (T. brcuei spp, T. evansi)*	Cattle, sheep, goats, dogs; toxic to horse, donkeys, dogs and camels	Same class as pentamidine, bind kDNA
Homidium bromide (licensed 1952; (dimidium bromide, Wilson, 1948) H. chloride	*T. congolense,* *T. vivax (T. b. brucei)*	Cattle, sheep, goats, pigs	DNA intercalator; toxic and resistance
Isometamidium chloride (Brown *et al*., 1961)	*T. congolense, T. vivax (T. brucei)*	Cattle, sheep, goats, horses, camels	Bind kDNA; does not cross blood-brain barrier
Melarsomine hydrochloride (Lun *et al*., 1991)	*T. evansi, T. equiperdum,* *T. b. brucei*	Camels, buffalo, goats, pigs, horses, cattle	Arsenical derivative, unknown action
Quinapyramine sulphate (Curd & Davey, 1949)	*T. evansi, T. brucei, T. congolense, T. vivax, T. equiperdum, T. simiae*	Camels, horses, pigs, dogs, (cattle - resistance); toxic at high dose	Action unknown; does not cross blood-brain barrier
Suramin (Haedel & Joetlen 1920)	*T. brucei spp., T. simiae*	Camels, horses (toxic), pigs	Resistance reported

TABLE 1.3: **Treatment of Pathogenic Trypanosomes.** Only selected *trypanosoma* spp. and the commonplace drugs are shown, adapted from Thomas et al., 2018, Alsford et al., 2012, Giordani et al., 2016 and Babokhov et al., 2013.

Surveillance and Treatment of Human Trypanosomiasis

Success in recent decades in the control of HAT has been due to a commitment to surveillance and systemic population screening in endemic areas and treatment of infected individuals. A small number of therapeutic drugs exist. Until recently, for human patients, these proved to have narrow safety margins and involved treatment requiring hospitalisation and IV infusions for prolonged periods.

For *T. b. rhodesiense*, the treatment of stage one of the disease remains to be suramin since 1916 (Bayer 205; Haendel and Joetlen, 1920). Suramin, polysulphonated naphthylurea, was based on a dye and enters the parasite by endocytosis, disrupting glycolysis (Alsford et al., 2012). For stage two, melarsoprol, a melaminophenyl-based organic arsenical introduced by Friedheim, 1949 is still in use despite its potential for encephalopathy resulting in 5% mortality; although one study claimed reported death of three out of nine patients (Aiyedun and Amodu, 1976). Melarsoprol enters the parasite *via* adenosine transporters, shared with pentamidine, the AT1 (or P2) and AQP2. Melarsoprol leads to parasite death by ultimately interfering with trypanothione metabolism. Trypanothione, N^1,N^8-bis(glutathionyl)spermidine, acts in the defence against oxidants in trypanosomes (Fairlamb et al., 1985).

T. b. gambiense traditionally was treated with pentamidine isethionate, for stage one HAT since the late 1930's (Yorke, 1940). Pentamidine is taken up by the parasite by P2 adenosine transporters (De Koning and Jarvis, 2001) and mutations in the related *TBAT1* gene were shown to lead to cross-resistance with arsenical drugs (Kazibwe et al., 2009). Alsford et al., 2012 added to this in their high-throughput loss-of-function screen identifying a single locus encoding two closely related aquaglyceroporins, AQP2 and AQP3, linked to pentamidine/melarsoprol cross-resistance. In recent years, a combination therapy, NECT (nifurtimox/eflornithine), was introduced for stage two (Priotto et al., 2009). Eflornithine, or D,L-α-difluoromethylornithine, is an inhibitor of ornithine decarboxylase, first trialed by Van Nieuwenhove et al., 1985. Nifurtimox is administered in tablet form *per os*, however eflornithine is approved for slow intravenous infusion every 12 hours for 7 days (WHO, 2009). A huge step forward in treatment was made in November 2018, when the first oral drug, Fexinidazole, was approved by the European Medicines Agency approval for HAT in Africa. This was an initiative of the Drugs for Neglected Diseases initiative (DNDi) and after over 10 years of research trials the goal was reached with the drug freely available, donated by Sanofi and distributed by WHO. However, this treatment remains only effective against *T. b. gambiense* and for patients $\geq$ 6 years old and weighing $\geq$ 20kg. Fexinidazole is given as a 10 day oral treatment, it is safe, easy to use, effective in both stage one and stage two of the disease, can be used out of a hospital setting by the patient at home and has been shown in clinical trials to be non-inferior to NECT, the previous drug of choice for second stage HAT caused by *T. b. gambiense* (Mesu et al., 2018). The WHO's goal of eliminating sleeping sickness as a public health problem by 2020 may now be in grasp, however, we should not rest on our laurels and a slackening of control strategies may lead

to flare-ups in the future with over 65 million people at risk (WHO, 2018). A benzoxaborole orally-active drug (SCYX-7158) is currently progressing through clinical trials to treat stage 2 HAT caused by both *T. b. gambiense* and *T. b rhoseiense* (Jacobs et al., 2011; https://clinicaltrials.gov/ct2/show/NCT03087955). Treatment of Chagas disease (*T. cruzi*) relies on two compounds: nifurtimox (Bock et al., 1969) and benznidazole (Richle, 1973) the current therapy of choice. Benznidazole induces the formation of free radicals by primarily oxidising the nucleotide pool and leading to lethal breaks in double-stranded DNA (Rajão et al., 2013).

Treatment for Animal Trypanosomiasis

For animal treatment, a number of drugs are licensed, however resistance has been reported for some, others are highly toxic in some animal species, notably horses, and lack of control of medication in terms of illegal trade, poor storage conditions and under-dosing of animals, means that more effective drug surveillance, regulation and novel molecules are needed (Baker et al., 2013). Diminazene aceturate (Berenil, MSD Animal Health) has been used for treatment of trypanosomosis in livestock in Africa since evidence of its effect against trypanosomes (Jensch, 1955). Within just 6 years of its use, resistance was already being reported in a *T. congolense* strain in Kenya (Whiteside, 1963). Cross-resistance with other arsenical derivatives such as melarsomine, due to uptake by the same P2/TbAT1 receptors has been reported (Matovu et al., 2003); also for pentamidine. Homidium salts, such as homidium bromide and homidium chloride (Novidium®, Merial, France) are highly toxic and their use is discouraged. Phenanthridium compounds were first shown to be trypanocidal by Browning et al., 1938, of which the derivative dimidium bromide was shown to be trypanocidal to *T. simiae* infection in pigs and *T. congolense* infection in Uganda (Wilson, 1948). In 1952, a safer, less toxic compound Homidium bromide (Ethidium®, CAMCO Animal Health, U.K.) was licensed. Isometamidium chloride (Trypamidium®, Merial, France) is used in treatment of many animal species since its effectiveness was first shown by Brown et al., 1961. Quinapyramine sulphate (Antrycide^{TM}) was shown to be effective against seven strains of trypanosomes by Curd and Davey, 1949. The modes of action of quinapyramine are still in speculation: reports include nucleic acid synthesis disruption (Newton, 1958) cytoplasmic ribosome inhibition (Newton, 1962), or a hypothesised mitochondrial action, suggested by the interpretation by Hawking and Sen, 1960 of the fluorescent inclusion bodies in trypanosomes as shown by Ormerod, 1951. Suramin (Naganol, Bayer 205, Germany) has been reported to be used for treatment of *T. evansi* in camels (Bennett, 1930), horses and cattle (Edwards, 1926). Suramin enters the trypanosome by endocytosis, resistance to suramin in animals, particularly *T. evansi* (Zhou et al., 2004) has emerged in horses and camels perhaps due to the single recommended dose and the immunosupressive effects of the disease in these animals. In humans, a regime of 5 injections maintains the plasma levels elevated for several weeks, thereby explaining how after a century of treatment, suramin remains effective for treating HAT.

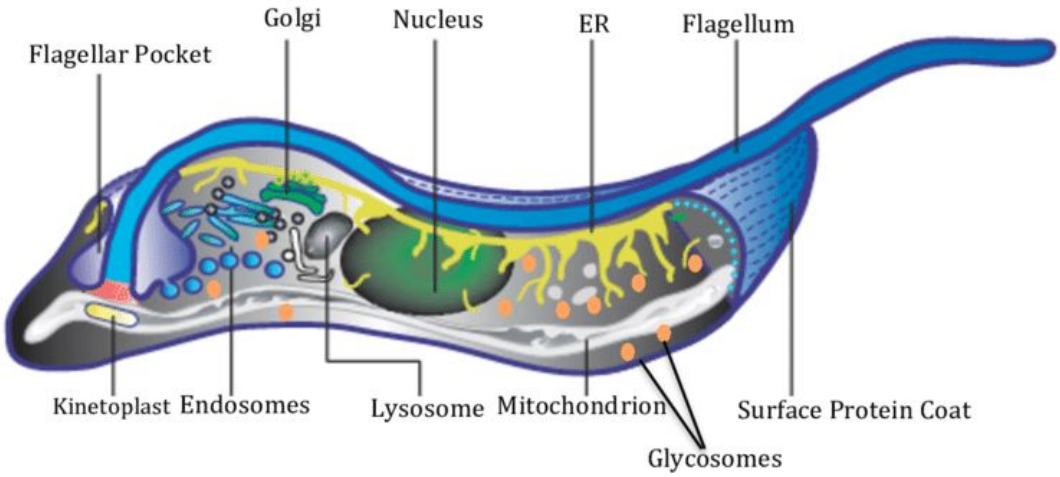

FIGURE 1.6: **The Ultrastructure of *T. brucei*.** A schematic diagram outlining the relative position of the organelles and structural components of *Trypanosoma brucei*, from Grunfelder, 2003.

Wiedemar et al., 2018 reported a variant surface glycoprotein (VSG^{SUR}) to be responsible for acquired resistance to suramin. Involvement of the VSG in binding suramin before endocytosis could explain this finding. Dourine, caused by *T. equiperdum* is a notifiable disease with only isolation, castration or euthanasia recommended as treatment (OIE), except in endemic countries. First reported for use in buffalo in China by Lun et al., 1991, melarsomine hydrochloride (Cymelarsan®, Rhône Mérieux, France) has had reported success in clearing infection with *T. equiperdum* (Hagos et al., 2010). At present there are no plans to further investigate fexinidazole for trials in the veterinary field (oral communication).

1.3 *Trypanosoma brucei* cell cycle

Cell division is necessary for the continuation of living cells and here I mainly focus on *T. brucei* as the model trypanosome used in my studies.

T. brucei (as other Kinetoplastids) possesses a number of single copy organelles, two DNA containing organelles: the kinetoplast (mitochondrial DNA) and the nucleus; a single flagellum in G1 phase (Sherwin and Gull, 1989); a golgi complex (He et al., 2004) and a single mitochondrion, see Figure 1.6. All these structures need to be faithfully replicated every time the cell divides. Orchestration of cell division is reliant upon elements of the cytoskeleton, in maintaining the mother cell whilst allowing replication and movement of new organelles within the cell and ending in cytokinesis and two daughter cells. An outline of the cell cycle of *T. brucei* is described here; more detailed information on each aspect of the cytoskeleton is given in Section 1.4.

The cell division events of *T. brucei* were well described by Sherwin and Gull, 1989 who categorised eight main events, starting with maturation of the pro-basal body, which subtends the growth of a new flagellum. The maturing basal body undergoes an anti-clockwise rotation around the flagellum to take up a posterior position, still within the old flagella pocket (Lacomble et al., 2010). Alongside the probasal body maturation event is the outgrowth of a new set of MTQ, which will continue to elongate alongside the new flagellum. As the new flagellum begins to elongate, a new pro-basal body is formed adjacent to each of the, now, mature basal bodies. As the new flagella exits the cell, the paraflagellar rod is formed running parallel to the axoneme (see more details on the PFR later). In PCF, a trans-membrane structure called the flagellar connector (FC) is positioned at the distal tip of the new flagellum, which connects the new flagellum to the lateral aspect of the old flagellum and appears to guide the new one along the length of the old (seen in Figure 1.7.B.; PCF; Briggs et al., 2004). The two DNA containing organelles go into S phase and divide separately; the first is the kinetoplast, which completes division before mitosis of the nucleus begins (Figure 1.7.A). The kinetoplast (kDNA or K) is a condensed mass of mitochondrial DNA, specific to kinetoplastids (giving them their name, although we now know petite mutants of *T. brucei*, *T. evansi* and *T. equiperdum*, are dys- or

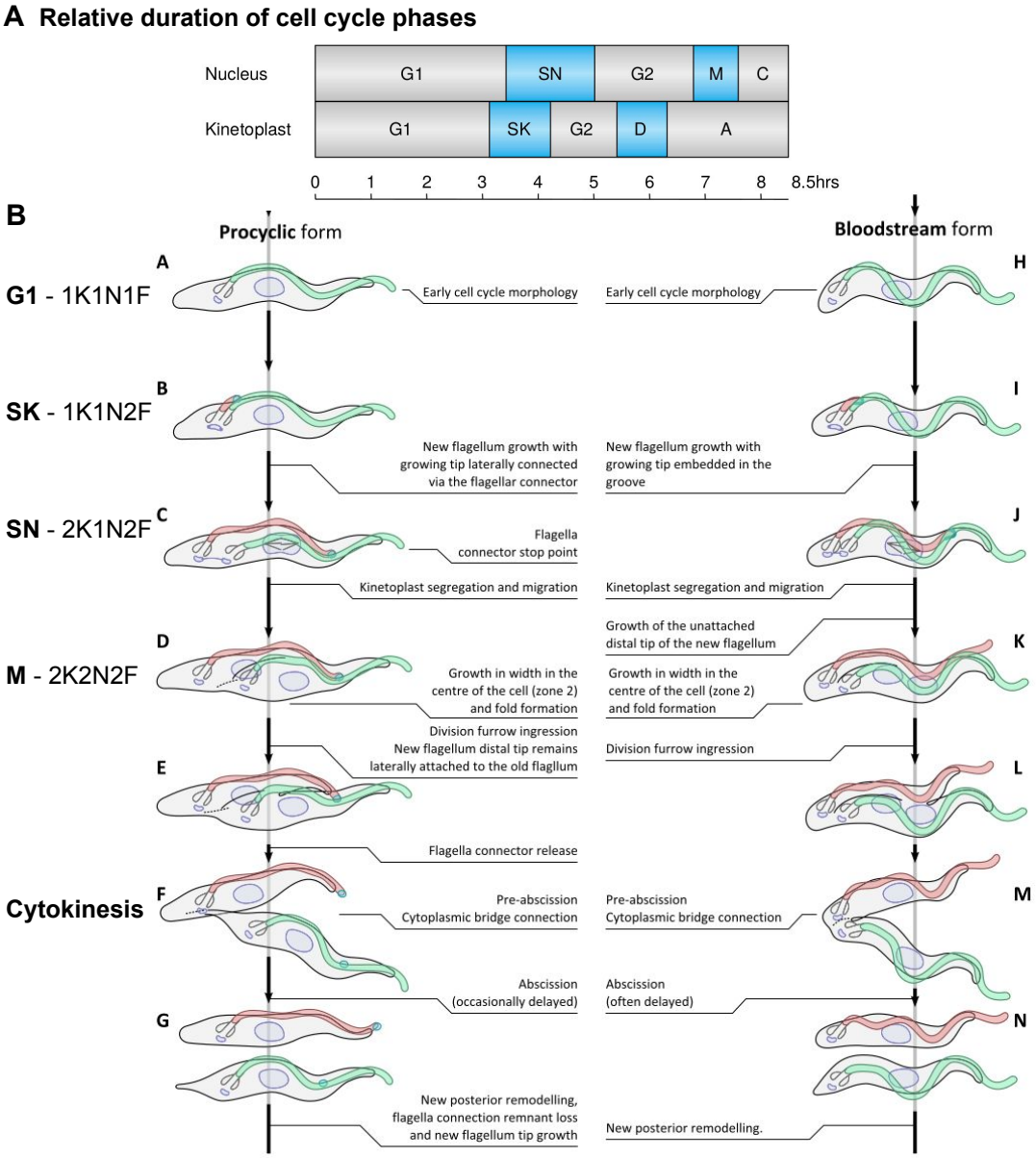

FIGURE 1.7: ***T. brucei* Cell Cycle.** **A** Relative length of each phase of the cell cycle, based on PCF. **B** Details of the cell cycle for both procyclic (insect midgut) forms, **A-G** and mammalian bloodstream forms, **H-N**. The new flagellum (F; red) grows posteriorly to the old flagellum (green). The kinetoplast (K) duplicates prior to the nucleus (N). Adapted from Woodward and Gull, 1990, McKean, 2003 and Wheeler et al., 2013.

akinetoplastic) and consists of a catenated network of around 10,000 mini- and 100 maxicircles of DNA (Borst and Hoeijmakers, 1979, Hoeijmakers and Weijers, 1980).

T. brucei is a diploid organism (Gibson et al., 1985) which undergoes a closed mitosis, forming an intranuclear spindle, whilst maintaining the nuclear envelope intact. The positioning of the newly formed kinetoplast and nucleus are different between PCF and BSF, with the linear organisation (posterior to anterior) of KNKN for PCF and KKNN for BSF (see Figure 1.7.B). Subsequent to mitosis, *T. brucei* undergoes cytokinesis, cleaving down a furrow starting at the anterior tip of the cell and possibly determined by the position of the flagellum attachment zone (FAZ) (Sunter and Gull, 2016). Known proteins required for furrow ingression in *T. brucei* are MOB1, *Tb*PLK (see later) and TRACK (Hammarton et al., 2007).

Key eukaryotic checkpoints are not present in *T. brucei*, for example the mitosis to cytokinesis checkpoint is absent in PCF, which enables the creation of zoids (anucleate cells) as seen in cell culture (Ploubidou et al., 1999). A number of cell cycle regulators have been identified in *T. brucei*, including eight cyclins CYC2-9 (CYC6; Hammarton et al., 2003) and six CDK homologues (CRK1-4 and *Tb*CRK6-7), with potential roles in different life cycle stages. Indeed regulation is also required for differentiation from proliferative forms, such as the procyclic and bloodstream form trypomastigotes, to non-proliferative forms such as the bloodstream stumpy form and metacyclics arrested in G0/G1; one such factor has recently been elucidated by Rojas et al., 2019, *Tb*GPR89 is a surface protein on long slender trypanosomes that can transport oligopeptides and the quorum-sensing signal thereby driving stumpy formation via the SIF signalling pathway.

1.4 Cytoskeleton

Ubiquitous amongst eukaryotes, the cytoskeleton provides a number of essential functions:

1. maintaining the integrity, shape and form of the cell;
2. enabling the cell to resist external forces and to drive and coordinate internal forces for movement and cell division;
3. spatial organisation of internal organelles are determined by the cytoskeleton;
4. spindle formation during mitosis;
5. transportation of intracellular cargo is made along the networks of filamentous polymers that traverse the cell (Fletcher and Mullins, 2010).

The term cytoskeleton was first proposed by the Russian scientist Nikolai Koltzoff, 1903 as "Ûber formbestimmende elastische Gebilde in Zellen" meaning "About

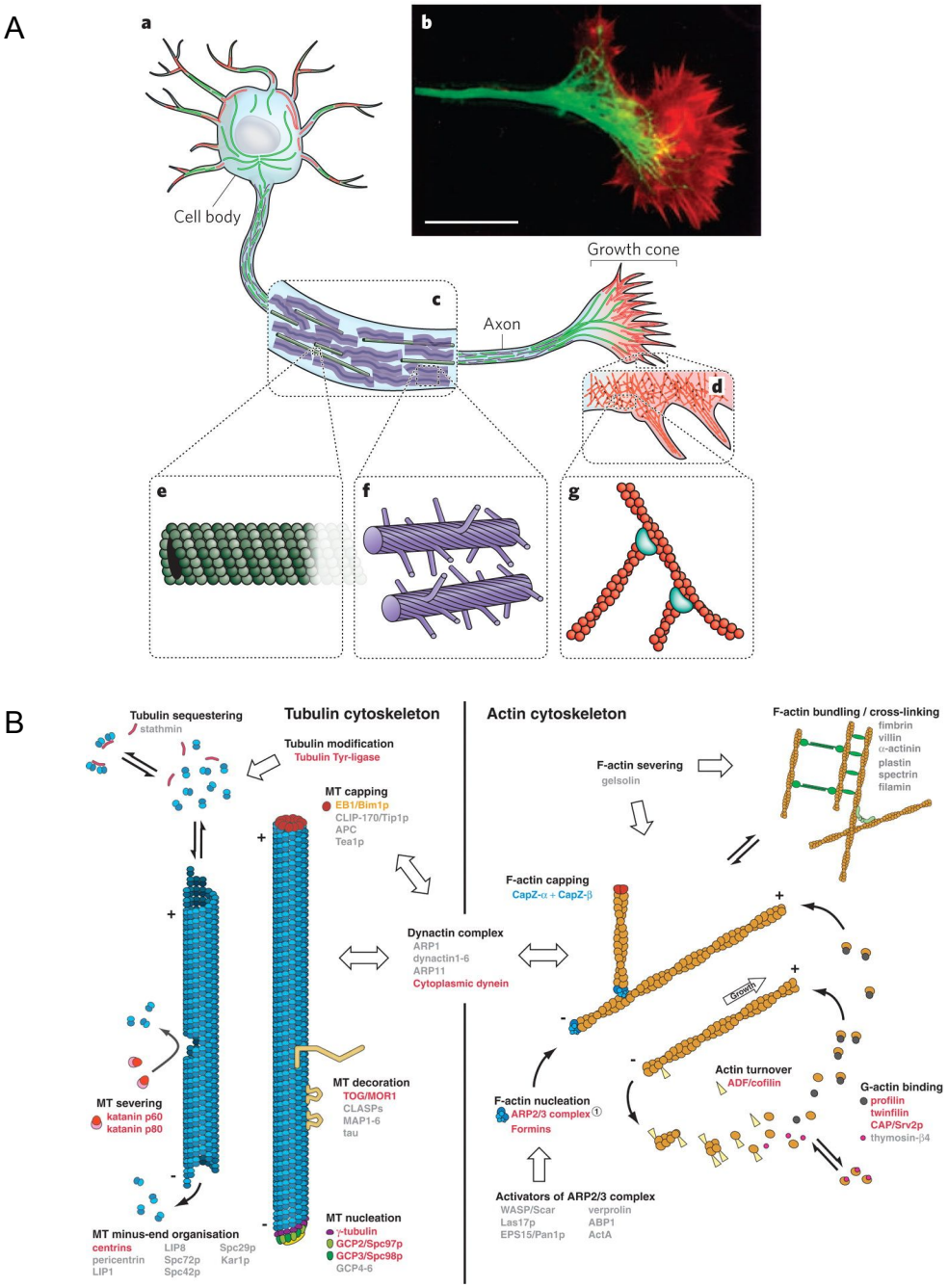

FIGURE 1.8: **The Cytoskeleton of Eukaryotic Cells. A**, **a** a neurone, schematic and **b** fluorescent micrograph magnifying the microtubules (green in **b** and **e**), intermediate filaments (purple in **f**) and actin (red in **b** and **g**); from Fletcher and Mullins, 2010. **B**. Homologues of core cytoskeletal components as found in the genome of *T. brucei*, *T. cruzi* and *L. major* in red; orange text in *T. brucei* and *T. cruzi* only; blue text in *L. major* only; grey text indicates no homologues; α- and β-tubulin subunits in light and dark blue; actin monomers in yellow; from Berriman et al., 2005.

form-determining elastic structures in cells". Today it is known that the cytoskeleton is a dynamic and adaptive structure.

In most eukaryotic cells the cytoskeleton is composed of three elements:

1. Microtubules
2. Intermediate filaments
3. Actin

Figure 1.8.A shows an example of a eukaryotic cell, a neurone, displaying the arrangement and microstructure of each of these three elements. Microtubules are the least flexible, followed by actin, with intermediate filaments, the most flexible. Microtubules themselves are polymers of subunits of α and β tubulin heterodimers arranged in a hollow tube, see Figure 1.8. Although the vast majority of tubulin in eukaryotic cells is α and β, 1% consists of γ tubulin; in classical mammalian cells, γ tubulin is located at the microtubule-organising centres (MTOC), namely the centrosome and spindle poles. A homologue of γ tubulin is present in *T. brucei* as a single copy gene, compared with 15 copies of α and β tubulin tandem repeats, reflecting their relative abundance (Scott et al., 1997). In *T. brucei*, γ tubulin is located primarily at the basal bodies and anterior tip of the cell (where the MT corset minus ends are located), as well as some labelling on the specialised set of four MT (all these structures are outlined in more detail below). In searching for homologues of δ tubulin, Vaughan et al., 2000 identified two new tubulin-like sequences. One of these sequences was identified as a homologue of mammalian ϵ tubulin and the other likely to represent a member a new member of the tubulin superfamily, a ζ tubulin.

Intermediate filaments are structural components of the cytoskeleton of cells of vertebrates and invertebrates. The abundance and role differ to suit the requirements of individual cell types; with keratin being an abundant, if atypical, example (Fuchs and Cleveland, 1998).

Actin is highly conserved among eukaryotes (animals, protists and plants) and its primary function in animal cells is in muscle contraction. In non-muscle cells, actin is involved in a wide range of functions including cytokinesis, endo-/exocytosis (Picco et al., 2018), mitosis, motility, structure and transport (Hightower and Meagher, 1986).

Trypanosomes possess a highly organised cytoskeleton that is comprised primarily of microtubules, but also many other novel proteins. This ensemble of proteins coordinate changes in cell morphology during the trypanosome cell cycle, differentiation from one stage to another within the vector and the host, as well as permitting cell motility.

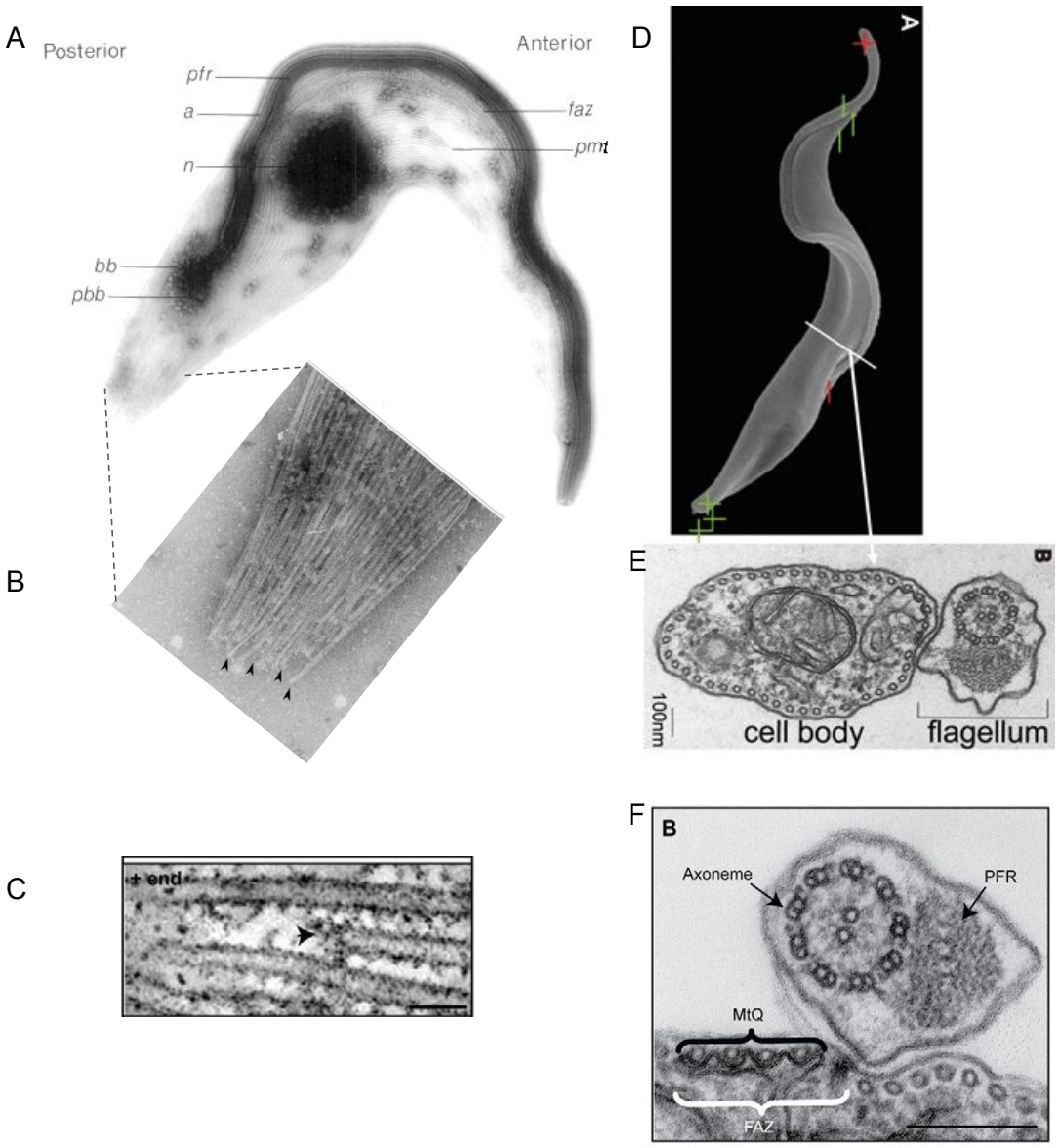

FIGURE 1.9: **The *T. brucei* Cytoskeleton. A** Sub-pellicular array of microtubules (pmt), in a PCF *T. brucei* cell. **B** Electron microscopy view of the posterior end of the cell, arrow heads indicate MT + ends. **C** A new MT (arrow head) growing between two existing MTs. **D** Scanning EM indicating the + and - ends of pmt (green) and the microtubule quartet (MtQ)/flagellum (red). **E** Cross-section TEM showing the pmt outlining the cell body, and **F** A magnified view of the MtQ and associated flagellar structures. PFR=paraflagellar rod, FAZ=flagellar attachment zone, a=axoneme, n=nucleus, bb=basal body, pbb=pro-basal body. Taken fromSherwin and Gull, 1989, Vaughan and Gull, 2008, Lacomble et al., 2009a and Wheeler et al., 2013.

Data obtained from sequencing of the trypanosome genome by Berriman et al., 2005, allow a detailed scrutiny of the genes present: those with homologues in *T. brucei*, *T. cruzi* and *Leishmania major* are shown in red in **B**, Figure 1.8. In fact, with regards to tubulin, these molecules are present and do indeed form microtubules, however, intermediate filaments are absent from the genome. Actin is present in the trypanosome genome, with a 60-70% homology to other eukaryotic actin genes (Ben Amar et al., 1988). However, in trypanosomes actin appears to carry out a more specific function than in animal eukaryotic cells, with a difference seen in function and essentiality between the insect vector procyclic form and bloodstream form found in the vertebrate host. Depletion of actin by RNAi in *T. brucei* PCF is not lethal, however in the BSF form it was found to be an essential protein. In PCF, actin was present throughout the cell, but in BSF it was polarised to the flagellar pocket membrane and required for formation of coated vesicles in endocytosis (García-Salcedo et al., 2004). In *T. brucei* endo- and exocytosis is polarised to the FP membrane, as described in more detail in Section 1.4.6.

1.4.1 Microtubules

The trypanosome cytoskeleton is composed of a highly cross-linked sub-pellicular array of microtubules running longitudinally beneath the cell membrane, see longitudinally in Figure 1.9**A** (pmt) and in cross-section in **F**. The microtubules of this corset are regularly spaced at an 18-22nm distance (Sherwin and Gull, 1989) as seen in the magnified view, in Figure 1.9.B. The microtubules are polarised, with the nucleated (positive ends) at the posterior of the cell (Robinson et al., 1995), whereas a specialised set of four microtubules, the microtubule quartet (MTQ) running alongside the flagellum, maintain their positive ends to the anterior end of the cell Figure 1.9.**D** and highlighted in **F**.

Cytoskeleton remodelling is essential for each step of the parasites' life cycle, to accommodate changes in cell morphology, re-positioning of organelles during cell division and the differentiation between the distinct life cycle stages (Hoare and Wallace, 1966). The distinctive fusiform shape of the parasite is maintained by the cytoskeleton. New MT grow in between existing filaments, as can be seen in Figure 1.9.C.

1.4.2 The Microtubule Quartet

The MTQ, otherwise known as the four microtubules (4MT), is a cytoskeletal structure, nucleated between the BB and kinetoplast, following a distal path, curving around the FP in a left-handed helical path and then running the length of the flagellum to the end of the cell body, beneath the cell membrane in close apposition, and physically connected to the FAZ filament (see MtQ in Figure 1.9.F.).

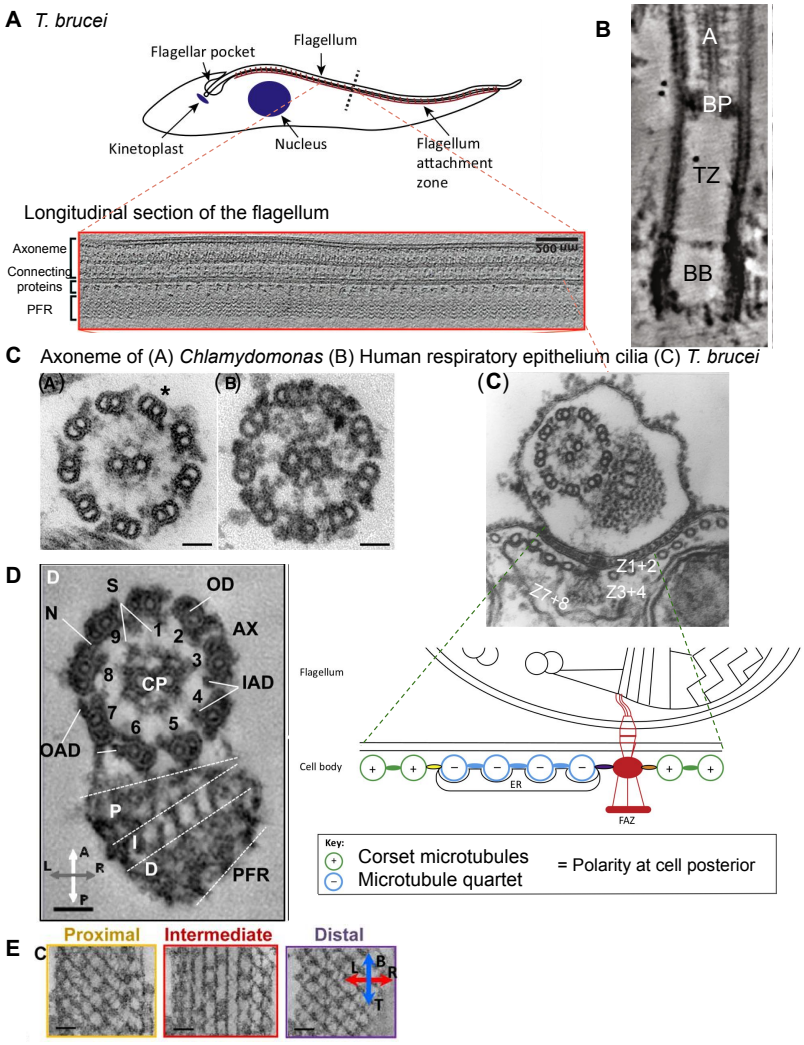

FIGURE 1.10: **The Flagellum, FAZ and PFR of *T. brucei*. A** longitudinal section of the flagellum; PFR=paraflagellar rod. **B** EM of the structures of the base of the flagellum BB=basal bodies, TZ=transition zone, BP=basal plate and A=axoneme. **C** Cross-section EM of axonemes from (A) *Chlamydomonas*, (B) human respiratory cilia and (C) *T. brucei* with a zoom schematic showing the FAZ structures: ER=endoplasmic reticulum, FAZ=flagellar attachment zone, Z=zone. **D** Classical numbering of the outer doublets in *T. brucei*; AX=axoneme, CP=central pair microtubules, IAD=inner arm dyneins, OD=outer doublet microtubules, N=nexin links, S=radial spokes. PFR zones: P=proximal, I=intermediate and D=distal, as shown in detail in **(E)**. Adapted from Koyfman et al., 2011, O'Toole et al., 2012, Sunter and Gull, 2016, Vaughan and Gull, 2016 and Hughes et al., 2012.

The MTQ was first identified in 1969 by Taylor and Godfrey D.G., 1969 using electron microscopy. They observed that a group of four microtubules were spatially organised distinct from that of the rest of the sub-pellicular microtubules; they provisionally termed this new structure the "subpellicular organelle". The function of the MTQ is as yet, unknown, however one theory is that it is the trafficking pathway for proteins going to the Flagellar Pocket Collar (FPC; see section 1.4.7), as seen by labelling of FPC and Hook Complex (HC; see 1.4.9) proteins on the MTQ structure, as seen by immunofluorescence (IFA) and immuno-electron microscopy (IEM). The only characterised protein specific to the MTQ is *Tb*Spef1, first identified by proteomics on immuno-isolated bilobe complexes (now known as the Hook complex). Spef1 (for Sperm flagellar protein1) was shown to localise to the MTQ region between the basal bodies and the bilobe structure (Gheiratmand et al., 2013). Protein depletion by RNA interference (RNAi) of *TBSPEF1* resulted in defects in cell motility, and growth arrest by 48 hours post-inductio in PCF (*Tb* 29.13). Structures further anterior such as the FPC, flagellum and FAZ were able to duplicate and divide, but structures originating more distal, such as the basal bodies, kinetoplast and flagellum were able to duplicate but not divide.

The MTQ together with a distinct complex of cytoskeletal structures make up what is known as the Flagellum Attachment Zone (FAZ) connecting the flagellum to the cell body first defined as a "zone of adhesion" by Vickerman, 1969, recent research has shed light on the complexity of this adhesion area, see Section 1.4.4.

1.4.3 Flagellum

T. brucei possess a single flagellum exiting the cell *via* a bulb-like or flask-shaped invagination of the pellicular cell membrane called the flagellar pocket (FP). This flagellum is attached along the length of the cell body in a left-handed spiral (as viewed from the posterior end); this chiral attachment leads to rotation of the cell during directional swimming motion (Heddergott et al., 2012).

Flagella and cilia are highly conserved among eukaryotes, with functions in motility and as sensory organelles. Motile flagella and cilia possess a conserved canonical 9 + 2 axoneme constructed from microtubules: 9 outer doublets and a central pair; see Figure 1.10.C for a comparison of examples of eukaryotic flagella and cilia: an example of a *Chlamydomonas* axoneme, a human respiratory epithelium cilia and a trypanosome flagellum are given (O'Toole et al., 2012 and Sunter and Gull, 2016).

The trypanosome flagellum axoneme is nucleated at the basal body (BB), analogous to the centriole in other eukaryotic cells (Dawe et al., 2007). Trypanosomes also possess a pro-basal body positioned alongside but at 90° to the mature BB, where the new flagellum will form and grow. As the new flagellum grows, the maturing probasal body undergoes a rotation anticlockwise around the old flagellum, to position the new flagellum anterior to the old flagellum. Robinson and Gull, 1991

showed that segregation of the kinetoplast was dependent on movements of the basal bodies, orchestrated via a cytoskeletal connection. With the aid of EM imaging, a tripartite attachment complex (TAC) was visualised that connects the kinetoplast to proximal end of basal body (Ogbadoyi, 2003).

Running alongside the axoneme within the trypanosome flagellum is a structure called the para-flagellar rod (PFR, seen in Figure 1.9.**F** and 1.10.**A**/**C**.). Initial pioneering studies of the structure of the PFR were made by Harold Fuge, 1969 when he described and showed clear images of a lattice-like patterned structure, indicative of the PFR by electron microscopy, due to longitudinal and oblique filaments running in different planes. More recent studies by Hughes et al., 2012 identified in more detail the three distinct layers of orientation of the filaments: proximal and distal layers consist of struts and laths which give rise to the cross-hatched or lattice-like appearance previously observed, and a newly identified intermediate zone consisting of longitudinal filaments running parallel to the length of the flagellum, see Figure 1.10.**D** and **E**.

A well-described system of intraflagellar transport (IFT) has been described in *T. brucei* and consists of a bi-directional movement of proteins necessary for flagellar formation (Absalon et al., 2007). IFT genes are conserved among eukaryotes, making *T. brucei* a useful model with a long flagellum of around 20μm. The flagellum is assembled at the distal tip and RNAi of IFT protein genes leads to absence of a new flagellum completely, shortened flagella or defects in antero- or retrograde transport dependant upon the specific proteins.

1.4.4 Flagellum Attachment Zone

The FAZ (Flagellum Attachment Zone) is a series of filaments including the four microtubules of the MTQ (Sunter et al., 2015) see Figure 1.10.C, schematic zoom.

The FAZ consists of three elements:

1. MTQ nucleated between the basal body and the probasal body, diagonally wrapping around the FP on cytoplasmic surface, then running parallel to flagellum to anterior tip of the cell
2. *Tb*Centrin4 - a rod-shaped complex in the FP neck region, running along the FAZ
3. Neck Microtubule - a single MT in the FP neck region

In the trypomastigote form of the parasite, the flagellum is attached along the cell body wall by a cytoskeletal structure termed the FAZ. This structure was first observed by Vickerman, 1969 (as earlier stated) and more recent cellular, molecular and microscopically analyses have elucidated its structure in more detail. In fact, analogies have been made to desmosomes in mammalian cells which join two cells

together. The FAZ comprises of radial fibres connecting the flagellum to the subpellicular microtubule array, traversing both the flagellar and cell body membranes; within the cell, the FAZ filaments are connected to the MTQ.

Interestingly, the FAZ filaments are assembled at their proximal end, in opposition to the flagellum; this assembly is made possible thanks to one of two theories: the "push" theory, whereby newly added proteins at the proximal end "push" the FAZ distally in opposition to the flagellum; and the second theory, is the "pull" theory, whereby a connector near the tip of the flagellum "pulls" the FAZ along as the flagellum extends anteriorly along the cell wall during its development (Sunter and Gull, 2016). The FAZ complex has been classified into roughly 8 different zones, spread over three main regions: the flagellum, intracellular and cell body regions. Interestingly, the phenotype upon RNAi of different proteins of the FAZ give rise to different phenotypes depending on the location of the target protein within the total FAZ structure. Knock-down of proteins within the flagellar compartment, such as FLAM3, leads to shortening of the total length of the flagellum (Sunter et al., 2015); knock-down of proteins with the intracellular compartment (e.g. FLA1) leads to flagella detached from the length of the cell body; and knock-down of protein in the cellular compartment (e.g. FAZ1) give rise to disruption of the FAZ cytoskeletal architecture.

1.4.5 The Flagellar Pocket

All pathogenic trypanosomatids, including the *Leishmania* kinetoplastids, possess an invagination of the pellicular membrane, called the flagellar pocket (FP), which is physically connected to the kinetoplast as described by Robinson and Gull, 1991. The FP is the site where the single flagellum (in G1 phase) exits the cell, passing through the lumen of the FP asymmetrically, see Figure 1.11.**A**. The FP is defined by two boundaries, at the base is the collarette (Figure 1.11.**C**.) and at the anterior end is the Flagellar Pocket Collar (FPC) seen in pink in Figure 1.11.B and C. The MTQ wraps around the FP on the cytoplasmic side and an additional microtuble, called the neck microtubule is located in the neck region of the FP. The FPC provides an annular architecture over which the plasma membrane folds (Florimond et al., 2015) and is the interface of three specialised membranes: the flagellar, pellicular and flagellar pocket membranes.

Importantly, with the exception of *T. cruzi* and its related species, the FP is the unique site for endo- and exocytosis for the parasite (Webster and Russell, 1993). *T. cruzi*, possesses an additional contractile vacuole, the cytostome, which continues as a long tubular internal structure, the cytopharynx. In organisms possessing a cytopharnyx, it takes over the process of endocytosis, whilst leaving the flagellar pocket the function of exocytosis and replacement of external protein coat (Alcantara et al., 2017).

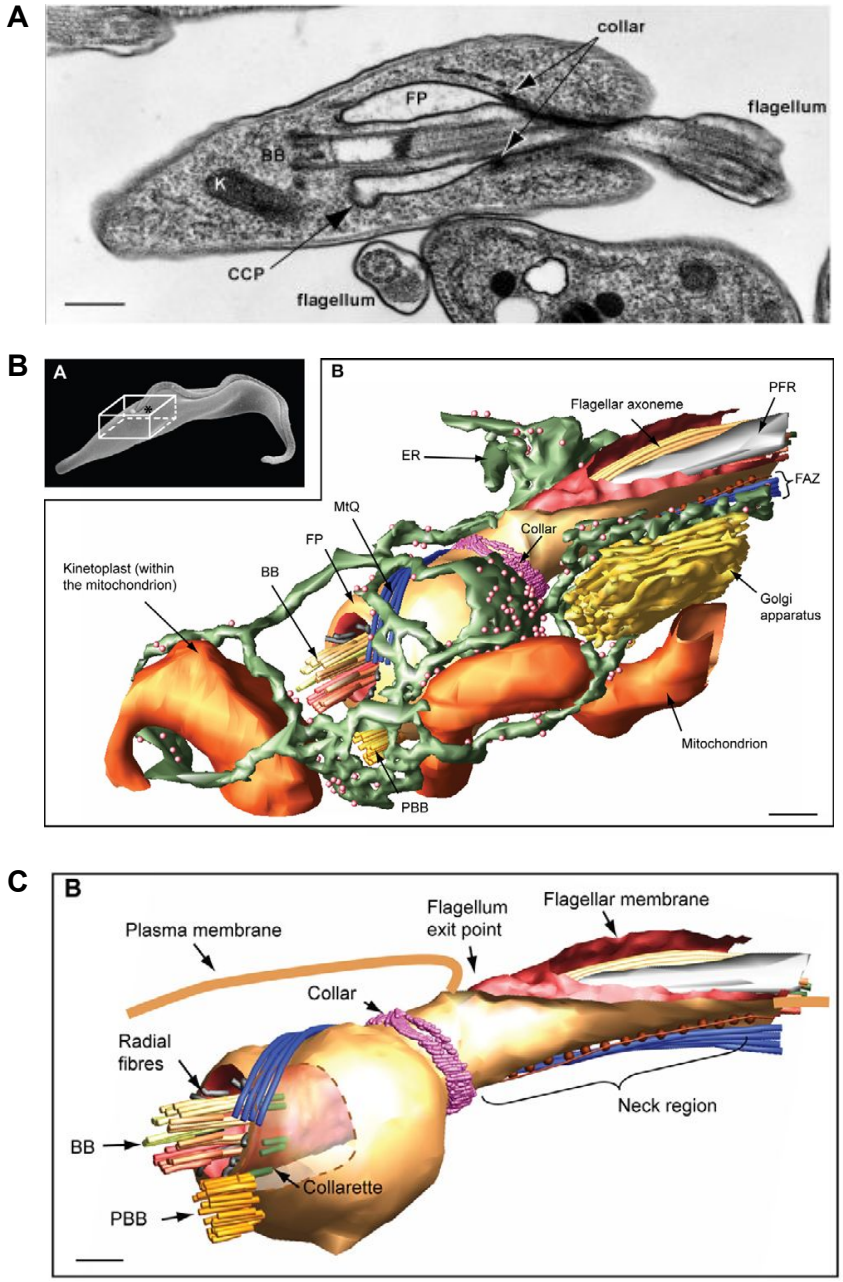

FIGURE 1.11: **The Flagellum Pocket of *T. brucei*.** **A** Electron micrograph of a cross-section of a *T. brucei*. **B** (A) Inset: location of the FPC; Zoom: tomogram of the FP and surrounding structures and organelles **C** Tomogram of the FP stripped of overlying membrane and structures. BB=basal body, CCP=clathrin-coated pits, ER=endoplasmic reticulum, FAZ=flagellar attachment zone, FP=flagellar pocket, K=kinetoplast, MtQ=microtubule quartet, PBB=probasal body, and PFR=paraflagellar rod; taken from www.catarinagadelha.com and Lacomble et al., 2009b. Scale bar in **A** = 250nm, **B** and **C** = 200nm.

Despite comprising less than 5% of the cell membrane surface area, the FP membrane and FP have a myriad of essential functions. The FP is involved in evasion of the host immune system by endocytosis of host immunoglobulin-bound surface VSG; protection of invariant receptors that can not be accessed by the host's immune system; nutrient uptake; trafficking and signalling (Engstler, 2004). A trafficking-specialised pocket organelle is conserved across cilia and flagella in epidermal and ependymal cells, and spermatids (Molla-Herman et al., 2010). Furthermore, expression of FP membrane components in *T. brucei* is life stage dependent, with receptors such as serum resistance-associated protein (SRA), transferrin and haptoglobin haemoglobin receptors (HPHBR) only present in the bloodstream from (BSF) exploiting host serum components which access the FP unrestricted (Field and Carrington, 2009); and CRAM receptors are present in the PCF. This trafficking pathway is the only macromolecular communication between the parasite and the host (Morgan et al., 2001).

Molecules from the extracellular space are able to enter the FP via a channel called the neck channel of 25-150nm in dimension, as visualized by EM by Gadelha et al., 2009. The intimate position of the single Golgi complex to the bulged side of the FP facilitates trafficking and recycling from the FP. Loss of many functions of the FP leads to cell death.

1.4.6 Endocytosis

As alluded to earlier, endo- and exocytosis are essential processes located exclusively at the flagellar pocket membrane in *T. brucei* (Allen et al., 2003). In fact, the rate of endocytosis in *T. brucei* is one of the highest of any known eukaryote (Engstler, 2004). Constantly exposed to the host immune system, trypanosomes have evolved mechanisms to survive such as antigenic variation, changing the surface coat antigens, the GPI anchored variant surface glycoproteins (VSG), periodically. In fact, the whole surface coat can be recycled in 7 minutes entirely by endocytosis through the FP. Endocytosed GPI are recycled back to the surface and any bound host immunoglobulins (Ig) are degraded. It has been demonstrated by Engstler et al., 2007 that hydrodynamic forces created as the trypanosomes swim in an anterior direction aid in propelling the Ig-VSG complex posteriorly towards the FP to be internalised and avoid complement mediated destruction of the trypanosomes.

In *T. brucei*, endocytosis is solely clathrin dependant (Allen et al., 2003) and takes place specifically at the flagellar pocket membrane. RNAi of the clathrin heavy chain, *TBCLH* was lethal in both procyclic (PCF) and bloodstream form (BSF) life stages (Hung et al., 2004), despite the fact that the rate of endocytosis in PCF is ten times lower than that in BSF (Natesan et al., 2007). Allen et al., 2003 observed a grossly enlarged FP in the BSF RNAi *TBCLH*, that eventually filled that entire cell and designated this phenotype "BigEye". Clathrin was first termed by Barbara Pearse, 1976 due to its lattice-like appearance by EM on coated vesicles. The steps

of clathrin-coated endocytosis are as follows: nucleation, cargo selection, coat assembly, scission and uncoating. Numerous proteins are necessary for this multi-step process, notably and in order of vesicle formation are: phosphatidylinositol 4,5 biphosphate (PI(4,5)P_2) concentrated in the plasma membrane (Antonescu et al., 2011) which recruits nucleation factors: PI(4,5)P_2 localises adaptor protein 2 complex (AP2) involved in cargo selection, as well as interacting with epsin-containing proteins that have a role in membrane binding and bending. AP2 recruits clathrin and dynamin which is required to complete scission (McMahon and Boucrot, 2011). Clathrin-mediated endocytosis is observed across eukaryotes and is involved in many vital roles, such as nutrient uptake, uptake of surface proteins for recycling or degradation, cell signalling and developmental regulation (Kaksonen and Roux, 2018).

The role of the Golgi-lysosome pathway in intracellular protein trafficking in *T. brucei* was shown by Price et al., 2007 who demonstrated that RNA interference of *TBARF1*, which localises to the Golgi, led to an enlarged FP, inhibition of endocytosis and cell death.

1.4.7 The Flagellar Pocket Collar and *Tb*BILBO1

An intimately-linked, cytoskeletal component of the flagellar pocket is the flagellar pocket collar (FPC), seen in pink on the tomogram, Figure 1.11.B and C. The FPC is a cytoskeletal structure consisting of polymer forming proteins that circumvents the flagellum at the site where it exits the cell. The FPC is located at the base of the neck of the FP, which in the trypomastigote form of *T. brucei* (the proliferative procyclic and the mammalian bloodstream forms) is located at the posterior end of the cell body. The FPC forms a cytoskeletal boundary or interface at the intersection of the pellicular, flagellar and FP membranes. To date, a handful of FP and FPC associated proteins have been identified but only two essential proteins have been characterised that are intimately associated with the FP.

The first structural protein of the FPC to be identified and characterised was *Tb*BILBO1 by Bonhivers et al., 2008. This novel and essential structural protein (Tb927.11.12150; 67kDa; 578aa) was named BILBO1 by virtue of the fact that the protein made up a structure that resembled a ring shape of 500-800nm in diameter, as can be seen in Figure 1.12.**A** and **B**, in the immunofluorescent image of over-expression of enhanced green fluorescent protein (eGFP) tagged *Tb*BILBO1 and in **C** of an electron micrograph using immuno-gold beads against anti-*Tb*BILBO1 antibodies.

A BLAST analysis of the parasite GeneDB database, revealed 20 orthologues of *TBBILBO1* in non-mammalian species including other *Trypanosoma* and *Leishmania* species; orthologues were not found in humans, therefore *Tb*BILBO1 could be a potential drug target (Perdomo et al., 2016).

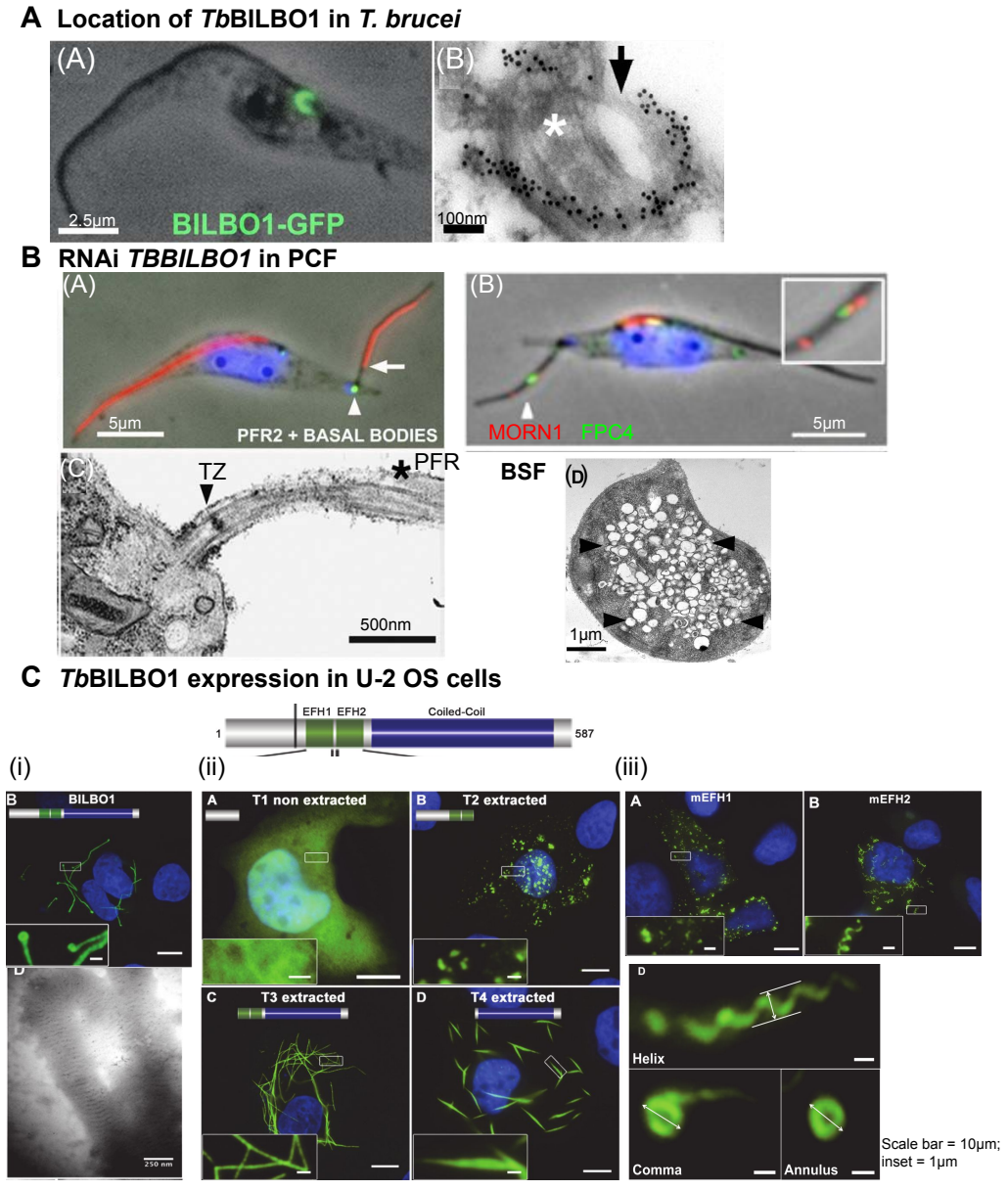

FIGURE 1.12: ***T. brucei* BILBO1.** **A** (B) Immunofluoresence image of a PCF *T. brucei* with BILBO1 labelled with GFP (C) Electron micrograph of the flagellar pocket collar showing *Tb*BILBO1 labelled with immunogold **B** RNAi *Tb*BILBO1 in PCF resulted in detached flagella and **C** abnormal location of *Tb*MORN1 and *Tb*FPC4; intracellular vescicles seen in BSF. **D** Schematic of domains of *Tb*BILBO1 and expression of (i) full-length, (ii) truncations and (iii) mutated EF-hands of *Tb*BILBO1 CCD=coiled-coil domain, GFP=green fluorescent protein, LZ=leucine zipper, NTD=N-terminal domain, PFR=paraflagellar rod and TZ=transition zone; taken from Bonhivers et al., 2008 Albisetti et al., 2017 and Florimond et al., 2015.

To assess the function of *Tb*BILBO1 in *T. brucei*, a tetracycline-inducible RNAi knockdown system was employed (Wirtz et al., 1999). Results of RNAi *TBBILBO1* in the procyclic form (PCF) resulted in aberrant flagellum re-positioning and detached flagella, which were not attached to the cell body along their length, but only at the basal body; often an extended posterior end was seen and the detached flagellum was observed extending from this elongated posterior end (as seen in Figure 1.12.B and C). The detached flagellum was no longer associated with a flagellar pocket at its base and components of the flagellum were positioned further outside of the cell, such as the transition zone (TZ in Figure 1.12.B) and the PFR which normally starts as the flagellum exits the cell, was seen at some distance from the external cell membrane. Albisetti et al., 2017 demonstrated that certain cytoskeletal components normally present in the hook complex, a cytoskeletal structure located just distal to the FPC along the flagellum (see section 1.4.9) were positioned at some distance along the flagellum outside of the cell. Swelling of the Golgi was also observed and cell death accrued 48-72 hours post induction. These data infer that *Tb*BILBO1 is necessary for the biogenesis of a new FP and indeed for cell survival (Bonhivers et al., 2008). Interestingly, in BSF, RNAi of *TBBILBO1* led to more rapid death, with rounding up of cells as early as 12 hours post-induction and accumulation of intracellular vesicles as seen in Figure 1.12.B and D. Initial bioinformatic analysis of the primary amino acid sequences of *Tb*BILBO1 did not predict any localisation or cytoskeletal functions, however, the following domains were determined: an N-terminal domain (NTD; from amino acid residues 1-110), two EF-hand domains (aa 185–213 and aa 221–249), followed by a coiled-coil domain (aa 263-566) and a putative leucine zipper (LZ) at the C-terminus (aa 534–578), see Figure 1.12.C and 1.13.B. These domains were the basis for truncations used throughout the experiments described below.

To explore further the functional properties of *Tb*BILBO1, the full-length (FL) protein, truncations thereof, and mutated versions of the protein were expressed in a heterologous system of U-2 OS mammalian cells, where this protein is not normally present. This cell line originated from human osteosarcoma cells derived from a 15 year old girl with a moderately differentiated sarcoma of the tibia in 1964 (Ponten and Saksela, 1967). In such a system, in the absence of other trypanosome specific proteins, it is possible to explore further intrinsic properties of non-native proteins.

Indeed, when FL-*Tb*BILBO1::GFP was transiently expressed in U-2 OS cells, linear polymers with comma and globular shaped termini were formed (Figure 1.12.C.(i).**B** IFA and **D** EM.). Expression of four different truncations of *Tb*BILBO1 in U-2 OS cells confirmed the requirement of the coiled-coil region for polymer formation (Figure 1.12.C.(ii).C and D). Florimond et al., 2015 also demonstrated that in a yeast 2-hybrid system, the coiled-coil region alone was required for BILBO1-BILBO1 interaction and in *T. brucei* the ectopic expression of truncations containing the coiled-coil domain formed long polymers in the trypanosome PCF cells. These data are in keeping with the known properties of coiled-coil domains as protein interaction sites. In fact, the coiled-coil protein structure was first described by Francis Crick, 1952 when observing α-keratin. Coiled-coil domains are omnipresent in life and constitute

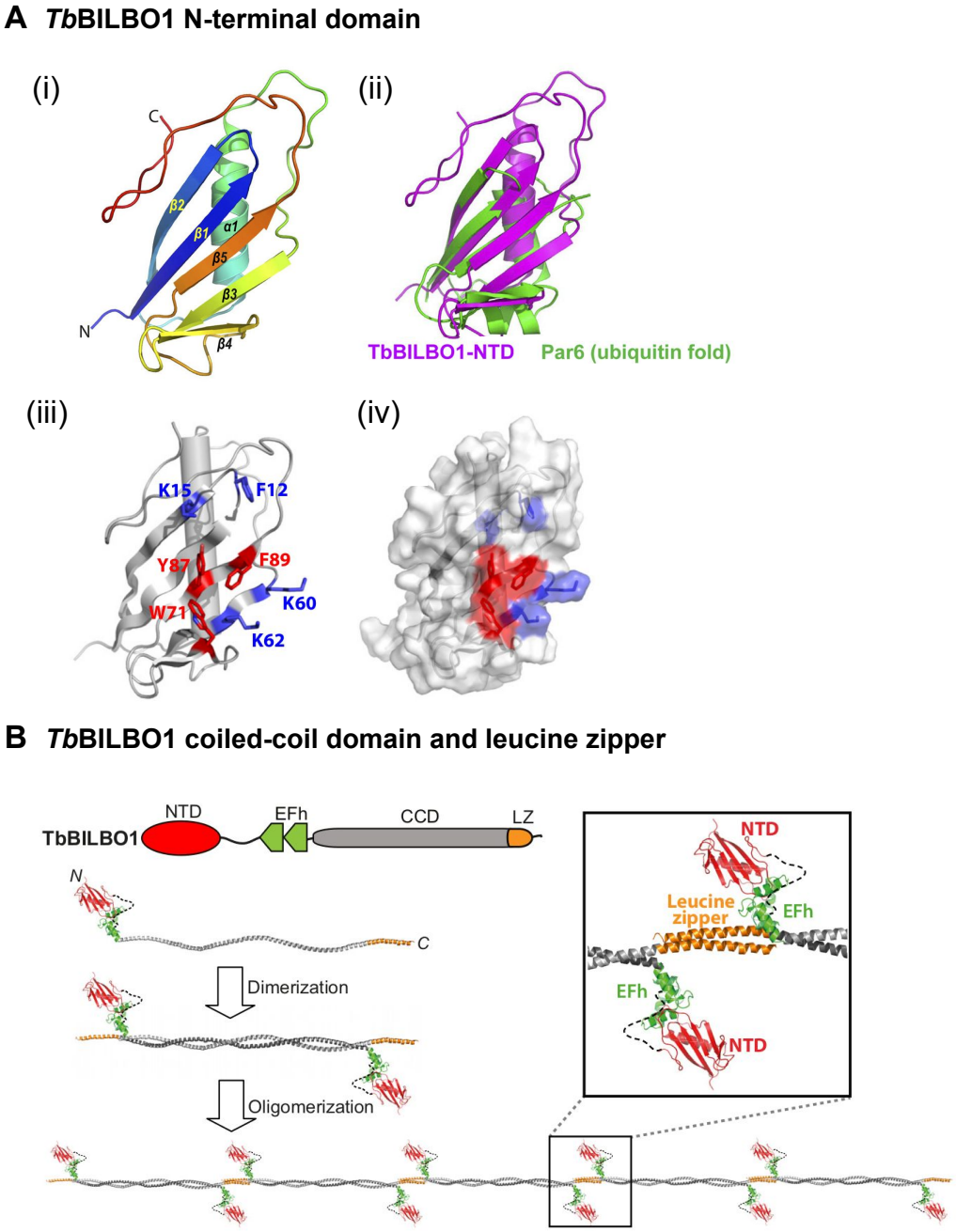

FIGURE 1.13: ***Tb*BILBO1 NTD, coiled-coil and LZ. A** Ribbon diagrams of (i) *Tb*BILBO1 N-terminal domain aa1-110 (ii) overlay of the NTD in magenta and a ubiquitin fold in green (iii) highlighting the conserved residues of the surface patch (iv) surface plot of previous; **B** Primary structure of *Tb*BILBO1 showing domains and hypothetical dimerisation and oligomerization, indicating the role of the leucine zipper (zoom); taken from Vidilaseris et al., 2014a and Vidilaseris et al., 2014b.

many roles including architecture of organelles, anchoring transport vesicles, within motor proteins, transferring conformational changes, and even within enzymes dictating catalytic site (Truebestein and Leonard, 2016). In their review, Truebestein and Leonard discussed the potential role of coiled-coil proteins as molecular scaffolds and lament that few examples exist, such as tropomyosin and dynein; therefore *Tb*BILBO1 could add to this list of scaffold proteins composed of an important coiled-coil domain.

*Tb*BILBO1 also contains two EF-hand (EFh) motifs. EF hand domains are extremely commonplace in eukaryotic cells, found almost exclusively in the cytoplasm and the vast majority binding calcium (Ca^{2+}). Named after the hand-like structure they form (Persechini et al., 1989), proteins containing EFh motifs perform an array of functions, with two main classes based on whether they transduce or modulate the Ca^{2+} signal. The conformational change induced by Ca^{2+} binding varies greatly between proteins, for example calmodulin takes on an open structure after binding Ca^{2+}, whilst calbindin remains in a closed structure (Nelson et al., 2009). To investigate the function of the EFh domains in *Tb*BILBO1, mutation of the domains was carried out and these mutated proteins were expressed in U-2 OS cells. A mutated version of each EFh was expressed individually and then together. The results showed that mutation of the canonical calcium-binding domain led to changes in the form of the polymers produced. Mutated EFh1 led to abolition of linear polymers and formation of punctate aggregates; mutation of EFh2 led to production of helical polymers, commas and annuli, as seen in Figure 1.12.C.(iii). These data demonstrate the influence that the EF-hand domain has on polymer-forming properties of *Tb*BILBO1 *in vivo*.

Confirmation that the EFh domain of *Tb*BILBO1 binds Ca^{2+}, wild-type and mutated versions of the EFh were tested for calcium binding by isothermal titration calorimetry (ITC). The results confirmed that wild-type EFh domain binds calcium but not the mutated version (Florimond et al., 2015) adding to the evidence that it is indeed binding of calcium which initiates conformational changes in *Tb*BILBO1 protein. This was further confirmed by Vidilaseris et al., 2014a who showed that indeed, the EFhands undergo a conformational change when binding to calcium.

The presence of the CC and the LZ, suggest possible roles in oligomerization and/or heterogeneous protein–protein interactions. These were investigated by Vidilaseris et al., 2014a who were able to confirm that the *Tb*BILBO1 coiled-coil domain forms anti-parallel dimers (see Figure 1.13.B) and that the leucine-zipper is required for filament assembly. The LZ was also shown to be necessary, but not sufficient alone, for targeting of *Tb*BILBO1 to the FPC (Florimond et al., 2015).

Further studies of *Tb*BILBO1 NTD by Vidilaseris et al., 2014b determined its three-dimensional structure by multidimensional NMR spectroscopy (see Figure 1.13.A)

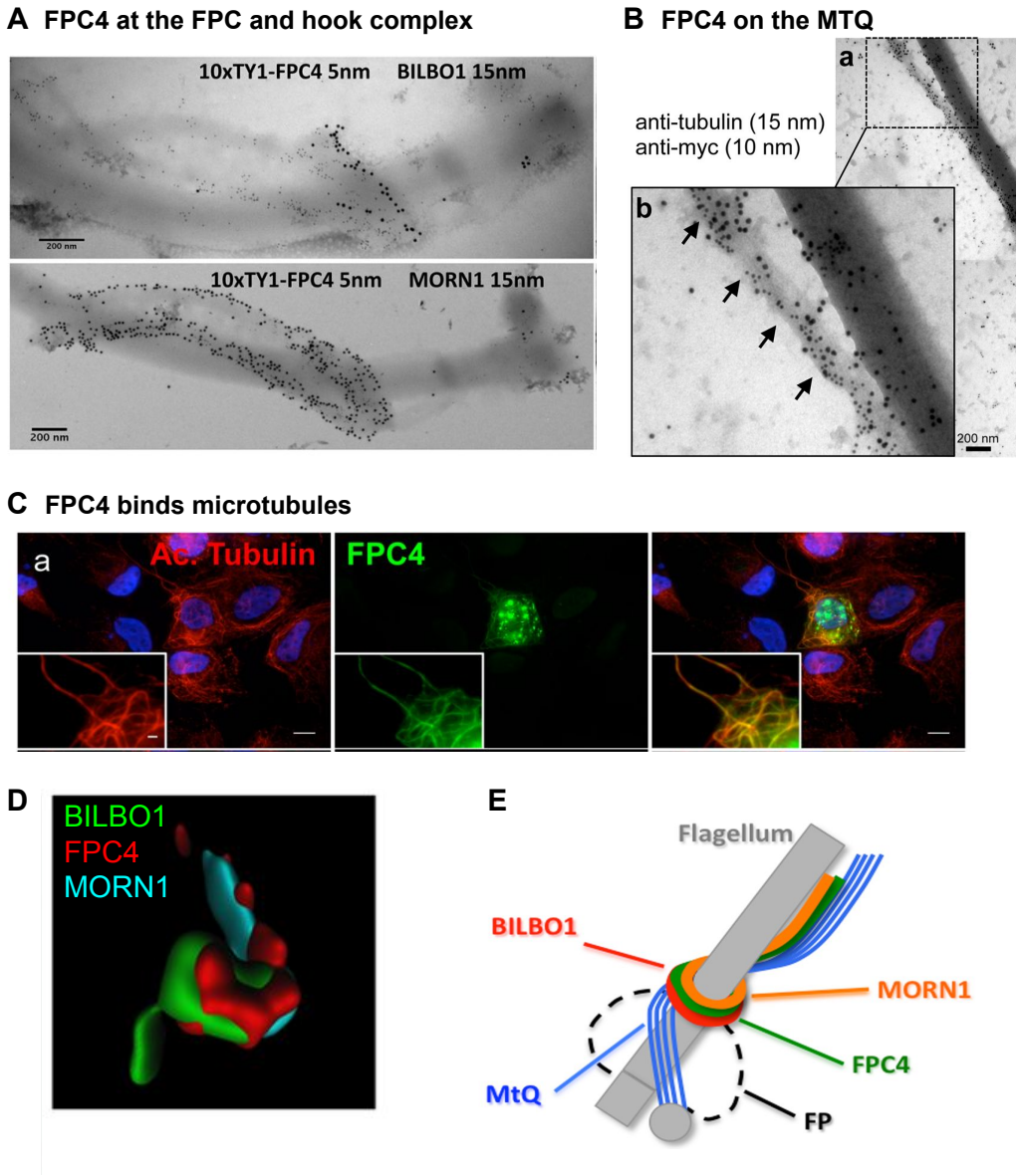

FIGURE 1.14: ***Tb*BILBO1's partner FPC4.** **A** FPC4 is found on the FPC, co-labelling with *Tb*BILBO1 and at the HC co-labelling with *Tb*MORN1. **B** FPC4 binds to the MTQ and **C** to the MT in U-2 OS cells. **D** 3-D reconstruction of STED confocal microscopy triple co-labelling of *Tb*BILBO1, FPC4 and *Tb*MORN1. **E** Schematic drawing of the FP showing the relative location of FPC and HC proteins, taken from Dr Anna Albisetti's PhD thesis and Albisetti et al., 2017.

consisting of five β strands and one α helix similar to a ubiquitin-like fold. A conserved surface patch was revealed containing four aromatic residues (Phe-12, Trp-71, Tyr-87, and Phe-89) and three basic ones (Lys-15, Lys-60, and Lys-62), as seen in Figure 1.13.A. The residues in red form the base of a crater-like structure, while the residues in blue form the rim. This patch is highly conserved amongst trypanosomatids and site-directed mutagenesis confirmed this site to be essential for cell viability, substantiating the result seen with deletion of the whole NTD (Florimond et al., 2015).

1.4.8 *Tb*BILBO1's partner: FPC4 (Tb927.8.6370)

Due to the essential nature of *Tb*BILBO1 and its strategic position at the FPC, investigation of binding partners were investigated. A technique for determining protein-protein interactions, yeast 2-hybrid, was carried out by Hybrigenics, using the full genome of *T. brucei* 927 with *Tb*BILBO1 as bait. Amongst several identified putative binding partners was FPC4 (Flagellar Pocket Collar protein 4; Tb927.8.6370; 48.9kDa; 444aa), a kinetoplastid specific gene. FPC4 contains a BILBO1-binding domain aa357-444 and a coiled-coil domain from aa218-252. Albisetti et al., 2017 demonstrated that the C-terminal domain of FPC4 interacts with the N-terminal domain of *Tb*BILBO1 using truncated versions of both proteins by yeast 2-hybrid and expression in U-2 OS cells. Indeed, two specific residues, Trp-87 and Phe-89, present in the conserved surface patch of *Tb*BILBO1 (as shown in Figure 1.13.A) were critical for this interaction. Localisation of FPC4 by IFA and EM showed it to be located at the interface of the FPC6 and HC in both PCF and BSF *T. brucei*. As shown in Figure 1.14.A, D and E. FPC4 is also seen on the MTQ, Figure 1.14.B. When expressed alone in U-2 OS cells FPC4 is observed localising on the microtubules, Figure 1.14.C. Although FPC4 was not shown to be essential using RNAi in either PCF or BSF, its function as a MT-binding protein (N-terminal domain) was confirmed when expressed alone in U-2 OS cells and by EM images of it on the MTQ. Over-expression of FPC4 in *T. brucei* suggested a role in the segregation of the FPC.

1.4.9 The hook complex and *Tb*MORN1

The hook complex (HC) is a cytoskeletal structure located just anterior to the FPC. The HC was first characterised under the name "bilobe" by He et al., 2005, who described a bilobed structure containing *Tb*Centrin2, which when knocked down by RNAi prevented duplication of the Golgi complex, confirming a cytoskeletal link with the Golgi. In 2008, Shi et al., 2008 localised another centrin protein *Tb*Centrin4 to the bilobe structure and found it to be involved in coordinating cell and nuclear division in *T. brucei*.

In trying to better understand this bilobe structure, Morriswood et al., 2009 compared the *T. brucei* extracted flagellum proteome with that of from *Chlamydomonas reinhardtii* flagella and *Tetrahymena thermophila* cilia. It was already known that the

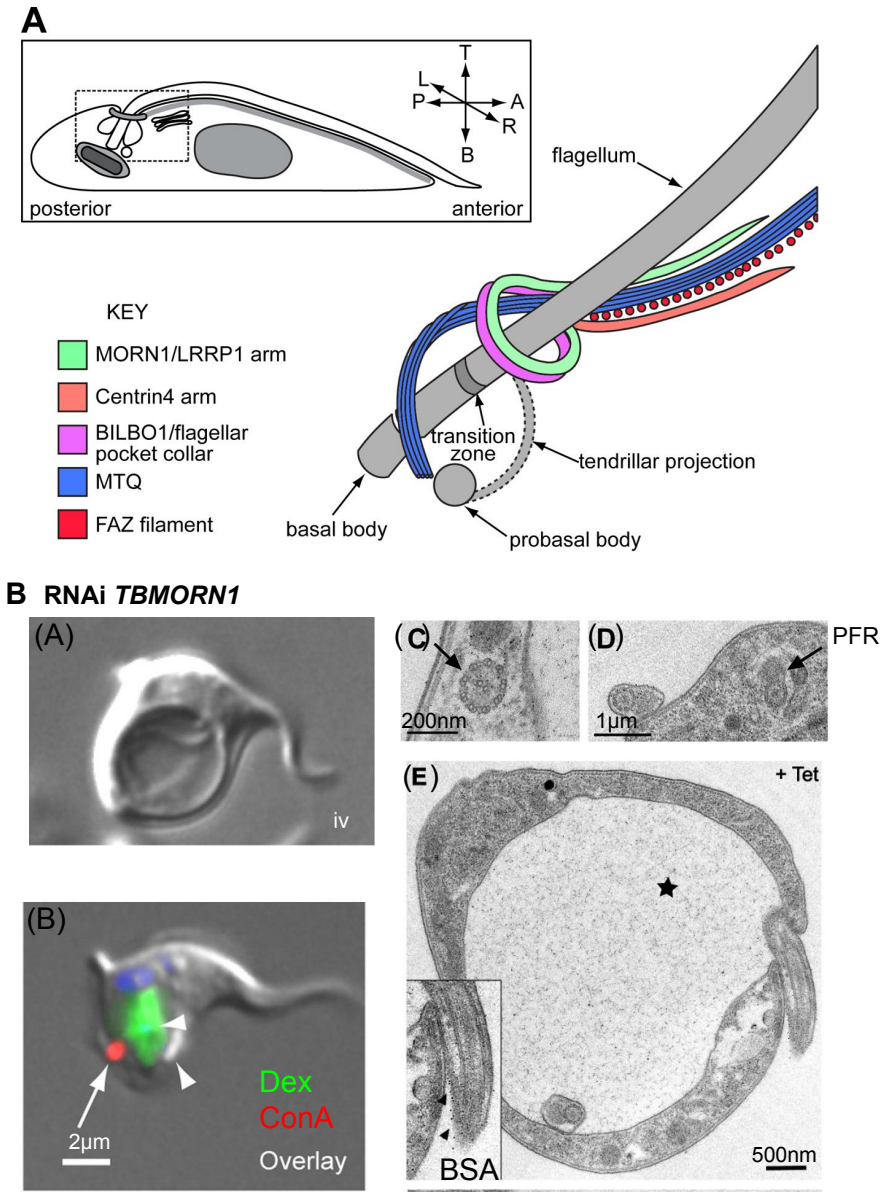

FIGURE 1.15: **The hook complex and *TBMORN1* RNAi. A** Components of the hook complex in *T. brucei*, taken from Esson et al., 2012. **B** RNAi *TBMORN1* leads to a Big-Eye phenotype **(A)** due to an enlarged FP **(B)** where Dextran accumulates and **(C)** the abnormal presence of intra-cellular axonemes and **(D)** PFR. RNAi *TBMORN1* impedes the entry of both ConA and BSA into the FP: **(E)** BSA is confined to a specific area of the flagellum just outside the FP (arrowheads); taken from Morriswood and Schmidt, 2015.

FPC, hook and centrin arm co-purify with flagella on high-salt extraction. With these results they were able to determine 180 putative bilobe/basal body proteins: 12 of them were tagged with yellow fluorescent protein (YFP) and localized in *T. brucei*. *Tb*MORN1 was identified (Tb927.6.4670; 358aa; 40kDa), with a highly repetitive primary structure of 15 tandem membrane occupation and recognition nexus (MORN) repeats. The MORN domain has previously been proposed to regulate plasma membrane localization and phosphatidic acid (PA)-inducible activation. *Tb*MORN1 was the first protein to be identified that localises exclusively to the bilobe (Morriswood et al., 2009). Immunofluorescence images show that *Tb*MORN1 forms a hook shape, with the head of this hook at the FPC, partially co-localising with *Tb*BILBO1, and the shank extending distally along the flagellum. A schematic of the location of *Tb*MORN1 is shown in Figure 1.14.E. and 1.15.A.

A leucine-rich repeat containing protein *Tb*LRRP1 was characterised the following year, by Zhou et al., 2010. RNAi of *TBLRRP1* led to inhibition of duplication of the bilobe structure, the Golgi, the FPC and the FAZ, suggesting an interlinked biogenesis of these structures. Continuing with the characterisation of *Tb*MORN1, Esson et al., 2012 described the bilobe as a bipartite entity: one arm of this hairpin contains *Tb*Centrin4 and might be synonymous with the previously described "neck microtubule"; the remainder of the hairpin, forming a fishhook shape, contains *Tb*MORN1 and *Tb*LRRP1.

Morriswood et al., 2009 confirmed that *Tb*MORN1 was essential in the BSF and, indeed, RNAi led to a block in endocytosis and cell death (Morriswood and Schmidt, 2015). Cell death was accompanied with a "BigEye" phenotype caused by enlargement of the FP, see Figure 1.15 .**B**. A "BigEye" phenotype was first described after RNAi of the clathrin heavy chain (Allen et al., 2003; see Section 1.4.6). Endocytotic assays using fluorescent dextran and concanavalin A (ConA) inferred that the function of *Tb*MORN1 may be in influencing the entry of molecules into the FP, with depletion of *Tb*MORN1 resulting in dextran remaining in the enlarged FP and ConA unable to access the FP fully, with neither being endoctytosed.

Replication of the HC is co-ordinated by *Tb*PLK, a polo-like kinase homologue of *T. brucei* that localises to the bilobe/HC during part of the cell cycle (Hu et al., 2017). *Tb*PLK plays roles in HC duplication, BB movements and segregation and cytokinesis. *Tb*PLK phosphorylates *Tb*Centrin2 in G1 and S phases. A potential substrate of *Tb*PLK and an additional component of the HC is *Tb*Smee1 (Tb927.10.8820). *Tb*Smee1 is necessary for maintaining the morphology of the HC, correct localisation of *Tb*PLK and efficient endocytosis (Perry et al., 2018).

1.4.10 Flagellar Pocket Collar protein 6 (FPC6)

FPC6 (Flagellar Pocket Collar protein 6; Tb927.4.3120; 100kDA; 933aa) was named by the Robinson laboratory after its discovery as a partner of *Tb*BILBO1 of the Flagellar Pocket Collar. In fact, FPC6 was identified on two separate occasions using different techniques and has appeared in the literature on a couple of occasions in large-scale genome studies. Here I shall summarise these preliminary data. Firstly, in the Robinson laboratory, FPC6 was discovered during a yeast 2-hybrid (Y2H) screen on the *T. brucei* 927 genome using *Tb*BILBO1 as bait (performed by Hybrigenics). Y2H is a technique used for determining protein-protein interactions and this screening identified a number of putative binding partners of *Tb*BILBO1 and amongst these was FPC6.

Preliminary studies in the Robinson laboratory by Dr Celia Florimond (a previous PhD student) found FPC6 to be located in close proximity to the FPC using a GFP tag. Further yeast 2-hybrid assays using full-length FPC6 and truncations of *Tb*BILBO1, confirmed that the BILBO1-binding domain of FPC6 (aa 661-781), initially identified by Hybrigenics, interacted with the EF hands region of *Tb*BILBO1 (aa 170-250), see Figure 1.16.A. In the Robinson laboratory, preliminary studies to investigate FPC6 protein depletion were made using a stem-loop RNA interference (RNAi) system for FPC6 protein depletion. Induction of RNAi by tetracycline, showed no effect on growth in PCF, however semi-quantitative RT-PCR of this same cell line revealed that the levels of mRNA were not diminished, indicating the stem-loop system was not effective.

In a separate laboratory in Vienna, Dr Brooke Morriswood was working on proteins of the hook complex, having already identified and characterised the essential protein *Tb*MORN1, Morriswood et al., 2013 employed a technique called close-proximity biotinylation (BioID) using *Tb*MORN1 as bait. In this technique the enzyme BirA is ligated to the bait and *in vivo* proteins within a 10nm vicinity are biotinylated, thus tagging lysine in proteins, which are then pulled down using streptavidin beads and identified by mass spectrometry, to identify interacting proteins, or at least those in very close proximity to the bait. BioID indicates spatial proximity but not direct interaction.

The candidates were tagged in *T. brucei* to determine their location by transient transfection of a pXS2 expression vector with a Ty1 epitope tag; FPC6 was seen to be located at the head of the hook-shaped structure formed by *Tb*MORN1 by immunofluorescence in trypanosomes (Figure 1.16.B.). Confirmation of the location of FPC6 within the cell can be seen on the Tryptag database showing transient tagging of FPC6 at both the N and C termini of the gene using monomeric NeonGreen (mNG), Figure 1.16.C. Preliminary evidence on the essentiality of FPC6 can be found by Horn, 2014 who developed a genome wide RNAi knockdown protocol and reported that FPC6 was essential in PCF, BSF and the differentiating stage between BSF to PCF.

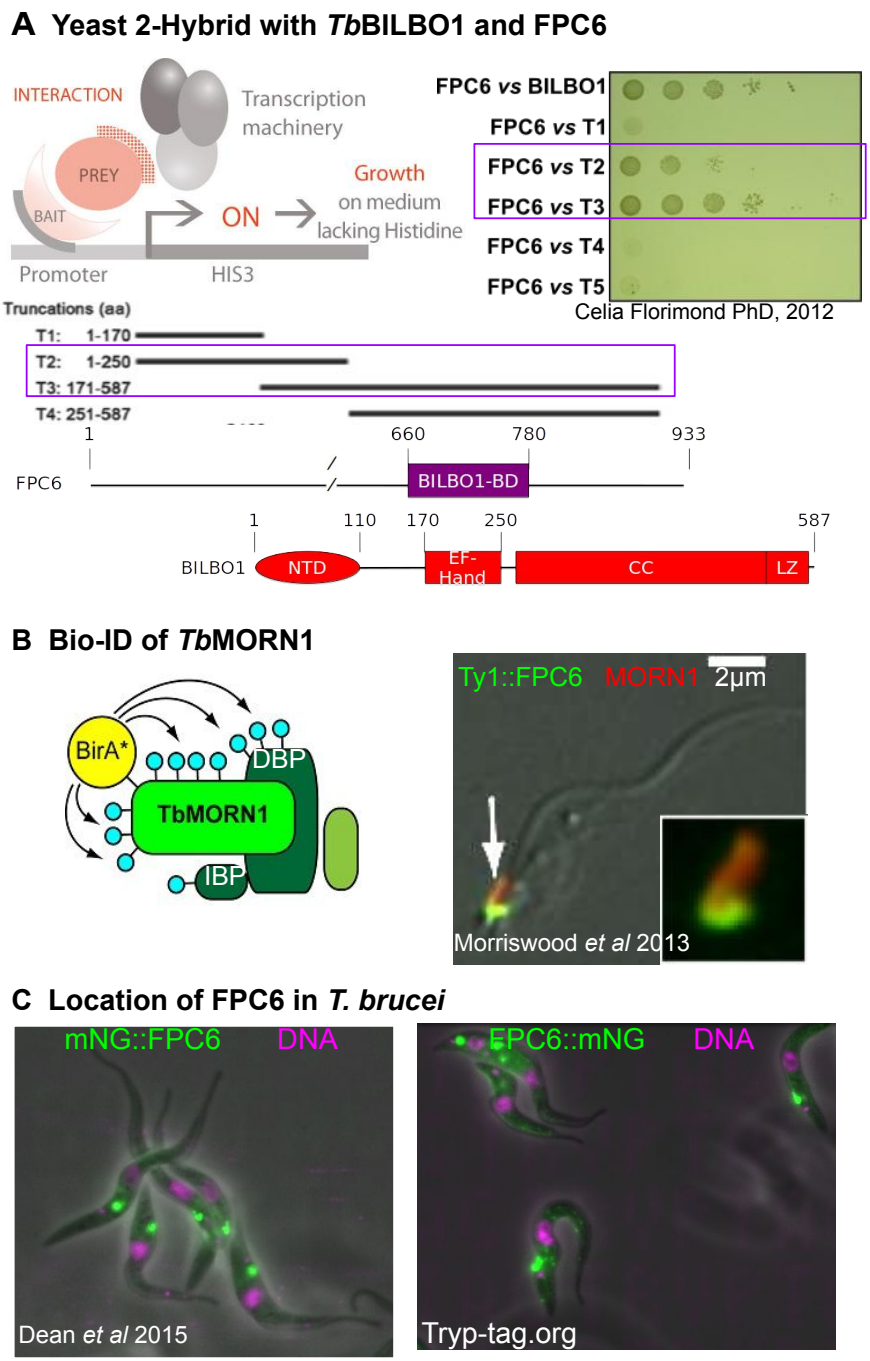

FIGURE 1.16: **Identification of FPC6.** by: **A** Yeast 2-hybrid of *Tb*BILBO1; **B** BioID of *Tb*MORN1; and **C** transient endogenous tagging of FPC6 at the N and C-termini (tryptag.org). From www.hybrigenics-services.com, Morriswood et al., 2013, Morriswood, 2015 and Dean et al., 2015a.

1.5 scFv and Nanobodies

1.5.1 Single chain variable domain fragment - scFv

Neutralizing antibodies are a part of the host's immune defence system. Since Köhler and Milstein, 1975 first described a technique to produce monocloncal antibodies (mAb) of defined specificity in large quantities in the laboratory, the use of mAb in biomedical science was unleashed. Their closing remark in their three page commentary was "Such cultures could be valuable for medical and industrial use." This statement could not have been closer to the truth and although, at the time of publication, the paper may not have been given a position of leading importance, nine years later in 1984, they both received the Nobel prize for contributions to scientific research. Today the use of mAb is vast, including medical diagnostics, therapeutics, and in experimental research. Indeed, in 2017 the number of antibody-based approved therapeutics by the European Medicines Agency and Food and Drug Administration, USA, reached its highest level of approval (Kaplon and Reichert, 2018) and the same year the global mAb therapeutics market was valued at $95,560 million with an expected annual growth rate in the market of 6.9% forecast to 2026 (coherent market insights, 2019).

Examples of murinised and humanised antibody drugs used for clinical purposes already exist: efalizumab is an anti-human CD11a-specific monoclonal antibody approved as a therapy for moderate psoriasis in humans since 2003 by the USDA (Gordon et al., 2003) and since September 2005 in France. In 2018, a record number of 12 mAb were licensed in the EU or USA: three for episodic migraine prevention, including eranumab (Goadsby et al., 2017) and cemiplimab (Libtayo®, Sanofi) licensed in the EU in April 2019 for treatment of advanced cutaneous squamous cell carcinoma (Migden et al., 2018). The first veterinary monoclonal antibody therapy was released onto the market in 2018, for atopic dermatitis. Lokivetmab is a caninized mAb targeting and neutralizing interleukin-31 (Cytopoint®, Zoetis; Furue et al., 2018). Regarding trypanosomes, a recent paper in May 2019 by MacGregor et al., 2019 described the conjugation of a human antibody against the trypanosome haptoglobulin-haemaglobulin receptor (HpHbR) with a pyrrolobenzodiazepine (PBD) toxin, which killed *T. brucei* leading to a cure in infected mice after a single therapeutic dose.

Limitations of the use of conventional antibodies can be encountered due to their size (150kDa) leading to reduced tissue penetration, especially in solid tumours (Jain, 1990), access to folds of proteins and having prolonged blood clearance. Production is costly, timely and may not be consistent. Advances in antibody engineering techniques, have led to the production of recombinant antibody fragments, notably Fab and scFv (55kDa and 28kDa respectively, see Figure 1.17.A). These smaller fragments normally retain the specificity in targeting of the monoclonal antibody derivative but can be produced with lower costs than conventional antibodies (Miller et al., 2005) and have improved pharmokinetics, specifically increased tissue penetration and lower immunogenicity due to lack of the Fc component.

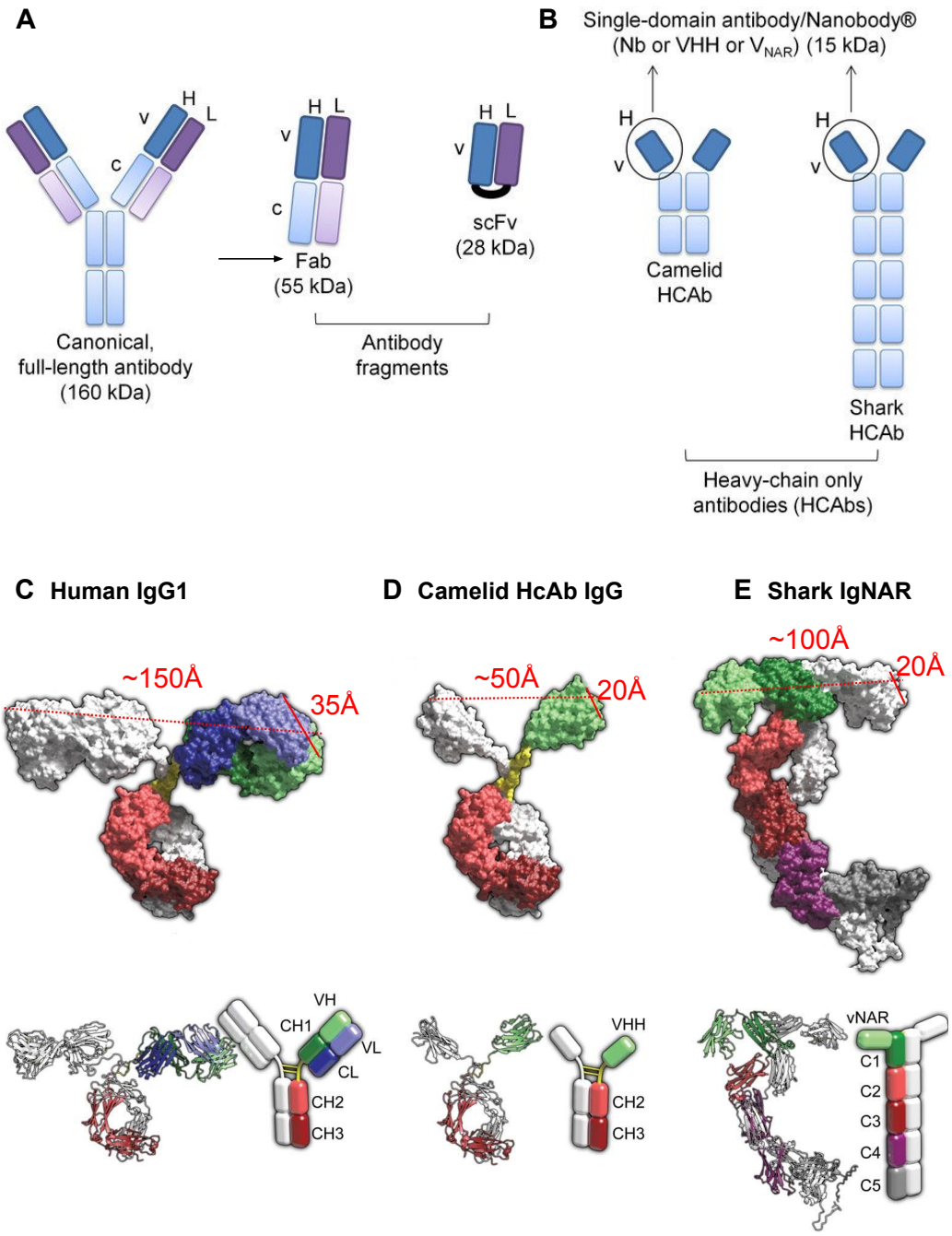

FIGURE 1.17: **scFv and Nanobody fragments.** A schematic diagram of **A** a conventional IgG molecule, a Fab and an scFv fragment; **B** examples of heavy chain only antibodies and their single domain variable fragments: VHH and V-NAR; **C** surface representations, ribbon and schematic diagrams showing the structural features of different antibody formats, taken from Doshi et al., 2014, Zielonka et al., 2015 and Brooks et al., 2018.

Fab (antigen binding fragments) were the first to be explored and led to the production of a number of commercial therapeutics, between 1994-2008, for clot prevention, macular degeneration and Crohn disease (Nelson, 2010). Following on from this recombinant single-chain variable domain fragments (scFv) were explored, consisting of only the smaller variable antigen-binding domain of conventional antibodies (Ahmad et al., 2012) seen in Figure 1.17.A. In a recombinant scFv molecule, the V_H (heavy chain variable domain) and V_L (light chain variable domain) are joined by a flexible peptide linker and can be constructed into multiple domains, tagged for identification and targeting, and bound to drugs for accurate delivery (Monnier et al., 2013). These recombinant proteins can be optimised for binding affinity and paired into diabodies or bi-specific fragments can be created, scFv can be isolated by hybridoma technology or by panning of a phage display library and afterwards, economically produced by expression in *Escherichia coli* (*E. coli*) or Yeast (Miller et al., 2005). The use of scFv molecules has been developed for cancer therapy (Chen et al., 2010), neurodegenerative diseases and to enhance *in vivo* imaging and study protein functions (Monnier et al., 2013).

1.5.2 Nanobodies: Discovery and properties

Nanobodies (Nb or VHH) are the variable domain of heavy chain only antibodies (HCAb) naturally occurring in camelidae: alpacas, camels, llamas and vicunas. The HCAb present in camels was discovered serendipitously by Hamers-Casterman et al., 1993 and lack the light chain and first constant domain (CH_1) of the heavy chain. Two isoforms of the HCAb exist in camelidae, with varying length of the hinge joining the CH_2 and VHH (Figure 1.17.B and D - only one isoform is shown here).

Roux et al., 1998 published a paper describing a **n**ew or **n**urse shark **a**ntigen **r**eceptor lacking the light chain and composed of one variable domain (V) and 5 constant (C) heavy chain domains. The variable domain in this case is termed V-NAR (Figure 1.17.B and E.). The presence of HCAb in elasmobranchs (a branch of cartilagenous fish, including sharks and rays) and in camelidae (camels, llamas, alpacas, vicuñas, and guanacos) is an example of convergent evolution (Brooks et al., 2018), whereby a mutation in the heavy chain gene occurred on more than one occasion and has been maintained in these species. Cases of heavy chain disease does occur in humans due to a mutation involving a genetic deletion of parts of the VH and CH_1 regions, however this is a pathological condition and these mutated antibodies are non-functional (Alexander et al., 1982).

Nanobodies are the smallest functional antigen-binding antibody-derived fragments, possessing characteristics that favour their use over conventional antibodies and, indeed, over scFv. There small size, 15kDa compared with 160kDa of a conventional IgG, enables Nbs to cross the blood-brain-barrier (a prerequisite for stage 2 clinical trypanosomiasis), have increased tissue penetration, including solid tumours, with access to cryptic epitopes inaccessible to their larger counterparts, due

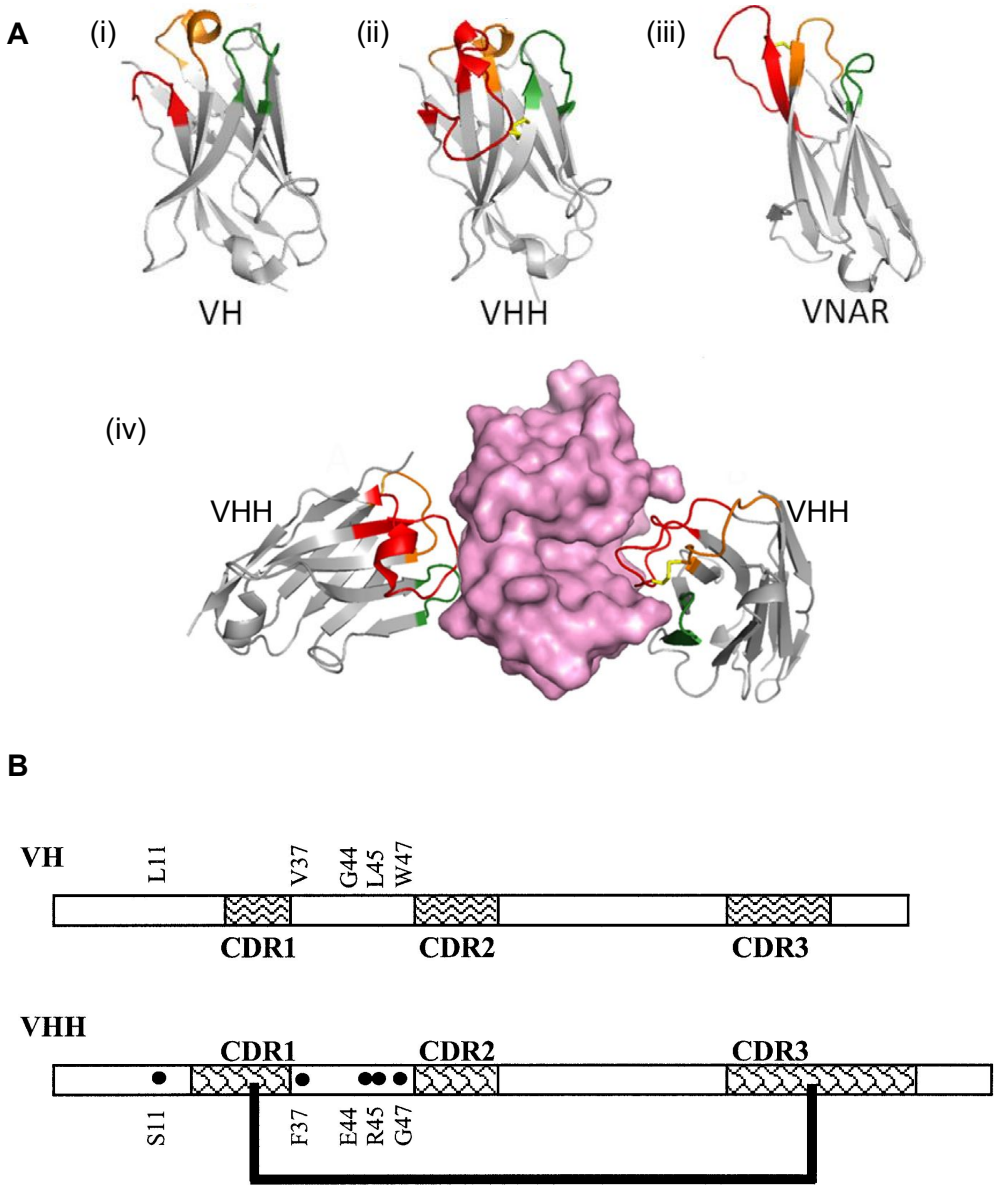

FIGURE 1.18: **Heavy-chain only Antibodies CDR H3 loop and amino acid substitutions in VHH. A** Ribbon diagrams showing the CDR1 in orange, the DCR2 in green and the CDR3 in red, for VH, VHH and VNAR; and the functional flexibility of range of paratopes of VHH. **B** conserved amino acid substitutions between VH and VHH; taken from Muyldermans, 2001, and Gonzalez-Sapienza et al., 2017.

to an elongated and more elaborate CDR H3 loop, see Figure 1.18.A in red. (Muyldermans et al., 1994). A number of conserved amino acid substitutions are seen between conventional VH and VHH; the first being L11S in framework region 1 the site of interaction with the CH_1 domain which is absent in VHH, with a hydrophilic substitution (L11S). The enhanced solubility properties of nanobodies are further enhanced due to a number of amino acid substitutions in framework two (V37F/Y, G44E, L45R and W47G) see Figure 1.18.B. Nbs have favoured kinetic and body clearance, desired in imaging and some therapies. Nbs are stable in extremes of temperature to 95°C and range of pH and may have an additional disulfide bond giving extra stability. Nbs are able to recognise a range of epitopes including structural forms and can distinguish between different isoforms of the same protein (Saerens et al., 2004).

The soluble VH domain isolated, called the VHH (single variable domain), or nanobody, binds antigen with higher affinity than the full antibody (Muyldermans, 2013). Nbs have increased tissue penetration, favoured kinetics, increased body clearance and an ability to recognise a wide range of epitopes. Importantly, functional Nbs can be produced from bacteria, fungi, plants, insects and even mammalian cell lines. The most commonly used are bacteria (periplasmic or cytoplasmic expression) and yeast (on an industrial scale).

Nanobody use is greatly expanding in cell and molecular biology, diagnostics, and medicine, for example, targeting cancer cells (including solid tumours; Iezzi et al., 2018) and immune pathways (Menzel et al., 2018). An interesting application of nanobodies against snakebite evenoming (a WHO Neglected Tropical Disease) was developed *in planta* by Julve Parreño et al., 2018. Tags can be fused to nanobodies for detection in living organisms, such as radio-isotopes for visualisation of tumours *in vivo* (Movahedi et al., 2012). In research, chromobodies, nanobodies fused to a fluorescent protein are used to visualise intracellular components; nanobodies can be used in immunoprecipitation and co-crystallisation of partner proteins by aiding in their stabilisation (Hassanzadeh-Ghassabeh et al., 2013). Drugs can be fused to nanobodies to refine their targeting (Siontorou, 2013), see below for an example in trypanosomes.

1.5.3 Nanobodies and Trypanosomes

Regarding trypanosomes, nanobodies have proved interesting, with a number of fields of research being developed. Direct targeting of conserved, hidden, regions of the surface VSG coat of *T. brucei* was investigated by Stijlemans et al., 2004. Nb-An33 was able to target cryptic VSG domain (Figure 1.19.A). A further three nanobodies, Nb-An05, Nb-An06 and Nb-An46 were able to induce loss of cell motility, FP swelling due to loss of endocytosis and cell death, *in vitro* and *in vivo* (Stijlemans et al., 2011); Figure 1.19.B shows the different effects of three nanobodies. These lethal effects of monovalent anti-*T. brucei* VSG are found in the absence of the Fc domain and are complement independent. Continuation of research using Nb-An33,

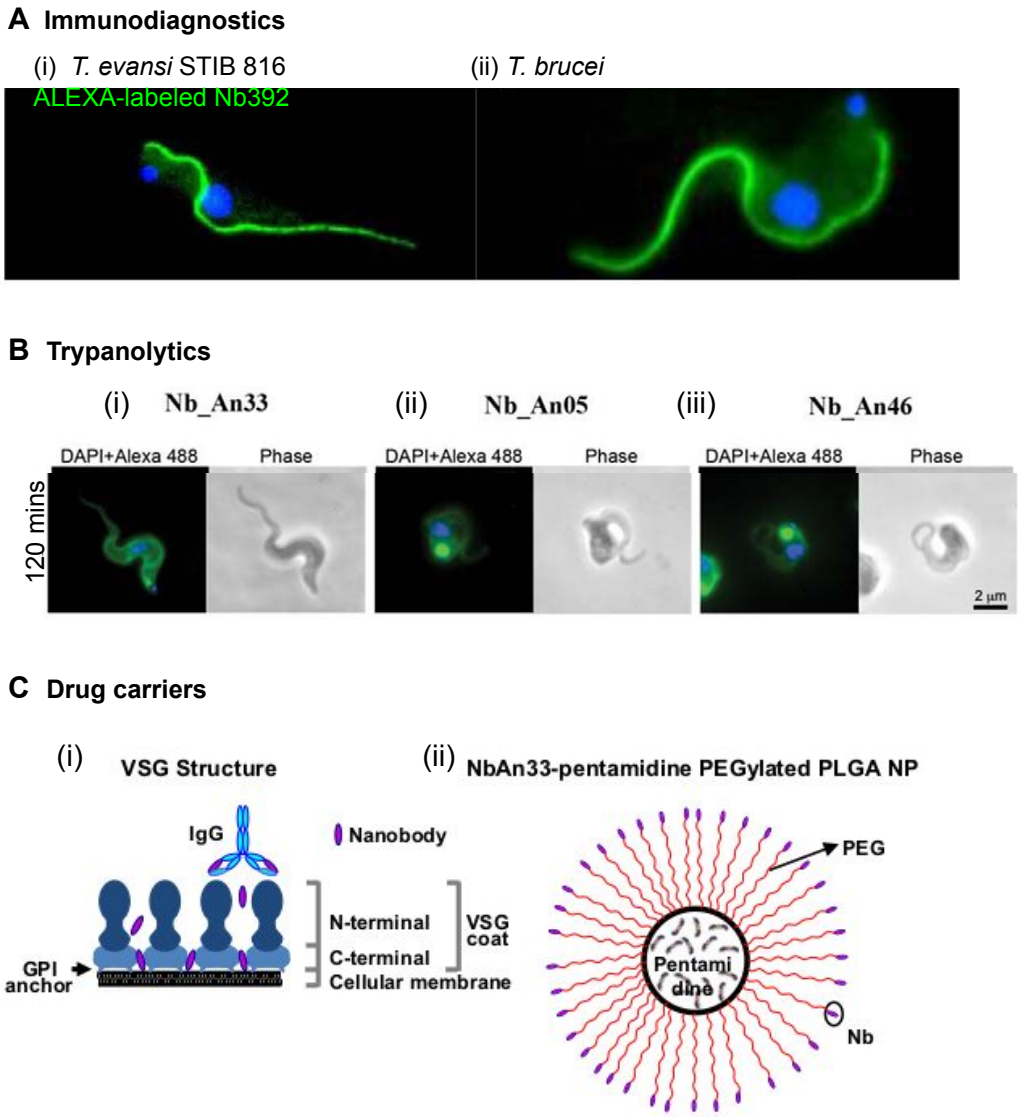

FIGURE 1.19: **Examples of nanobodies used in trypanosome research. A** As immunodiagnostics using a Nb targeting PFR1. **B** As trypanolytics against VSG, and **C** as drug-carriers, showing (i) the targeting of Nb-An33 to the conserved hidden region of the surface VSG, and (ii) the nanoparticle complex of conjugated nanobody loaded with pentamidine. GPI = glycophosphatidylinositol, PEG = poly ethylen glycol, PLGA = poly(D,L-lactide-co-glycolide acid), NP = nano- particles; taken from Obishakin et al., 2014, Stijlemans et al., 2011 and Arias et al., 2015.

led to the creation of two different conjugated forms. The first by Baral et al., 2006, conjugating a truncated *T. b. rhodesiense* apolipoprotein-L1 by deleting the SRA interacting domain rendering it lytic for *T. b. rhodesiense*, and fusing this to Nb-An33. Treatment of mice with this engineered immunotoxin complex resulted in cure from *T. b. rhodesiense* paving the way for potential therapy for both trypanosomes sensitive and resistant to normal human serum. Secondly, Nb-An33, targeting cryptic VSG domains was coupled to a nanocarrier: poly ethylen glycol (PEG) covalently attached (PEGylated) to poly(D,L-lactide-co-glycolide acid) (PLGA) to generate PEGylated PLGA nanoparticles. These nanoparticles were loaded with pentamidine (Arias et al., 2015; Figure 1.19.C.), a known trypanolytic with a transporter resistance mechanism, that is now endocytosed into the parasite; results showed an enhanced drug effect with cure of mice at a 10-100 fold lower dose rate.

A novel transparagenic approach was taken by De Vooght et al., 2012, expressing nanobodies in the *T. brucei* endosymbiont *Sodalis glossinidus* to deliver nanobodies to trypanosome *in vivo* in the tsetse fly. Nb-An33 was again employed and preliminary data show that the nanobody could be produced and released extracellularly in *Sodalis glossinidus* with no reduction in fitness *in vitro* in bacteria and with detection of the nanobody in the tsetse fly (De Vooght et al., 2014).

Nbs have been explored as immunodiagnostic tools for detection of trypanosome infection. By immunizing an alpaca with lysates of *T. evansi*, (Obishakin et al., 2014) were able to identify a nanobody, Nb392 targeting the paraflagellar rod protein, PFR1. This nanobody showed cross reaction with *T. brucei, T. congolense, T. evansi* and *T. vivax*, enabling the possibility of a one-step direct nanobody based immunofluorescence test for Animal African Trypanosomiasis (AAT). On the other hand, Odongo et al., 2016 immunized an alpaca with a whole-parasite proteome from *T. congolense* TC13 and through phage library panning identified a nanobody, Nb474, that was specific for *T. congolense* and not for *T. brucei, T. evansi* nor *T. vivax*. Mass spectrometry determined the nanobody target to be *T. congolense* glycosomal aldolase, proposing a unique biomarker for diagnostic development. Another study, by Pinto Torres et al., 2018 looking into diagnostics for AAT, immunized an alpaca with the secretome mix from two strains of *T. congolense* IL3000 and IL1180. A pair of nanobodies were identified, Nb44/Nb42, which targeted the glycolytic enzyme pyruvate kinase. An ELISA was developed that could detect parasitaemia in infected mice and cattle and proved to be a "test-of-cure" in a lateral flow assay. Regarding the vector, an epidemiological tool was investigated by Caljon et al., 2015, using a nanobody to detect Tsal proteins from tsetse fly saliva as a biomarker for bite exposure.

These data demonstrate some of the possible applications of Nb in the quest for novel therapeutic and diagnostic approaches to trypanosomiasis.

1.5.4 Intrabodies and Intra-nanobodies

Intrabodies are recombinant antibodies expressed intracellularly to inhibit the function of a specific intracellular protein (Carlson, 1988). The advantages of using intrabodies to modulate protein function compared with other techniques, such as CRISPR Cas9 or RNA interference, are reduced off-targets effects due to high antigen specificity, the ability to target a specific cell compartment, a particular isoform or post-translational modification of a protein (Marschall et al., 2015) and indeed, the ability to recognise and bind to a structural epitope, compared with a simple linear sequence. There is increasing potential for therapeutic intrabodies for neurological disease (Alzheimers; Meli et al., 2013), cancer (VEGF; Alirahimi et al., 2017), viral infections (HIV; Da Silva et al., 2004 and autoimmune disease (TLR9; Reimer et al., 2013).

Nbs are proving to be invaluable as research tools as well as promising therapeutics. Due to their small size, ability to cross the blood-brain barrier, to access cryptic epitopes, high specificity, pH and thermal stability, ease of production and malleability to conjugate to toxins, they have proven to have desirable properties (Abulrob et al., 2005, Arias et al., 2015, Muyldermans, 2013 and Pardon, 2014). Nbs are also proving innovative for advancing medical diagnostics, imaging, treatment of in breast cancer (Van Impe et al., 2013), monitoring of animal disease (Pinto Torres et al., 2018) and resistance to plant viruses (Ghannam et al., 2015). Nbs exhibit a low immunogenicity and are easy to adapt to a new host e.g. humanize or caninize, for therapeutic perspectives with numerous clinical trials involving nanobodies in progress and the recent approval by the European medicines agency (EMA) of the first therapeutic nanobody, caplacizumab for treatment of acquired thrombotic thrombocytopenic purpura (aTTP), a rare blood-clotting disorder (Duggan, 2018).

1.6 Aims and Objectives of my PhD studies

My thesis comprised of two parts: part one the study and characterisation of a novel cytoskeletal protein of the trypanosome Flagellar pocket collar/Hook complex, FPC6. Part two, the purification of nanobodies and scFv raised against *Tb*BILBO1, and expression intracellularly in trypanosomes in culture in the laboratory.

My aims and objectives for these two parts were as follows:

1.6.1 Part one: FPC6

The aims of this study were:

1. To characterise a cytoskeletal protein, FPC6, a partner of *Tb*BILBO1 and possible component of the hook complex.

2. To assess the essentiality of FPC6 in trypanosome cell culture PCF and BSF after depletion of protein by RNAi.
3. To determine which domain of FPC6 targets to the flagellar pocket collar region and if any of these domains alone rescue any RNAi phenotype.
4. To ascertain the function of FPC6.

The specific objectives for each aim were:

1. To describe the cell phenotype and growth after RNAi induction of *FPC6* in PCF and BSF cell cultures.
2. To replace one allele of *FPC6* with a recoded gene resistant to RNAi, tagged with a different tag to the wild type allele. To describe the position of the recoded FL and truncations of FPC6 in *T. brucei* and to record any effect on growth of the cells after RNAi *FPC6*; to determine if the recoded full-length or truncated versions can rescue the RNAi lethal phenotype.
3. To express truncations of FPC6 in *T. brucei* and determine by immunofluorescence which domain of FPC6 is necessary for targeting to the flagellar pocket collar region.
4. To complete endocytotic assays of BSF *T. brucei* cells after induction of FPC6 *RNAi* and record the uptake of fluorescent dextran and concanavalin A into the trypanosome cells.

1.6.2 Part two: scFv and Nanobodies

In seeking new immunological tools for use in the laboratory as well as methods to obstruct FPC activity and thus cell viability, through targeted inhibition of *Tb*BILBO1 function, I examined the use of nano-technology *via* scFv and nanobodies.

The aims of this study were:

1. To develop new antibody fragments as tools for the laboratory, that can be used to detect *Tb*BILBO1 proteins in techniques such as immunofluorescence assay (IFA) and western blot (WB), replacing larger conventional antibodies.
2. To further characterise *Tb*BILBO1 by investigating the binding of small antibody fragments against *Tb*BILBO1, to novel epitopes, *in vivo*.
3. To investigate if scFv and/or nanobodies raised against *Tb*BILBO1 can influence cell growth and morphology, specifically, whether they are inhibitory or trypanocidal to *T. brucei* when inducibly expressed in the parasite or,
4. when placed in the culture medium.

The specific objectives for these aims were:

1. To transfect and inducibly express antibody fragments against *Tb*BILBO1, in the procyclic (PCF) and mammalian blood stream forms (BSF) of *T. brucei*, recording any affect on cell growth, viability and morphology and using IFA to visualise if (and where) these intrabodies bind *Tb*BILBO1.
2. To use anti-*Tb*BILBO1 peptides as probes in western blot analysis to see if they can detect *Tb*BILBO1 protein in whole cell lysates.
3. To clone and express anti-*Tb*BILBO1 peptides in *E. coli* bacteria, purify them and determine their ability to detect endogenous *Tb*BILBO1 protein by probing fixed trypanosomes by WB and IFA and to determine if *Tb*BILBO1 has an exposed cytoplasmic domain.
4. To add anti-*Tb*BILBO1 peptides directly to living BSF trypanosomes to ascertain whether the domain of BILBO1 recognised by the Nb is exposed in the lumen of the FP, and if co-culture is deleterious for parasite survival.

Chapter 2

Materials and Methods

2.1 Cell culture

2.1.1 Trypanosome cell culture

Medium

Procyclic forms (PCF) were grown in SDM-79 medium (GE Healthcare, G3344-3005). This semi-defined medium was first described by Brun and Schonenberger, 1979 and is made up in the laboratory with Aguettant water (OTEC H_2O, Aguettant Essential Medicine, 600500). The pH is adjusted to 7.4, and completed by the additions of 10% Foetal Bovine Serum (FBS; Gibco, 11573397; complement deactivated at 56°C for 30 minutes) and 2mg/mL haemin (Sigma Aldrich, H-5533). PCF are incubated at 27°C without supplementary CO_2.

Bloodstream forms (BSF) were grown in Iscove's Modified Dulbecco's Medium, developed by Hirumi and Hirumi, 1989, containing: IMDM (Gibco 42200-014); 3.024g/L Sodium Bicarbonate (Euromedex 6885-1); 0.136g/L Hypoxanthine (Sigma H-9636); 0.11g/L Sodium Pyruvate (Sigma P-3662); 0.039g/L Thymidine (Sigma T-9250); 0.028g/L Bathocuproinedisulfonic acid (Sigma B-1125); 2μM mercaptoethanol (Sigma M-6250); 1.7μM L-Cysteine (Sigma C-1276); 55μg/mL Kanamycin (Sigma K-4000); 10% FBS, made up to 1L with Aguettant water (Aguettant Essential Medicine, 600500). BSF cells were incubated at 37°C with 5% CO_2.

Cell lines for all scFv and nanobody experiments

The PCF cell line Tb427 29.13 and BSF Tb427 90.13 were used. *Trypanosoma brucei* 427 Lister is a monomorphic strain, originally isolated in 1960 from a sheep in Uganda and transferred to the Lister Institute in London in 1961 by Keith Vickerman, as listed by Cunningham and Vickerman, 1962. Cells were grown with selection antibiotics hygromycin (25μg/mL for PCF and 5μg/mL for BSF) and neomycin (10μg/mL for PCF and 2.5μg/mL for BSF) added to the media to maintain the plasmid vectors pLew29/pLew90 and pLew13 harboured by the parasites Wirtz et al., 1999. These

Antibiotic (Manufacturer / ref.)	**Stock concentration**	**Culture concentration for**	
		***T. brucei* PCF**	***T. brucei* BSF**
Blasticidin (InvivoGen #ant-bl-1)	1 mg/ml	10 µg/ml	5 or 10 µg/ml[1]
Hygromycin (InvivoGen #ant-hg-1)	2.5 mg/ml	25 µg/ml	5 µg/ml
Phleomycin (InvivoGen #ant-ph-1)	1 mg/ml	5 µg/ml	2.5 µg/ml
Puromycin (InvivoGen #ant-pu-1)	100 µg/ml	1 µg/ml	0.1 µg/ml
Neomycin (G418[2]) (InvivoGen #ant-gn-1)	1 mg/ml	10 µg/ml	2.5 µg/ml
Antibiotic (Manufacturer / ref.)	**Stock concentration**	**Bacterial culture concentration**	
Ampicillin (Sigma-Aldrich #A9518)	100 mg/ml	100 µg/ml	
Kanamycin (Sigma-Aldrich #K4000)	10 mg/ml	50 µg/ml	
Antibiotic (Manufacturer / ref.)	**Stock concentration**	**RNAi induction in *T. brucei***	
Tetracycline (Sigma #T3383)	1 mg/ml / 10 mg/ml	0.1 ng - 10 µg/ml	

TABLE 2.1: **Table of Antibiotics.** List of antibiotics used for *T. brucei* cell culture, bacterial culture for gene cloning and range of concentration of tetracycline used for RNAi induction. [1]according to Brooks et al., 2000: $2/5/10\mu g/mL$; and MacGregor et al., 2013 and Mazet et al., 2013: $10\mu g/mL$; [2]geneticin = G418 sulphate.

plasmids contain the tetracycline repressor (TetR - integrated in the tubulin locus), T7 promotor and bacteriophage T7 RNA polymerase genes, which are required for the tetracycline inducible gene expression system. In the absence of tetracycline, the TetR binds the EP procyclin promotor upstream of the gene of interest and the scFv or nanobody (Nb) is not transcribed Wirtz et al., 1999. In the presence of tetracycline, the TetR binds to tetracycline, inducing a conformational change, reducing TetR binding to the DNA and allowing the transcription and expression of the scFv or Nb.

Phleomycin (5μg/mL for PCF and 2.5μg/mL for BSF) was added to the media of cells transfected with the pLew100-3Myc vector (containing the scFv or Nb sequence), to select for those harbouring the antibiotic selection gene and hence the desired, tagged, gene. Expression of tagged scFv or Nb intracellularly was induced with tetracycline at 10μg/mL – 0.1ng/mL tetracycline. Observations ranging from 1 to 300 hours of induction were assessed to detect any effect of scFv or Nb expression on cell growth and viability. For all antibiotic concentrations used, see Table 2.1.

Cell lines for all experiments involving FPC6

PCF and BSF Tb427 Single marker Oxford strain (SmOx; Poon et al., 2012) cell lines was used with selection antibiotic puromycin 1μg/mL for PCF and 0.1μg/mL for BSF. This cell line replaces the first tubulin gene in the locus with both the TetR and T7 promotor. Transfection of SmOx cell line with the RNA interference (RNAi) vector, p2T7$^{Ti:TAblue}$-FPC6 (from Dr Brooke Morriswood, University of Würzburg, Germany; original vector from Alibu et al., 2005) were selected for with hygromycin. Endogenous tagging of selected genes (see Section 2.5.6; Dean et al., 2015a) were selected for by the required antibiotic: either blasticidin (10μg/mL for PCF and 5-10μg/mL for BSF; 5μg/mL for culture and 10μg/mL for selection) for Ty1 tagging or neomycin for cMyc tagging. For all antibiotic concentrations used, see Table 2.1.

Cloning and growth curves

Clones were obtained by serial dilution in 96 well plates and maintained in logarithmic phase growth at 2x10^6 cells/mL for PCF and 1x10^5 cells/mL for BSF. Growth curves representing logarithmic number of cells were calculated by counting the number of cells every 24 hours using counting chamber slides (Globe Scientific Inc., ref. 3805). Cells were fixed with 3.7% formaldehyde in phosphate-buffered saline (PBS) for PCF and 3.7% formaldehyde in vPBS (Voorheis's modified PBS: PBS supplemented with 10mM glucose and 46mM sucrose) for BSF.

Trypanosome transfection

Trypanosomes were transfected with either linearised plasmids or purified PCR products. Plasmids, either pLew100-3cMyc or p2T7$^{Ti:TAblue}$ (Alibu et al., 2005),

were linearised with *Not*1 (restriction emzyme), then concentrated and purified by ethanol precipitation of DNA (see Materials and Methods, Section 2.5.18). Four PCR products (total 200μL) were pooled, ethanol precipitated and resuspended in 10μL sterile H_2O. Laboratory cell lines of PCF were grown to 5-10x10^6 cells/mL, then 3x10^7 cells were counted, washed twice in ice-cold 1xPBS, before being re-suspended in Roditi's buffer (90mM sodium phosphate, 5mM potassium chloride, 0.15mM calcium chloride, 50 mM HEPES, pH 7.3) (Schumann Burkard et al., 2011). The DNA, either 10μg of plasmid or 4 pooled PCRs, was added to the trypanosomes in the Roditi's buffer and gently mixed before placing the cells into a transfection cuvette with a 2mm gap (VWR International; cat. no. 732-1136). Transfection by electroporation was carried out using a Biosystems Nucleofector®II, AMAXA, using programme X-001 or Z-001. A total of 3x10^7 log growth cells were collected, centrifuged at 800 x g, washed twice in 1xPBS (at 4°C for PCF) or washed once in vPBS (at room temperature for BSF), resuspended in Roditi's buffer, then transfected as above. Clones were obtained post transfection by serial dilution in media containing the selection antibiotic(s). For all antibiotic concentrations used, see Table 2.1.

Trypanosome culture in presence of purified nanobody

Anti-*Tb*BILBO1 nanobodies were added to the culture medium of *T. brucei* BSF *Tb*427 90.13, in serial dilutions (500μg, 100μg, 50μg, 10μg), after 17 hours, cell concentration and viability were counted using Guava Viacount®(EMD Millipore Corp. USA). Trypanosomes were prepared for IFA, extracted and fixed with methanol (see Material and Methods, Section 2.3.1. Purified nanobodies were labelled using anti-HIS and anti-HA, followed by secondary fluorescent antibodies. For all primary antibodies used see Tables 2.2 and 2.3; for all secondary antibodies used, see Table 2.4.

2.1.2 Bacterial culture

Bacterial cell lines

Bacteria used were Stellar^{TM}competent (Clontech; ref. 636766), XL1 blue, and WK6 (VIB nanobody service). They were grown either on solid agar in plates or liquid lysogeny broth (LB) in flasks, impregnated with the appropriate antibiotic: ampicillin 100μg/mL (Sigma-Aldrich; ref. A9518) or kanamycin 50μg/mL (Sigma-Aldrich; ref. K4000).

Transformation of bacteria

Twenty-five μL of bacteria were transformed with 5μL of In-Fusion or aqua-cloning reaction or 100ng of plasmid construct from classical ligation, as follows: bacteria taken from -80°C stocks were first rested on ice for 20 minutes, then the plasmid

construct/vector added, mixed by flicking and placed on ice for 30 minutes. Bacterial cells were exposed to a thermal shock at 42°C for 45 seconds, then placed on ice for 2 minutes. Next, 250μL of SOC medium (Hanahan, 1983) was added to the bacterial cells and incubated for 1 hour at 37°C at 220rpm. The bacterial cells were centrifuged at 2000 x g for 3 minutes, then the pellet resuspended in 200μL of SOC medium (super optimal broth: Clontech; cat. no. 636763). Bacteria were plated out on LB + selection antibiotic on solid agar (according to the plasmid) in two plates: 50μL on the first plate and the rest of the culture was centrifuged at 16,000 x g for 2 minutes, resuspended in 150μL fresh SOC then spread on the second plate with the aid of glass beads. The plates were incubated overnight at 37°C.

2.2 Endocytotic Uptake Assays

To assess endocytosis of fluorescent marker molecules, a protocol was adapted from that used by Morriswood and Schmidt, 2015. WT BSF Tb427 SmOx and cells endogenously tagged with 10xTy1::FPC6 also harbouring the p2T7$^{Ti:TAblue}$ plasmid for RNAi *FPC6* (clone 5.6), were diluted to 1x10^5 cells/ml and grown overnight at 37°C either non-induced or induced with 1μg/mL tetracycline. 17-19 hours post-induction trypanosomes were counted and 2x10^6 cells from each condition were centrifuged at 800 x g for 10 minutes at 4°C; cells were then resuspended in 1mL of ice-cold serum-free IMDM and transferred to 1.5mL microfugation tubes (Sarstedt; ref.72.706.700). Cells were pelleted by centrifugation at 800 x g for 5 min at 4°C, then resuspended in 100μL of ice-cold serum-free IMDM, and chilled for 10 minutes on ice. Dextran, fluorescein, 10,000MW, anionic (Life Technologies Corporation; ref. D1821) final concentration 5 mg/mL and Concanavolin A, Texas Red^{TM}conjugate (Life Technologies Corporation; ref. C825) to a final concentration of 10μg/mL) were added and mixed to the trypanosomes in the tubes by flicking. The cells were then incubated to allow Flagellar Pocket loading for 15 minutes on ice. Half the samples were then fixed (time, t = 0). The other half (t = 30 minutes) were shifted to 37°C and incubated for 30 minutes to allow uptake. For both sets of samples (t = 0 and t = 30 minutes), uptake was stopped by the addition of 1mL of ice-cold serum-free IMDM and fixed as described in Section 2.3.1.

2.3 Imaging

2.3.1 Immunofluorescence assay

For PCF

One mL of log-phase cells were collected, centrifuged for 5 minutes at 1000 x g, washed in 1xPBS (phosphate-buffered saline), resuspended in 500μL of 1xPBS, then 20μL was loaded onto poly-L-lysine 0.1% solution (Sigma-Aldrich; P8920) coated

Antibody	Species made in	Immunoglobulin class	Manufacturer/ ref.	Dilution
Anti-GFP	rabbit	polyclonal	Clontech, 632460	IF: 1:1000; WB: 1:10,000
Anti-HA	mouse	IgG1	Biolegend MMS-101R	IF: 1:1000; WB: 1:1000
Anti-HA	mouse	IgG2a	Santa-Cruz 7392	IF: 1:200; WB: 1:1000
Anti-His	mouse	IgG2a	Sigma H-1029	IF: 1:100; WB: 1:3000
Anti-cMyc	mouse	IgG1	Ersfeld, 9E10	IF: 1:20; EM: 1:10
Anti-cMyc	rabbit	polyclonal	Santa-Cruz, 789	IF: 1:500; WB: 1:1000
Anti-cMyc	rabbit	polyclonal	Sigma, C3956	IF: 1:200; WB: 1:1000
Anti-Ty BB2	mouse	IgG1	Bastin	IF: 1:200; WB: 1:100-150 Purified: EM: 1:5; WB: 1:50,000

TABLE 2.2: **Table of primary antibodies against tags.**

slides for 4 minutes to adhere. Slides used were ThermoScientific Cel-line diagnostic microscope slides, 30-225H-RED-CE24. Whole cells were fixed with either 1% paraformaldehyde (PFA; Electron microscopy Sciences; Cat.no. 15714) for 10 minutes and permeabilized with 0.1% triton TX-100 (Aldrich; 23,472-9) for 10 minutes, neutralised in 100mM glycine (Euromedex; ref. 26-128-6405-Ca-630; ref. I3021) twice for 10 minutes, washed in 1xPBS, then blocked in 0.1% bovine serum albumin (BSA; Sigma; P-0834) and 0.1% Tween®20 (Sigma; P7949), or, fixed in methanol at -20°C for at least 60 minutes. Cytoskeleton extraction was with 0.25% NP40 (IGEPAL®in PIPES buffer (100 mM PIPES pH 6.8 (Piperazine-N,N'-bis-(ethanesulfonic acid); Euromedex; 1124), 1mM $MgCl_2$) for 5 minutes, and then washed twice in PIPES buffer; cells were fixed with 1% PFA or methanol (as for whole cells).

For BSF

Five mL of log-phase cells were collected, centrifuged at 800 x g for 5 minutes, then washed in V-PBS. Whole cells were fixed in 3% PFA for 10 minutes or methanol for 60 minutes; cytoskeleton extraction was with 0.25% NP40 (as above). Slides used were as above or ThermoScientific Superfrost®plus 1800AMNZ.

For fixation of BSF from endocytotic assays

After incubation with fluorophore-conjugated dextran and ConA (see Section 2.2), cells were pelleted at 800 x g for 5 minutes at 4°C and then resuspended and incubated in 1mL 4% paraformaldehyde – 0.1% glutaraldehyde (Sigma; G5882) in ice-cold vPBS for 20 minutes on ice, for fixation of the cells. Cells were then centrifuged at 800 x g for 5 minutes at 4°C, resuspended in 50μL vPBS at 4°C and 50μL was spread over a slide well coated in poly-L-lysine. Cells were left to adhere for 20 minutes at room temperature (RT), then dried for 10 minutes. Cells were then permeabilized with 0.25% Triton TX-100 in 1xPBS for 4 minutes, washed twice for 5 minutes with 100mM glycine, washed twice for 5 minutes with 1xPBS, incubated with 25μL DAPI (Sigma; D-9542) for 2 minutes at RT, washed twice with 1xPBS, then a drop of Slowfade®Gold anti-fade reagent (Invitrogen; S36936) was added to each well before covering with a coverslip (Knittel Glass) and sealing with nail varnish. Trypanosomes were imaged directly, using the same acquisition settings and exposure times for both induced and non-induced samples.

For flagella preparations

Ten mL of log growth *T. brucei* were collected and washed once in 1xPBS for 5 minutes at 1000g at RT. Cells were extracted with 1mL 1% NP40 in 100mM PIPES buffer + 1mM $MgCl_2$ for 7 minutes at RT. Cytoskeletons were centrifuged for 10 minutes at 5,000 g at 4°C. To extract flagella, cytoskeletons were incubated for 15-30 minutes on ice with 1% NP40 in 100mM PIPES buffer + 2mM $MgCl_2$, containing 1M KCl. Flagella were centrifuged for 5 minutes at 5,000 g at 4°C, the supernatant was removed

Antibody	Species	Immunoglobulin	Manufacturer/ ref.	Dilution
Anti-*Tb*BILBO1 coiled-coil	mouse	IgM	Robinson, 5F2B3-C8	IF: 1:1
Anti-*Tb*BILBO1 NTD aa 1-110	rabbit	polyclonal	Robinson, bleed 1 1517028	IF: 1:4000; EM: 1:200-400 WB: 1:1000; ELISA: 1:100
Anti-Enolase	rabbit	polyclonal	Bringaud	WB: 1:10,000
Anti-FAZ	mouse	IgG1	Bastin, L3B2	IF: neat
FAZ signal - uncharacterised (mAb37)	mouse	IgM	Robinson	IF 1:10
Anti-FTZC	rabbit	polyclonal	Bringaud	IF: 1:10,000
Anti-*Tb*MORN1	rabbit	polyclonal	Morriswood	IF 1:5000; EM: 1:400 WB: 1:20,000-1000
Anti-PFR2 (*Tbgl mamaissata*)	rabbit	polyclonal	Baltz	IF: 1:200
Anti-*Tb*SAXO (mAb25)	IgG2a	monoclonal	Robinson	IF: 1:10-100; WB: 1:1000-3000
Anti-tubulin TAT1	mouse	IgG2a	Bastin	IF: 1:50-100; WB: 1:1000

TABLE 2.3: **Table of Primary Antibodies against *T. brucei* proteins.**

and flagella were resuspend in 500μL PIPES buffer. Flagella were washed twice in 100mM PIPES buffer + 1mM $MgCl_2$ for 5 minutes 5000g at 4°C before being deposed on poly-lysine coated slides and left to adhere for 5–10 minutes. The flagella were fixed at -20°C in MeOH or in 3% PFA as described above.

Cells were incubated with single or combination of antibodies: anti-cMyc monoclonal antibody IgG1 9E10 (a kind gift from Professor K. Ersfeld, University of Bayreuth, Germany 1:20) to detect expressed scFv or Nb, anti-*Tb*BILBO1 (amino acids 1–110 Rabbit Bleed 1 201-10-14 1:4000), anti-*Tb*MORN1 (rabbit, polyclonal, a kind gift from Dr Brooke Morriswood diluted 1:5000), anti-PFR2 rabbit (Prof Baltz), anti-FAZ monoclonal (a kind gift from Dr Philippe Bastin) for 60 minutes, washed twice in 1xPBS, then incubated with secondary antibodies: anti-mouse IgG (subclasses 1 + 2a + 2b + 3) specific FITC (Jackson, 115-095-164), anti-mouse far red (Fischer, A21235), and anti-rabbit Ig(H+L) Alexa fluor 594 (Invitrogen, A-11012). Slides were stained with 10μL DAPI in 1xPBS for 2 minutes and Slowfade®loaded before covering and sealing with nail varnish.

For all primary antibodies used, see Tables 2.2 and 2.3; for all secondary antibodies used, see Table 2.4.

2.3.2 Nanobodies used as probes in IFA of fixed trypanosomes

PCF Tb427 29.13 wild-type (WT), Tb427 29.13 pLew100-BILBO1::3cMyc (overexpressing *Tb*BILBO1 induced 24 and 48 hours with 1μg/mL tetracycline) and BSF Tb427 90.13 WT were fixed (as above) incubated with Nb for 1 hour, followed by anti-HIS (mouse mAb, Sigma IgG2a) diluted 1:100 or anti-HA (mouse mAb, Santa Cruz 7392) diluted 1:200. For co-labelling with *Tb*BILBO1, anti-*Tb*BILBO1 (aa 1-110 rabbit 151-70-28 bleed 1) was used at a dilution of 1:4000 in 1xPBS. Secondary antibodies were used at 1:100 dilution: goat anti-mouse IgG2a Alexa fluor 488 (Sigma, A21131), anti-rabbit IgG(H+L) Alexa fluor 594 (Invitrogen, A11012). For all primary antibodies used see Tables 2.2 and 2.3; for all secondary antibodies used, see Table 2.4.

2.3.3 Electron microscopy

Electron microscopy of trypanosome sections: TEM (transmission electron microscopy)

10mL of mid-log phase procyclic *T*b427 29.13 wild-type (WT) cells, pLew100-Nb48::3cMyc, and pLew100-Nb9::3Myc cells (induced for 24 and 48 hours) were fixed, dehydrated and embedded as previously described by Pradel, 2006.

Antibody	Species	Immunoglobulin class	Manufacturer/ ref.	Dilution	Fluo/ HR / gold
Anti-chicken	goat	IgG (H+L)	Molecular probes, A11039	IF 1:400	Alexa fluor 488
Anti-chicken	goat	IgG (H+L)	Jackson, 103-035-155	WB: 1:10,000	HRP
Anti-mouse	goat	IgG	Sigma, F2012	IF: 1:100	FITC (green)
Anti-mouse	goat	IgG (subclasses 1 + 2a + 2b + 3) Fc**γ** specific	Jackson, 115-095-164	IF: 1:100-(200)	FITC
Anti-mouse	goat	IgM (μ chain specific)	Sigma, F9259	IF: 1:100	FITC
Anti-mouse	goat	IgG2a	Sigma, A21131	IF: 100	Alexa fluor 488
Anti-mouse	chicken	IgG (H+L)	Molecular probes, A21201	IF: 1:200	Alexa fluor 594 red
Anti-mouse	goat	IgG (H+L)	Fischer, A21235	IF: 1:100	far red, 647
Anti-mouse	goat	IgG	BB International, GMTA 5	EM: 1:15-20	5nm gold
Anti-mouse	goat	IgG + IgM	Jackson, 115-035-044	WB: 1:10,000	HRP
Anti-mouse	sheep	IgG (H+L)	Jackson, 515-035-062	WB: 1:1000	HRP
Anti-mouse	goat	IgG	BIO-RAD, 12005867	WB: 1:2500	StarBright™ Blue 520
Anti-rabbit	goat	IgG (whole molecule)	Sigma F-9887	IF: 1: 100-200	FITC
Anti-rabbit	goat	IgG (H+L)	Invitrogen A11012	IF: 1:(100)-200	Alexa fluor 594
Anti-rabbit	goat	IgG	BB International, GAR15	EM: 1:15	15nm gold
Anti-rabbit	goat	IgG (whole molecule)	Sigma, A9169	WB: 1:10,000 ELISA: 1:10,000	HRP
Anti-rabbit	goat	IgG	BIO-RAD, 12004162	WB: 1:2500	StarBright™ Blue 700

TABLE 2.4: **Table of secondary antibodies.**

Immuno-electron microscopy: IEM

Ten mL of mid log phase $\sim$ 5 x 10^6/mL pLew100-Nb48::3Myc cells were induced with 1μg/mL tetracycline for 1 or 2 hours. Five mL of induced cells were harvested (1000 x g for 5 minutes), washed twice with 1xPBS by centrifugation (1000 x g for 5 minutes) then re-suspended in 500μL of 1xPBS. Five mL of 2 x 10^6/mL procyclic *Tb*427.29.13 cells were used as control and harvested as above. Freshly glow-discharged, butvar and carbon-coated G2000-ni nickel grids (EMS) were floated on the droplets and the cells allowed to adhere for 15 minutes. Grids were then moved onto a drop of 1% NP-40 in PEME buffer (100 mM PIPES pH 6.8, 1mM $MgCl_2$, 0.1mM EGTA) for 5 minutes at RT, followed by incubation on a 500μL drop of 1% NP-40, 1M KCl in PEME buffer to depolymerise the sub-pellicular microtubules for 15 minutes, (3 x 5 minutes, 40°C). Flagella were then washed twice (2 x 5 minutes) in PEME buffer at RT. Flagella were equilibrated and blocked by transferring to four 50μL drops of 2% fish skin gelatin (Sigma-Aldrich G7041) or 0.5% BSA, 0.1%tween 20 in 1xPBS and then incubated in 25μL of primary antibody diluted in blocking buffer; each primary antibody was used either alone, or mixed with a second primary antibody, for 1 hour at RT. For Nb experiments: mouse IgG anti-cMyc monoclonal supernatant (Ersfeld) was diluted 1:10-50 or protein G purified/concentrated supernatant (diluted 1:50) and anti-*Tb*BILBO1 (rabbit polyclonal IgG) was diluted 1:200 or 1:400. Additionally, for FPC6 experiments: anti-Ty1 (Bastin) was diluted 1:5 and anti-*Tb*MORN1 (Morriswood) was diluted 1:400 The grids were then moved through four drops of blocking solution and incubated in secondary antibody for 1 hour at RT (goat anti-mouse GMTA 5nm gold, and/or goat anti-rabbit 15nm gold GAR15, BB International). Grids were then incubated in blocking solution 4 x 5 minutes at RT, then 2 x 5 minutes in 0.2% fish skin gelatin in PBS and fixed in 2.5% glutaraldehyde in 0.2% fish skin gelatin in 1xPBS. Flagella were then negatively stained with 1% aurothioglucose, 10μL for 30 seconds, (Merck, 1045508). Micrographs were taken on a Phillips Technai 12 transmission electron microscope at 100 kV.

2.4 Alpaca immunization and Nb library construction

The alpaca (*Vicugna pacos*) immunization experiment was approved by the Ethical Committee for Animal Experiments of the Vrije Universiteit Brussel, VUB, Brussels, Belgium (Permit Number:0000). A recombinant 6xhistidine::*Tb*BILBO1 protein was over-expressed in bacteria, purified in urea on Ni-NTA resin (by affinity column purification), and then 200μg of purified *Tb*BILBO1 protein was injected subcutaneously into an alpaca on days 0, 7, 14, 21, 28 and 35 (Nanobody Service Facility, Belgium). On day 39, anti-coagulated peripheral blood was collected for lymphocyte isolation, mRNA extraction and cDNA synthesis using oligo(dT) primers. A VHH library was constructed and screened for antigen-specific Nb as follows. Total RNA from peripheral blood lymphocytes was used as a template for cDNA synthesis; from the cDNA, the VHH (Nb) encoding sequences were amplified by PCR using specific primers CALL001 and CALL002 (Conrath et al., 2001). The identified

VHH sequences were digested with *Pst*I and *Not*I, and cloned into the phagemid vector pMECS. All primers used in scFv and nanobody experiments are listed in Table 2.5.

A nanobody library of 2 x 10^8 independent transformants was obtained as previously described in Arbabi Ghahroudi et al., 1997 and Stijlemans et al., 2004, and subjected to two rounds of panning, performed on solid-phase coated full-length *Tb*BILBO1 antigen (10μg/well). Enrichment for antigen-specific phages after each round of panning was assessed by comparing the number of phages eluted from antigen-coated wells with those from negative control wells. Ninety-five colonies from round two were randomly selected and analysed by ELISA for the presence of antigen-specific Nbs in their periplasmic extracts.

Thirty-four colonies scored positive, representing seven different Nbs from three different groups based on their gene sequences: Nbs in each group have very similar sequence data, predicted as recognising the same epitope (Figure 4.3.A). The Nb genes were cloned into a pMECS vector containing a PelB leader signal sequence at the N-terminus, to direct the Nb to the periplasmic space of *E. coli* during bacterial expression (Conrath et al., 2001) a hemagglutinin A (HA) tag and a hexa-histidine (6xHis) tag at the C-terminus, for purification (by IMAC) and immunodetection. These vectors were cloned into TG1 *E. coli* and stored at -80°C.

2.5 Molecular Biology

2.5.1 Cloning of nanobodies and scFv for bacterial expression and purification

Nanobodies were sub-cloned from pMECS to pHEN6c vector as follows: TG1 *E. coli* harbouring the Nbs, were grown overnight on solid agar + ampicillin (100μg/mL). The Nb genes were amplified by PCR directly on colonies using Q5®Hot Start High-Fidelity DNA Polymerase (New England, BioLabs, USA) and specific primers A6E and PMCF, see Table 2.5. Fragments of around 400bp were amplified, purified using Illustra^{TM}GFX^{TM}DNA purification kit (GE Healthcare Life Sciences, 28-9034-70) and digested overnight with the restriction enzyme *Pst*I at 37°C. The product was purified with GFX^{TM}and digested overnight with *Bst*II at 60°C. The product was purified with GFX^{TM}and was ready for ligation.

Digested fragments (Nbs) were ligated into the pHEN6c vector as follows: the pHEN6c vector was harboured in XL1 blue *E. coli* with ampicillin resistance stored at -80°C, they were grown overnight in 100mL LB + ampicillin (100μg/mL) liquid medium, then the plasmid was extracted using Wizard®Plus SV Minipreps DNA Purification System (Machery Nagel, 740588.250). The amount of vector was quantified (UV spectrometry, Omega), then digested with *Pst*I for 3 hours at 37°C, purified

Protein / construct	Sequence (5' - 3')	ID number
VHH amplification from cDNA	F: GTCCTGGCTGCTCTTCTACAAGG R: GGTACGTGCTGTTGAACTGTTCC	CALL001 CALL002
VHH from pMECS to pHEN6c	F: GATGTGCAGCTGCAGGAGTCTGGRGGAGG R: CTAGTGCGGCCGCTGAGGAGACGGTGACCTGGGT	A6E PMCF
Mutagenesis of R2BIL48 (T-C)	F: CTATGAGGGCACAcATGAGTATGAC R: GTCATACTCATgTGTGCCCTCATAG	1170* 1171*
scFv from pLew-100 to pHEN6c	F: CAGGTGCAGCTGCAGatgGAAATTGTGCTCACCCAG R: GAGGAGACGGTGACCgtTGAGGAGACTGTGAGAGTGG	993* 994*
scFv specific for colonies	R: GATCctcgagTGAGGAGACTGTGAGAGTGG	707
For vector pHEN6c on colonies	TCACACAGGAAACAGCTATGAC	M13R
For vector pJET28a on colonies	TAATACGACTCACTATAGGG	T7 promotor

TABLE 2.5: **Table of primers for scFv and nanobody cloning.** *Primers designed by Christine Reix.

(GFX), then digested with *Bst*II for 2.5 hours and purified by GFX^{TM}. The digested vector was run on 1% agarose gel and the band (3288bp) was cut from the gel and purified by GFX^{TM}. Cohesive ligation of the Nb inserts and pHEN6c vector using Anza^{TM}T4 Ligase Master Mix (Invitrogen, ref. 15535720) was performed, using a ratio of 1:3 (vector:insert).

All primers used in scFv and nanobody experiments are listed in Table2.5.

2.5.2 Transformation of scFv and nanobodies into non-suppressor WK6 *E. coli*

Competent WK6 *E. coli* were transformed with the ligation reaction (pHEN6c + Nb) overnight on solid agar LB + ampicillin (100μg/mL) at 37°C. PCR was carried out directly on transformed colonies, using one primer specific for the vector, universal reverse primer M13R and one primer specific for the Nb, PMCF (see Table 2.5. Fragments of 500bp were obtained confirming the Nb insert was present.

For the scFv fragment, In-Fusion was initially used to ligate the insert (scFv sequence) into the pHEN6c vector. The vector was digested with *BstE*II and *Pst*I and primers designed for the ligation of scFv: forward primer 993 and reverse primer 994 (see Table 2.5). After failure to obtain positives clones, the vector and insert were digested with *BstE*II and *Xba*I and cohesive ligation was performed using Anza^{TM}T4 DNA ligase, at a ratio of 1:3 (vector:insert).

Two colonies from each of the scFv/Nb groups were chosen and grown in LB + ampicillin liquid culture overnight at 37°C and the plasmids harbouring the Nb/scFv inserts were extracted using Miniprep (Wizard®). The extracts were quantified and digested (as above: *Pst*I/*Bst*II) to check for bands specific in size for pHEN6c and scFv/Nb insert. Clones were sequenced to confirm absence of mutations by comparing with theoretical sequences *in silico*.

2.5.3 Transformation of scFv into pJET28a for expression in *E. coli*

The pJET28a-HIS vector and scFv insert were digested with *EcoR*I and *Xho*1, then ligated using In-Fusion reaction and transformed into XLI Blue *E. coli*. Colonies were picked and confirmed for the presence of the insert by PCR, using one primer specific for the vector (T7 promotor) and one specific for the insert (707), see Table 2.5. Minipreps were prepared and the purified plasmid doubly digested with *EcoR*I and *Xho*I to confirm the size. All primers used in scFv and nanobody experiments are listed in Table 2.5.

2.5.4 Cloning of scFv and nanobodies into a trypanosome expression vector

The scFv construct had previously been cloned into a plasmid. pJet 5F3-B2-C8 scFv and confirmed by sequencing of the insert. The scFv insert was then subcloned into a pLew100-3cMyc vector (completed by Dr Aya Takemura, a visiting PhD student to the Robinson laboratory, 2013). The cMyc tag allowed identification of the expressed protein in trypanosome cells by IFA and western blot.

Nanobody inserts previously subcloned from pMECS to pHEN6c (as described above) were digested out with *Hind*III and *Nde*I. The plasmid pLew100-3cMyc was double-digested with *Hind*III and *Nde*I and purified from 1% agarose gel (GE Healthcare illustra ^{TM}28-9034-70). Nanobody 73 was cloned into pLew100-3cMyc by In-Fusion, whilst nanobodies 9 and 48 were cloned into a pLew100-3cMyc vector using cohesive ligation into Stellar^{TM}*E. coli* on LB + ampicillin (100μg/mL). Clones of *E. coli* harbouring Nb were sequenced, the plasmid was extracted from bacteria using a midiprep kit (Sigma-Aldrich, GenElute ^{TM}HP Plasmid, NA0200-1KT).

2.5.5 Site-directed mutagenesis

The nucleotide sequence encoding nanobody 48 (Nb48, R2BIL48) contained the restriction site *Nde*I (CATATG), therefore, I performed a site-directed mutagenesis to change a single nucleotide from T to C, thereby changing the code at this site from CATATG to CACATG. A kit called Quick Change Lightning Site-Directed Mutagensis (Agilent Technologies, 210518-5) was used. 50ng of purified plasmid, pHEN6c-Nb48-6HIS was mixed with 5μL 10x reaction buffer (from the kit), 1μL of dNTP 5nM and 2.5μL of each primer: Forward 1170; reverse 1171, see Table 2.5. To this mix, 1μL of pfuTurbo DNA polymerase was added and a PCR reaction was carried out with a 4 minute extension time, to allow full amplification of the entire plasmid containing Nb48. The PCR product was treated with *Dpn*I for 1 hour at 37°C, Stellar *E. coli* were transformed (see below). PCR on colonies confirmed the plasmid was present, minipreps were carried out on overnight growth of two selected colonies, which were double digested to confirm the vector and then both were sequenced. One out of the two had acquired the desired mutation. All primers used in scFv and nanobody experiments are listed in Table 2.5.

2.5.6 Endogenous tagging of FPC6, Tb927.4.3120

Primers were designed according to Dean et al., 2015a using the vector pPOTv7-BLAST-10Ty1, inserting an endogenous 10xTy1 tag to the gene *FPC6* and simultaneously inserting an antibiotic selection cassette, in this case for blasticidin (see Table 2.1). Both N-terminal and C-terminal tags were inserted to determine if either would affect the localisation of the protein or growth curve of the trypanosomes.

Protein / construct	Sequence (5' - 3')	ID number
Endo-tag Nter FPC6	F:TATATACAACATACGCAGTTACGCAACAAAATAGAGGAGATTTTAGAGTTTAGAACAATAATTAGT GGTGGCATAAAACgtataatgcagacctgctgc R:CCTTCGGTTCTTCCACATTCCGTCGGGTCATATTTGGTAGCCGTTGGCATGGCTTCGGTCTCAT GCCCTTCAATTTCCATactacccgatcctgatcc	1054 1055
Endo-tag Cter FPC6	F:TGGCGGCGAAAAACTTTGCACGTGATCTCTCGTCGCTAGCATCCGCTGTACGGGGCAGTGAAC TATTTAGCATGATATCGggttctggtagtggttcc R:CCATGCACAGCAGAAGTGCATTCGACTCCGCTATAAACCGTTCATTTCCTCACATTTTTGATTTA TTCGCCATAGTGTCCaatttgagagacctgtgc	1189 1190
RNAi FPC6 sequence in colonies	F: AGAGGTCCCTTTGTGTGGTG R: GACGAGAGATCACGTGCAAA	1108 1109
FPC6 genomic DNA	F: CAACATACGCAGTTACGC R: GACGAGAGATCACGTGCAAA	1168 1169
FL FPC6 from pEX-K4	F: GCGAAGAAGATCTTGGATCCGAGATCGAAGGTCATGAAAC R: ATTTAAGCGCAGCGGAGCTCTTATGAAATCATACTGAAGA	1452 1453
10Myc:FL FPC6	R: ccatgcacagcagaagtgcattcgactccgctataaaccgttcatttcctcacattttgatttattcgccatagtgtccTTATGAAATCATAC TGAAGAGCTC	1240
For pPOTv7 vector	F: TGTAAAACGACGGCCAGT	M13F (U)
T1 from pPOTv7	R: CTCCGTTTCATGACCTTCGATCTCtcctgatccggatccaagatcttc	1238
T2/T3 from pPOTv7	R: CGACGCTGATTTGCTAGCGGATCCtcctgatccggatccaagatcttc	1242
T1 from pEX	F: gaagatcttggatccggatcaggaGAGATCGAAGGTCATGAAACGGAG	1239
T2/T3 from pEX	F: gaagatcttggatccggatcaggaGGATCCGCTAGCAAATCAGCGTCG	1243
T1/T2/T3 from pEX	R: CAGGCTTTACACTTTATGCTTCCGGC	1314
10Myc::T1	R: ccatgcacagcagaagtgcattcgactccgctataaaccgttcatttcctcacattttgatttattcgccatagtgtccttaCTTACGAATACC TTTGTTCGT	1241
10Myc::T2	R: CCATGCACAGCAGAAGTGCATTCGACTCCGCTATAAACCGTTCATTTCCTCACATTTTTG ATTTATTCGCCATAGTGTCCttaACTTGGTGAGTAAGCCTGTGTCCA	1244
10Myc::T3	R: ccatgcacagcagaagtgcattcgactccgctataaaccgttcatttcctcacattttgatttattcgccatagtgtccTTATGAAATCATAC TGAAGAGCTC	1240

TABLE 2.6: **Table of Primers for Endogenous Tagging and Cloning of FPC6.** All primers were designed by Christine Reix.

For the N-terminal tag, the primers included the last 80 nucleotides of the target gene's 5'UTR and the first 80 nucleotides of the target gene's Open Reading Frame (ORF): the forward primer for the N-ter tag was 1054, and the reverse primer for the N-ter tag was 1055 (see Table 2.6.

For the C-terminal tag, the primers included the last 80 nucleotides of the target ORF (excluding the STOP codon) and the first 80 nucleotides of the target gene's 3'UTR: the forward primer for the C-ter tag was 1189, and the reverse primer for the C-terminal tag was 1190 (see Table 2.6.

Four polymerase chain reactions (PCR) of 50μL each were used per transfection, the DNA was ethanol precipitated (see Section 2.5.18), resuspended in 10μL sterile H_20 before transfection using electroporation (see Section 2.1.1). PCR reactions were performed with Q5^{TM}High-Fidelity polymerase, Q5^{TM}enhancer and Q5^{TM}reaction buffer (New England, BioLabs, ref. M0491L). Verification that the tag had been inserted in the trypanosomes was made by PCR on genomic DNA extracted from transfected cell lines, for PCF and BSF. Specific primers for the *FPC6* were used: Forward in the N-terminal UTR, 1168, and the reverse at the C-terminal end of *FPC6*, 1169. All primers used in cloning of FPC6 for experiments involving trypanosomes are listed in Table 2.6.

2.5.7 Endogenous tagging of *Tb*PIPKA, Tb927.4.1620

A 10xcMyc N-terminal tag was designed and produced by PCR as for the 10xTy1 tag of *FPC6* (above), using a different pPOTv7 vector: pPOTv7-NEO-10cMyc and primers: forward (1513) 5' ATATATAAGCTCGCCCACGCTCACTACCATCGGTCGACCCGGGCGGCAGGAAGGCCTTAATTTCGTTGGCGCGGGGAGCCgtataatgcagacctgctgc 3' and reverse (1514) 5' CGACGTGCCGCTATCTCCGCTGAGGAAAGGGGTCCAGATTCAAAGGAGATGGCGGCAAGTATTTCTCTATTGAACGGCATactacccgatcctgatcc 3'.

2.5.8 Cloning of FPC6 recoded gene: full-length and truncations for replacement of one allele in *T. brucei*

A recoded sequence for *FPC6* (Tb947.4.3120) was produced by (Eurofins Genomics, Germany) such that the nucleotide sequence was sufficiently different to be resistant to the double stranded RNA inducibly expressed in the cell as part of the RNA interference (RNAi) system, but still encoding for the same amino acids and hence the same protein. The sequence for *FPC6* recoded was previously cloned into a pEX-K4 plasmid named pEX-K4-FPC6-opt.

To produce a construct for the full-length (FL) FPC6 recoded gene, firstly, the pPOTv7-NEO-10Myc vector as described by Dean et al., 2015a, was double digested

Protein / construct	Sequence (5' - 3')	ID
FL FPC6 in U-2 OS	F: TTGGTACCGAGCTCGgatccATGGAAATTGAAGGGCATGAGACC R: GTTTAAACGGGCCCTTCACGATATCATGCTAAATAGTTCAC	1545 1537
T1 FPC6 in U-2 OS	R: GTTTAAACGGGCCCTTCACTTTCGTATGCCTTTGTTTG	1538
T2 FPC6 in U-2 OS	F: TTGGTACCGAGCTCGgatccGGGAGCGCATCCAAATCC R: GTTTAAACGGGCCCTTCAAGAGGGGGAATATGCCTGAGT	1546 1540
T3 FPC6 in U-2 OS	R: GTTTAAACGGGCCCTTCACGATATCATGCTAAATAGTTCAC	1537
T1 FPC6 in Y-2-H pGAD	F: CAGTGAATTCCACCCGGGTATGGAAATTGAAGGGCATGAG R: CAGCTCGAGCTCGATGGATCCtcaCTTTCGTATGCCTTTGTTTG	1547 1548
T2 FPC6 in Y-2-H pGAD	F: CAGTGAATTCCACCCGGGTGGGAGCGCATCCAAATCC R: CAGCTCGAGCTCGATGGATCCtcaAGAGGGGGAATATGCCTGAG	1549 1550
T3 FPC6 in Y-2-H pGAD	R: CAGCTCGAGCTCGATGGATCCTCACGATATCATGCTAAATAGTTCAC	1551
T1 FPC6 in Y-2-H pGBKT7	F: GACCTGCATATGGCCATGGAGATGGAAATTGAAGGGCATGAG R: CTGCAGGTCGACGGATCCtcaCTTTCGTATGCCTTTGTTTG	1552 1553
T2 FPC6 in Y-2-H pGBKT7	F: GACCTGCATATGGCCATGGAGGGGAGCGCATCCAAATCC R: CTGCAGGTCGACGGATCCtcaAGAGGGGGAATATGCCTGAG	1554 1555
T3 FPC6 in Y-2-H pGBKT7	R: CTGCAGGTCGACGGATCCTCACGATATCATGCTAAATAGTTCAC	1556

TABLE 2.7: **Table of primers for cloning of full-length and truncations of *FPC6* into expression vectors for U-2 OS and yeast 2-hybrid experiments.** All primers were designed by Christine Reix.

with *BamH*I and *Sac*I, treated with *Dpn*I for 30 minutes at 37°C to linearise any undigested vector. The vector was then purified from 1% agarose gel using GFX (GE Heathcare, Illustra^{TM}, 28-9034-70). The full-length FPC6 recoded gene was obtained via a PCR reaction on the pEX-K4-FPC6-opt plasmid adding sufficient overhangs to allow recombination during AQUA cloning (see Section 2.5.12). Primers used were: forward 1452 and reverse 1453, see Table 2.6. The PCR product was purified with HiPrep Sephacryl S-300 HR (GE Healthcare, Ref.17059901), to remove any unused primers.

Following AQUA cloning into Stellar^{TM}competent bacteria, single colonies were tested by PCR for the correct construct using a specific primer for the insert and another for the vector. One positive colony was grown in liquid LB (+ selective antibiotic) overnight and a miniprep (Machery Nagel, 740588.250) of the vector prepared for confirmation by gene sequencing (Eurofins genomics, Germany). Bacterial glycerol stocks were made and stored at -80°C and a midiprep was made using GenElute^{TM}HP plasmid (Sigma-Aldrich, Life Sciences). A final PCR was carried out using primers containing the 5'and 3' UTR for the gene *FPC6*, to insert the desired construct into the genome by homologous recombination, replacing one allele of *FPC6* with the FL *FPC6* recoded and inserting an antibiotic cassette for selection, in this case neomycin (selected at concentration in Table 2.1) with an N-terminal cMyc tag. Primers used were: forward 1054 (as for 10Ty N-ter tagging) and 1240; see Table 2.6.

Three truncations of *FPC6* recoded gene were constructed:
T1: Δ B1BD/Cter (aa 1-595);
T2: the BILBO1 binding domain (B1BD) including an overlapping globular domain (aa 596-800);
T3: Δ Nter (aa 596-933).

To obtain the truncations, overlapping PCRs were used: in the first step, using pPOTv7-NEO-10cMyc as a template to produce a construct containing the neomycin resistance cassette and 10xcMyc tag for N-terminal tagging. Alongside this, the PCR product of the desired sequence of *FPC6* recoded gene was amplified from the pEX-K4-FPC6-opt plasmid with an overhang homologous to the pPOTv7 vector at the 5'.

In the second step, the two PCR products from the first step were mixed and a PCR reaction run using primers designed with overhangs of 80bp matching the 5' and 3' UTR of *FPC6*, to allow homologous recombination into the trypanosomes genome replacing one allele of *FPC6*. The size of the final PCR products, were verified on agarose gel then purified by ethanol precipitation (see later) before transfection into trypanosomes.

The following combination of primers were used (see Table 2.6):
T1: first step (pPOT: M13F(U)/1238) (pEX: 1239/1314), second step (1054/1241)

T2: first step (pPOT: M13F(U)/1242) (pEX: 1243/1314), second step (1054/1244)
T3: first step (pPOT: M13F(U)/1242) (pEX: 1243/1314), second step (1054/1240)

All primers used in cloning of FPC6 for experiments involving trypanosomes are listed in Table 2.6.

2.5.9 Cloning full-length FPC6 and truncations for transfection of U-2 OS cells

The vector pcDNA3.1-3Ty1-X was used to clone the full-length and truncations (as above) of *FPC6* wild-type sequence. The vector was prepared by double digestion with *BamH*I and *Xba*I, for 2 hours at 37°C, the size was verified on 1% agarose gel, then the vector was purified from agarose gel using GFX^{TM}kit (GE Healthcare Life Sciences, 28-9034-70). FL *FPC6* and truncation sequences were prepared by PCR from a vector already harbouring the wild-type sequence, pcDNA3-BILBO6-GFP (FPC6 was previously named BILBO6). The PCR products were treated with *Dpn*I for 1 hour at 37°C and purified by S300. See Table 2.7 for primers used in FPC6 truncations cloning into the pcDNA3.1-3Ty1-X vector for expression in U-2 OS cells. AQUA Cloning was used to recombine the insert (PCR product of *FPC6*) into the vector and transformed into competent Stellar^{TM}*E. coli* bacteria; single colonies were picked from agar plates. PCR using specific primers confirmed the presence of the insert and miniprep extraction of plasmid DNA was carried to prepare purified DNA for sequencing (Eurofins Genomics, Germany). All primers used in cloning of FL *FPC6* and truncations into the U-2 OS expression vector are listed in Table 2.7.

2.5.10 Cloning of FPC6 full-length and truncations for yeast 2-hybrid assay

I designed primers to clone the same truncations of *FPC6*, as outlined above, into both pGAD and pGBKT7 vectors for yeast 2-hybrid assays (Y2H) to enable all constructs to be used for both bait and prey. See Table 2.7 for primers used to clone *FPC6* truncations cloning into the pGAD and pGBKT7 vectors for expression in U-2 OS cells. All primers used in cloning of FPC6 truncations into the Y2H expression vectors are listed in Table 2.7.

2.5.11 In-Fusion®cloning

Firstly, 5μg of plasmid was linearised and the DNA purified from 1% agarose gel by Illustra^{TM}GFX purification (GE Healthcare; Ref: 28-9034-70). Secondly, the PCR fragment was produced using primers with at least 15bp homologous with the vector's ends; the PCR product was purified by size-exclusion using Sephacryl S-300 HR resin (GE Healthcare no.17-0599-01), see below. The DNA

concentrations of the linearised vector and the PCR product were measured using FLUOstar Omega (BMG LABTECH) and the ratio of 260/280 was checked for DNA purity (see later, section 2.5.21). An optimal In-Fusion ratio 1:2 (plasmid:insert) was calculated taking into account the length of the vector and insert (http://bioinfo.clontech.com/infusion/molarRatio.do). For the In-Fusion reaction: 50ng of linearized vector and 5-100ng of insert (PCR product) were mixed with 1μL 5x In-Fusion mix (Clontech no.638910) and the total made up to 5μL with ddH_2O (Millipore). The In-Fusion reaction mix was incubated for 15 minutes at 50°C, then put on ice. Five μL of the reaction mix was used to transform 25μL Stellar bacteria (as in Section 2.1.2).

2.5.12 AQUA cloning

The vector and insert were prepared as for In-Fusion®(above). If the PCR product was taken from a template vector with the same antibiotic resistance as the target vector, the PCR product was treated with *Dpn*I for 30 minutes at 37°C. An optimal AQUA cloning ratio 1:3 (plasmid:insert) was used taking into account the length of vector and insert.

Formula: V_{insert} = (($SIZE_{insert}$ / $SIZE_{vector}$) x m_{vector} x R) / [Insert]

V= volume (μL)
SIZE = base pair number (bp)
m = mass (ng)
R = ratio plasmid:insert (usually 3)
[ ] = concentration (ng/μL).

The AQUA cloning mix consisted of: 50-100ng linearized vector, insert calculated according to the previous formula, made up to 5μL with double distilled H_2O. The mix was incubated for 60 minutes at room temperature on the bench, then put on ice. Five μL of the reaction mix was used to transform 25μL Stellar^{TM}bacteria (as for In-Fusion®).

The benefit of AQUA cloning is the cost benefit of the omission of In-Fusion mix (Clontech), the bacteria's own machinery is used for the recombination of insert into plasmid (Beyer et al., 2015) with similar success rates. In fact, I used AQUA cloning in preference to In-Fusion for most cloning reactions.

2.5.13 RNAi constructs

Two different sequences and constructs for RNAi *FPC6* were used. The first was a stem-loop designed and tested by Dr Celia Florimond (former PhD student in the Robinson laboratory). The sequence of *FPC6* in this construct was cloned into a

RNAi construct	FPC6 target seqeunce
pSL-FPC6-pLew100	CAACAAGCGACTTGGACTCACGGTACGAAACCAAACCCTGGA CTCAGGCATATTCCCCCTCTGGTGCCACCACCGACACCCTTG ACAACGGTTACACTTCATCGATTGATCCCCCACGCTCAAAGTA TTGGGACAGGGAAATGGCCGGAGGCACTTCTAAGAGGCATAA CTCAAGACCGAGATCACTGTTTCCGCCGCCGCACTCACCCGT CAAAACCTCAGCTGATCCACCGGTGGACGGCCTCATTTACAC ACCAGCGAAAACTGCATCGGCACGCAGCGCTTCCTGGATGTT TGAAAGGAGTCCTGATGAGGATAGGTACAACTCGTACTTCATG GACGCAAACTCACGGCTGCAGGAACTCCGTGTATGTGATTCA ATGGCGGCGAAAAACTTTGCACGTGATCTCTCGTCGCTAGCAT CCGCTGTACGGGGCAGTGAACTATTTAGCATGATATCGTGA
p2T7$^{Ti:TAblue}$FPC6	AGAGGTCCCTTTGTGTGGTGCAACCATGTGGGGGAAAGGTAA GTGCAAGTGAACTAAGTGCACTGGCTTCCACGCAGCTGATGT CCAAGGACACCTCGTTGAGCGAAGACTGCGCGAGCAGGTTGC GGAAGAAGTGGGGAGTAACGCCGAAGAAGGCAGAAAAAGAG GATGATGAAGAAGAGAGGATACGTCGGGCAGAACGTTTTGAG AGGATCAACCTCGCGTTGCTAAAGCTAGAAGTCTGCAGAAAG AACAATCATTCATCTCATGACACAAGGGGGTGGGCGTCACCA ACAAGCGACTTGGACTCACGGTACGAAACCAAACCCTGGACT CAGGCATATTCCCCCTCTGGTGCCACCACCGACACCCTTGAC AACGGTTACACTTCATCGATTGATCCCCCACGCTCAAAGTATT GGGACAGGGAAATGGCCGGAGGCACTTCTAAGAGGCATAACT CAAGACCGAGATCACTGTTTCCGCCGCCGCACTCACCCGTCA AAACCTCAGCTGATCCACCGGTGGACGGCCTCATTTACACAC CAGCGAAAACTGCATCGGCACGCAGCGCTTCCTGGATGTTTG AAAGGAGTCCTGATGAGGATAGGTACAACTCGTACTTCATGGA CGCAAACTCACGGCTGCAGGAACTCCGTGTATGTGATTCAAT GGCGGCGAAAAACTTTGCACGTGATCTCTCGTC

TABLE 2.8: **Table of *FPC6* target sequences for RNAi.**

pLew100 vector for inducible expression: pSL-FPC6-pLew100, 406bp sequence of FPC6 was used, as seen in Table 2.8.

The second RNAi sequence was designed by Dr Brooke Morriswood and cloned into a p2T7$^{Ti:TAblue}$ plasmid (Alibu et al., 2005) which integrates into the rRNA locus. The plasmid was received by post on filter paper in a 1cm drop. I cut out half the circle and placed it in a 1.5mL tube with 10μL of sterile H_2O. This was left at RT for 1 hour then centrifuged at 14,000 x g to recuperate the liquid. XL1 *E. coli* were transformed with 8μL of the recovered liquid containing the plasmid. PCR on colonies was carried out using primers specific for the FPC6 sequence: Forward 1108 and reverse 1109 (see Table 2.6).

I transfected both PCF and BSF Tb427 SmOx already endogenously tagged with a 10xTy1 N-terminal tag on *FPC6*, with this RNAi construct. Induction of RNAi *FPC6* was made by the addition of tetracycline at 1 and/or 10μg/mL. The sequence of *FPC6* used for this construct is 706bp; seen in Table 2.8.

2.5.14 Extraction of RNA

Starting with 10x10^8 PCF cells or 2x10^7 BSF cells, trypanosomes were centrifuged at 800 x g for 10 minutes at 4°C, washed once in 1xPBS (vPBS for BSF) at RT. The supernatant was discarded and the pellet was well re-suspended in 0.5mL of TRIzol or Isol-RNA Lysis Reagent (5 PRIME 2302700) 400μL for 2x10^7 BSF cells. The pellet was then stored at - 80°C for up to 1 month. The tube was incubated for 5 minutes at RT, then 0.1mL of chloroform was added (0.2mL for 1mL of TRIzol). The tube was mixed vigorously (by vortex) for 15 seconds, before centrifugation at 4°C for 20 minutes at 12,000 x g. The RNA remained exclusively in the upper aqueous phase which was transferred to a fresh eppendorf tube. The RNA was precipitated by mixing with 250μL of isopropyl alcohol (or isopropanol); 0.5mL per 1mL of TRIzol and incubated for 1 hour at -80°C. The tube was then centrifuged at 4°C for 10 minutes at 16,000 x g and the supernatant discarded. 0.5mL of 100% isopropanol (or 70% ethanol) was added to the RNA pellet (1mL for 1mL of TRIzol) and the tubes were stored at -20°C. When ready for use: the tubes were centrifuged at 7,500 x g for 5 minutes at 4°C, and the pellet is re-suspended in 50μL ddH_2O (Aguettant, 600500).

2.5.15 Treatment of RNA with DNAase

Prior to RT-PCR, the extracted RNA samples were subjected to treatment with Turbo DNA-free^{TM}(Invitrogen, AM1907). To 4μg of RNA, 1μg Turbo DNAase was added, plus Turbo DNAase 10x buffer and made up to 50μL with sterile ddH_2O (Aguettant, 600500) and incubated at 37°C for 30 minutes. The addition of 2μL DNAase inactivation reagent was added to stop the reaction and incubated for 5 minutes at room temperature, before centrifugation at 10,000 x g for 90 seconds. The supernatant was transferred to a fresh tube, this was the RNA fraction.

Protein / construct	Sequence (5' - 3')	ID number
FPC6 WT - wild type protein	F: CAAGAGAGTCGTGGTACTG R: GTATGCGAGGCAACACTTC	210 211
Recoded RNA T1 FPC6	F: ACAGGAAGGATGTGAAGGCG R: ACCTTGGGAGGTCATCCGTA	1480* 1481*
Recoded RNA T1 FPC6	F: GTAGAACGGAGGGCAGTCAC R: GTGCTAGTGCCGGTAGTGTT	1482* 1483*
Recoded RNA T1 FPC6	F: ATGTGAAGGCGGTGGATCTG R: ACGGGGAGTGGGATAGAACA	1484* 1485*
Recoded RNA T2 /T3 FPC6	F: GAAAGAGCAGCCCAAAGTGC R: AAGCTGCGTTCCTTACTGCT	1472* 1473*
Recoded RNA T2 /T3 FPC6	F: AGTAGAGGTAGTGGCCGGAG R: AGGCCGATAGTTCACTTGCC	1474* 1475*
Recoded RNA T2 FPC6	F: AGCCCAAAGTGCTTGCAGTA R: GCACAAGCTGCGTTCCTTAC	1476* 1477*
Recoded RNA T3 FPC6	F: GCGGCATAATTCACGTCCAC R: TTGGCTGCCATGCTATCACA	1478* 1479*
18s - ribosomal RNA small subunit	F: ACGGAATGGCACCACAAGAC R: GTCCGTTGACGGAATCAACC	476 477
TERT - telomerase reverse transcriptase	F: GAGCGTGTGACTTCCGAAGG R: AGGAACTGTCACGGAGTTTGC	478 479
Hsp60 - heat shock protein	F: ATGAGGACATGGAGCAGGAT R: CTTCACGGGGTCGACAATAC	480 481

TABLE 2.9: **Table of Primers used in RT-PCR.** * primers designed by Christine Reix.

2.5.16 Semi-quantitative RT-PCR

The purified RNA was used as a template for PCR, with a low number of programme cycles to prevent over-amplification and allow a semi-quantitative measurement of mRNA to be obtained. Primers for RT (reverse transcriptase)-PCR were designed to be specific for either *FPC6* wild-type sequence or *FPC6* recoded sequence; primers were designed in triplicate, targeting different regions of the gene sequence to allow for optimisation in the RT-PCR reaction. A negative control reaction was made with dNTPs to determine if there was any DNA contamination using specific primers for the DNA sequence. Positive and loading controls were used: 18s ribosomal unit, TERT (telomerase reverse transcriptase) and Hsp60 (heat shock protein 60). A kit was used called SuperScript®III One-step RT-PCR with Platinum®Taq (Invitrogen, 12574-018). Each RT-PCR reaction consisted of 25μL 2x reaction buffer (from the kit), 100ng template RNA, 1μL of 10μM forward and reverse primers, 2μL SuperScript Taq polymerase and 20μL H_2O. The PCR program had 25x cycles so as not to over-amplify any RNA present in the sample and to give a semi-quantitative result. The DNA control reaction contained 100ng template RNA, 1μL each of the forward and reverse primers for the DNA sequence, 2.5μL 5nM dTNPs, 1μL Taq G polymerase, 2.5μL thermopol buffer 10x, made up with H_2O to 25μL. A list of primers specific for recoded RNA *FPC6* is found in Table 2.9. PCR reaction products were run on 1% agarose and measurements of amplified nucleic acid was made using G:BOX (Syngene).

2.5.17 Nucleic acid purification

For some BSF transfections a nucleic acid purification step was carried out prior to the ethanol precipitation (see below). PCR products were pooled and an equal volume of Phenol:Chloroform:Isoamyl alcohol (25:24:1) was added and mixed by vortexing for 1 minute at room temperature, until the mix was dense and white in colour. the tube was then centrifuged at 16,000 x g for 5 minutes at room temperature. The supernatant was taken and placed in a fresh tube. An equal volume of Chlorofrom:Isoamyl alcohol (24:1) was added to the supernatant and vortexed for 1 minute to mix. The new mix was then centrifuged for 5 minutes at 16,000 x g at room temperature. The supernatant was taken, Chlorofrom:Isoamyl alcohol (24:1) added in equal volume and the mix and centrifugation steps repeated. The final supernatant was taken and an ethanol precipitation of the DNA was performed.

2.5.18 Ethanol precipitation of DNA

For all transfections, the DNA was prepared by a single ethanol precipitation as described here. Sodium acetate (0.3M final concentration, pH 5.2) was added at a ratio of 1:10 of the original volume and mixed by vortexing well. Three times the original volume of 100% ethanol (kept at -20°C) was added and mixed by inversion. The tube was than placed at either -20°C overnight, or 2 hours at -80°C. The mix

was centrifuged for 30 minutes at rpm max (16,100 x g), at 4°C. The supernatant was removed and the pellet is washed twice with 1mL 70% ethanol (kept at 4°C) by centrifugation for 30 minutes at rpm max (16,100 x g), at 4°C; the pellet was not re-suspended. After the final wash, the tube was opened under a culture hood (sterile) and left to air dry for approximately one hour. The DNA was then suspended in sterile water. Either 10μg of DNA or 4 PCR products were diluted in 10μL sterile H_2O, for one parasite transfection.

2.5.19 Purification of PCR products by S300

The S-300 resin was in 10mM TRIS + 1mM EDTA pH 7.5 - 8. Seven hundred μL of resin was loaded into a column (micro spin Biorad) and the column was inserted into a 2mL collection tube. The tube/column was centrifuged for 1 minute at 700 x g; the column was removed from the collection tube and put it into a new 1.5mL tube. The PCR reaction was added onto the resin and this was centrifuged for 2 minutes at 700 x g. The recovered eluate was the purified PCR product. The resin was removed and discarded from the column and the column was recycled.

2.5.20 Extraction of genomic DNA from *T. brucei*

Cells were counted and 1.5x10^7 cells were taken and pelleted by centrifugation at 1,200 x g for 10 minutes. The cells were washed with 1mL of 1xPBS before centrifuging again for 10 minutes. The pellet was re-suspended in 150μL of lysis buffer: TELT (50mM Tris-HCl pH8, 62.5mM EDTA pH8, 4% Triton X-100) gently by inversion three times to completely re-suspend the cells (not by vortex). The cells were incubated for 5 minutes, then 150μL of Phenol/chloroform/isoamyl alcohol (25:24:1) was added and the tube shaken slowly without vortexing and then centrifuged at 16,000 x g for 5 minutes. The upper phase was collected and transferred to a new tube before adding 150μL of phenol/chloroform 1:1 and shaking gently without vortex. The tube was then centrifuged for 5 minutes at 16,000 x g. The upper phase was precipitated by addition of 300μL absolute ethanol (at -20°C), gently swirled for 15 seconds to mix to see the DNA pellet and then centrifuged for 10 minutes at 13,000 x g. The supernatant was removed and 300μL of 70% ethanol was added (pre-cooled to -20°C) without re-suspending the white pellet. A second wash of 70% ethanol was carried out, centrifuged at 13,000 x g for 10 minutes. The pellet was dried to eliminate any ethanol by evaporation and the pellet was suspended in 100μL of sterile ddH_2O. PCR reactions were made directly using 1μL of sample.

2.5.21 Quantification of DNA/RNA

The absorbance of UV light was measured using UV spectrometry (FLUOstar Omega, BMG LABTECH). Nucleic acids (DNA and RNA) absorb light at 260nm;

the ratio of absorbance 260/280 was checked for purity: ideally 1.8 for DNA and 2 for RNA.

2.6 Protein Production

2.6.1 scFv-*Tb*BILBO1 production

The sequences of the variable regions of immunoglobulin genes from a mouse monoclonal IgM-producing hybridoma, made previously in the Robinson laboratory, were identified and cloned to produce a single chain variable fragment (scFv). The purified IgM was proven to identify *Tb*BILBO1 by IFA and western blot and binds to the C′ terminus of the protein (coiled coil domain). Variable regions of the immunoglobulin genes expressed by the mouse hybridoma were amplified with specific primers, from the cDNA generated from the anti-*Tb*BILBO1 producing hybridoma cells, using RT-PCR and sequenced. The product containing the variable regions of the heavy and light chain genes were assembled into a single chain antibody using overlapping PCR with custom designed primers. The two variable regions, from the heavy and light chains being joined by a linker sequence; the resultant construct was cloned into pJet-5F3-B2-C8 (Aldevron, Germany).

2.6.2 Periplasmic expression of scFv and nanobodies in WK6 *E. coli*

Freshly transformed WK6 colonies were inoculated into 10mL LB + ampicillin (100μg/mL) + 1% glucose and incubated overnight at 37°C, shaking at 250rpm. Terrific broth (TB) medium was prepared for scFv/Nb expression (Pardon, 2014). TB per litre: 2.3g KH_2 PO_4, 16.4g K_2 $HPO_4.3H_2O$, 12g Tryptone, 24g Yeast, 4mL 100% glycerol. One mL of culture was added to 330mL TB + 100μg/mL ampicillin, 2mM $MgCl_2$ and 0.1% glucose, incubated at 37°C, shaking 250rpm, until a mid-log phase of growth OD600 of 0.6-0.9 was reached, to maximise protein yield. scFv/Nb expression was induced with 1mM Isopropyl β-D-1-thiogalacto-pyranoside (IPTG - Pardon, 2014), which binds the lactose repressor (lacI) allowing the lac promotor to transcribe T7 RNA Polymerase which binds the T7 promotor upstream of the gene of interest i.e. scFv/Nb (Studier, 2005) which is then expressed. The culture was incubated for 17 hours at 28°C with shaking at 220rpm. For scFv expression, a range of incubation temperatures (25-28°C) and concentrations of IPTG were tested (0.1-1mM final concentration). scFv/Nb was extracted from the periplasm of WK6 *E. coli* where the oxidising environment contains disulphide bond catalysts and protein chaperones for protein folding (Salema and Fernández, 2013) proteolysis is reduced and purification simpler. Overnight induced cultures were centrifuged for 16 minutes at 4,500 x g. The pellet was re-suspended in 4mL of TES (0.2 M Tris pH8.0, 0.5 mM EDTA, 0.5M sucrose), then shaken for 1 hour on ice at 110 rpm (osmotic shock). Four mL TES/4 (TES diluted 1:4 in water) was added and further incubated on ice

for 1 hour with shaking, then centrifuged for 60 minutes at 4,500 x g at 4°C. The supernatant contained the periplasmic extract with scFv/Nb. A control periplasmic extraction was performed using the same procedure as above, without the scFv/Nb insert in the vector, as a negative control.

2.6.3 Purification of protein by IMAC

Immobilised metal affinity chromatography (IMAC, using and ÄKTA-purifier^{TM}10, GE Healthcare) was used to purify the scFv, Nbs (Pardon, 2014) and *Tb*BILBO1. 1.5mL of His-select ®resin (Nickel affinity gel, Sigma-Aldrich P6611) was equilibrated with PBS: the resin was washed 3 times, centrifuging at 700 x g for 2 minutes between each wash, discarding the supernatant The periplasmic extract was added to the resin, incubated for 45 minutes with gentle shaking, then loaded into a PD-10 column (GE healthcare, cat no. 17-0435-01). The column was washed with 100mL PBS, and the 6xhistidine-tagged protein was eluted with 1mL PBS/0.5M imidazole per 1mL of resin. Imidazole competitively displaced the 6His-tagged Nb bound to Ni ions on the beads of the resin in the column, (Bornhorst and Falke, 2010) releasing the purified protein.

2.6.4 Dialysis of purified protein

Purified elutions were dialysed, initially overnight at 4°C in 1xPBS using Spectra/Por®molecular porous membrane tubing (Spectrum Laboratories Inc, USA) with a cut-off of 3500 daltons (Nb = 15000 daltons), changing the buffer 3 times; the Nbs were stored in 100μL aliquots in 1xPBS or 50% glycerol at 4°C and -20°C. Later dialysis was carried out using Slide-A-Lyzer®cassettes with a 10,000 dalton molecular weight cut-off (Thermo Fischer Scientific^{TM}Ref:87730) in 1xPBS, 10% glycerol, changing the dialysis buffer 4 times every 2 hours; then stored at -20°C, or 4°C when in use.

2.6.5 Quantification of protein

The extinction coefficient of each eluted Nb was determined using ProParam (ExPASy, Bioinformatics resource portal, Swiss Institute of Bioinformatics) calculated from the amino acid sequence; this was then used to measure the absorption of light at 280nm using protein quantification (Omega Fluostar BMG Labtech) or using Nanodrop^{TM} 2000 (Thermo Fisher).

2.7 Western Blot Analysis

Cells were collected, centrifuged at 800 x g for 10 minutes, and washed in 1xPBS for PCF, or V-PBS for BSF. For whole cells, the required number of cells were calculated, then re-suspended in protein sample buffer 2x plus benzonaze ®nuclease (Sigma, Ref. E1014). For cytoskeletons, the washed cells were re-suspended in 1% NP4O, 100mM PIPES, 1mM MgCl for 7 minutes; cytoskeletons were checked by microscopy, then cells were washed in 100mM PIPES buffer before being resuspended in sample buffer 2x (as above). For flagella preparations, the cells were incubated for 15-30 min on ice with 1% NP40 in 100mM PIPES buffer + 1mM $MgCl_2$, 1M KCl containing Benzonase (1:10,000 dilution, Sigma E1014) and protease inhibitors (1:10,000 dilution Protease Inhibitor Cocktail Set III Calbiochem, Ref. 539134-1). Flagella were centrifuged for 5 minutes at 5,000 g at 4°C, the supernatant was removed and flagella were resuspended in 500μL PIPES buffer. Flagella were washed twice in 100mM PIPES buffer + 1mM $MgCl_2$ for 5 minutes, 5000g, at 4°C before re-suspension in sample buffer 2x at the required volume. The samples were boiled at 100°C for 5 minutes then stored at -20°C until required.

Sodium dodecyl sulfate polyacrylamide gel electrophoresis (SDS-PAGE) gels were prepared and samples loaded at $5x10^6$ cells per well. For Nb samples 15% SDS was used, for scFv 12% SDS was used and for FPC6 8% SDS-PAGE was used; with a higher percentage gel corresponding to a smaller sized protein of interest. Samples were separated at 25mA per gel for the stacking (concentrating) portion and then at 35mA for the remaining gel for 90 minutes then transferred in a semi-dry system (BIORAD Trans-Blot®Semi-dry transfer cell 221BR54560) onto Polyvinylidene difluoride (PVDF) membrane and blocked with 5% milk, 0.2% Tween 20 in 1xTBS (blocking solution) for 45 minutes at 25V for scFv and Nb, and for 60 minutes for FPC6 (to allow efficient transfer of the larger protein). For detection of the scFv and Nb 3xcMyc tag, an anti-cMyc antibody (rabbit Santa-Cruz, SC-789) was diluted in blocking solution (BS) 1:1000 and incubated with the membranes overnight at 4°C. Membranes were washed in 1xTBS and then BS before probing with a secondary antibody conjugated to Horse Radish Peroxidase (HRP) diluted 1:10000 in BS anti-rabbit (Sigma goat anti-rabbit IgG + IgM A9169) for 60 minutes.

To identify the Ty1 tag, an anti-Ty1 antibody (purified BB2 mouse monoclonal) was diluted 1:50,000 in BS followed by an anti-mouse secondary (HRP). For *FPC6* recoded gene and truncations the anti-cMyc tag was detected using anti-cMyc rabbit (Sigma, Ref. C3956). The following antibodies were also used as primaries: anti-*Tb*BILBO1 1-110 NTD rabbit; anti-*Tb*MORN1 rabbit (Morriswood). Anti-*Tb*SAXO (Robinson) and anti-tubulin (TAT1 mouse, Bastin) were used as loading controls. For all antibodies used refer to Tables 2.2 (primaries against tags), 2.3 (primaries against proteins), and 2.4 (secondaries). Revelation was using Image Quant LAS 4000 (luminescent Image Analyser) or Chemidoc^{TM}(Bio-Rad).

Antibody	Species made in	Immunoglobulin class	Manufacturer/ ref.	dilution
Anti-FPC6	Chicken, from eggs	IgY	Robinson lab, H018 (Eurogentec)	IF: 1:500 /250 /100 WB: 1:500 /1000 /2000 /2500 /5000 /10000 purified ADEM-KIT IF: 1:10-200
Anti-FPC6	Rabbit	polyclonal	Morriswood, 420	IF: 1:50 WB: 1:100
Anti-FPC6	Rabbit	polyclonal	Morriswood, 421	
Anti-FPC6	rabbit	polyclonal	Robinson, 1730024 (D0, D53, D74)	IF: 1:10 /100 /200 /250 /500 /1000 /2000 /5000 WB: 1:100 /250 /1000 /2000 /4000 /6000 /8000
Anti-FPC6	rabbit	polyclonal	Robinson, 1734045 (D0, D53, D74)	

TABLE 2.10: **Table of Antibodies raised against FPC6.**

2.7.1 Nanobodies used as probes in western blot assays

To detect the presence of *Tb*BILBO1 in whole cells: PCF *Tb*427 29.13 wild type, BSF *Tb*427 90.13 wild type, PCF *Tb*427 29.13 pLew100-BILBO1::3cMyc over-expressing *Tb*BILBO1 (induced with tetracycline 1μg/mL, 24 or 48 hours) and BILBO1::6HIS purified protein. To determine which peptide sequence of BILBO1 was targeted by the Nbs, firstly truncations of *Tb*BILBO1 expressed in trypanosomes were prepared and tested (T1: aa1-170, T2: aa1-250, T3: aa171-250, T4: aa251-587), then smaller, overlapping peptide sequences were prepared and using a western blot test to determine more specifically the peptide sequence of *Tb*BILBO1 recognized by the Nbs.

2.7.2 Verification of Nb present in purified elutions

Ten μL from each elution was run on a 15% sodium dodecyl sulfate polyacrylamide gel electrophoresis (SDS-PAGE) gel was stained with Coomassie Brilliant Blue (Instant Blue ^{TM}Expedeon Ltd); the proteins from the second gel were transferred to a polyvinylidene difluoride (PVDF) membrane using a semi-dry transfer method (BIORAD Trans-Blot ®Semi-dry transfer cell 221BR54560) and a western blot was performed using anti-HIS and anti-HA antibodies to detect the Nb.

2.8 Testing anti-FPC6 antibodies

A number of antibodies raised against FPC6 were tested (see Table 2.10).

Previously, in the Robinson laboratory, an antibody against FPC6 was purified from chicken eggs as first described by Polson et al., 1980; this extracted the IgY fraction, reference H018. This antibody was tested by western blot (WB) and immunofluorescence (IFA) on PCF and BSF cells using whole cell (WC) and cytoskeleton (CSK) extraction. The IgY antibody was later purified using ADEM-KIT (Ademtech, 04400) and re-tested by WB and IFA. A secondary antibody, anti-chicken IgG(H+L) (Molecular probes, A11039) was used which binds to IgY.

Two anti-FPC6 antibodies made in rabbit (420 and 421) from Dr Brooke Morriswood were also tested. These had previously been tested by Morriswood with limited success due to non-specific labelling of the FAZ proteins.

Two further anti-FPC6 antibodies were ordered by the Robinson laboratory from Covalab, using 3 peptide sequences identified using BLAST searches of the full sequence of FPC6 to determine short amino acid sequences that were specific to FPC6:

Peptide 1 (aa91-107) C-YFSTPESNSEEGSVDSR-coNH2;
Peptide 2 (aa267-281) C-KIPIQESRGTDYKEN-coNH2;
Peptide 3 (aa878-891). C-FERSPDEDRYNSYF-coNH2.

Two rabbits (1730024 and 1734045) were immunized with the 3 peptides and good immunoreactivity was determined at day 53 post injection. Testing of pre-immune serum, and serum collected on days 53, 74 and 116 post-immunization were tested by WB and IFA, using anti-rabbit HRP (Sigma, 9169) for WB and anti-rabbit fluor 594 (Invitrogen, A11012), see Table 2.10 for dilutions tested.

2.9 ELISA Assays

An enzyme-linked immunosorbent assay (ELISA) was carried out to confirm the ability of the purified Nb to bind to *Tb*BILBO1 protein *in vitro* (Salema and Fernández, 2013). A 96 well plate (Nunc MaxiSorp®) was coated with Nb, at a range of concentrations from 160μ/mL to 1.9x10^{-5} μ/mL, overnight at 4°C. Wells were purified Nbs to bind to *Tb*BILBO1 protein saturated in 0.2% gelatine for 1 hour at 37°C, and then washed with 0.05% Tween 20 in 1xPBS, before incubating truncated, soluble *Tb*BILBO1 protein (aa 1-110) at 37°C for 1 hour. Wells were washed (as above), then incubated with anti-*Tb*BILBO1 (aa 1-110 rabbit 151-70-28 bleed 1) 1:100 in 1xPBS, at 37°C for 1 hour, washed again, then incubated with an anti-rabbit IgG (H+L whole molecule HRP, Sigma A9169) 1:10000 for 1 hour at 37°C, for detection. Wells were washed and revealed with chromogen substrate buffer (ABTS (2,2'-azino-bis(3-ethylbenzothiazoline-6-sulphonic acid)), citric acid, 1M NaOH, H_2O_2 30%), then stopped with Block Buffer (10 mM NaOH 1M, 0.35% hydrofluoric acid, 1mM EDTA (ethylenediaminetetra acetic acid). A spectrophotometer (Fluostar Omega, BMG Labtech) was used to measure the absorbance of light at 405nm giving a quantification of the result.

2.10 Surface Plasmon Resonance Assays

Surface plasmon resonance (SPR) was used to measure the binding affinity of the nanobodies to *Tb*BILBO1 purified protein, the benefits being it is measured in real-time and is label-free (Marschall et al., 2015). SPR analysis was carried out at the Institut Européen de Chimie et Biologie (IECB), Bordeaux, using a Biacore T200. Previously purified *Tb*BILBO1::6HIS protein (see above) was immobilised in a dextran matrix on a Series S, sensor chip CMS (CM dextran general purpose; GE healthcare 180809DD Lot no. 10266084), supporting a gold layer for SPR. The chip was first primed using EDC (1-Ethyl-3-(3-dimethylaminopropyl) carbodiimide) + NHS (N-hydroxysuccinimide) at a flow rate of 5μL/minute to produce carboxymethylated dextran. *Tb*BILBO1-6HIS (500μg/mL) was diluted in HBS-EP+ Buffer pH7 10x (0.1M HEPES, 1.5 M NaCl, 0.03M EDTA and 0.5% v/v Surfactant P20) to a

concentration of 50μg/mL, then flowed over the chip at a rate of 5μL/minutes for 630s. Ethanol amine (HCl, IM pH8.5 GE Healthcare) was injected for 420s to remove unbound *Tb*BILBO1 protein and to bind unbound or exposed carboxyl groups. A test regeneration was performed using 10mM glycine-HCl pH 2.1 (GE healthcare 10mM glycine HCl pH2.1 LOT NO. 10220772) at 30μg/minute for 30 seconds with *Tb*BILBO1 alone to ensure no loss of signal. Each Nb was drop dialysed on filter paper with running buffer (RB = HBS-EP+) in a petri dish half full of RB, at 4°C in fridge for 1 hour, then diluted as necessary to obtain 500nM solutions. The K_D (dissociation constant) was calculated for each Nb over an average of at least three separate recordings, with regeneration of the chip between each Nb sample.

2.11 Statistics

Experimental data for growth curves and cell counts are representative of at least n=3 independent experiments with values represented as mean and Standard error of the mean (SEM). Student t-test was used to determine differences between values, with statistical significance given as $p < 0.005$ and $p < 0.001$.

Chapter 3

Results Part One: FPC6

3.1 *In silico* analysis of FPC6, Tb927.4.3120

3.1.1 A *Trypanosoma* specific protein

As described in the introduction, FPC6 was identified as a *Tb*BILBO1 binding protein through a yeast 2-hybrid screen. Bioinformatical analysis of FPC6 revealed orthologues present only in *Trypanosoma* spp., using a nucleotide sequence database search, BLASTn (NCBI, 2019a). 100% identity was seen within *Trypanosoma brucei brucei* strains (Lister 427 and TREU 927) and therefore an assumed 100% identity with *T. b. rhodesiense* according to the reported similarity in the genome sequence between *T. b. rhodesiense* and *T. b. brucei*. (Wellcome Sanger institute, 2019). A 99.2% sequence identity seen with *T. b. gambiense* also indicates a close similarity in genome sequence with this sub-species, as shown in the phylogenetic tree calculated by phylogengy.fr using Maximum Likelihood, in Figure 3.1.A. This phylogram was constructed from the syntenic orthologues of FPC6 found in *Trypanosoma brucei Lister strain 427*, *Trypanosoma brucei gambiense* DAL972, *Trypanosoma congolense* IL3000 and *Trypanosoma evansi* strain STIB 805, as reported on TriTrypDB, 2019.

BLASTp (NCBI, 2019b) gave further information regarding conserved proteins with similar amino acid sequences: 99% amino acid sequence identity between *T. b. brucei*927 FPC6 and *T. equiperdum* IVM-t1 (Davaasuren et al., 2019). *Trypanosoma grayi* DQ04, a parasite of *Crocodylus niloticus* has only 46% similarity in amino acid sequence to *T. b. brucei*, similar to *T. rangeli* (a parasite of rodents in South America) with 45% similarity. *T. cruzi* strains have no more than 37% identity, fitting with their closeness to *T. grayi* as opposed to *T. b. brucei* (Kelly et al., 2014). These *in silico* analyses recapitulate the phylogenetic findings from Chapter 1, Figure 1.1, in that *T. brucei*, *T. evansi* and *T. equiperdum* are very closely related compared with *T. congolense*, *T. vivax* and other kinetoplastids.

3.1.2 Domain analyses showed low prediction

Information about the function of a protein can be determined form its primary sequence and specific domains. To try to determine the tentative function of FPC6

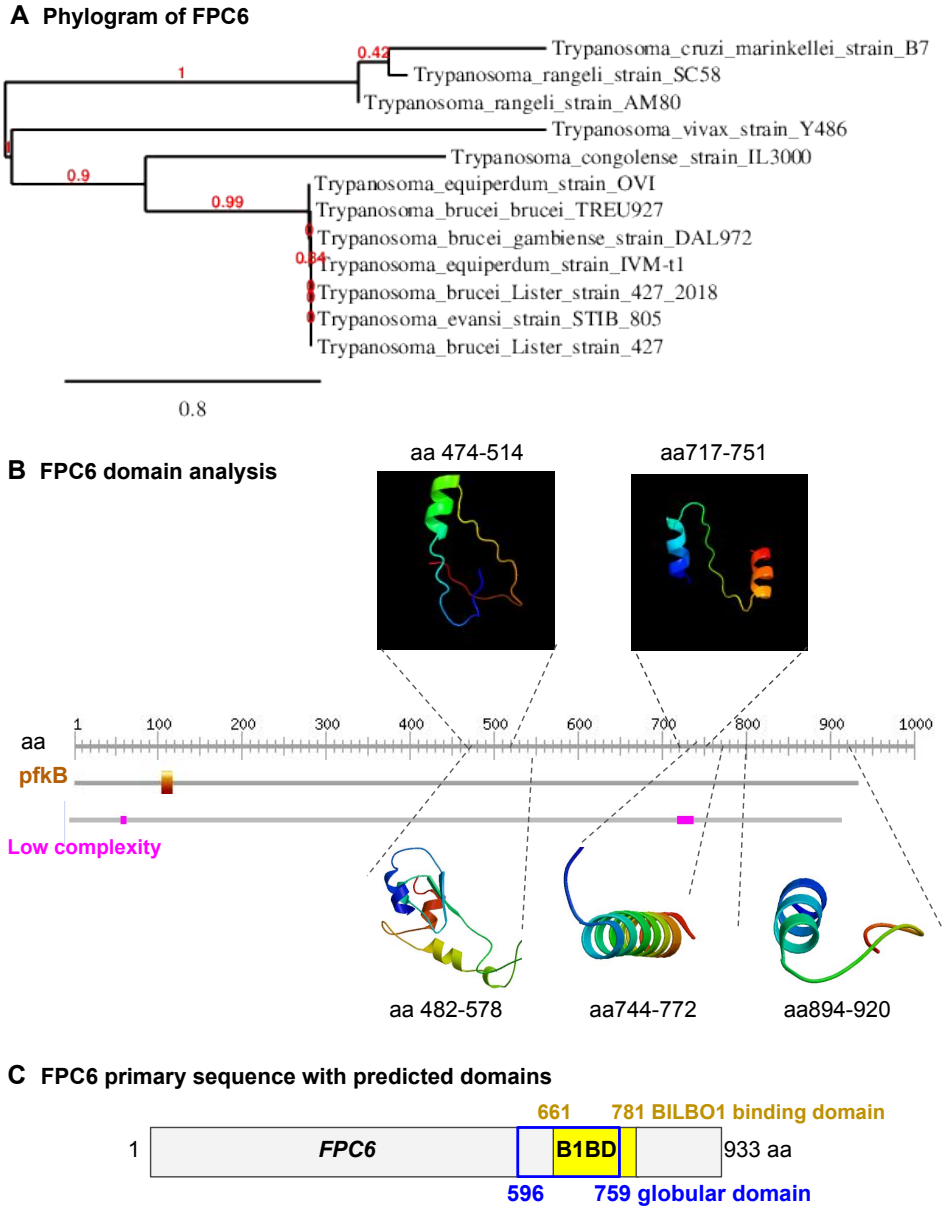

FIGURE 3.1: **Phylogenetic tree of FPC6 orthologues and predicted domain analysis.** **A** Sequences taken from TriTrypDB, 2019 and NCBI protein BLAST (NCBI, 2019b). Calculations made by Dereeper et al., 2008 and Dereeper et al., 2010 on phylogeny.fr **B** Predicted domain searches using prosite.expasy.org, swissmmodel.expasy.org, Phyre[2] and SMART. **C** The primary sequence of FPC6 with predicted domains used in this study.

in silico, I screened a number of databases to determine any predicted domains.

FPC6 is a protein comprised of 933 amino acids. It was shown, in an earlier yeast 2-hybrid assay, that the *Tb*BILBO1 binding domain of FPC6 was from amino acids (aa) 661-781 (see Chapter 1.4.10). Analysis of the amino acid sequence on the NCBI conserved domain search engine (NCBI, 2019c) gave no predicted domains. Interpro (EMBL-EBI, 2019) analysis also gave no predicted protein family, domains or function. The ExPASy, Prosite engine (SIB, 2019a) gave a short signature between aa 105-118: DSrGGGDnigAAAA. This is a pfkB family of carbohydrate kinases signature 2, seen as the orange box in Figure 3.1.B. From a Phyre2 analysis (Kelley et al., 2015) the two models with the highest confidence had 33.3-33.7% and 20-31% identity, respectively. The ribbon diagrams of these two models are shown in Figure 3.1.B; the sequence aa 474-514 was revealed as a pyruvate kinase C-terminal domain-like fold, and aa 717-751 was modelled on a sugar cane carbohydrate binding protein. Using swissmodel (SIB, 2019c) three short regions were allocated a predicted structure, as seen in the ribbon diagrams in Figure 3.1.B; however these predictions were based on only a 17.24-29.3% similarity. SMART (a Simple Modular Architecture Research Tool; Letunic and Bork, 2018) classified two zones as low specificity: aa 62-69 and aa 734-754. A globular domain was predicted from aa 661-781 and this was included with the BILBO1 binding domain (B1BD) when making FPC6 truncations, see 3.1.C.

Preliminary data (see Chapter 1.4.10) had shown that FPC6 co-localised to the centriole and basal body when expressed in mammalian U-2 OS (an heterologous system). Micrototubule binding proteins are often repeated and basic, therefore, a search for basic repeats was made using RADAR (EMBL-EMI, 2019). Data revealed that FPC6 domains aa 627-644 and aa 722-739 contained higher concentration of basic amino acids: H = histidine, R = arginine, and K = lysine. Data from Nett et al., 2009 and Urbaniak et al., 2013 showed that FPC6 had 12 phosphorylation sites at 140S, 144S, 213S, 82S, 786S, 870S, 135T, 139T, 143T, 781T, 864T and 868T (TriTrypDB, TriTrypDB, 2019). Phosphorylation can induce conformational changes in proteins, influence protein-protein interactions and indeed degradation.

One interesting finding was a Spermatozal protamine family motif from aa 622-646, using motif scan (SIB, 2019b). In *T. brucei* FPC6 is located near the base of the trypanosome flagellum and it is reported by Coutton et al., 2018 that human spermatozoa and *T. brucei* share an extremely conserved axoneme. All in all, very limited data regarding predicted domains was obtained and a final, working primary sequence showing the only predicted domain: a globular domain from aa 596-759 (globplot.embl.de), as seen in Figure 3.1.**C**. This annotated sequence was used to design truncations for experiments in the rest of this study on FPC6.

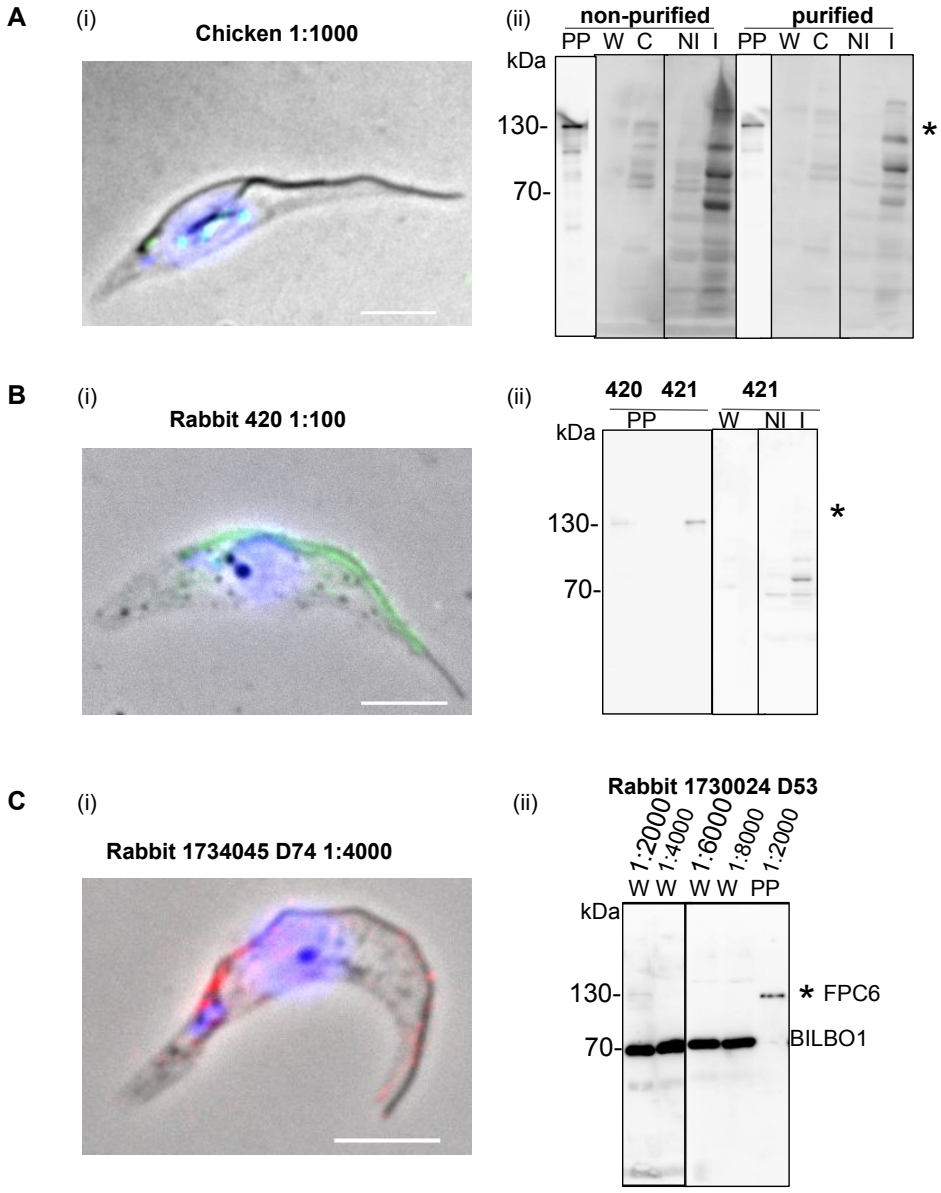

FIGURE 3.2: **Testing of anti-FPC6 antibodies.** **A** Anti-FPC6 chicken from eggs IgY H018 Eurogentec, tested by (i) IFA, seen at FPC and spindle poles, and (ii) WB, non-specific. **B** Anti-FPC6 rabbit 420 and 421 (i) IFA gave a FAZ signal and (ii) WB, FPC6 was not detected. **C** Anti-FPC6 rabbit 1730024 and 1734045 (Covalab), by (i) IFA at the FPC but not clean and by (ii) WB signal too low for use. PP=50ng 6HIS::FPC6 purified protein; D=day, W=whole cells, C=cytoskeletons, NI=non-induced, I=induced. Scale bar = 5μm.

3.2 Location of FPC6 in *T. brucei*

To be able to characterise FPC6, it was first necessary to be able to determine accurately, its location in trypanosomes precisely. To this end, it was necessary to be able to do so consistently in fixed trypanosomes by immunofluorescence assays (IFA) and also in western blot analysis (WB) of denatured protein. A reliable and accurate antibody was required either against FPC6 endogenous protein or FPC6 needed to be tagged *in situ* and an antibody used against this tag.

3.2.1 Anti-FPC6 antibodies were not suitable for use

I tested several antibodies raised against FPC6 and summarise the results here. The list of antibodies can be found in Table 2.10.

Five antibodies were tested in total:
1. Chicken, from eggs IgY (H018, Eurogentec); from the Robinson laboratory
2. Rabbit: two rabbits (420 and 421); from Brooke Morriswood (Würzburg, Germany)
3. Rabbit: two rabbits (1730024 and 1734045, Covalab); from the Robinson laboratory

1. The first antibody to be tested was an antibody made in Chicken and recovered and purified from eggs; the immunglobulin class was IgY. I tested the ability of this antibody to detect FPC6, before and after I purified it using ADEM-KIT (see Methods 2.8). By IFA, with whole cells a non-specific labelling of the entire cell was seen. With detergent-extracted cells i.e. cytoskeletons, a signal could be seen in the location of the Flagellar Pocket Collar in both PCF and BSF. The best dilutions were 1:100, 1:250 and 1:500. However extra labelling could also be seen within the trypanosome cells, including at the spindle poles (see Figure 3.2.**A**.**i**.). Unfortunately, the location given by fluorescence was not consistent between experiments and in PCF whole cell (W) the signal was not specific at all. Purification of the chicken anti-FPC6 antibody gave very similar results on IFA, with a signal at the FPC, but some cells still showed extra labelling. By western blot, the chicken anti-FPC6 recognised purified 6HIS::FPC6, in *T. brucei* samples, a possible band was seen when FPC6 was over-expressed in the cells (GFP::FPC6) at the predicted size, however multiple bands were seen, so it was not possible to determine if this was specific or not; with cytoskeleton samples by WB, no detection of FPC6 was seen (see Figure 3.2.**A**.**ii**.). The chicken anti-FPC6 antibody was not used for any further experiments as it was deemed to be neither consistent nor specific enough.

2. Two polyclonal antibodies from rabbit, affinity purified, were given as a kind gift to the Robinson laboratory by Brooke Morriswood for this study. Preliminary testing of these antibodies by Morriswood concluded that they were not specific for FPC6. I tested both of these antibodies on *T. brucei* by IFA and WB. By IFA, both

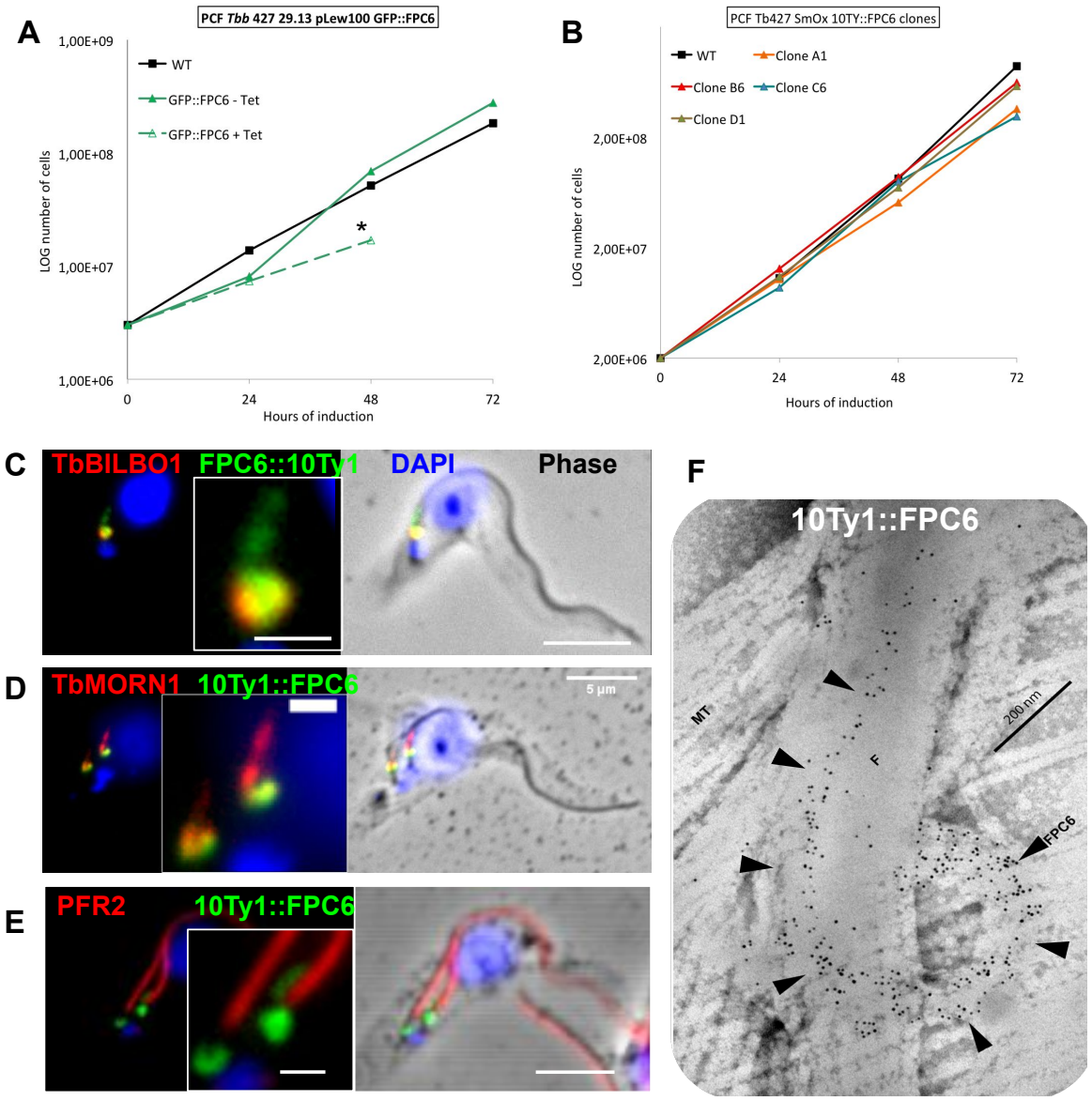

FIGURE 3.3: **FPC6 forms a hook-shaped structure at the base of the flagellum in *T. brucei*** **A** GFP::FPC6 expression was lethal after 72hpi; **B** 10Ty1::FPC6 clonal cell lines grew as the WT; **C** FPC6::10Ty1 forms a hook-shaped structure that partially co-localised with *Tb*BILBO1; **D** 10Ty1::FPC6 co-localised with the strongly with the head of the hook of *Tb*MORN1 and also along the shank; **E** curving around the base of the flagellum as it exits the cell (PFR2); **F** EM of 10Ty1::FPC6 curving around the FPC and extending up the flagellum. IFA scale bar = 5μm; inset = 1μm; IEM scale bar = 200nm.

anti-FPC6 rabbit 420 and 421 gave a strong FAZ signal on cytoskeletons, as seen in Figure 3.2.**B**.**i**.; whole cells gave a non-specific signal across the entire cell with PCF and BSF; with BSF cytoskeletons no labelling was seen. On WB, rabbit 421 gave a stronger signal with purified 6HIS::FPC6 protein, but using *T. brucei* whole cells samples, no band was seen around the expected size. Multiple attempts, dilutions and addition of a 1mM NaCl wash, did not improve the results. Therefore these antibodies (rabbit 420 and 421) were no longer used for any further experiments due to the lack of a specific IFA or WB signal.

3. Due to the previous antibodies being unsuitable for use, a polyclonal antibody was ordered from Covalab (Villeurbane, France). Two rabbits (1730024 and 1734045) were immunized with three short peptides from the FPC6 sequence: aa 91-107, 267-281, 878-891 (see Methods Section 2.8). Serum was collected from the rabbits on day 0 (pre-immune), day 53, day 74 and day 116. I tested rabbit sera from all time points on IFA and western blot. By IFA, a signal was seen at the FPC but also within the cell and sometimes along the FAZ. For rabbit 1730024 the best time point was day 74 with dilutions 1:4000 and 1:8000 and for rabbit 1734045 the best signal was given at day 74 with dilutions 1:1000, 1:4000, 1:6000 and 1:8000; an example is given in Figure 3.2.C.i. By western blot, rabbit 1730024 was able to recognise purified 6HIS::FPC6 protein, however using trypanosome whole cell samples, results were either negative, had a lot of background, or a possible weak signal only. Neither of these antibodies were specific enough to be used in this study.

At this point, I had commenced the cloning for an endogenously tagged FPC6 *T. brucei* cell line and once this was successful, I stopped any further testing of antibodies. The tag used was Ty1 and we had a very specific monoclonal antibody in the laboratory to detect this tag on IFA and WB, see Table 2.2 and Results below.

3.2.2 GFP::FPC6 expression is lethal at 72 hours

Initial tagging of FPC6 in PCF had been carried out by Marie Eggenspieler (Robinson laboratory) using a pLew100-GFP::FPC6 PCF cell line i.e. over-expressing GFP (green fluorescent protein) tagged FPC6 in the cell. I re-tested clone D5H7 from this cell-line: the tag was detectable, however, cells died after 72 hours post induction (hpi) with tetracycline, see Figure 3.3.**A**. It has been shown previously in the Robinson laboratory that tagging of essential cytoskeletal proteins in *T. brucei* with a GFP tag can lead to aberrant location of the protein in the cell and cell death (data not published). Therefore no further studies were done with this cell line. This FPC6::GFP cell line was, however, used at 24 and 48hpi to provide samples for western blot as a GFP positive control at the predicted size of FPC6, when testing other antibodies specific for FPC6.

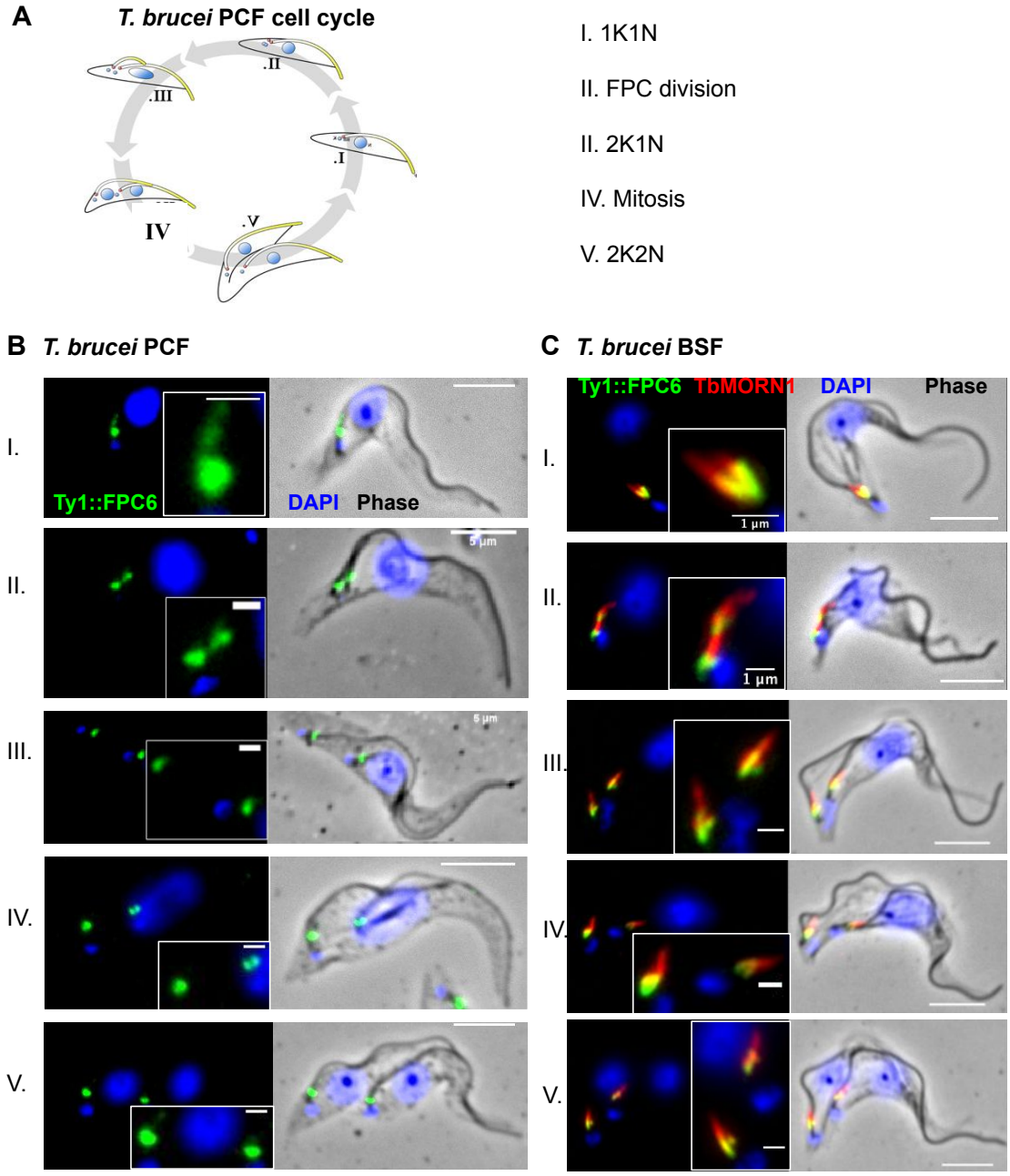

FIGURE 3.4: **FPC6 is present throughout the cell cycle in PCF and BSF *T. brucei*. A** 10Ty1::FPC6 was located at the FPC/Hook complex throughout all phases of the cell cycle in PCF; **B** 10Ty1::FPC6 follows the same localisation in the BSF, seen here co-localising strongly at the head of *Tb*MORN1 and tapering into the shank throughout the cell cycle. IFA scale bar = 5μm; inset = 1μm.

3.2.3 10Ty1::FPC6 forms a hook-shaped structure

Due for a need to identify FPC6 protein in vivo in trypanosomes and the fact that the FPC6 antibodies were unsuccessful and the GFP tag had an affect on cell growth, a small endogenous tag was required. Recent success by Dean et al., 2015b as seen on the tryptag.org website, showed how a 10xTy1 tag could be easily and successfully added to trypanosome gene *in situ*, even for low expressed genes, which due to the initial inability to detect clearly with the antibodies tested, could be a possibility. I successfully placed an endogenous 10xTy1 tag (Brookman et al., 1995, Bastin et al., 1996) on FPC6 at both the N- and C-termini, to determine if the location of the tagged protein in *T. brucei* and the growth of the cells was affected by which terminus the tag was placed. I chose Tb427 SmOx because it was a single marker cell line (puromycin; Poon et al., 2012) allowing the maximum potential for a range of additional constructs to be transfected into the same cell line using a range of other antibiotic selection drugs; this cell line contains the tetracycline inducible system: T7 promoter and TET repressor allowing induction of RNAi (Wirtz et al., 1999). In PCF, I saw no effect on cell growth with either 10Ty1::FPC6 or FPC6::10Ty1, see Figure 3.3.B showing the growth curve for four clones (A1, B6, C6 and D1) tagged with 10Ty1 on the N-terminus, resembling the growth curve of the wild-type parental cells (WT). The location of the fluorescent signal in both instances was identical, an example of the C-terminus tag is shown in Figure 3.3.C. The tag confirmed the location and distinctive hook-shaped structure, as seen in preliminary data published by Morriswood et al., 2013 and TrypTag.org (Dean et al., 2015a). The signal was best in detergent-extracted cells (i.e. cytoskeletons) therefore these were used in all future IFA. I also decided to use the N-terminal tag for both PCF and BSF for all further experiments.

3.2.4 FPC6 co-localises with *Tb*BILBO1 and *Tb*MORN1

To determine more precisely the location of FPC6 in relation to other known FPC and hook complex (HC) proteins, I carried out co-labelling with different antibodies using IFA. *Tb*BILBO1 is located on the FPC and MTQ and FPC6 was observed partially co-localising with *Tb*BILBO1, Figure 3.3.**C**. *Tb*MORN1 protein forms a distinctive hook-shaped protein structure within the hook complex (Morriswood et al., 2009); FPC6 co-localised exactly with the head of *Tb*MORN1 tapering into the shank of the hook, see Figure 3.3.**D**. To determine the location of FPC6 in relation to the flagellum, an antibody against the Paraflagellar rod (PFR2; see Table 2.3) that passes along the length of the flagellum after the flagellum has exited the cell, was used. In Figure 3.3.E, the structure formed by 10Ty1::FPC6 protein can clearly be seen at the base of the flagellum and the shank of FPC6 is seen continuing along the PFR2. Immuno-electron microscopy (IEM) was used to explore in more detail the precise location of FPC6, using 5nm gold beads against the Ty1 endogenous tag. The gold beads were seen at the FPC curving around the flagellum, then extending distally

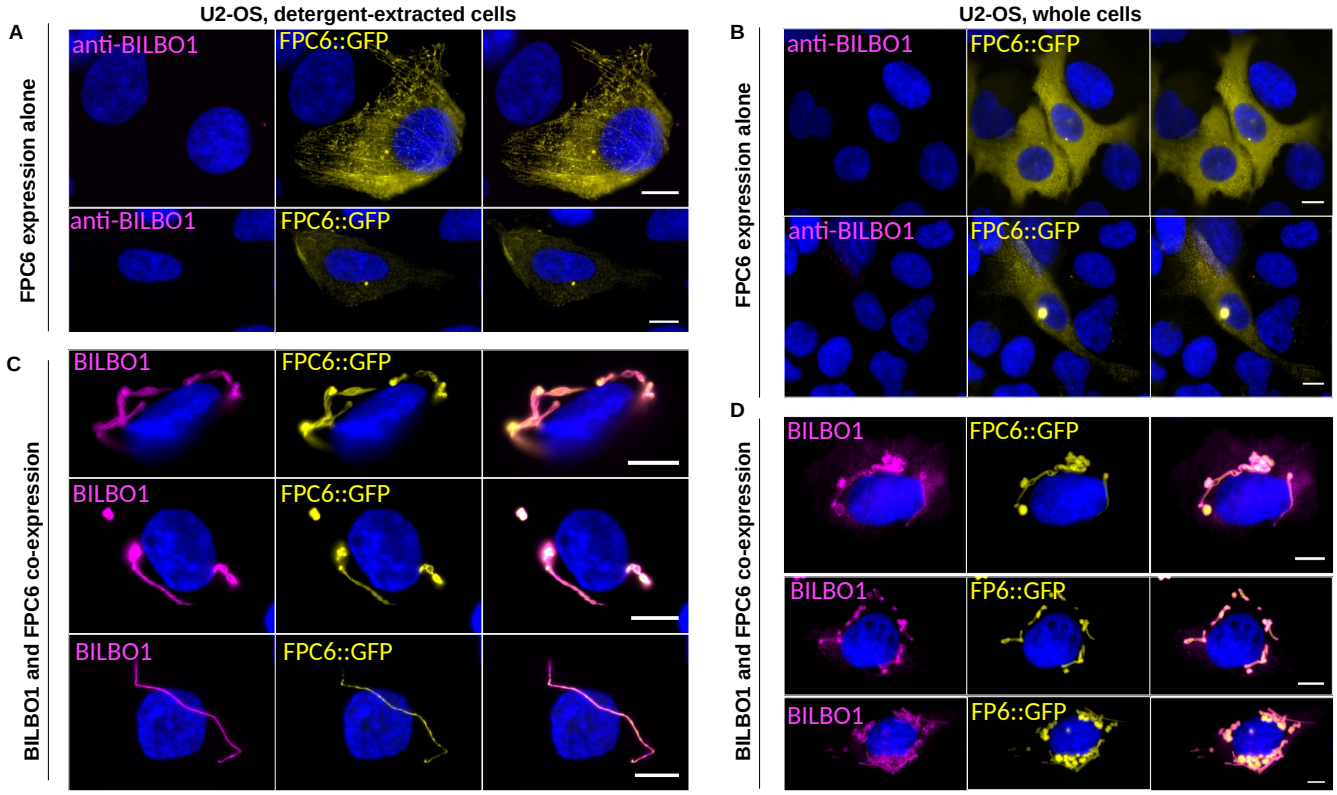

FIGURE 3.5: **Expression of FPC6 in U-2 OS cells. A** FPC6::GFP expressed alone in U-2 OS cells was seen throughout the entire cell with a concentration at the centrosome in both detergent extracted cells and **B** whole cells. **C** and **D** When *Tb*BILBO1 was co-expressed with FPC6::GFP, the GFP signal was seen only on the polymers formed by *Tb*BILBO1 giving rise to distinct shapes with globular heads present in the cytoplasm. Scale bar = 5μm.

along the flagellum, gradually diminishing and tapering off, see Figure 3.3.F. Additional electron microscopy images of the location of FPC6 protein in PCF *T. brucei* cytoskeleton preparations can be seen in Appendix A, Figure A.1 and on isolated flagella in Appendix A, Figure A.2. Electron microscopy images showing the co-labelling of FPC6 and *Tb*MORN1 on isolated flagella can be seen in Appendix A, Figure A.4 and co-localisation with *Tb*BILBO1 on isolated flagella in Appendix A, Figure A.3.

3.2.5 FPC6 is located at the hook complex throughout the cell cycle

I observed the labelling of 10Ty1::FPC6, in both PCF and BSF in detergent-extracted cells fixed in methanol, throughout the cell cycle using an anti-Ty1 antibody (BB2; see Table 2.2). *T. brucei* goes through a clearly determined sequence of cell cycle events, shown in the schematic in Figure 3.4.A. of the *T. brucei* PCF cell cycle depicting the main phases I-IV (adapted from Ooi and Bastin, 2013). In summary: starting in G1 phase there is a single kinetoplast (K), single nucleus (N) and single flagellum (1K1N), the K is first to divide, along with a new flagellum and flagellar pocket to give a 2K1N cell; next the nucleus divides by mitosis to give A 2K2N cell. In the BSF, the main phases are the same as for PCF, but the linear order of the kinetoplast and nucleus (posterior to anterior) that are different, specifically that the 2K2N stage in PCF is KNKN, whilst in BSF it is KKNN, as explained in Chapter 1.3 and Figure 1.7.

In Figure 3.4.**B**, (left panel) the main phases of the cell cycle are described and is based on number of kinetoplasts (K) and nuclei (N) per cell. Expression of FPC6 can be seen with the green fluorescent signal, which often appeared to be strongest and exhibited the most hook-like shape in the 1K1N phase, possibly related to an increase in incoming FPC6 protein prior to division. As the new flagellum was seen starting to grow and a new FPC was being formed at its base, so too could the FPC6 signal be seen to become two structures of equal size and intensity. As the kinetoplast divided and then the cell went through mitosis, the signal for FPC6 was always at both FPC, although the hook-shape was often less obvious.

In BSF Tb427 SmOx, I also endogenously tagged FPC6 at the N-terminus with 10xTy1; this was not straightforward and took many transfection attempts to obtain positive clones (see Trouble-shooting, Chapter 5.2.14). As for the PCF, I checked that the tag had no effect on cell growth compared with the WT. The location of 10Ty1::FPC6 in BSF was the same as in PCF: at the FPC/Hook complex. However an interesting observation in BSF, was that the "head" of the hook appeared to be more pointed in shape compared with the rounder "head" in PCF, as can be seen in Figure 3.4.**C**.

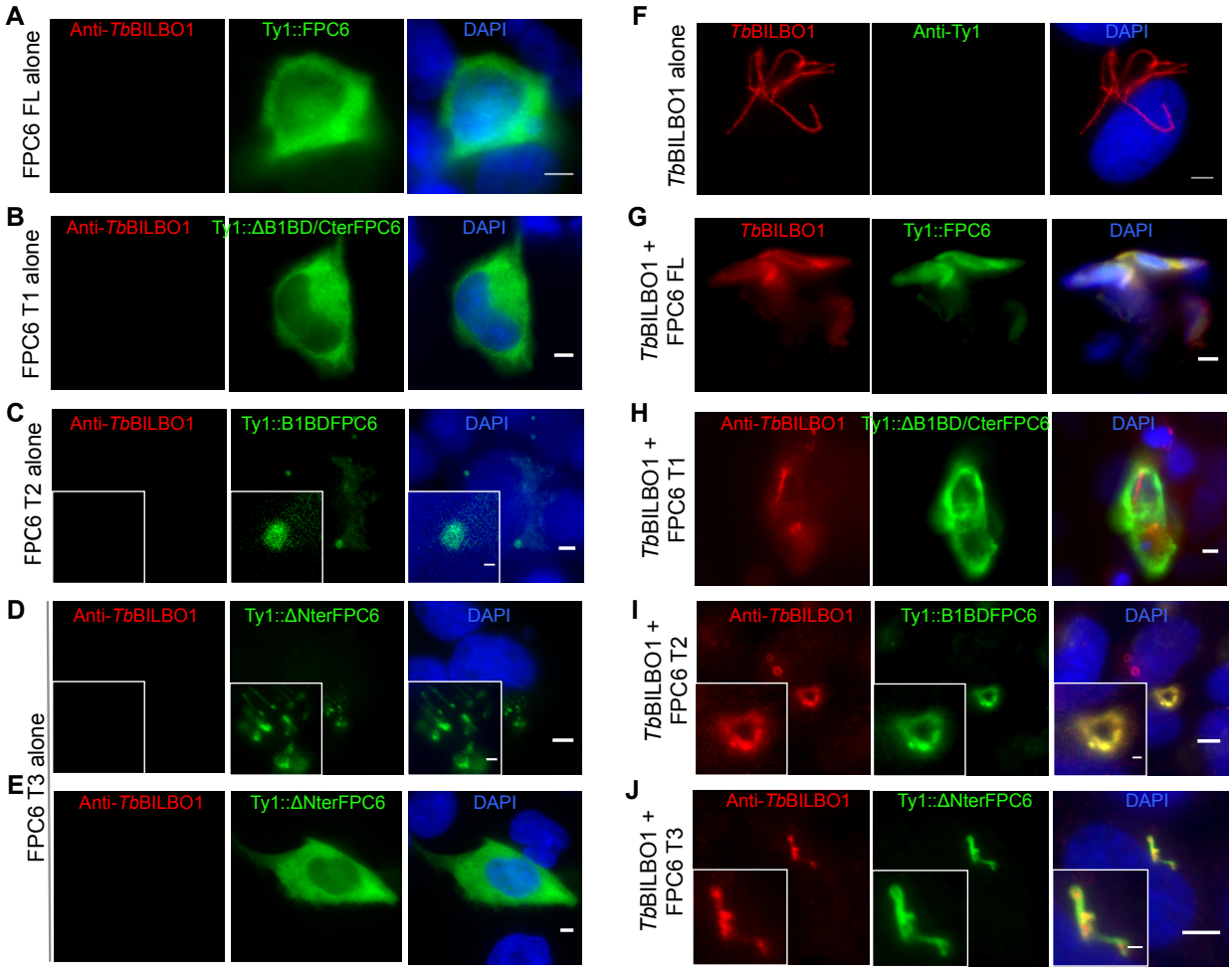

FIGURE 3.6: **Co-expression of *Tb*BILBO1 and FPC6 in U-2 OS cells.** **A** Expression of FPC6 FL alone, **B** Expression of FPC T1 alone, **C** Expression of FPC6 T2 alone, **D** and **E** Expression of FPC6 T3 alone, **F** Expression of *Tb*BILBO1 alone, **G** Co-expression of *Tb*BILBO1 and FPC6 FL, **H** Co-expression of *Tb*BILBO1 and FPC6 T1, **I** Co-expression of *Tb*BILBO1 and FPC6 T2, **J** Co-expression of *Tb*BILBO1 and FPC6 T3. Scale bar = 5μm, inset = 1μm.

3.2.6 In U-2 OS cells, FPC6 is located at the centrosome, on the MT and on *Tb*BILBO1

Orthologues for FPC6 do not exist in organisms other than trypanosomatids, however, expressing trypanosome-specific proteins in a novel environment can give surprising and insightful information about the properties of the protein. Previous preliminary data from the Robinson laboratory regarding the expression of FPC6 in mammalian cells revealed FPC6::GFP located at the centrosome when expressed in U-2 OS cells and located to the mature basal body in RPE-1 cells possessing a primary cilia (Dr. Celia Florimond, PhD thesis). Expression in U-2 OS cells was repeated with FPC6::GFP expressed alone and in co-expression with *Tb*BILBO1. These experiments confirmed that expression of FPC6::GFP localised to microtubules with a concentration at the centrosome (the microtubule organising centre), Figure 3.5, in detergent extracted cells (A) and whole cells (B). When *Tb*BILBO1 was expressed in U-2 OS cells it was seen to form distinctive structures: either simple polymers or complex polymers with globular/comma-shaped ends (as shown in Figure 1.12 Florimond et al., 2015) In contrast, when *Tb*BILBO1 and FPC6::GFP were co-expressed, FPC6::GFP was seen only on the structures formed by *Tb*BILBO1, however the shape and form of the polymers created by *Tb*BILBO1 were altered, producing long filaments of polymers periodic globular enlargements, see Figure 3.5 in both detergent extracted cells (C) and whole cells (D). These dual protein structures showed some hook-shape characteristics with a concentration of GFP labelling at a globular head followed by a shank-like structure. Furthermore long polymers of repeated patterns were observed, that appeared to twist around themselves with areas of alternating increased and weaker fluorescence. It is worth bearing in mind that Florimond et al., 2015 saw artefacts using *Tb*BILBO1::GFP in U-2 OS cells and therefore rejected these results. To this end, I designed primers and began cloning FPC6 with a 10xTy1 tag on the N-terminus because I knew this had no effect on FPC6 protein in *T. brucei*. I also designed truncated constructs to match those expressed in *T. brucei* (see later, in Figure 3.10).

3.2.7 Truncated versions of FPC6 show different characteristics co-expressed with *Tb*BILBO1 in U-2 OS

The experiment shown above (Figure 3.5) was repeated using FPC6 tagged with 3xTy1 at the N-terminus. I have already shown that an N-terminal Ty1 tag on FPC6 protein in *T. brucei* has no effect on growth and localises as expected, therefore this same tag was used here. Figure 3.6 shows whole cell U-2 OS cells fixed and probed with both anti-**Tb**BILBO1 and anti-Ty1 (BB2). In row **A**, expression of FPC6 full-length (FL) alone gave the same labelling as with the GFP tag (Figure 3.5.**B**.), Ty1 signal was seen on the MT with a concentration at the centromere. To gain information on the function of individual domains of FPC6, truncations were engineered, in relation to the BILBO1 binding domain (B1BD)/globular domain, giving three truncations: T1 = N-terminus (ΔB1BD + Cter); T2 = B1BD + globular domain; T3 =

B1BD/globular domain + Cter (ΔNter). This experiment could also aid in confirming the identification of the BILBO1 binding regions of FPC6, found earlier in Y2H assays. When truncation 1 (T1) the ΔB1BD/Cter of FPC6 was expressed alone, row **B**, labelling was seen throughout the cell in a similar patter to the FL, however this needs to be repeated with CSK preparations to be certain T1 is on the MT and not just cytoplasmic. Row **C** shows expression of T2, the B1BD of FPC6 alone, forming small rounded aggregates in the U-2 OS cells. For truncation 3, the ΔNter of FPC6 alone a less consistent pattern was seen with some cells showing aggregates of protein with globular heads (row **D**), and other cells showing a whole cell signal (row **E**). Again this needs to be repeated with detergent-extracted U-2 OS cells.

The right-hand panel of images in Figure 3.6 shows, in row **F**, expression of *Tb*BILBO1 alone, forming long polymers within the U-2 OS cells. When full-length FPC6 was co-expressed with *Tb*BILBO1, row **G**, FPC6 (Ty1 labelling) was seen on the polymer shapes with *Tb*BILBO1, but the form seemed to be more ribbon-like; this needs to be repeated with detergent extracted U-2 OS, i.e. cytoskeletons. Row **H** shows T1 expressed with *Tb*BILBO1. *Tb*BILBO1 can be seen forming polymers as when alone, and the ΔB1BD/Cter of FPC6 can be seen throughout the whole cell, indicating that the N-terminal domain of FPC6 alone is not sufficient to bind to *Tb*BILBO1. The BILBO1 binding domain of FPC6 was previously identified by yeast 2-hybrid, ad when this domain alone (B1BD; T2) was expressed with *Tb*BILBO1 in U-2 OS cells, very interesting annular structures were seen as in row **I**. Finally, when the ΔNter of FPC6 was expressed with *Tb*BILBO1, again a mixture of cell labelling was seen (as for T3 alone). Some cells showed co-labelling of polymer structures with anti-*Tb*BILBO1 and anti-Ty1 (FPC6 T3) as seen in row **J**, however some cells gave a whole cell signal (as for row **E**). in conclusion, the expression of Full-length and truncated versions of FPC6 in U-2 OS cells demonstrate an inherent propensity for FPC6 to bind microtubules, the centromere and *Tb*BILBO1 (when present). These data also confirm the BILBO1 binding domain of FPC6 and the necessity of this domain for FPC6 truncated protein to bind to *Tb*BILBO1.

3.3 Depletion of FPC6 protein by RNAi

3.3.1 RNAi *FPC6* in PCF is not lethal

To determine if FPC6 was an essential protein in *T. brucei* and to aid in determining its function, RNA interference (RNAi) was used to deplete the levels of mRNA and hence protein in the cell. RNAi is a well-established technique in trypanosomes since Ngô et al., 1998 observed that transfection of double stranded RNA (dsRNA) into *T. brucei* leads to degradation of the mRNA from the targeted gene and therefore a reduced level of protein. Although RNAi can never completely eliminate all the mRNA and therefore protein (it is not a knock-out), it can diminish the protein levels sufficiently to see an effect, or not, on cell growth, morphology and function. There are in fact two constructs to achieve RNAi: stem-loop, whereby a sequence

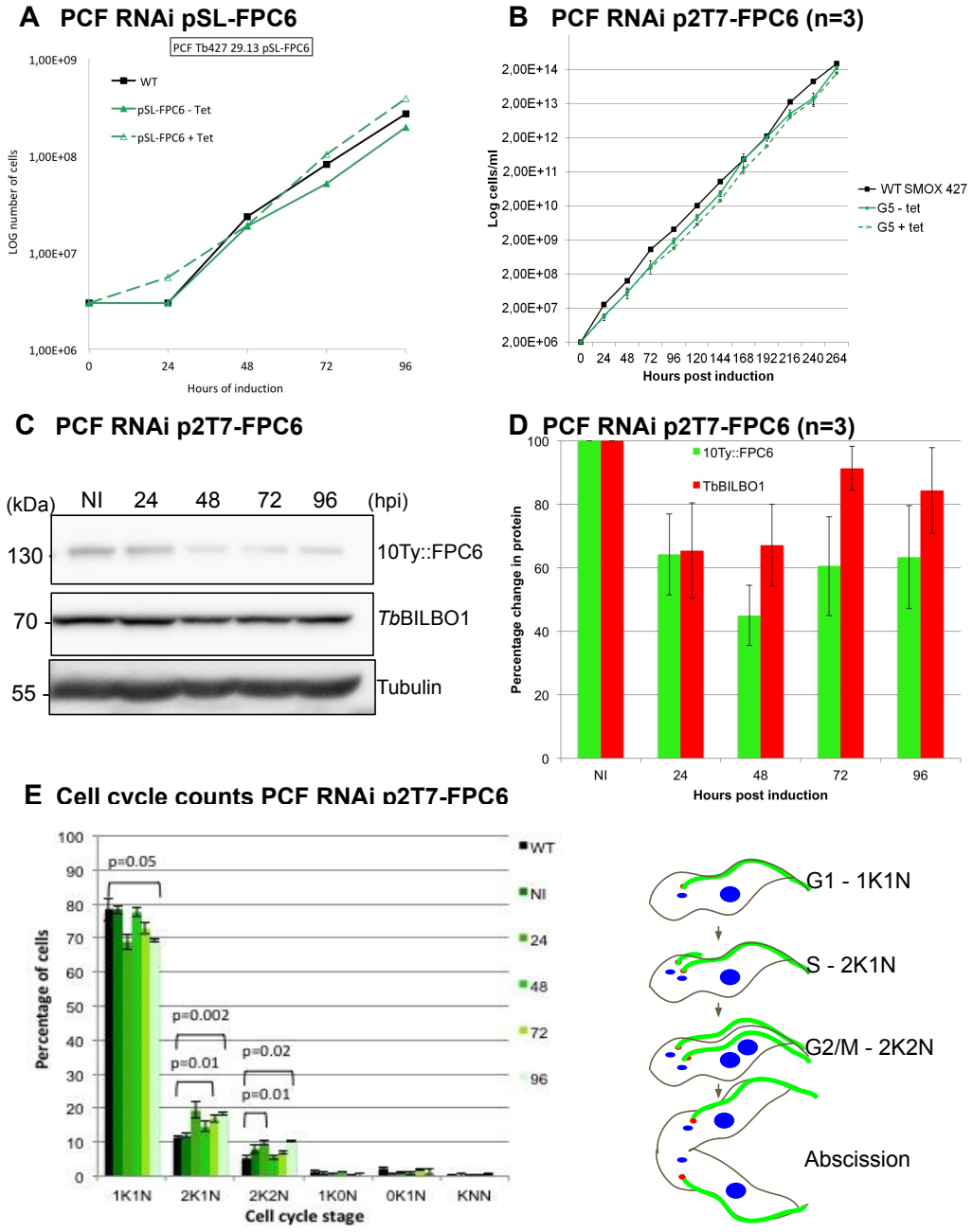

FIGURE 3.7: **RNAi *FPC6* in PCF. A** Growth curve of stem-loop RNAi pSL-FPC6, clone B4F10; **B** Growth curve of twin promoter RNAi, p2T7^{Ti}:TAblue-FPC6, clone G5: RNAi induction had no effect on growth; **C** Western blot of *T. brucei* CSK samples probed with anti-Ty1 (FPC6), anti-*Tb*BILBO1 and anti-TAT1 (tubulin); **D** Bar graph of quantification by densiometry of western blot images from three separate inductions of FPC6 in PCF; **E** Cell cycle stage counts showing a decrease in 1K1N and an increase in 2K1N and 2K2N cells.

of the target gene is repeated, one copy in the sense direction and the other in the anti-sense direction, joined by a "stuffer" sequence that allows the formation of a "hairpin" when the two complementary regions combine; this transfected construction integrates into the ribosomal RNA (rRNA) spacer and is a highly regulated inducible system (Shi et al., 2000). The other system, twin promoter, uses a T7 promoter at either end of the gene sequence to create two single strands of RNA which recombine *in vivo*. In this study of FPC6, the vector p2T7$^{Ti:TAblue}$ was used, this has a hygromycin selection antibiotic cassette to select for transfected trypanosomes in culture, as described by Alibu et al., 2005. This vector containing the targeting sequence for FPC6 was kindly given to the Robinson laboratory by Dr Brooke Morriswood (as described in the Methods Chapter 2.5.13.)

Firstly, I re-tested an RNAi cell line created by Dr Celia Florimond (previous PhD student in the Robinson laboratory). This was a stem-loop RNAi system in PCF Tb427.29.13 (pSL-FPC6-pLew100) and preliminary studies showed that tetracycline induction of dsRNA targeting *FPC6* had no effect on the growth of PCF *T. brucei*. To ensure that this RNAi system was working, mRNA levels were measured by semi-quantitative RT-PCR: the analysis showed no reduction in *FPC6* mRNA. This meant that either the RNAi system was not working or that the trypanosomes were able to regulate the level of protein, indicating FPC6 could be important in their survival. On re-testing two clones from this cell line (B4F10 and D4F10), I obtained the same result as Dr Florimond and growth was not effected by RNAi induction with 1μg/mL tetracycline; an example growth curve of clone B4F10 is shown in Figure 3.7.**A**.

The second RNAi construct that I tested was designed by Dr Brooke Morriswood, who previously identified FPC6 close proximity biotinylation (BioID) with *Tb*MORN1 (see section 1.4.10. This RNAi construct targeting *FPC6*, used a twin promoter system, p2T7$^{Ti:TAblue}$-FPC6 (Alibu et al., 2005). This construct was kindly given to the Robinson laboratory for this FPC6 study and is the construct that I used in all further RNAi experiments.

I transfected the p2T7$^{Ti:TAblue}$-FPC6 construct into the Tb427 SmOx PCF cell line (Poon et al., 2012) already endogenously tagged with 10Ty1::FPC6, to be able to detect levels of FPC6 protein on IFA and WB before and after induction of RNAi *FPC6*. When stable clones were achieved, I first tested their growth to ensure that the non-induced cells grew as for the wild-type (WT). I then induced RNAi *FPC6* with both 1 and 10μg/mL tetracycline, however no effect was seen on the growth of the cells as compared to the WT, or non-induced (NI), see growth curve for clone G5 in Figure 3.7.B, (n=3). I checked that the RNAi system was working and that FPC6 protein was knocked-down, by western blot up to 96 hours post-induction (hpi), Figure 3.7.C. Protein levels reduced to a minimum of 26% of non-induced cells (average 44%), see Figure 3.7.D. This bar graph shows quantification by densiometry of western blot images for three separate inductions of RNAi *FPC6* in procyclics. The

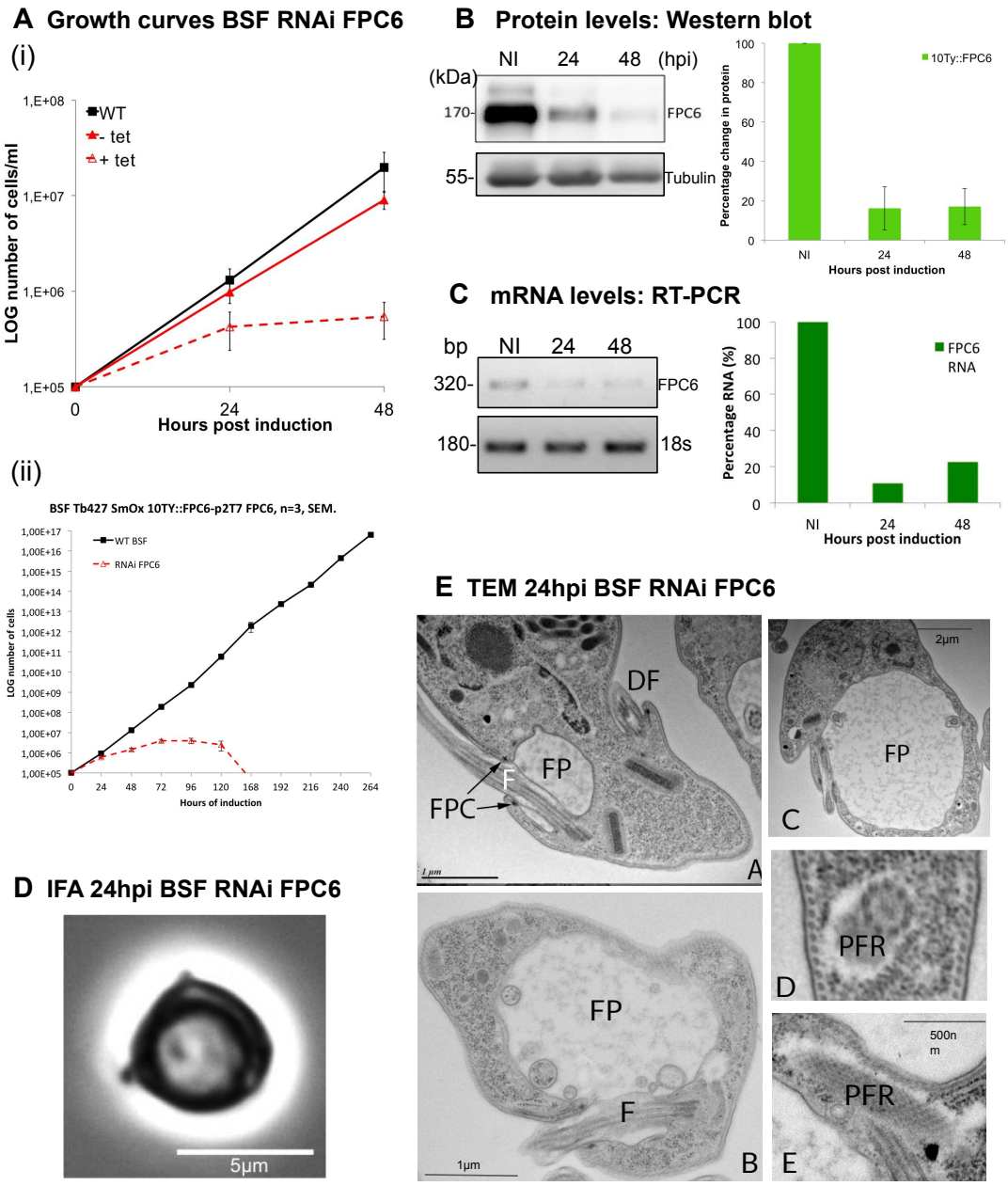

FIGURE 3.8: **RNAi *FPC6* in BSF A** (i) Growth curve of BSF RNAi *FPC6* to 48 hpi (ii) to 264 hpi: rapid growth arrest and cell death was seen; **B** Western blot and quantification by densiometry showing reduction in FPC6 protein with RNAi *FPC6*. **C** a reduction in mRNA *FPC6*; **D** BigEye phenotype of BSF RNAi *FPC6*; **E** TEM showing "BigEye" phenotype and intracellular PFR.

relative change in protein levels for FPC6 and *Tb*BILBO1 were calculated using tubulin (anti-TAT1) as a loading control, relative to NI cells. Levels of *Tb*BILBO1 protein appears to be decreasing post-induction of RNAi *FPC6*, although never reducing to less than 67% of non-induced levels. Possible due to up-regulation of production of this protein by trypanosomes, indicating its importance for the parasite, or that clones were selected for post-transfection that were less amenable to RNAi.

3.3.2 RNAi *FPC6* in PCF leads to a delay in cytokinesis

To explore further any effects of RNAi *FPC6* on cell division in PCF, I carried out cell cycle counts on clone G5, counting 200 cells at each time point of induction (n=3). A statistically significant reduction in 1K1N ($p < 0.05$) and a significant increase in 1K2K and 2K2N ($p < 0.01$) cell cycle stages were detected, indicating a delay in cytokinesis, see Figure 3.7.E. A schematic is shown alongside representing the different cell cycle stages for *T. brucei* PCF.

3.3.3 RNAi *FPC6* in BSF is rapidly lethal

I first assessed the effect of RNAi *FPC6* in the BSF cell line kindly given to the Robinson laboratory by Brooke Morriswood. I tested two clones of BSF Tb427.1313.514, single marker (neomycin resistance) transfected with p2T7^{Ti}:TAblue-FPC6 (hygromycin resistance marker; Alibu et al., 2005). Induction of RNAi in this cell line led to rapid cell death within 48 hours. Due to the fact that I did not have a reliable antibody for FPC6, I made numerous attempts to transfect this cell line with an endogenous 10xTy1 tag for FPC6. However, due to lack of success, I decided to start from scratch with BSF Tb427 SmOx (puromycin resistance marker; Poon et al., 2012). I first, endogenously tagged the N-terminal of FPC6 with 10xTy1 (see earlier Results section 3.2.5, then I transfected this stable cell line with the RNAi construct: p2T7$^{Ti:TAblue}$-FPC6. Induction of RNAi *FPC6* in BSF, led to a severe growth defect and rapid cell death within 48 hours of induction and complete population death in 168 hpi (ii), see Figure 3.8.**A**.**i**. Samples of trypanosomes were taken at each induction time point and cytoskeleton preparations were made for western blot, see Figure 3.8.**B**. Quantification by densiometry of the western blot images from two independent experiments revealed a reduction of FPC6 protein to 16% of non-induced cells by 24hpi. To assess the level of mRNA produced in the cells and verify the specificity and effectiveness of the RNAi system. RNA was extracted from cells at each time point and a semi-quantitative RT-PCR was performed, see Figure 3.8.**C**. The results mirrored those of the western blot, with a 90% reduction of mRNA FPC6 at 24hpi compared to non-induced cells. I could therefore conclude, that the RNAi system *FPC6* was effective and specifically targeting *FPC6* mRNA.

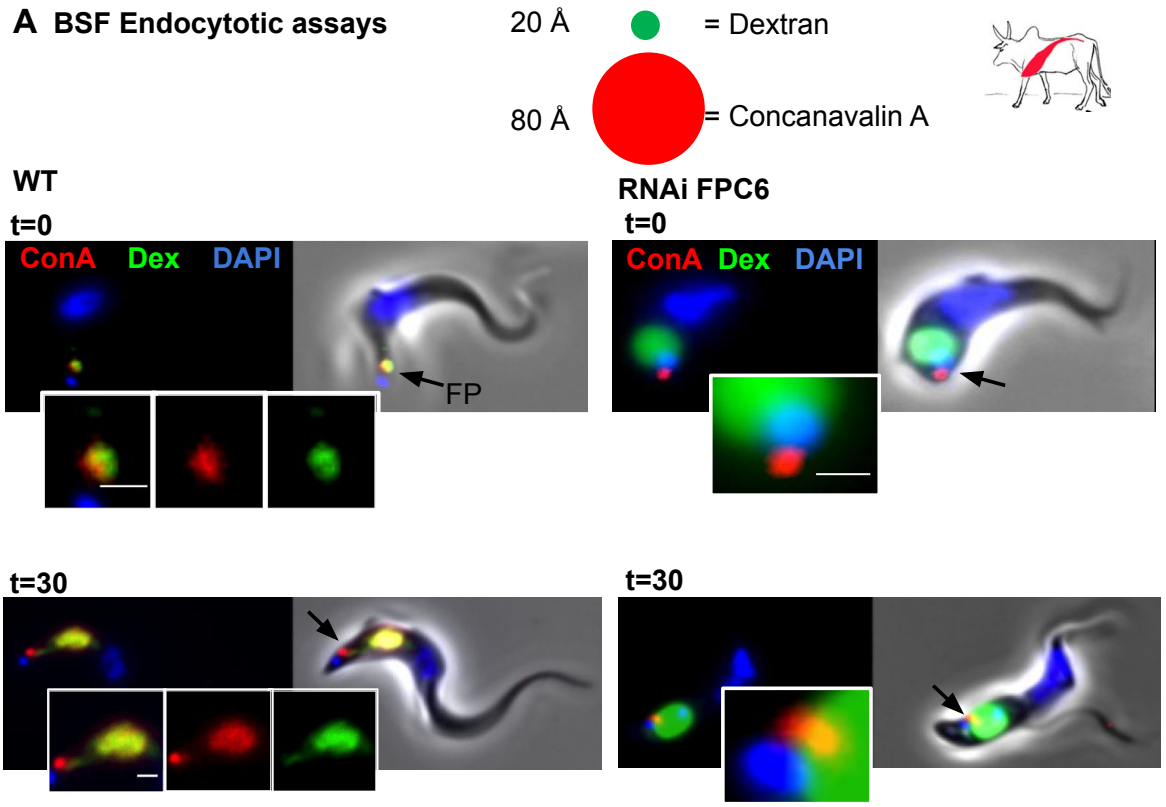

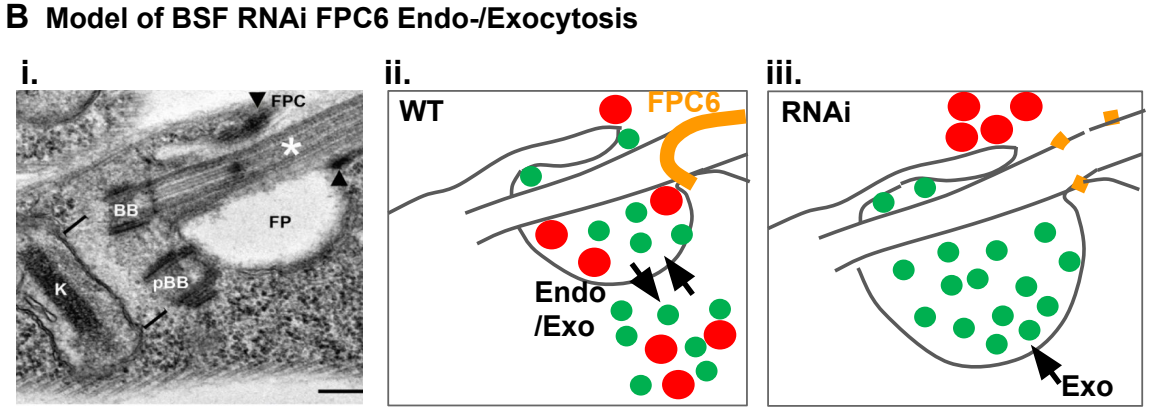

FIGURE 3.9: **Endocytotic assays in BSF. A** IFA in WT cells: dextran and ConA loaded in the FP at t=0 and both markers entered the cell after 30 minutes at 37°C. In RNAi *FPC6* cells (17 hpi), dextran loaded the enlarged FP at t=0, but ConA remained outside; after 30 minutes at 37°C, the position of both markers remained unchanged. **B.i**. TEM cross-section through the FP of WT *T. brucei* PCF; **ii**. schematic of TEM for WT at t=30; **iii**. after RNAi *FPC6* 17hpi. Endo=endocytosis, Exo=exocytosis, FP=flagellar pocket, FPC=flagellar pocket collar, K=kinetoplast, BB=basal body, pBB=pro-basal body, t=time, WT=wild type.

3.3.4 RNAi *FPC6* in BSF produces cells with a "BigEye" phenotype

Initial observation by eye of live BSF cells induced with RNAi *FPC6* revealed a rounded morphology of cells as they died. I first observed these cells by light microscopy to explore this abnormal phenotype. I saw rounding up of the usual long fusiform shape of the cells, see Figure 3.8.**D**. by IFA, in these cells, the *Tb*BILBO1 signal could still be seen at the FPC as well as an anti-Ty1 (FPC6) signal, despite a reduction of the level of FPC6 protein in the cells as observed by western blot. This could have been due to variation cell-to-cell and the fact that at this time-point around 16% of FPC6 protein is still present in the cells.

To explore in further detail what was happening intracellularly, thin sections of parasites were made for transmission electron microscopy (TEM), see Figure 3.8.**E**. A "BigEye" phenotype was observed, (Allen et al., 2003; Chapter 1.4.6): this is where the ordinarily small sized flagellar pocket (FP) became grossly enlarged and eventually filled almost the entire trypanosome cell as shown in images **B** and **C**. A detached flagellum (DF) can be seen in image **A** and the abnormal intracellular location of normally extracellular structures, such as the paraflagellar rod (PFR) was seen by its distinctive lattice in images **D** and **E**, in Figure 3.8.**E**. Additional transmission electron microscopy images of thin sections of bloodstream form trypanosomes showing the lethal BigEye phenotype can be seen in Appendix A, Figure A.5 and A.6.

3.4 RNAi *FPC6* in BSF leads to a block in endocytosis

To investigate the hypothesis that the "BigEye" phenotype seen in BSF after RNAi *FPC6* was due to perturbation in endocytosis, I performed an endocytotic assay as outlined in Methods Section 2.2; adapted from Morriswood and Schmidt, 2015. In these assays, TbSmOx BSF WT and BSF induced with RNAi *FPC6* for 17 hours were incubated with different sized fluorescent molecules: Dextran 10,000Da, 20Å and Concanavalin A (ConA) calculated at 80Å diameter (see Figure 3.9.**A**). Dextran enters the cell in the fluid phase whilst ConA binds to glycoproteins close to the neck of the pocket and is then taken up by endocytosis. The purpose of this experiment was to determine if these molecules were able to enter the FP and to be endocytosed into the cells upon induction of RNAi *FPC6*, to ascertain if a depletion in FPC6 protein has an effect on endocytosis.

Firstly, I looked at WT cells: the cells were temporarily incubated on ice for 15 minutes to prevent endocytosis (Brickman et al., 1995), in the presence of fluorescent Dextran and ConA. At this time point (t=0), I fixed the cells (see Methods Chapter 2.3.1) and could see labelling for dextran and ConA within the FP. At this stage not all cells were labelled with ConA in the FP, but all the cells did have labelling in the FP for dextran; an image for double labelling of dextran and ConA in the FP can be seen in Figure 3.9.B, WT t=0. After warming the cells up to 37°C for 30 minutes to

allow endocytosis to recommence, I fixed the cells and observed that both Dextran and ConA were labelled within the cell in the location of the endosomal-lysosomal system, indicating that both molecules had been internalised and that the endocytotic process was active. At this stage some ConA could still be seen in the FP, whilst all the Dextran had been internalised, see Figure 3.9.A, WT t=30.

Next, I took the BSF cell line possessing the inducible RNAi sequence for FPC6 (clone 5.6 as shown in Figure 3.8) and induced the RNAi for 17 hours using 1μg/mL tetracycline. After incubation with dextran and ConA for 15 minutes on ice (t=0), dextran was seen loading, the now enlarged FP, however ConA was seen in close proximity to the FP and kinetoplast but not co-localising with Dextran, i.e. outside of the FP, see Figure 3.9.A; RNAi FPC6, t=0. After warming the cells for 30 minutes at 37°C the pattern of labelling was unchanged, in stark contrast to that seen with the WT cells. The dextran was still observed filling the enlarged FP and ConA was observed at a distinct location in the region of the neck of the FP, see Figure 3.9.A, RNAi FPC6, t=30. This indicated that endocytosis was blocked and neither molecule could be taken up into the cell. ConA no longer had access to the FP and was located at the edge of the pocket near to the kinetoplast and external surface of the trypanosome cell.

To explain this finding, a model is shown in Figure 3.9.B. (adapted from Morriswood and Schmidt, 2015). In this panel (i) shows a cross-section EM of the FP, modelled in (ii) showing in gold the position of the hook-like structure formed by FPC6 protein at the FP neck and extending along the flagellum. In these WT cells, endo- and exocytosis continues as normal with dextran (green circles) and ConA (larger red circles) moving into the FP and then into the cell. In (iii) a cell induced for 17 hours with RNAi *FPC6* is modelled. In this case, FPC6 protein is depleted (dashed gold line), the FP is enlarged, dextran (green circles) is filling the FP and ConA (red circles) is blocked in a position near the neck of the FP; exocytosis continues unabated, whilst endocytosis appears to be arrested.

3.4.1 Endogenous tagging of *Tb*PIPKA

To investigate a possible connection between the knock-down of a cytoskeletal protein and an effect on a membranous process, a potential link was seen in the paper by Demmel et al., 2016, here they identified a novel protein with phosphatidylinositol phosphate (PIP) kinase activity in *T. brucei*: *Tb*PIPKA. They showed that *Tb*PIPKA was located specifically at the flagellar pocket neck and its product phosphatidylinositol 4,5 biphosphate (PI(4,5)P_2) was only present at the FP membrane; an essential factor for clathrin-dependent endocytosis, as described earlier in Chapter 1.4.6. In their paper, Demmel et al., 2016 described that knock-down of *TBPIPKA* by RNAi led to enlargement of the flagellar pocket and inhibition of endocytosis. This is a very interesting finding and could explain the link between the FPC/Hook complex and the FP membrane. To this end, I designed primers to enodogenously

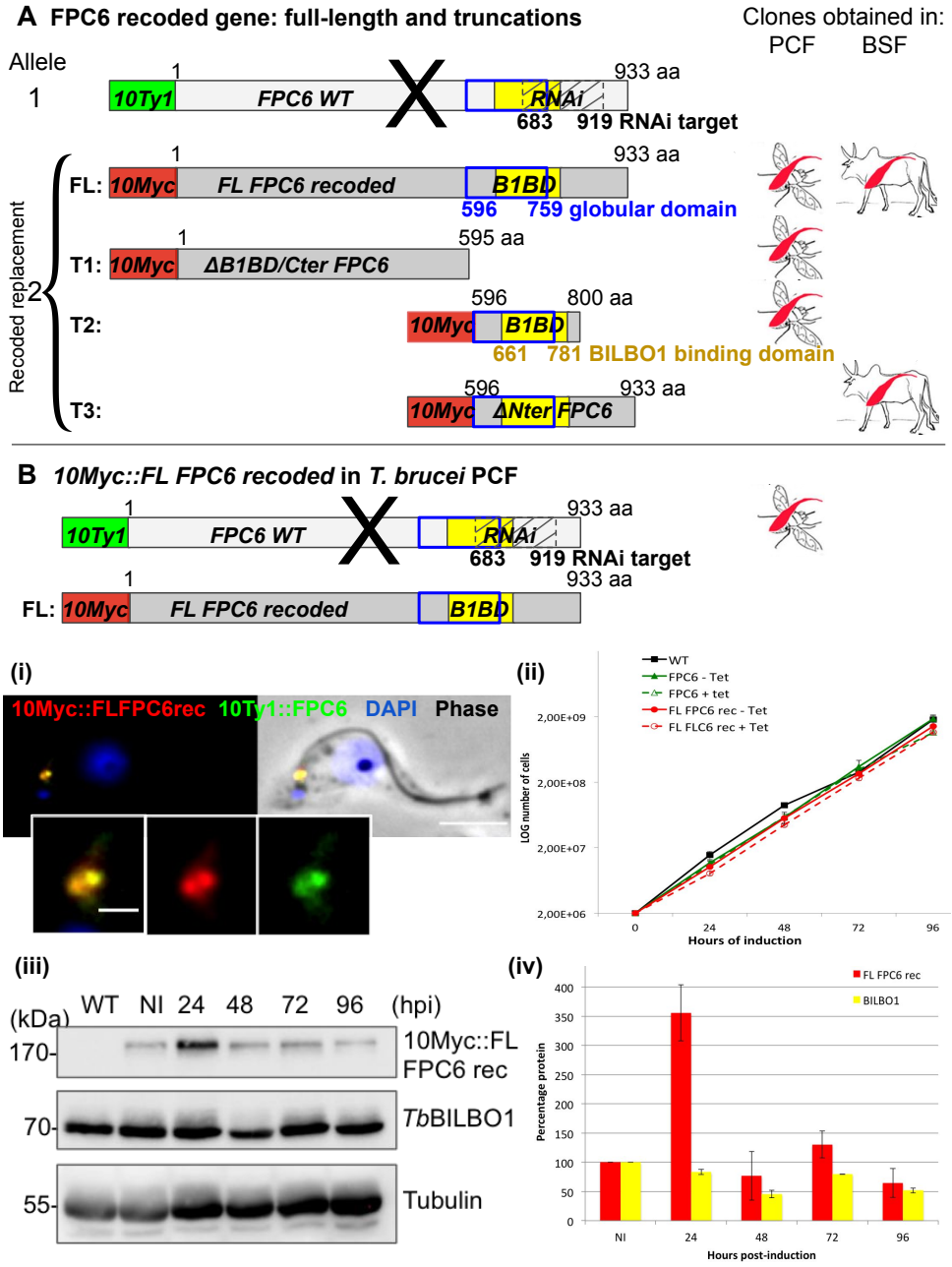

FIGURE 3.10: **Recoded FPC6: full-length and truncations. *FL FPC6* recoded gene expression in PCF. A** Schematic of FPC6 WT allele and FPC6 recoded FL and truncations (T1, T2, T3). Successful transfections in either PCF or BSF *T. brucei* is indicated to the right of each construct. **B** (i) Immunofluorescence showing 10cMyc::FLFPC6rec co-localising with 10Ty1::FPC6. (ii) Growth curve to show replacement of one allele with a recoded version has no effect on growth. (iii) WB showing that levels of 10cMyc::FLFPC6rec protein increase at 24hpi. (iv) Quantification of WB in triplicate. aa=amino acid, BSF=bloodstream form, FL=full-length, hpi=hours post induction, NI=non-induced, Tet=tetracycline, WT=wild type. Scale bar=5μm, inset=1μm.

tag *Tb*PIPKA on the N-terminus with a 3xcMyc tag using the vetor pPOTv7-3cMyc-NEO (adapted from Dean et al., 2015a), in the BSF cell line 10Ty1::FPC6/RNAi-FPC6. However, clones obtained after transfection were negative for the tag by IFA. Therefore, I increased the tag to 10xcMyc, using a pPOTv7-10cMyc-NEO vector; however on testing by IFA, the tag on *Tb*PIPKA was not detectable, despite the cells growing normally in the presence of the neomycin selection antibiotic. This might be due to low expression levels of the *Tb*PIPKA protein, or loss of the tag yet retention of the antibiotic selection cassette. This hypothesis warrants further investigation.

3.5 Expression of recoded FPC6 in *T. brucei*

A recoded version of the *FPC6* gene was obtained from Eurofins Genomics (Germany) to provide a template nucleotide sequence that would be resistant to the RNAi and yet code for the same amino acids and therefore the same protein. It has been shown by Sinclair-Davis et al., 2017 that a recoded sequence of a gene in *T. brucei* can lead to a normally functioning protein that is resistant to RNAi of the wild-type allele. The full-length (FL) FPC6 recoded gene was cloned into a pPOTv7-10cMyc-NEO vector by classical ligation (see Methods 2.5.8). Truncations of FPC6 were determined according to preliminary data of the primary structure (see Figure 3.1.**C** and 3.10.**A**.), thereby three truncations were used in all further experiments:

FL: Full-length FPC6 recoded, amino acids 1-933
T1: ΔB1BD/Cter FPC6 recoded, amino acids 1-595
T2: B1BD (BILBO1 binding domain) FPC6 recoded, amino acids 596-800
T3: ΔNter FPC6 recoded, amino acids 596-933

The FPC6 recoded gene truncations were produced by nested PCRs (see Methods 2.5.8). The resulting constructs were transfected into both PCF and BSF Tb427 SmOx already containing the RNAi *FPC6* inducible system (under hygromycin selection) and endogenously tagged 10Ty1::FPC6 (under Blasticidin selection). In this way, one allele of FPC6 would possess a 10xTy1 tag and be targetable by RNAi, and the other allele would be replaced with a recoded version (full-length or truncation) with a 10xcMyc tag (10cMyc::FLFPC6rec) and be resistant to the RNAi system, producing a cell line: 10Ty1::FPC6/10cMyc::FPC6rec/RNAi-FPC6.

3.5.1 Full-length recoded FPC6 in PCF co-localises exactly with WT FPC6 and increased after RNAi *FPC6*

The FL construct was obtained in PCF after two transfections. The location of the 10cMyc::FLFPC6rec protein (from the recoded gene), was observed on IFA of detergent-extracted cells (CSK) to co-localise exactly with the wild-type 10Ty1::FPC6

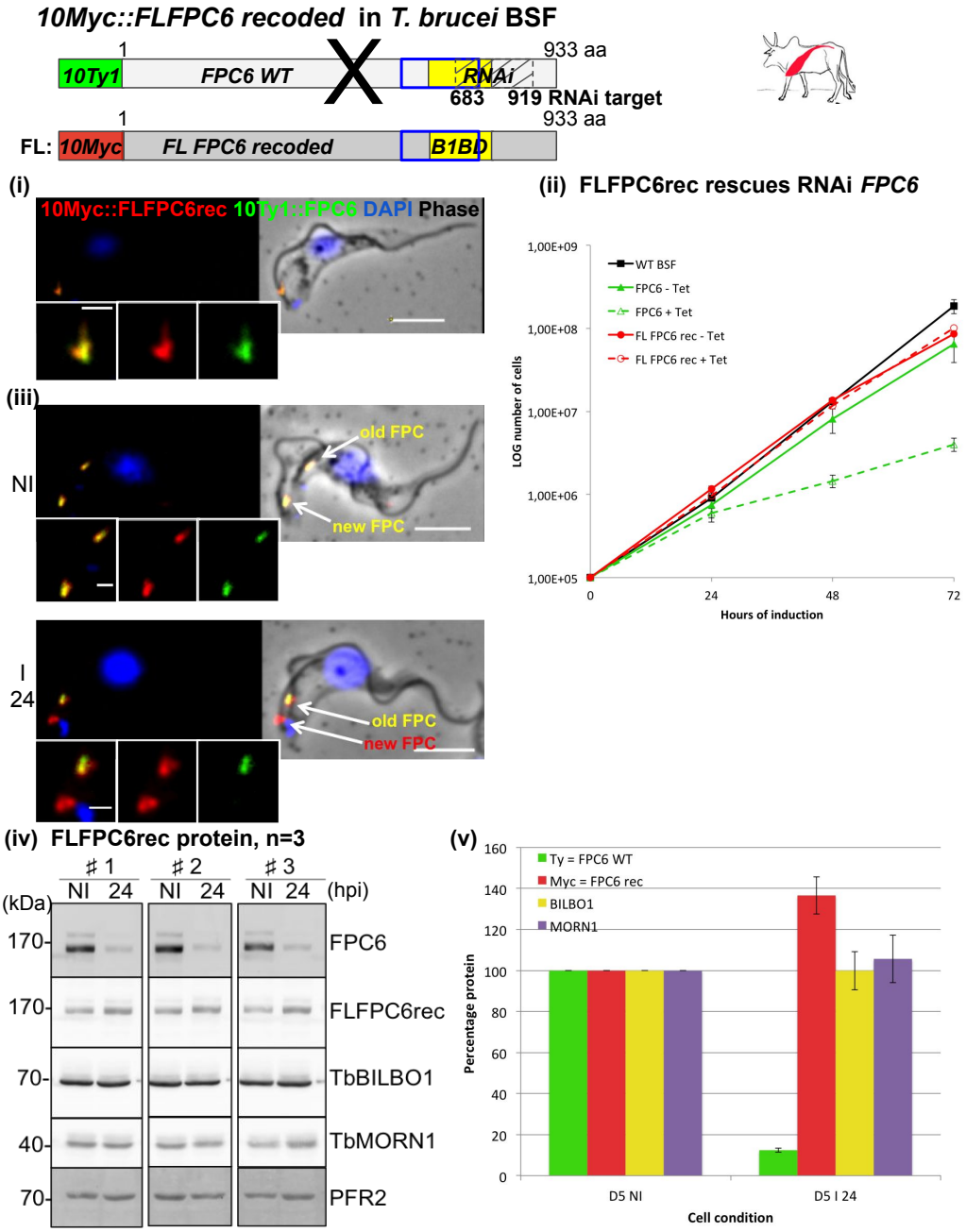

FIGURE 3.11: **Expression of *FL FPC6* recoded gene in BSF.** (i) IFA showed co-localisation of 10cMyc::FLFPC6rec with 10Ty1::FPC6. (ii) Growth curve revealed replacement of one allele with a FL recoded version was able to rescue the FPC6 *RNAi* phenotype. (iii) RNAi *FPC6* reduced 10Ty1::FPC6 signal in the new FPC, but not 10cMyc::FLFPC6rec. (iv) WB showed that levels of recoded protein were not affected by RNAi *FPC6*. (v) Quantification of 3 separate inductions by WB showing loss of FPC6 protein and slight increase in recoded FPC6. aa=amino acid, BSF=bloodstream form, FL=full-length, hpi=hours post induction, NI=non-induced, Tet=tetracycline and WT=wild type. Scale bar=5μm, inset=1μm.

protein, Figure 3.10.B.(i). Growth of non-induced and induced RNAi *FPC6* cells grew as for the WT cells, as for all experiments involved in RNAi FPC6 in PCF (Figure 3.10.B.(ii)). Western blotting confirms the size of 10cMyc::FLFPC6rec protein to be the same as the 10Ty1::FPC6 protein (Figure 3.10.B.(iii)). Quantification of 3 separate inductions by western blot reveal in increase in FPC6 protein at 24hpi of 350% (Figure 3.10). Interestingly, an increase in 10cMyc::FLFPC6rec protein is seen at 24 hours post induction with tetracycline, coinciding exactly with the time-point that the wild-type FPC6 protein is reduced due to RNAi, see Figure 3.7.D. This result indicates that the recoded protein is compensating for a reduction in wild-type FPC6. Two clones were fully tested (G5, H12) and the results obtained were the same in each case.

3.5.2 FL FPC6 recoded protein rescues the RNAi *FPC6* in BSF

In the BSF, I carried out four transfections to obtain clones with one allele of FPC6 replaced with a 10cMyc tagged FL FPC6 recoded version, whilst maintaining the other allele tagged with 10Ty1::FPC6 and RNAi *FPC6*, to produce a cell line identical to that in the PCF, above: 10Ty1::FPC6/10cMyc::FLFPC6rec/RNAi-FPC6.

IFA revealed that 10Myc::FLFPC6rec co-localised with 10Ty1::FPC6 (wild-type), see Figure 3.11.(i). When RNAi of the wild-type *FPC6* sequence was induced, the cells grew as for the WT and the NI, see Figure 3.11.(ii). The green lines show, the cell line 10Ty1::FPC6/RNAi-FPC6 (NI=solid line; I=dashed line) and the red lines indicate the new cell line compensated for with the recoded allele 10Ty::FPC6/10cMyc::FLFPC6rec/RNAi-FPC6. Instead of the cells dying from 24hpi, they continued to grow with no detriment to growth. Examination of CSK, by IFA, in NI cells and those induced for 24 hours with RNAi *FPC6* in the compensated cell line, revealed that the fluorescence signal for 10Ty1::FPC6 (the wild-type allele) normally present at both the old and new FPC, was only present at the old FPC and not at the new FPC in 2K1N cells, after RNAi. The fluorescent signal for 10cMyc::FLFPC6rec, however, retained a strong signal at both the old and new FPC, see Figure 3.11.(iii). In 2K2N cells the signal for 10Ty1::FPC6 was even weaker and even disappeared altogether at both the old and new FPCs (not shown). By western blot, protein for 10Ty1::FPC6 is seen to disappear at 24hpi (n=3), however 10cMyc::FLFPC6rec protein could be seen before (NI) and after induction of RNAi *FPC6* for 24 hours. This confirms that the recoded protein has not been depleted by RNAi (see Figure 3.11.(iv)) Quantification of this WB shows that 10Ty1::FPC6 reduced to less than 20% of NI levels, that 10cMyc::FLFPC6rec increased more than 30% above NI levels and both *Tb*BILBO1 and *Tb*MORN1 remained the same. These data provide evidence that not only is the recoded gene not targeted by the RNAi, but it was up-regulated to compensate for the loss of the native FPC6 protein from the wild type alelle.

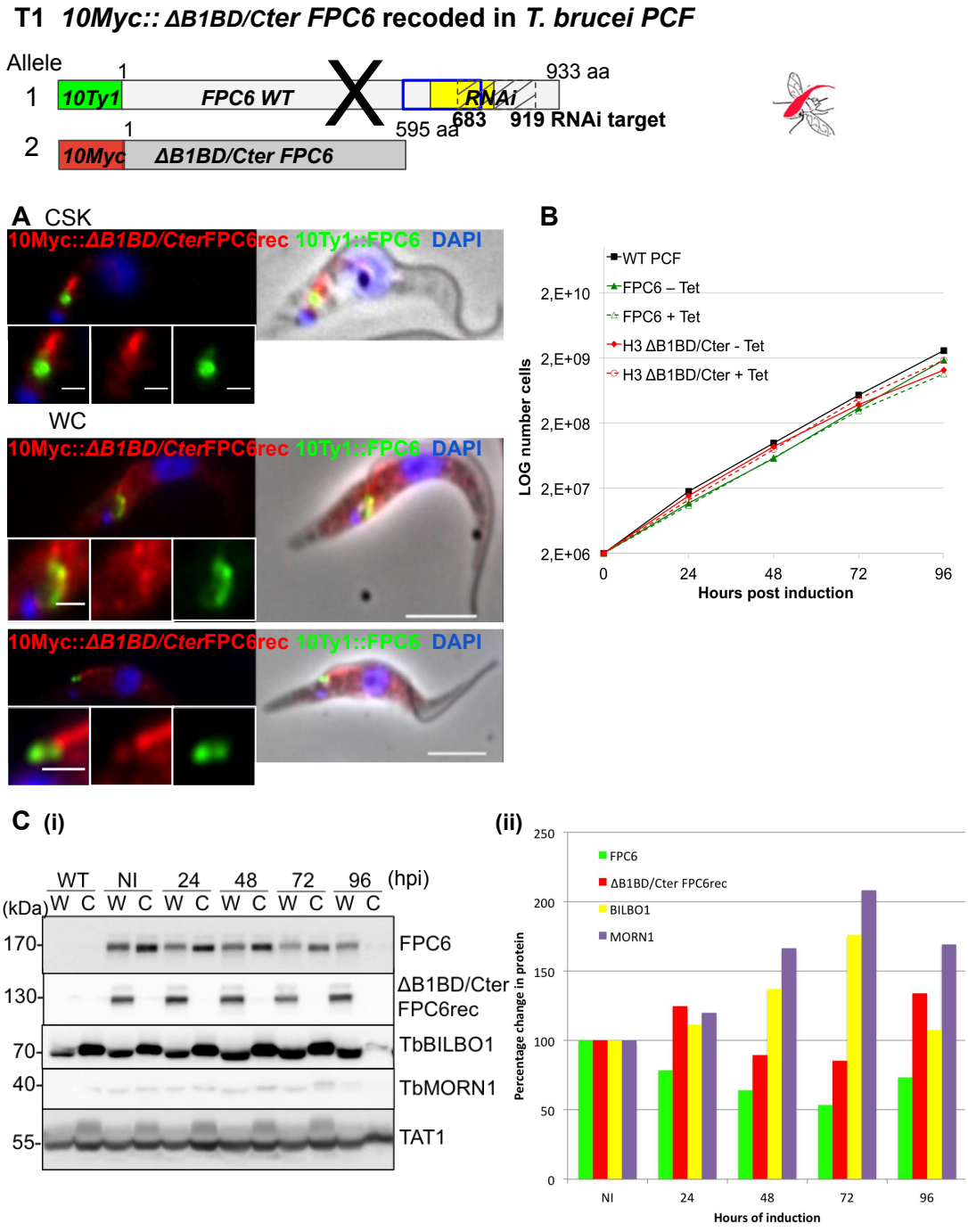

FIGURE 3.12: **Expression of T1: ΔB1BD/Cter FPC6 recoded in PCF. A** IFA revealed mainly cytoplasmic location of 10Myc::ΔB1BD/CterFPC6rec. **B** Growth curve showed no effect on growth upon RNAi *FPC6*. **C(i)** Western blot confirming cytoplasmic location of ΔB1BD/Cter FPC6 rec protein in *T. brucei*. **(ii)** Western blot showing the presence of 10Myc::ΔB1BD/CterFPC6rec after RNAi *FPC6*. aa=amino acid, PCF=procyclic form, hpi=hours post induction, NI=non-induced, Tet=tetracycline, WT=wild type. Scale bar=5μm, inset=1μm.

3.5.3 Truncation 1: ΔB1BD/Cter FPC6 recoded gene expression in PCF

This truncation was only obtained in the PCF, on the first transfection to give a cell line: 10Ty1::FPC6/10cMyc::ΔB1BD/CterFPC6rec/RNAi-FPC6. Numerous transfections were made in the BSF but were unsuccessful in obtaining clones. Confirmation of the expression of this truncation was made initially by IFA whereby a vague signal was seen in CSK with a concentration in the FPC area; on whole cell (WC) preparations a definite cytoplasmic signal was seen, Figure 3.12.A. When RNAi *FPC6* was induced, the cells containing the recoded truncation 10cMyc::ΔB1BD/CterFPC6rec (clone H3; the red lines) continued to grow as the WT (black line), the NI and the cell-line containing the 10Ty1::FPC6/RNAi-FPC6 (the green lines), see Figure 3.12.B. The cytoplasmic location of the ΔB1BD/Cter FPC6 recoded truncation was confirmed by western blot which labelled the cMyc tagged protein (10cMyc::ΔB1BD/CterFPC6rec) almost entirely in the whole cell (W) sample and very little in the cytoskeleton (C) preparation, see Figure 3.12.C.(i). This is in contrast to FPC6 wild-type protein which always gave a stronger signal with CSK preparations. When trypanosome samples were collected from each time-point after induction, the recoded truncation 10cMyc::ΔB1BD/CterFPC6rec protein levels did not diminish. Two clones were fully tested and gave the same result. Quantification of the western blot, showed the reduction in wild-type 10Ty1::FPC6, the resistance (and even increase) in the recoded truncation 10cMyc::ΔB1BD/CterFPC6rec, and an increase in both *Tb*BILBO1 and *Tb*MORN1 after RNAi *FPC6* induction. The increase in the later two proteins might be to aid in compensation of the loss of a protein of the FPC/Hook complex, Figure 3.12.C.(ii).

3.5.4 Truncation 2: B1BD FPC6 recoded expression in PCF

This truncation was obtained only in the PCF after the first transfection, to give a cell line: 10Ty1::FPC6/10cMyc::B1BDFPC6rec/RNAi-FPC6. A number of attempts were made in the BSF but were unsuccessful and all the cells dying within days of transfection and addition of the selection antibiotic (neomycin).

Extremely interesting, was the location of the 10cMyc::B1BDFPC6rec truncation protein in *T. brucei*: it was almost identical to *Tb*BILBO1, see Figure 3.13.A.(i) The prediction of this BILBO1-binding domain (B1BD) was originally made by yeast 2-hybrid and it was nice to see this being confirmed *in vivo*. Co-labelling with anti-Ty1 and anti-cMyc enabled labelling of both native and recoded FPC6 protein, respectively. IFA showed that apart from an area of co-localisation at the FPC, the green fluorescence for 10Ty1::FPC6 extends in a hook shape distally along the flagellum (as usual for the native protein), whilst the red fluorescence for 10cMyc::B1BDFPC6rec protein extends in the opposite direction towards the basal bodies, as seen previously with *Tb*BILBO1, see Figure 3.13.A.(ii). Upon RNAi *FPC6* induction, the cells containing the recoded B1BD truncation continued to grow as for the WT PCF and the 10Ty1::FPC6/RNAi-FPC6; see Figure 3.13.B.

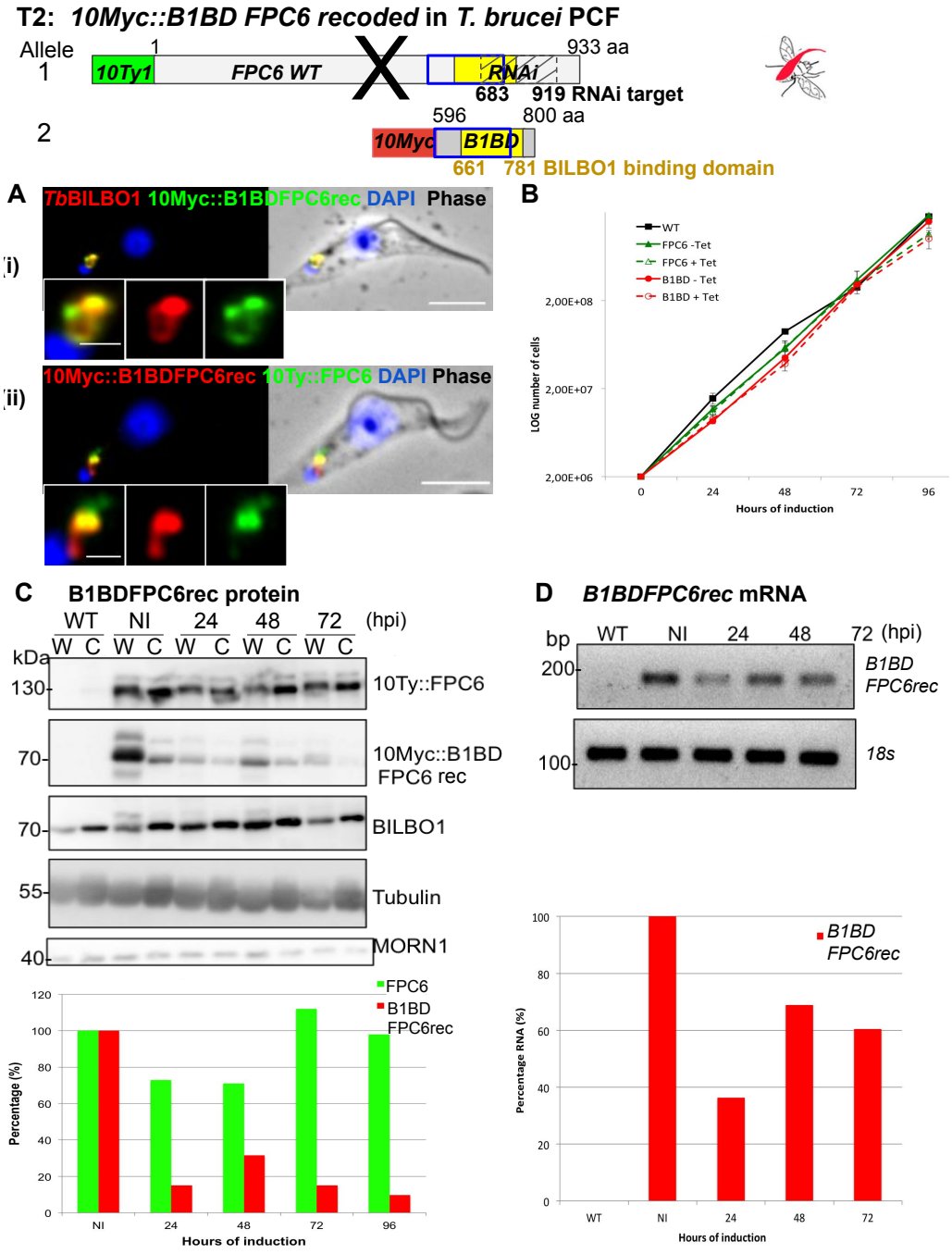

FIGURE 3.13: **Expression of T2: B1BD FPC6 recoded in PCF. A** (i) Co-localisation of 10Myc::B1BDFPC6rec with *Tb*BILBO1, (ii) but not with 10Ty1::FPC6 WT. **B** No effect on growth upon RNAi *FPC6*. *C* Western blot to show the disappearance of B1BD FPC6 recoded protein upon RNAi *FPC6* and quantification bar graph of whole cells. **D** Levels of mRNA for recoded B1BD after RNAi *FPC6* and quantification bar graph. B1BD=BILBO1 binding domain, C=cytoskeletons, PCF=procyclic form, NI=non-induced, W=whole cells, WT=wild type. Scale bar=5μm, inset=1μm.

Confirmation of the size of the recoded truncation was made by western blot probing the cMyc-tag. However, when samples of induced cells collected at 24 hour intervals post induction with tetracycline, were probed on western blot, an extremely surprising finding was observed. The recoded truncation 10cMyc::B1BDFPC6rec protein was seen to disappear after the induction of RNAi *FPC6* to a greater extent than the native protein 10Ty1::FPC6, as seen in Figure 3.13.C. This was an unexpected finding because the recoded sequence has been shown not to be targeted by the RNAi system (Section 3.5.1) despite the fact that the amino acid sequence of the B1BD and that targeted by the RNAi sequence overlap, as can be seen in the schematic at the top of Figure 3.13. To try to understand this finding, I collected trypanosome samples for semi-quantitative RT-PCR, to determine if the mRNA of the recoded sequence really was being targeted by the RNAi system in this case. Figure 3.13.D shows the mRNA specific for the recoded truncation 10cMyc::B1BDFPC6rec (for primers used see Table 2.9). mRNA *B1BDFPC6rec* was present at each timepoint of induction, concluding that the RNAi *FPC6* was not targeting the mRNA from the recoded gene sequence. Quantification of this image showed that there was still a reduction in mRNA for *B1BDFPC6rec* after RNAi *FPC6*; this might be an artefact in this single experiment, and this would need to be repeated a number of times to ensure the result was real and repeatable.

3.5.5 Truncation 3: ΔNter FPC6 recoded expression in BSF rescues the RNAi phenotype

This truncation was only obtained in BSF, with one clone (D2) obtained on the first transfection, to give a cell line: 10Ty1::FPC6/10cMyc::ΔNterFPC6rec/RNAi-FPC6. I attempted PCF transfections twice, but each time all of the cells grew in the selection antibiotic and yet were negative for the cMyc-tag on IFA and WB.

Immunofluorescence revealed that this truncation of FPC6 (10cMyc::ΔNterFPC6rec) was located at the FPC but the form that it exhibited was not the same as that for native FPC6. Figure 3.14.A. shows detergent-extracted *T. brucei* BSF cells: in the NI cells, the green fluorescence displayed the hook-like shape of 10Ty1::FPC6 and in red the recoded truncated ΔNterFPC6rec protein showed some overlap at the FPC with wild-type FPC6 protein, but the recoded truncation then extended towards the basal bodies and kinetoplast, possibly along the MTQ. In conclusion the location in the cell and protein structure formed by truncation 10cMyc::ΔNterFPC6rec was not the same as the full-length native FPC6 protein.

Induction of RNAi *FPC6* led to a sudden and surprising complete disappearance of the recoded truncation at 24hpi with tetracycline, as seen in IFA, Figure 3.14.A. When RNAi *FPC6* was induced, cell growth was reduced from 24

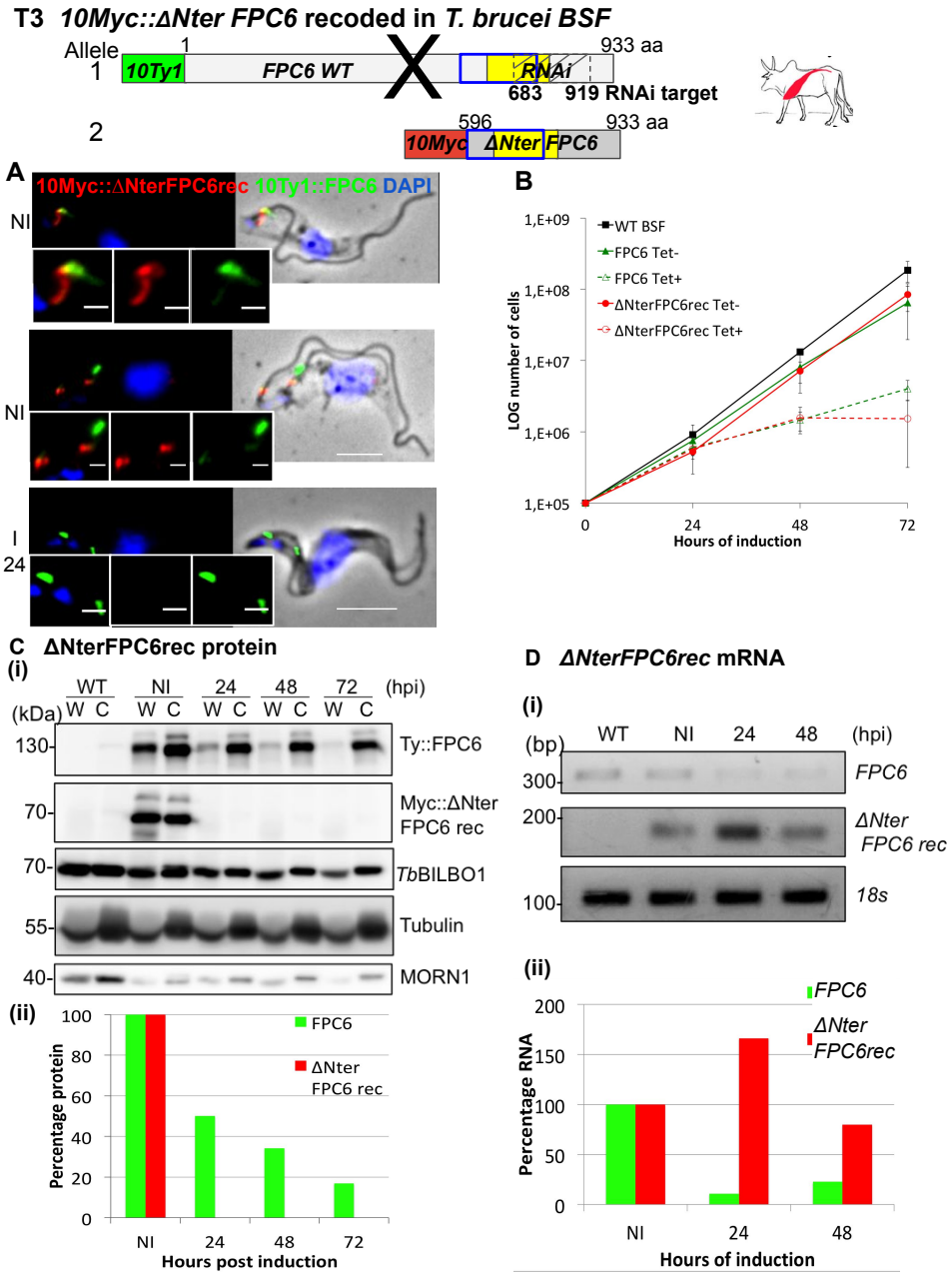

FIGURE 3.14: **Expression of T3: ΔNter FPC6 recoded in BSF. A** 10cMyc::ΔNterFPC6rec does not co-localise with 10Ty1::FPC6. **B** ΔNterFPC6rec does not rescue RNAi *FPC6*. **C** (i) WB showing a sudden disappearance of 10cMyc::ΔNterFPC6rec protein after RNAi *FPC6*, with (ii) quantification from whole cells. **D** (i) mRNA for 10cMyc::ΔNterFPC6rec before and after RNAi *FPC6* and (ii) quantification bar graph reveals mRNA *FPC6* present and increased. C=cytoskeletons, NI=non-induced, W=whole cells, WT=wild type. Scale bar=5μm, inset=1μm.

hours post induction, with cell death appearing at a similar rate to the cell-line containing the Ty1 tagged protein and RNAi alone, 10Ty1::FPC6/RNAi-FPC6, see Figure 3.14.B. The black line is the WT BSF, the green line represents the parental cell line 10Ty1::FPC6/RNAi-FPC6, and the red line represents the cell line with one allele of FPC6 replaced with the recoded truncation: 10Ty1::FPC6/10Myc::ΔNterFPC6rec/RNAi-FPC6.

To confirm the expression of the cMyc tagged recoded truncation at the expected size in this cell line (clone D2) and also to investigate further what was happening with regards to the disappearance of the 10Myc::ΔNterFPC6rec signal, samples of trypanosome cells were collected before (NI) and 24, 48 and 72 after induction with RNAi *FPC6* for western blot. Curiously, the signal for the 10cMyc::ΔNterFPC6rec protein had completely disappeared in all induced samples from 24hpi, as seen in Figure 3.14.C.(i). This blot was quantified and the graph below (ii). The green bars represent 10Ty1::FPC6 reducing gradually due to the RNAi *FPC6*, as usual. Remarkably, however, the levels of 10Myc::ΔNterFPC6rec disappeared completely after RNAi *FPC6* (24, 48 and 72hpi).

As for the B1BD truncation, the RNAi *FPC6* should be specific for the mRNA from the wild-type sequence only and not the recoded sequence, as confirmed by the full-length expression (Section 3.5.2; Figure 3.11). To try to explain this unexpected finding, I took cell samples were taken from non-induced cells and those at 24 and 48hpi for semi-quantitative RT-PCR. In Figure 3.14.D. the level of mRNA *FPC6* (wild-type) can be seen reducing, whereas mRNA for Δ*NterFPC6rec* is not reduced and in fact at 24 hours post induction can be seen to increase above baseline (non-induced) levels. This result not only confirms that the recoded truncation is not being targeted by the RNAi *FPC6*, it appears to be up-regulated and is compensating for the loss of wild-type FPC6 mRNA (and therefore protein) in the cell. As for the previous truncation (B1BDFPC6rec), this result will need to be re-confirmed.

3.6 Either RNAi *TBMORN1* or RNAi *FPC6* alone is sufficient for cell death; neither can compensate for the other

Due to the exact co-localisation of FPC6 with *Tb*MORN1 at the hook complex in *T. brucei*, the relationship between these two proteins was explored further.

Firstly, using the clone 5.6 of the cell line that I created with 10Ty1::FPC6/RNAi-FPC6, I looked at the labelling for *Tb*MORN1 by IFA and WB after RNAi *FPC6* induction. Figure 3.15.A.(i) shows the growth curve seen earlier in Figure 3.8 displaying the rapid cell death seen after 24hpi RNAi *FPC6* in the BSF. IFA of cells before (NI) and 24hpi RNAi *FPC6* with tetracycline, showed the normal location of

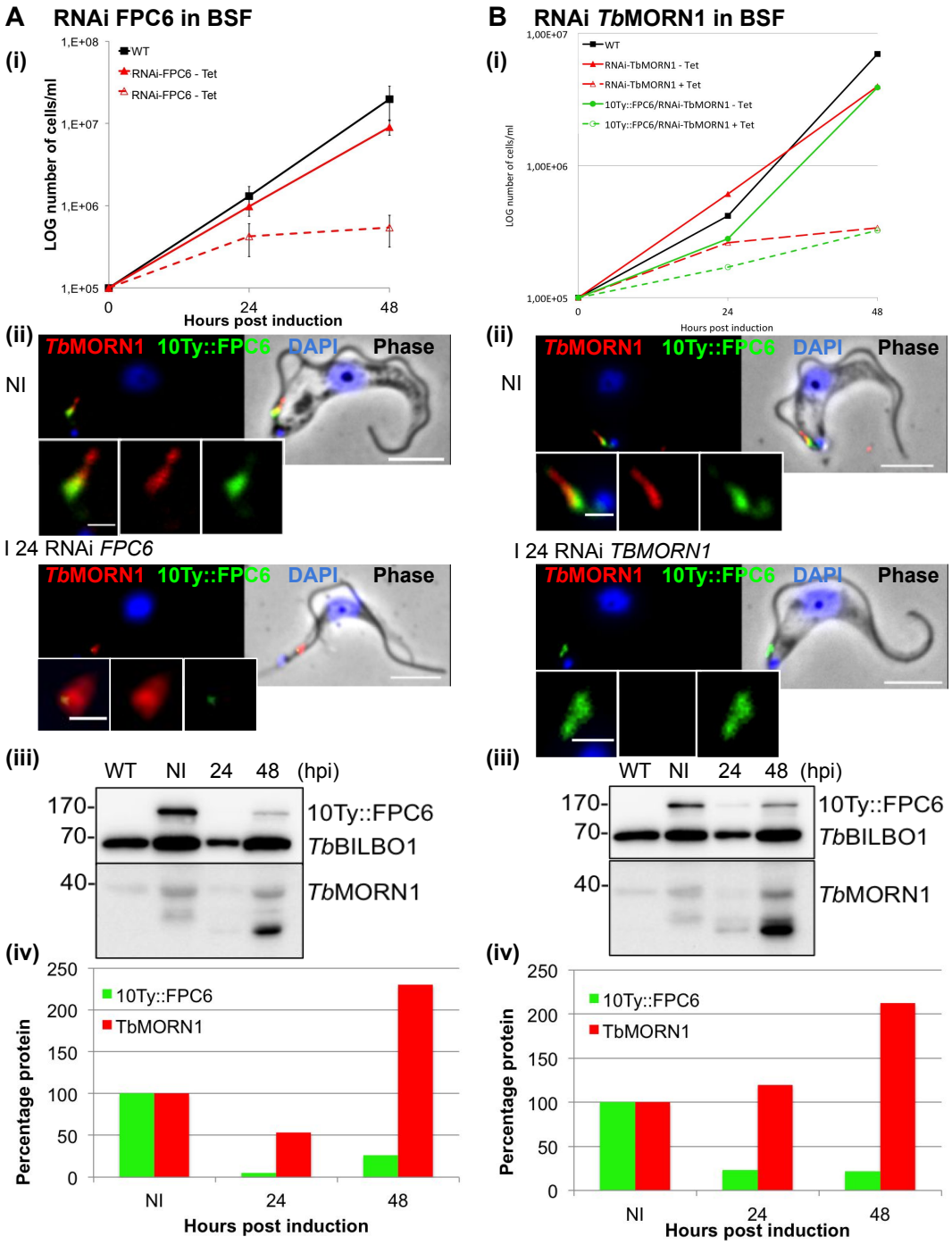

FIGURE 3.15: **RNAi depletion of either FPC6 or *Tb*MORN1 is sufficient for cell death.** **A** RNAi *FPC6* in the cell line 10Ty1::FPC6 led to (i) rapid cell death 24 hpi (ii) loss of 10Ty1::FPC6 protein 24 hpi (iii),(iv) a decrease in 10Ty1::FPC6 protein post induction but an increase in *Tb*MORN1 **B** RNAi *FPC6* in the cell line 10Ty1::FPC6/RNAi-*Tb*MORN1 (i) cell death as for RNAi *FPC6* (ii) *Tb*MORN1 protein disappeared after RNAi *TBMORN1*, but 10Ty1::FPC6 protein was unaffected. (iii),(iv) A surprising decrease in 10Ty1::FPC6 was seen and an increase in *Tb*MORN1 protein upon RNAi *TBMORN1*. NI=non-induced, WT=wild-type. Scale bar=5μm, inset=1μm.

10Ty1::FPC6 at the hook complex: at the head of *Tb*MORN1 (anti-*Tb*MORN1) and tapering into the shank. When RNAi *FPC6* is induced for 24 hours, either reduced or no labelling with 10Ty1::FPC6 was seen, however *Tb*MORN1 was still present and strongly labelled at the Hook complex, see Figure 3.15.A.(ii). This result, confirms that the RNAi *FPC6* is working and that it does not interfere with the location or presence of *Tb*MORN1 at the newly developed FPC. Trypanosome whole cell samples taken for western blot before (NI) and 24 and 48hpi RNAi *FPC6* showed a reduction in 10Ty1::FPC6 and an increase in *Tb*MORN1, see the blot and quantification in Figure 3.15.(iii) and (iv) respectively.

To explore the effect of RNAi *Tb*MORN1, Brooke Morriswood kindly sent the BSF RNAi *TBMORN1* cell line to the Robinson laboratory (as used in Morriswood and Schmidt, 2015). On receipt of this cell line, I induced RNAi *TBMORN1* to confirm the rapid cell death of the cells, and then transfected this cell line with an endogenous N-terminal 10Ty1 tag on FPC6: 10Ty1::FPC6. Once this new cell line was established (clone A5), I induced RNAi *TBMORN1* and observed the effect, being able to track the effect on FPC6 in this cell line. The growth curve in Figure 3.15.B.(i) showed rapid cell death after RNAi induction in this new cell line (10Ty1::FPC6/RNAi-*Tb*MORN1; green lines) as for RNAi FPC6 (cell line 10Ty1::FPC6/RNAi-FPC6). IFA, in Figure 3.15.B.(ii), showed in NI cells, the normal labelling for *Tb*MORN1 at the hook complex, and the co-localisation of 10Ty1::FPC6. After induction of RNAi *TBMORN1* for 24 hours the signal for *Tb*MORN (anti-*Tb*MORN1) had disappeared, but FPC6 was unaffected.

Western blot samples were taken for non-induced cells and those induced cells for 24 and 48 hours RNAi *TBMORN1*. Somewhat unexpectedly, the results were synonymous with that for RNAi *FPC6*, see Figure 3.15.(iii) and (iv), showing a reduction in 10Ty1::FPC6 and increase in *Tb*MORN1 protein. I was certain that the samples were correct: this result needs to be re-affirmed.

Overall, this set of results indicate that the two RNAi systems are working, at least as seen by IFA, where they are specific for the target mRNA seen by a reduction in protein. The loss of either one does not seem to affect the other, but depletion of either one leads to cell death.

3.7 Yeast 2-hybrid assays of FPC6 truncations

Previously in the Robinson laboratory, yeast 2-hybrid analysis of full-length FPC6 (by Dr Celia Florimond, PhD) showed an interaction with *Tb*BILBO1 FL, and two truncations of *Tb*BILBO1: T2 and T3 (see Chapter 1.4.7; Figure 1.12). T2 was the N-terminus and EF hands, and T3 was the EF-hands, coiled coil and C-terminus. Full-length FPC6 also interacted in one direction with *Tb*MORN1, however, truncations of FPC had not been tested previously. To this end, I designed the primers for constructs of the same truncations of FPC6: T1, T2 and T3 as above (see Figure 3.10).

These truncations of FPC6 were designed to be obtained by PCR from a plasmid harbouring the full-length sequence for *FPC6* (pcDNA3-FPC6-GFP) and to be used with aqua-cloning to insert the sequences into both pGAD and pGBKT7 vectors for bait and prey in Yeast 2-hybrid assays (see Methods 2.5.10, and Table 2.7). Unfortunately, due to lack of time at the end of my PhD, I was unable to complete this experiment.

Chapter 4

Results Part Two: scFv and Nanobodies

With the aim of further characterising *Tb*BILBO1 through the use of small antibody fragments that would be able to assess hidden epitopes and bring fluorescent imaging closer to the target, as well as with the aim of using these small antibody fragments as potential drugs to target *Tb*BILBO1 in vivo, an scFv and nanobodies were investigated. The scFv came from an IgM in the Robinson laboratory, already known to recognise *Tb*BILBO1 and the nanobodies were produced by immunising an alpaca with purified *Tb*BILBO1. The potential of scFv and Nbs is already known, however to express the Nbs as intra-bodies within the trypanosomes is novel and could indicate further the biogenesis of the flagellar pocket collar by studying its interaction with a Nb *in vivo*.

4.1 scFv

4.1.1 scFv sequence and *in silico* modelling

The single chain variable fragment (scFv) against *Tb*BILBO1 was produced by identifying and sequencing the variable regions of the immunoglobulin genes expressed by a mouse IgM-secreting hybridoma produced in the Robinson Laboratory. This monoclonal IgM was proven to identify *Tb*BILBO1 protein *in vivo* by immunofluorescence assay and western blot and binds to the C-terminal, coiled-coil region of the protein (see Figure 1.13.B.). The scFv was assembled from the identified variable regions with a short peptide linker sequence joining them together (see Figure 4.1.A.) and the assembled genes were then cloned into a generic vector (by Aldevron, Germany; for full details see Methods, Chapter 2.6.1). Modelling of this scFv using Phyre^2 (Kelley et al., 2015) was able to provide an *in silico* structural representation with 100% coverage and 100% confidence fit. Figure 4.1.B. shows a ribbon diagram and surface reconstruction.

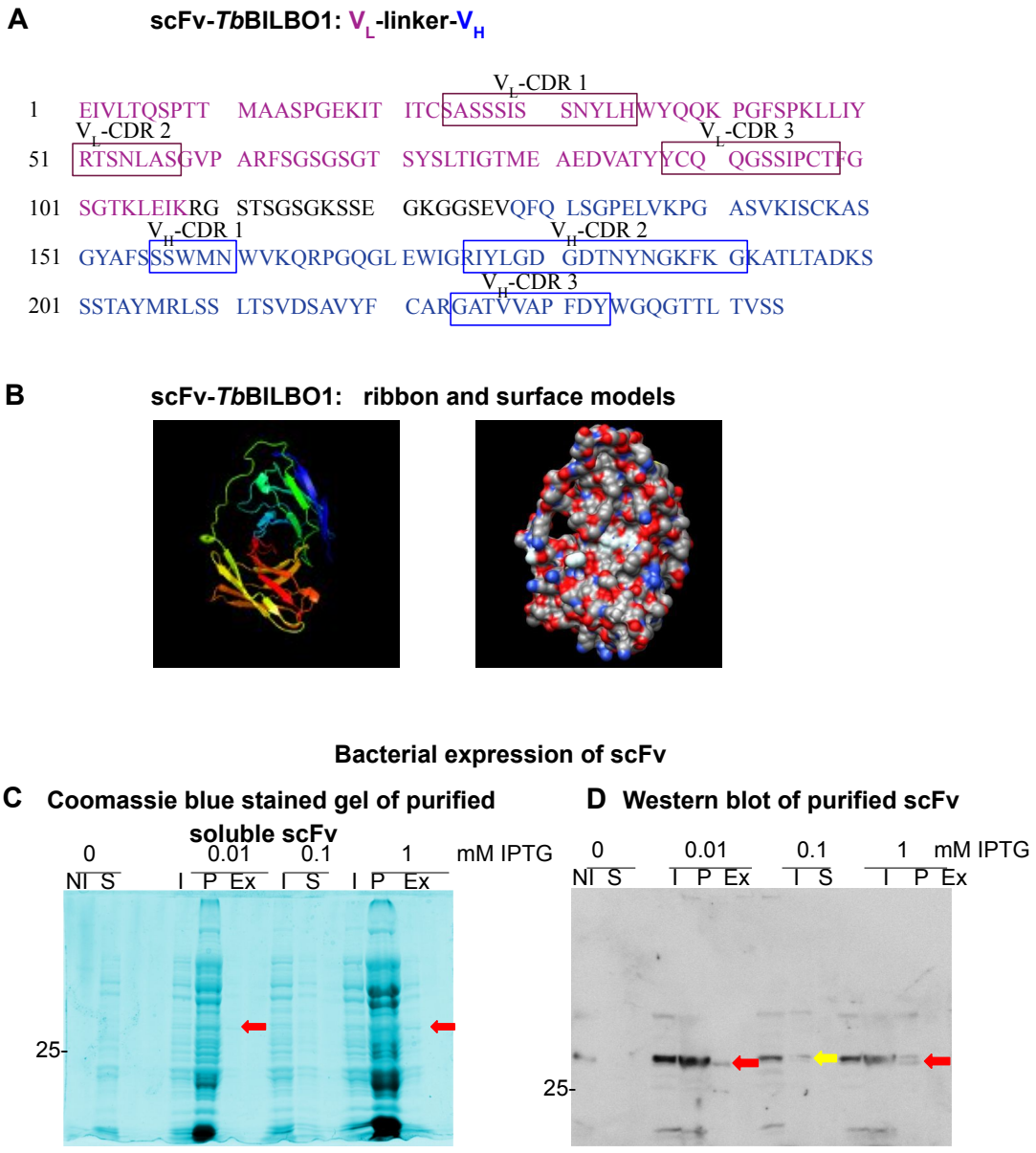

FIGURE 4.1: **scFv-*Tb*BILBO1 sequence and models.** **A** Amino acid sequence of scFv*Tb*BILBO1, annotated with the CDR regions for both light (V_L) heavy (V_H) variable regions. **B** Ribbon and surface diagrams modelled by Phyre^2 with 100% confidence (Kelley et al., 2015). **C** Bacterial expression of scFv, extraction and purification, seen on Coomassie blue stained gel and **D** western blot probed with anti-HIS (scFv::6HIS). NI=non-induced, I=induced, S=supernatant, P=pellet, Ex=periplasmic extract; arrows indicate the presence of scFv protein.

4.1.2 scFv-*Tb*BILBO1 was poorly expressed in *E. coli*

I made numerous attempts to purify scFv-*Tb*BILBO1 protein from *E. coli* bacteria. The scFv gene had been previously cloned into a pJET vector for cytoplasmic expression, however, I sub-cloned the scFv gene into a pHEN6c vector for periplasmic expression, with a *pelB* leader seqeunce to direct the protein to the periplasmic space. Pectate Lyase B (pelB) was identified in *Erwinia carotovora* (Lei et al., 1987) and directs the protein to the periplasmic space of gram negative bacteria. Both the heavy and light chain variable regions contain a disulphide bond and this requires the oxidising environment of the periplasmic space to be formed and allow stability of the scFv and fully functional antigen binding (Glockshuber and Schmidt, 1992). At the C-terminus, a 6xHIS tag was fused to the protein to allow purification by Immobilized Metal Affinity Chromatography (IMAC).

I used a range of concentrations of Isopropyl β-D-1-thiogalactopyranoside (IPTG) for induction of expression (0.01, 0.1, 0.5 and 1mM final concentrations) to try to find the optimal because higher concentrations of IPTG appeared to be slowing down the growth of the bacteria. I also varied the overnight incubation temperatures from 25 to 28°C to try to maximise the yield of the scFv*Tb*BILBO1 (see Methods Chapter 2.6.2 for full details of protein expression in bacteria). Figure 4.1.C. shows an example of a Coomassie blue stained gel of protein samples (InstantBlue™, Expedeon Ltd., ISB1L) and Figure 4.1.D. shows a western blot of the same samples taken from a representative purification experiment. The samples included: non-induced bacteria (NI), induced bacteria before (I) and after centrifugation to giving supernatant (S), pellet (P) and purified periplasmic extract (Ex). The results from 3 different induction concentrations of IPTG are shown, resulting in only a faint band at the correct size for scFv in the periplasmic extract (red arrows, 27kDa). A band was also seen in the sample from the supernatant by western blot (yellow arrow). This is not an ideal finding because it means that some protein is being lost, but according to Dewi et al., 2016 it has been shown previously that small antibody fragments can cross the outer cell membrane and be detected in the culture medium. A test was made by transforming BL21(DE3) competent *E. coli* with the scFv construct, however the same profile was obtained as with pHEN6c. Following purification of the periplasmic extract by IMAC using an (ÄKTA-purifier™10, GE Healthcare), a small peak was seen on the elution graph but these elutions were negative when tested by western blot, concluding that the HIS tag had been cleaved. In conclusion, expression and therefore extraction and purification of scFv*Tb*BILBO1 protein was very limited. It would be worth trying a yeast expression system, such as *Pichia pastoris* to try to improve expression and yield, as used by Vallet-Courbin et al., 2017 who found low yield with bacteria but much higher yields with a yeast system.

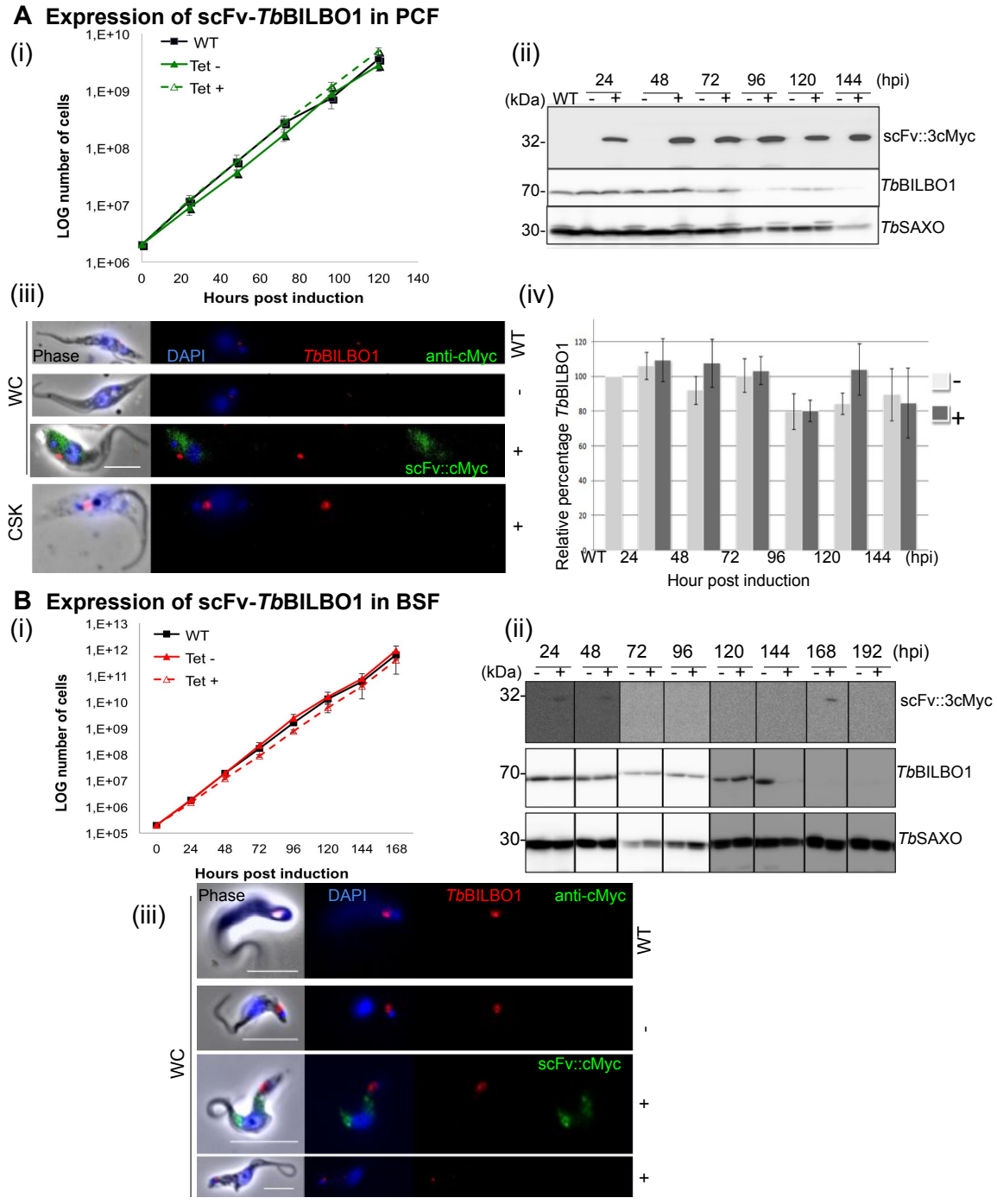

FIGURE 4.2: **scFv-*Tb*BILBO1 expression in PCF and BSF *T. brucei*.** **A** (i) Growth curve of scFv-*Tb*BILBO1::3cMyc expression in PCF *T. brucei*. (ii) Western blot confirming expression of scFv-*Tb*BILBO1::3cMyc. (iii) Cytoplasmic expression of scFv*Tb*BILBO1::3cMyc in WC from induced cells (+). (iv) Quantification of *Tb*BILBO1 present in trypanosomes at different time points of scFv expression post induction **B** (i) Growth curve of scFv expression in BSF. (ii) Weak and inconsistent expression of scFv seen on western blot. (iii) Only few *T. brucei* cells show weak cytoplasmic expression of scFv-*Tb*BILBO1::3cMyc. Scale bar = 5μm.

4.1.3 Expression of scFv*Tb*BILBO1 in *T. brucei* is cytoplasmic and not lethal

I successfully transfected both procyclic forms (PCF, Tb427.29.13) and bloodstream forms (BSF, Tb427.90.13) with pLew100-scFv-3cMyc. Below, I give a description of the resulting phenotypes.

In vivo expression of scFv in PCF

I tested three PCF clones expressing scFv-*Tb*BILBO1::3cMyc for up to 144 hours of induction, with 1μg/mL of tetracycline. Population growth curves were carried out for all three clones (clones 5, 8 and 9). None of the clones showed a difference in growth rate compared with non-induced (NI) or wild-type (WT) *T. brucei* cells. Figure 4.2.A.(i) shows a representative growth curve of one of the clones (clone 8) averaged over three independent experiments, the error bars represent standard error of the mean (SEM). During the induction period, the expression of scFv*Tb*BILBO1::3cMyc was monitored by western blot analysis using an antibody against the cMyc tag (see Table 2.2). Probing of whole cell samples of induced PCF trypanosomes revealed a protein band at 32kDa, the expected size for scFv-*Tb*BILBO1::3cMyc, in all induced cells. Figure 4.2.A.(ii) shows clone 8, as representative of the three clones tested. This result shows that all induced PCF cell lines, in this study, expressed scFv (against *Tb*BILBO1) and the protein was not degraded. Anti-*Tb*BILBO1 was used to probe the western blot membrane to detect any changes in *Tb*BILBO1 expression in the induced cells lines compared with wild-type (WT) and non-induced (NI). Anti-*Tb*SAXO, a protein of the axoneme (Dacheux et al., 2012) was used as a loading control. It appears that *Tb*BILBO1 protein levels are reducing over time, however the loading control (*Tb*SAXO) is also seen reducing so it is likely that this area of the membrane was poorly transferred or exposed. *Tb*BILBO1 is essential and if *Tb*BILBO1 really was reducing to this extent in the parasites, they would be dying (as seen by RNAi; Bonhivers et al., 2008).

The cellular localisation of scFv-*Tb*BILBO1::3cMyc was investigated by immunofluorescence assay (IFA) at each induction time-point in whole cells (WC) and detergent-extracted cells (cytoskeletons, CSK). From 24 to 144 hours of induction cells expressed scFv-*Tb*BILBO1::3cMyc was seen throughout the cell cytoplasm, as detected using anti-cMyc (Figure 4.2.A.(iii)). In fixed cytoskeletons, no labelling was seen with anti-cMyc in induced clones confirming the cytoplasmic localisation in WC. Indeed, when the concentration of extraction detergent (NP40) was reduced, the labelling was restored. These results confirm that scFv-*Tb*BILBO1::3cMyc is expressed in induced cell lines and is present in a soluble form within the cytoplasm of these cells. However, at no time point, did the cMyc labelling co-localise with endogenous *Tb*BILBO1 protein.

Finally, quantification of band intensity by western blot was carried out to confirm that expression of scFv-*Tb*BILBO1 had no effect on the levels of *Tb*BILBO1 protein

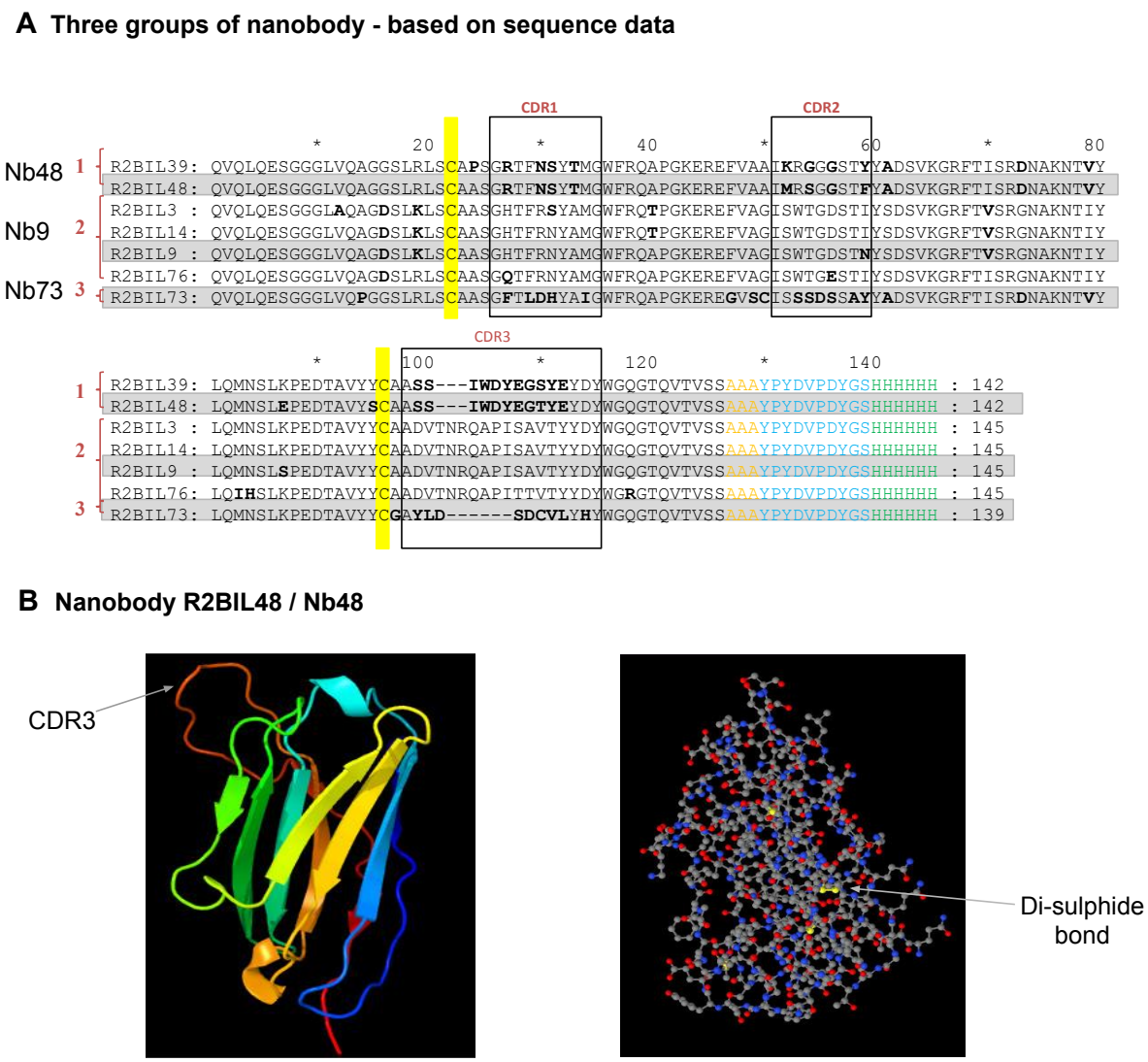

FIGURE 4.3: **Nanobody sequences and modelling.** **A** Amino acid sequence for the seven nanobodies produced against *Tb*BILBO1, grouped according to similarity in gene sequences. Complementarity-determining regions (CDRs) are outlined with boxes and disulphide bonds are highlighted in yellow **B** Ribbon diagram and surface modelling of Nb48 from Phyre[2] (Kelley et al., 2015).

in the trypanosomes. The bar graph in Figure 4.2.A.(iv) shows no real change over time in the relative levels of *Tb*BILBO1 protein in induced cells relative to wild-type in comparison to the ratio of *Tb*SAXO levels.

In vivo expression of scFv in BSF

In bloodstream forms, induced cell lines showed no difference in growth rate compared with non-induced or wild-type parasites, as seen previously with PCF. Figure 4.2.B.(i) shows representative data from one clone out of three tested (clones 12, 17 and 18) up to 168 hours induction, averaged over three independent experiments. By western blot, not all induced BSF cell lines revealed a band at 32kDa, the expected size for scFv-*Tb*BILBO1::3cMyc. Revelation of a band was only seen after almost 60 minutes exposure, see Figure 4.2.B.(ii). This indicated that not all induced cell lines were expressing scFv-*Tb*BILBO1::3cMyc and at those time-points were expression was seen it was limited. Additionally, in some cell lines, a band was revealed at some time points whilst not at others. Expression of scFv-*Tb*BILBO1::3cMyc was less consistent and much lower than in procyclic forms, which might indicate that the BSF parasites were controlling the expression of scFv within the cell and implying some degree of toxicity or adverse effect of expression of scFv in the parasites.

Detection of scFv-*Tb*BILBO1::3cMyc by IFA on BSF whole cells did not show consistent labelling WITHIN the parasites, compared with PCF. One induced cell line (clone 18) at one induced time point, had some cells with cytoplasmic labelling (seen in Figure 4.2.B.(iii)) but this was not a uniform finding compared with what was seen in PCF. The anti-cMyc labelling did not co-localise with endogenous *Tb*BILBO1 in these instances. Cytoskeleton fixation was negative for labelling with anti-cMyc, as for PCF. These data together indicate that the scFv against *Tb*BILBO1 expressed intracellularly in *T. brucei* was, generally, not highly expressed in BSF and seems to be cytoplasmic when it was detectable. Overall these results demonstrate the successful expression of scFv-*Tb*BILBO1 in PCF *T. brucei*, but limited expression in BSF, indicating a possible suppressive effect by BSF parasites, or selection of low/non-expressing forms post transfection.

4.2 Nanobodies

4.2.1 Seven anti-*Tb*BILBO1 nanobodies were identified following alpaca immunisation

Since *Tb*BILBO1 is an essential protein and required for the biogenesis of the flagellar pocket, a vital organelle for parasite survival (see Introduction Chapter 1.4.7), nanobodies were generated against *Tb*BILBO1 with the aim to use them as generic tools but also as protein drugs. Full-length, 6xhistidine-tagged, *Tb*BILBO1 protein was purified (as described in Methods Chapter 2.4) and sent to Nanobody Service

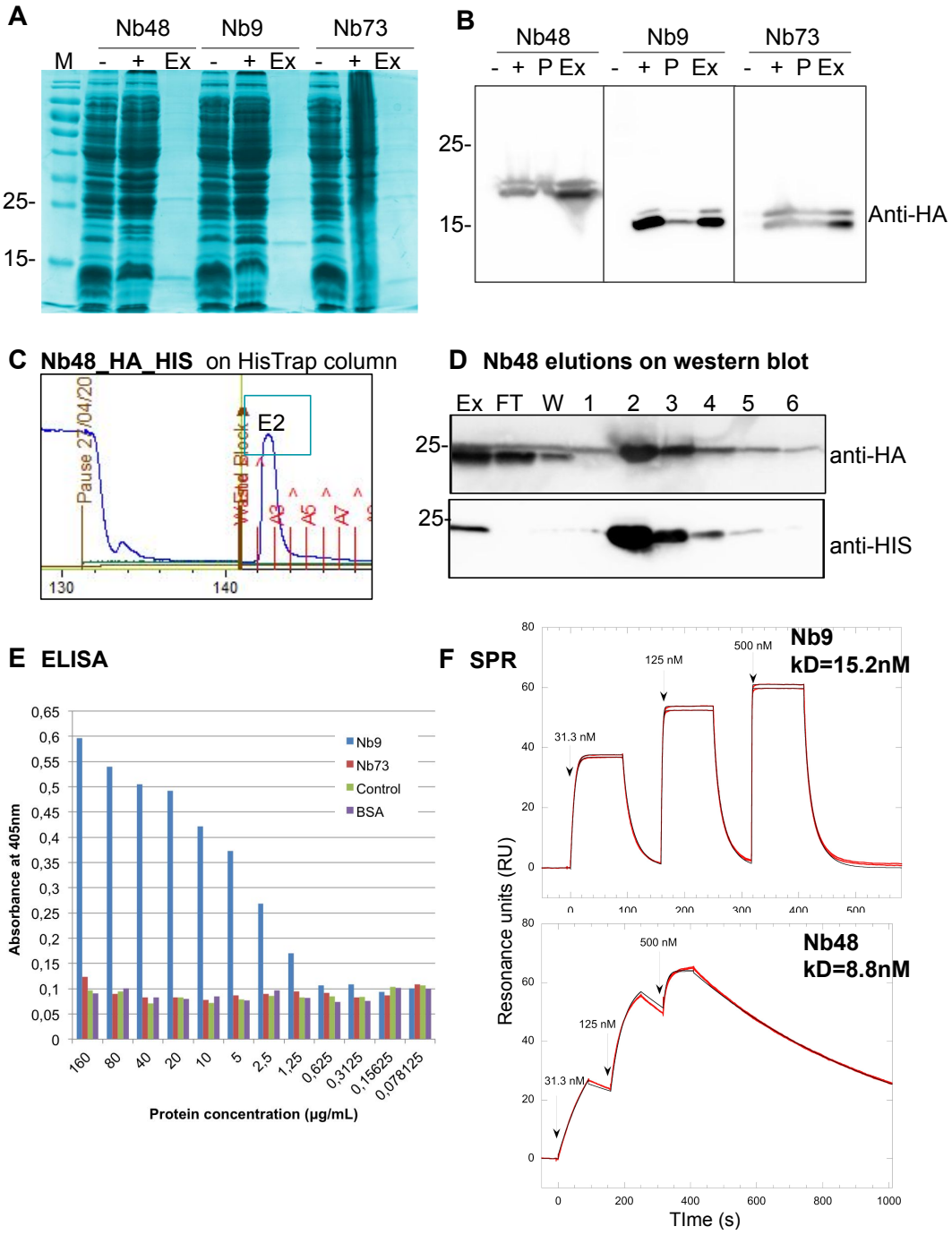

FIGURE 4.4: **Purified nanobody can recognise *Tb*BILBO1 *in vitro*.** **A** Coomassie blue stained gel of Nb expression in bacteria, before induction (-), after induction (+) and the periplasmic extract (Ex). **B** Samples run on WB and probed with anti-HA. **C** A peak seen with elution 2 on the purification profile for Nb48; p=pellet. **D** Samples of periplasmic extract (Ex), flow through (FT), wash (W) and elutions (1-6) run on WB. **E** ELISA results showing detection of *Tb*BILBO1 protein by Nb9. **F** Kinetic analysis by SPR of Nb9 and Nb48 binding to *Tb*BILBO1 *in vitro*.

Facility (Vrije Universiteit Brussel, Belgium). There an alpaca was subcutaneously injected with the soluble *Tb*BILBO1 protein once per week for 5 weeks to initiate an immune response. Anti-*Tb*BILBO1 nanobodies were subsequently derived from alpaca peripheral blood lymphocytes (full details in Methods Chapter 2.4). Seven different nanobodies were identified; the amino acid sequences of these nanobodies (Nbs) are shown in Figure 4.3.A. These seven nanobodies were assigned to three different groups based on similarities in their amino acid sequences. Group 1 contained R2BIL39 and R2BIL48; Group 2 contained R2BIL3, R2BIL9, R2BIL14 and R2BIL76; and Group 3 contained R2BIL73. It could be assumed that each group was derived from clonally-related B-cells, which are the result of somatic hypermutation, or from the same B-cell but diversified due to PCR error during library construction. It was hypothesised that Nbs in the same group would recognise the same epitope, but their other characteristics such as affinity, potency, stability, expression yield, *etc.*, could be different. A Phyre^2 model of the 3 dimensional structure of Nb48 (group 1), is shown in Figure 4.3.B. I worked with one nanobody from each group, from hereafter termed: Nb48, Nb9 and Nb73.

4.2.2 Functional anti-*Tb*BILBO1 nanobodies produced from *E. coli*

The gene sequences for *Nb48*, *Nb9* and *Nb73* were fused with a *pelB* leader sequence and a C-terminal 6 x histidine tag. Each Nb construct was cloned independently into a pHEN6c vector and transformed into WK6 *E. coli*. Periplasmic expression of Nb was induced by addition of ImM IPTG, as seen in Figure 4.4.A. showing whole bacterial cells before (-) and after (+) induction of Nb expression and the periplasmic extract (Ex). A faint band seen between 15 and 18kDa is the Nb protein. Initial expression appeared low and this was hypothesised to be due to cleavage of the HIS tag, therefore an additional HA tag was inserted between the Nb sequence and the HIS tag. Confirmation of cleavage of the HIS tag can be seen in the western blot probed with anti-HA in Figure 4.4.B. The upper band represents Nb with a HA::6HIS tag and the lower band represents the Nb with the HA tag alone.

The periplasmic extracts containing the soluble anti-*Tb*BILBO1 Nb were purified using immobilized metal affinity chromatography (IMAC) using an ÄKTA-purifier^{TM}10 (GE Healthcare). Elution of the purified protein was performed using 10mM imidazole, which displaces the HIS tagged Nb bound to nickel ions, allowing the eluted Nb to be recovered. A peak was seen with elution 2, shown on the graph in Figure 4.4.**C**, for Nb48. The samples from this purification can be seen by western blot in Figure 4.4.D, probed with both anti-HA and anti-HIS; labelling with anti-HA is seen throughout the samples and anti-HIS is concentrated in elution 2. This confirms again that the HIS tag was being cleaved and that a large proportion of the purified Nb was not being recovered.

4.2.3 Purified nanobody binds to *Tb*BILBO1 by ELISA

To assess the binding of purified nanobodies (6HIS-tagged) to purified *Tb*BILBO1 protein, indirect enzyme-linked immunosorbent assays (ELISA) were performed. The Nbs were first absorbed on to the plates, then purified *Tb*BILBO1 protein was added, followed by an antibody specific for *Tb*BILBO1 (rabbit polyclonal, aa1-110; see Table 2.3). Detection of the primary antibody was carried out using an HRP-linked secondary anti-rabbit antibody (Sigma A9169; Table 2.4). ELISA was carried out with Nb9, Nb73, a negative periplasmic control was used produced from the periplasmic extract of bacteria transformed with an empty pHEN6c vector, and BSA (bovine serum albumin) was also used as a negative control. The results indicated that Nb9 (group 2) displayed a positive concentration dependent binding curve (absorbed at 405nm) with *Tb*BILBO1 protein, as seen in Figure 4.4.E. Nb73 was negative in this experiment, potentially due to its inability to bind to the denatured form of *Tb*BILBO1 in this particular ELISA. Both of the negative controls were negative.

4.2.4 Surface Plasmon Resonance confirms a strong binding affinity of Nb48 to *Tb*BILBO1

Once Nb48 had been purified, a superior test to characterize the binding kinetics of the Nb48, Nb9 and Nb73, with *Tb*BILBO1 was desired and SPR (surface plasmon resonance) was carried out by the IECB (Institut Européen de Chimie et de Biologie, Pessac, France). In this assay the dissociation constant (K_D) was measured: this is a measure of the dissociation (physical separation) of each Nb from *Tb*BILBO1. The binding affinity of the Nb to *Tb*BILBO1 is the inverse of the K_D, i.e. the lower the K_D, the higher the affinity. The benefits of SPR compared with other assays, are that it is measured in real-time and is label-free (Marschall et al., 2015). The K_D of one nanobody from each group was investigated: Nb48, Nb9 and Nb73. SPR assays were performed using a BIAcore T200 and a sensor chip (Series S, GE Healthcare), for further details see Methods Chapter 2.10. *Tb*BILBO1 was bound to the dextran matrix on the chip and the three different Nbs were flowed over at a rate of 30μL/minute. All Nb were previously drop-dialysed in running buffer. All Nbs showed low non-specific binding to the reference surfaces and all experiments were replicated on at least three separate occasions.

The sensorgrams are shown in Figure 4.4.F., the Nbs are represented by the red curves and the black line represents the theoretical fit as obtained from the Biaevaluation software to a kinetic titration data set of three concentrations of the nanobodies: 31.3 nM, 125 nM and 500 nM. It was not possible to assess Nb73 (group 3) using SPR due to the very limited and un-pure expression and extraction of this nanobody from bacteria. The results here, show that Nb9 and Nb48 bind to *Tb*BILBO1, but do not behave kinetically in the same way. The 100 times slower rate of dissociation of Nb48 with *Tb*BILBO1 compared to Nb9, affirms the higher affinity of Nb48 for *Tb*BILBO1 protein *in vitro*. The very good superposition of the sensorgrams with the

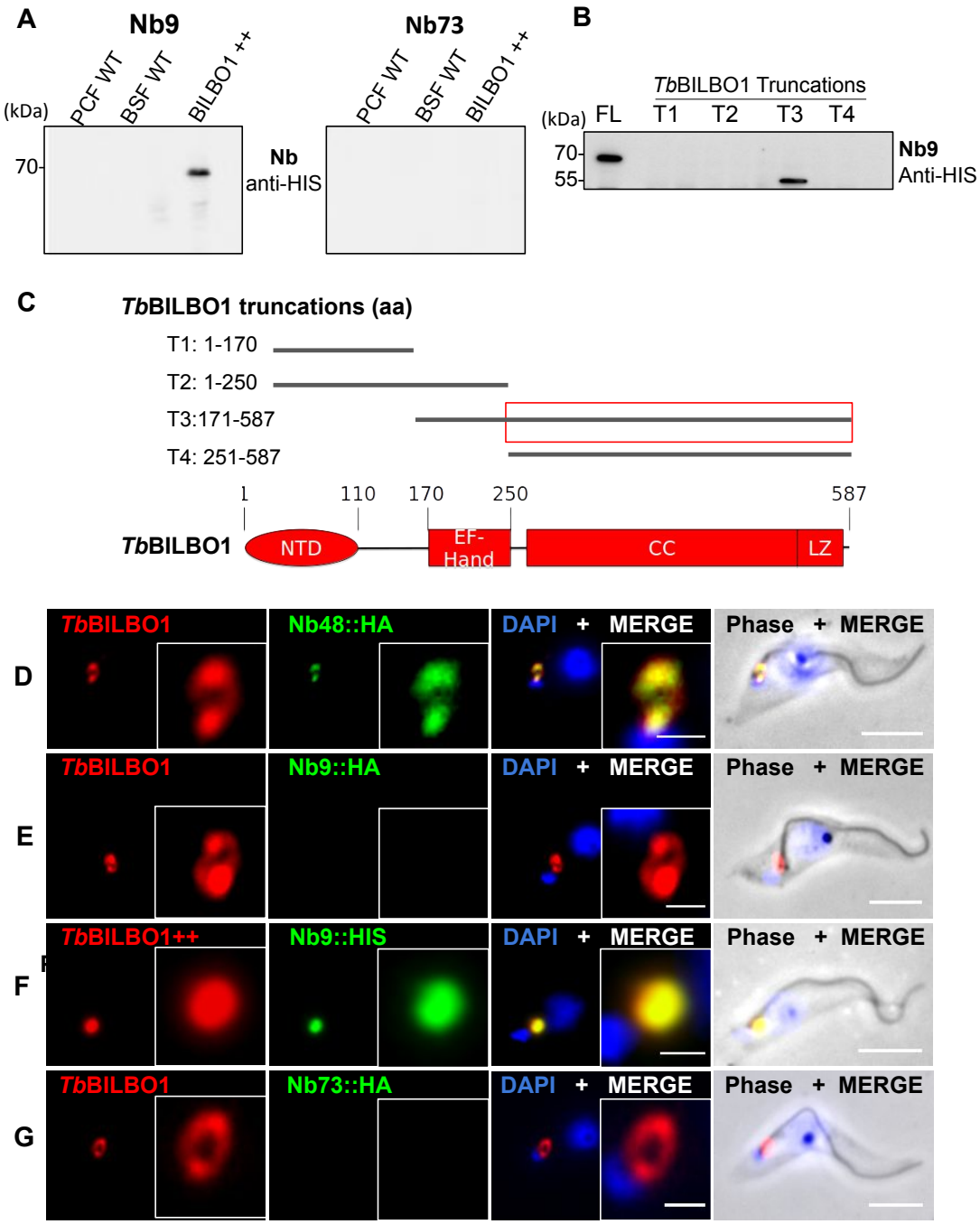

FIGURE 4.5: **Purified nanobody can recognise *Tb*BILBO1 in *T. brucei*** Testing of **A** Using Nb9 and Nb73 as probes for western blot. **B** Probing full-length (FL) and truncations (T) of *Tb*BILBO1 with Nb9 by Western blot. **C** Identification of the *Tb*BILBO1 domain recognised by Nb9. **D** Nb48 on wild-type (WT) *T. brucei* cytoskeletons by IFA, **E** Nb9 on WT, **F** Nb9 on *T. brucei* over-expressing *Tb*BILBO1, and **G** Nb73 on WT. Scale bar = 5μm, inset = 1μm.

fitting curves validates the Langmuir 1:1 model of interaction for analysing them. These data confirm that Nb48 (group 1) has the highest affinity for *Tb*BILBO1, followed by Nb9 (group 2).

4.2.5 Nb9 recognises over-expressed *Tb*BILBO1 in PCF *T. brucei*

Purified Nb9 and Nb73 were used as immuno-probes by western blot, see Figure 4.5.**A**. Nb9::6HIS was probed on whole cell trypanosome samples of *T. brucei* PCF, BSF and cells over-expressing *Tb*BILBO1, a positive signal was only seen with Nb9 for cells expressing an extra copy of *TBBILBO1* (BILBO1++). When Nb73 was used as an immuno-probe on the same western blot samples, a negative result was observed for all lanes, showing that Nb9 did not recognise *Tb*BILBO1 in these experiments.

4.2.6 Nb9 recognises the coiled coil region of *Tb*BILBO1

In order to identify the domain of *Tb*BILBO1 that was recognised by the nanobodies, 3cMyc-tagged full-length (FL) and truncated versions of *Tb*BILBO1 were expressed in PCF *T. brucei* (pLew100-*Tb*BILBO1FL/T1/T2/T3::3cMyc; pLew100-T4::GFP). Whole cell samples of protein extracts from trypanosomes from these cell lines were taken, run on a western blot and probed with Nb9, see Figure 4.5.**B**. Nb73 was not tested due to the previous negative result with whole cell samples by western blot. Nb9 recognised a linear epitope in truncation T3 (aa171-587), the coiled-coil region, of *Tb*BILBO1, see Figure 4.5.**C**. In this experiment, T4 was negative. In fact, T4 was a sample produced from *T. brucei* over-expressing aa251-587 with a different tag to the FL and other truncations. The T4 sample was also an old sample, therefore the protein may have degraded, or the expression of this truncation in the trypanosomes could have been much lower than the others, therefore undetectable in this experiment. This experiment was later repeated and gave a positive result for both T3 and T4 (not shown), confirming that Nb48 recognised a region of *Tb*BILBO1 in the coiled-coil domain.

4.2.7 Nb48 recognises endogenous *Tb*BILBO1 in *T. brucei*

Once each of the three purified and dialysed nanobodies, Nb48 (group 1), Nb9 (group 2) an Nb73 (group 3), had been obtained, they were tested as immunological tools on fixed trypanosomes by IFA (see Methods 2.6.4 for the nanobody dialysis protocol). The purified nanobodies were tagged with HA::6HIS. Preliminary testing by IFA showed that the use of anti-HA gave more sensitive and clearer results than anti-HIS; this might be due to cleavage of the HIS tag (as previously identified), less accessibility to the HIS tag in the folded protein, or differences in detection of the two separate antibodies used for detection (anti-HA mouse and

anti-HIS mouse, see Table 2.2). Figure 4.5.**D-G** show a panel of immunofluorescence images summarising the findings of testing Nb48 (group 1), Nb9 (group 2) and Nb73 (group 3). Nb48::HA::6HIS was able to recognise endogenous *Tb*BILBO1 in PCF (Figure 4.5.**A**.) and BSF *T. brucei*. The anti-cMyc labelling (Nb) co-localises exactly with *Tb*BILBO1 as seen in the merged fluorescence image in row **D**. Testing of Nb9::HA::6HIS on wild-type (WT) *T. brucei* was negative, as seen in row **E**. However, testing of purified Nb9::6HIS as a probe on PCF *T. brucei* over-expressing *Tb*BILBO1 (pLew100-*Tb*BILBO1::3cMyc) was positive, see Figure 4.5.**F**, showing that Nb9 is able to detect *Tb*BILBO1 but only when a larger quantity of *Tb*BILBO1 is present in the trypanosomes, in these experiments. NB73::HA::6HIS was not able to detect endogenous *Tb*BILBO1 in WT *T. brucei*, see row **G**, or in trypanosomes over-expressing *Tb*BILBO1 (not shown). These data of the nanobodies used as immuno-probes on IFA correspond with those observed by WB and confirm that Nb48 is the best Nb with regards recognising endogenous *Tb*BILBO1 in trypanosomes under these conditions.

4.2.8 Culture of *T. brucei* with Nb48 has no effect on growth

Bloodstream forms of *T. brucei* were incubated with different concentrations of purified Nb48 for 48 hours: 0.1μg/mL, 0.5μg/mL, 1μg/mL and 10μg/mL. No effect was seen on growth of trypanosomes incubated with purified nanobody, compared with the wild-type bloodstream form trypanosomes or those incubated with a negative nanobody control (the periplasmic extract from *E. coli* transformed with an empty pHEN6c vector i.e. no nanobody). Fixation of trypanosomes incubated with Nb48 for IFA were negative for detection of labelling of the HA tag of the purified Nb48 either in or on the FPC or on the outside of the trypanosome cells.

4.2.9 Anti-*Tb*BILBO1 intra-nanobodies are cytotoxic in *T. brucei*

*Tb*BILBO1 is an essential protein of the flagellar pocket collar in *T. brucei* and has the ability to form polymers and dimers *in vivo* and *in vitro* (Florimond et al., 2015). The expression of nanobodies inside the trypanosomes (intracellularly) was explored to determine: if these "intra-nanobodies" (INb) can be functionally produced in *T. brucei*, can find their target *Tb*BILBO1, can bind (tightly) to that target, and challenge the structures formed *in vivo* by *Tb*BILBO1.

The same three Nb gene sequences as used for purification earlier, Nb48, Nb9 and Nb73, were independently cloned into a trypanosome inducible expression vector (pLew100-Nb::3cMyc). I successfully transfected this construct into procyclic cells with all three nanobodies, but only Nb73 produced viable clones in bloodstream forms. The expression of each intra-nanobody was induced respectively with 1μg/mL tetracycline initially and daily cell counts were taken. Independent induction of each Nb resulted in phenotypes that ranged from rapid cell death from

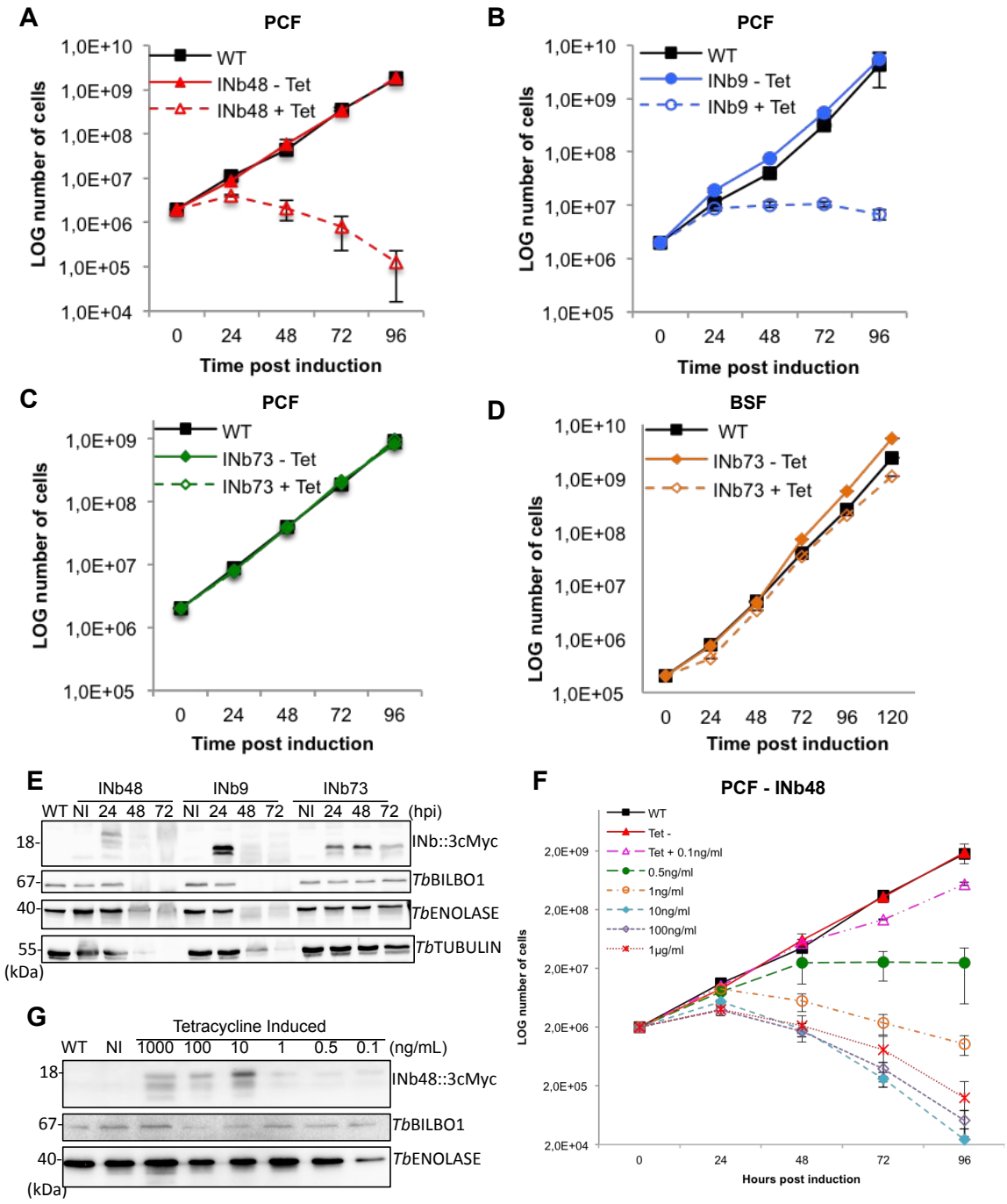

FIGURE 4.6: **Expression of intra-nanobodies was trypanocidal** Growth curves of **A** INb48 (group 1) in PCF, **B** INb9 (group 2) in PCF, and **C** INb73 (group 3) in PCF and **D** INb73 in BSF. **E** Western blot of INb48, 9 and 73 expression in PCF, **F** Tetracycline dose-dependent effect on trypanosome growth and cytotoxicity for INb48. **G** Western blot of expression of INb48 at different tetracycline concentrations.

24 hours post induction for INb48 (group 1; Figure 4.6 growth curve **A**), to a moderate rate of cell death for INb9 from 24 hours post-induction (group 2; growth curve **B**), to no change in growth rate for INb73 in PCF (group 3; growth curve **C**), or in BSF (clone 2; growth curve **D**). Figure 4.6 shows representative growth curves for each group plotting the mean of three independent induction experiments, error bars represent standard error of the mean (SEM). These data implies that Nb9 does recognise endogenous *Tb*BILBO1 in trypanosomes when expressed as an INb and that it does not need to be over-expressed to be recognised. this might imply that the results of the use of Nb9 as an immuno-probe are probably below the level of detection in the conditions used or that INb9 only binds to newly made or modified *Tb*BILBO1 *in vivo*.

The western blot in Figure 4.6.**E**. shows whole cell samples taken from wild-type (WT) *T. brucei*, non-induced (NI) and induced (I) PCF trypanosomes at 24, 48 and 72 hours post induction with 1μg/mL tetracycline. INb proteins are only detected after induction of expression. Interestingly, after intra-cellular expression, some INb degradation is observed. There is disappearance of INb48 and INb9 from 48 hours post-induction, as the parasites begin to die. At 48 hpi of INb48 and INb9, *Tb*BILBO1 is also seen to disappear; this might be due to degradation of *Tb*BILBO1 protein after targeting by INb48 or INb9, followed by death of the cells. Inversely, this may be due to death of the cells following INb targeting of *Tb*BILBO1, and degradation of all proteins in the cells, as seen by a loss of *Tb*ENOLASE and *Tb*TUBULIN, in this western blot. These results substantiate those found earlier with the purified nanobodies. Nb48 (group 1) proves to be the most potent, with highest affinity for *Tb*BILBO1 by SPR, able to detect endogenous *Tb*BILBO1 in fixed trypanosomes by IFA and rapidly trypanocidal when expressed as an intra-nanobody.

4.2.10 INb induced trypanosome death is dose-dependent

I monitored the effect of expression of INb48 in procyclic forms using different concentrations of tetracycline as shown in Figure 4.6.F. Concentrations of 1μg/mL, 100ng/mL and 10ng/mL produced very similar growth curves, with rapid death of cells from 24hpi. 1ng/mL produced death after 24 hours but with a more gradual decline of the population over 72 hours. 0.5ng/mL produced a growth arrest after 48hpi and 0.1ng/mL had a slight reduction in growth after 48hours compared with non-induced and WT, but the trypanosomes continued to grow thereafter. The expression was confirmed by western blot, see Figure 4.6.G. Here it is clear to see the reduction in expression of INb48 in whole cell PCF *T. brucei* samples as the dose of tetracycline was reduced. A concentration of 1μg/mL tetracycline was used as the standard concentration for INb48 induction because it killed the entire population of cells within a 48 hour period allowing biochemical and cellular study of the resulting phenotype.

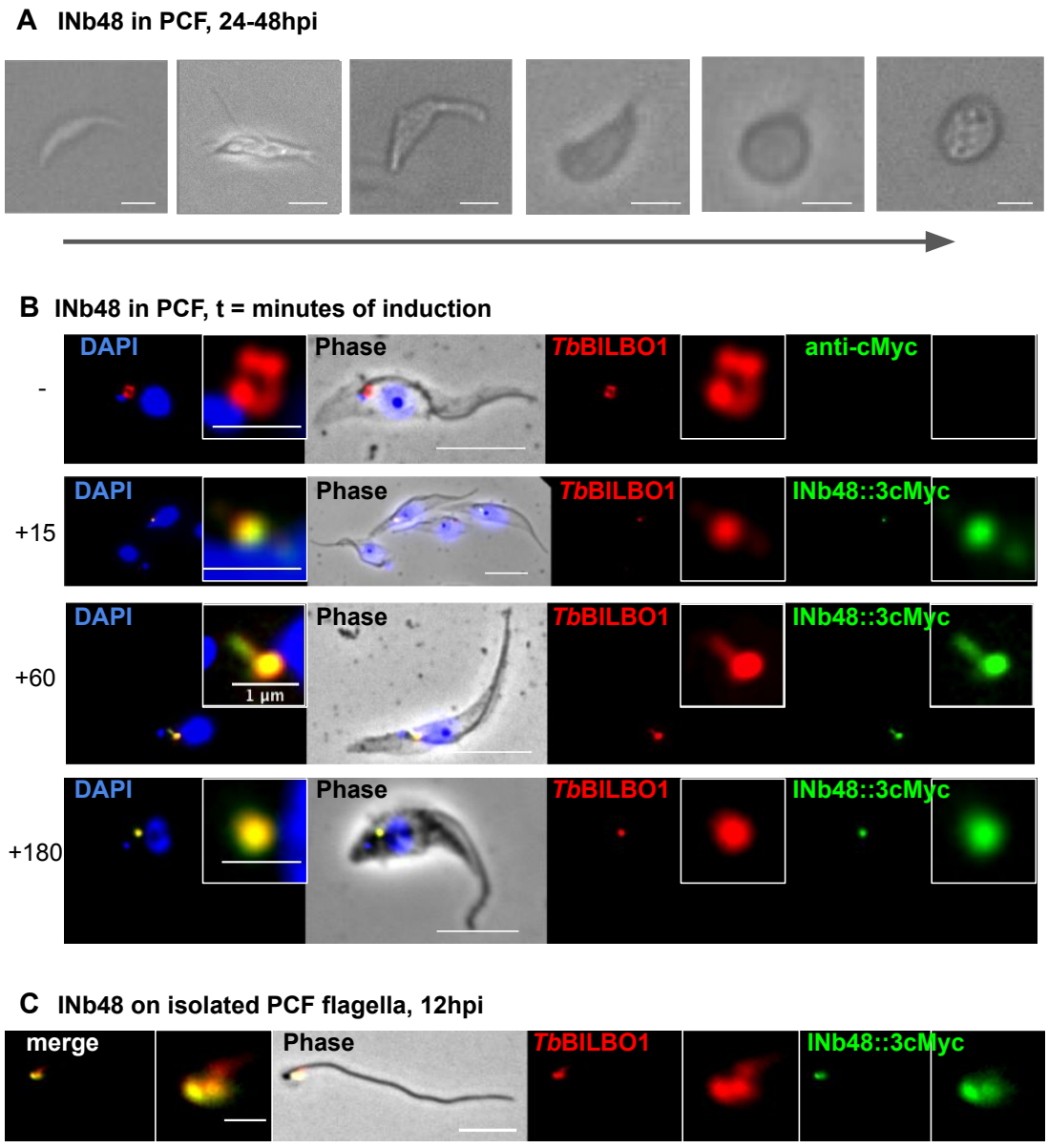

FIGURE 4.7: **INb48 expression targeted *Tb*BILBO1 *in vivo*.** **A** Images of live cells expressing INb48 **B** IFA of fixed PCF trypanosomes showing co-localisation with *Tb*BILBO1 from 15 minutes post-induction **C** Co-localisation of INb48::3cMyc with *Tb*BILBO1 on isolated *T. brucei* PCF flagella. Scale bar = 5μm, inset = 1μm.

4.2.11 Dying cells become rounded

I observed trypanosomes expressing INb48, induced at 1μg/mL tetracycline, using a light microscope. Cells became rounded-up, exhibiting a reduced mobility and aggregated together as they died. Images of representative cells taken at progressive stages of death are shown in Figure 4.7.**A**. A detached flagellum is evident in the second image from the left.

4.2.12 INb48 co-localises with *Tb*BILBO1 *in vivo*

PCF *T. brucei* expressing INb48 were fixed for immunofluorescence at different time points of induction, with 1μg/mL tetracycline. Figure 4.7.**B**. shows a panel of immunofluoresence images of fixed trypanosomes showing no detection of INb48::3cMyc in non-induced cells (-), precise co-localisation between *Tb*BILBO1 (anti-*Tb*BILBO1 1-110) and INb48::3cMyc (anti-cMyc monclonal) in 20% of cells at just 15 minutes of induction, and then co-localisation in 100% of cells from 60 minutes of induction. The lower panel in Figure 4.7.**B** at 180hpi shows fixed whole cells, whilst other panels are of detergent extracted cells (CSK). At 60 minutes post induction an interesting signal was seen for both *Tb*BILBO1 and INb48, extending from the FPC towards the basal bodies. This signal is seen frequently with *Tb*BILBO1 using the anti-*Tb*BILBO1 polyclonal antibody (aa1-110) and it was intriguing to see the intracellularly expressed nanobody also present at this location. Based on unpublished immuno-EM data, this signal is most likely the MTQ.

4.2.13 INb48 co-localises with *Tb*BILBO1 on isolated flagella

Flagella extractions were made (see Methods 2.3.1) from PCF trypanosomes induced for 12 hours with 1μg/mL tetracycline and these were fixed for IFA. The flagella were probed with anti-*Tb*BILBO1 and anti-cMyc, and again there was co-localisation between the two signals, indicating that the intra-nanobody was bound tightly to its target, *Tb*BILBO1, and was not removed with the KCl extraction.

4.2.14 INb9 shows a weaker co-localisation with *Tb*BILBO1 *in vivo*

INb9 was seen co-localising with *Tb*BILBO1 at 6 hours post induction in some cells (Figure 4.8.**B**) and in other the labelling of anti-cMyc was seen in the vicinity of the FPC, apparently along the FAZ, but not co-localising with *Tb*BILBO1 (Figure 4.8.**C**). After 24 hours induction of expression of INb9, labelling of anti-cMyc was seen within the cell, not only co-localising with *Tb*BILBO1 but elsewhere in the cell. Figure 4.8.**E** shows a trypanosome with a detached flagellum, co-labelling of INb9::3cMyc and *Tb*BILBO1 at the location of the FPC for the new flagellum, but a

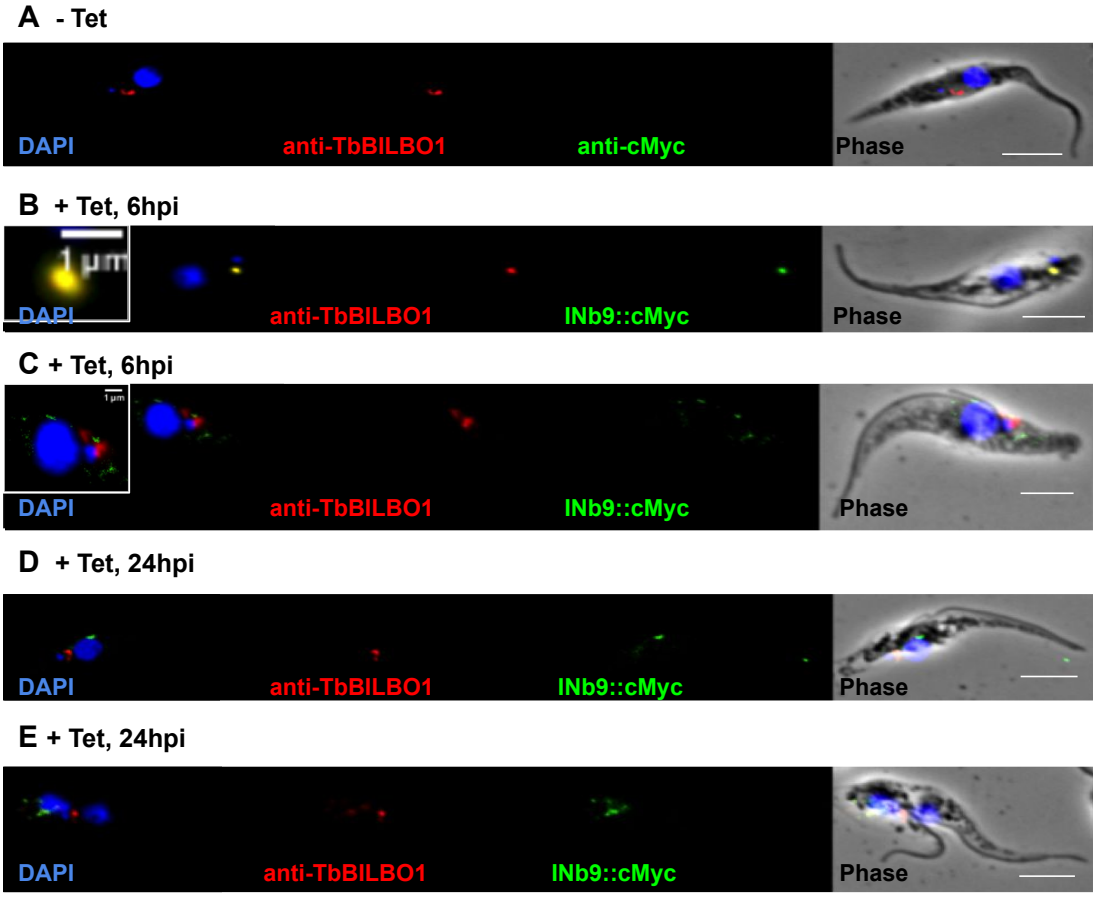

FIGURE 4.8: **Immunofluoresence of intra-nanobody 9 expression in PCF *T. brucei*. A** Shows a non-induced trypanosome with no labelling for anti-cMyc. **B** After 6 hours induction of expression of INb9 co-labelling is observed of INb9::3cMyc and *Tb*BILBO1 **C** In some cells it was observed that the labelling for cMyc was not co-localising with *Tb*BILBO1 and dispersed in the vicinity of the FPC region. **D** After 24 hours post induction of INb9 expression labelling of cMyc is seen in the trypanosome cell but not co-localising with *Tb*BILBO1. **E** A detached flagellum is seen and labelling of INb9::3cMyc is observed at the location of the FPC for the detached flagellum where a weak *Tb*BILBO1 co-labelling signal is seen. Scale bar = 5μm; inset = 1μm.

weaker signal at the old FPC and additional labelling for anti-cMyc in the surrounding area of the cell.

4.2.15 Intra-nanobody expression in *T. brucei* gives an RNAi *TBBILBO1*-like phenotype

To describe in more detail the unusual phenotype of trypanosomes expressing INb48, cells were fixed at 24 and 48 hours post-induction (hpi), see Figure 4.9. Non-induced trypanosomes displayed the classic immunofluorescence signal for *Tb*BILBO1, the annular labelling at the flagellar pocket collar (FPC) as seen in **A**; no labelling of anti-cMyc was seen in non-induced cells, signifying that Nb48 was not being expressed in these cells. **B** represents a typical induced *T. brucei* cell expressing INb48::3cMyc, with precise co-labelling of the intra-nanobody with *Tb*BILBO1. This cell is also starting to show the more rounded phenotype observed by light microscopy of live cell (Figure 4.7.**A**.) *in vivo*. In these cells, labelling of anti-cMyc was only ever seen in conjunction with *Tb*BILBO1. After induction of INb48, the new flagellum was always detached from the length of the cell body as seen with RNAi *TBBILBO1* (Bonhivers et al., 2008; see Introduction 1.4.7). In almost all *T. brucei* cells observed, *Tb*BILBO1 and INb48 were only observed at the old FPC (always positioned anteriorly in PCF *T. brucei*).

Investigation of the detached flagella phenotype was carried out by co-labelling with anti-*Tb*PFR2 and anti-FAZ (L3B2). *Tb*PFR2 is a protein of the paraflagellar rod, running alongside the axoneme of the flagellum outside of the cell body (see Introduction 1.4.3) and FAZ/L3B2 is a protein marker of the flagellum attachment zone (FAZ), anchoring the flagellum to the cell body along its length (see Introduction 1.4.4). Figure 4.9.**C**. shows a non-induced trypanosome cell labelled with *Tb*PFR2 along the flagellum (an additional basal bodies signal is always seen with this antibody in the Robinson laboratory) and no detection of INb48::3cMyc in these cells. **D** shows labelling of *Tb*PFR2 along the old flagellum (anteriorly) and in the newly detached flagellum at the base of an extended posterior end. A kinetoplast is seen at the base of the extended posterior end in this cell; this was a frequent finding and was also seen with RNAi *TBBILBO1*. In this cell, INb48::3cMyc can be clearly seen at the old FPC (at the posterior of the cell body in PCF *T. brucei*). When anti-FAZ labelling was carried out on 24 hour induced cells, a signal could be seen as usual alongside the old flagellum which is attached along its length from its exit from the cell at the FP anteriorly towards the anterior tip of the trypanosome cell, as seen in Figure 4.9.**E**. Also seen in this cell is a short FAZ signal, apparent at the base of the new detached flagella(DF) indicating that this structure was in the process of being formed. The appearance of a FAZ signal at the base of the DF was variable in the population, possibly due to a variation of the stage of the cell cycle the trypanosome cell was at when the induction of expression of intra-nanobody was induced.

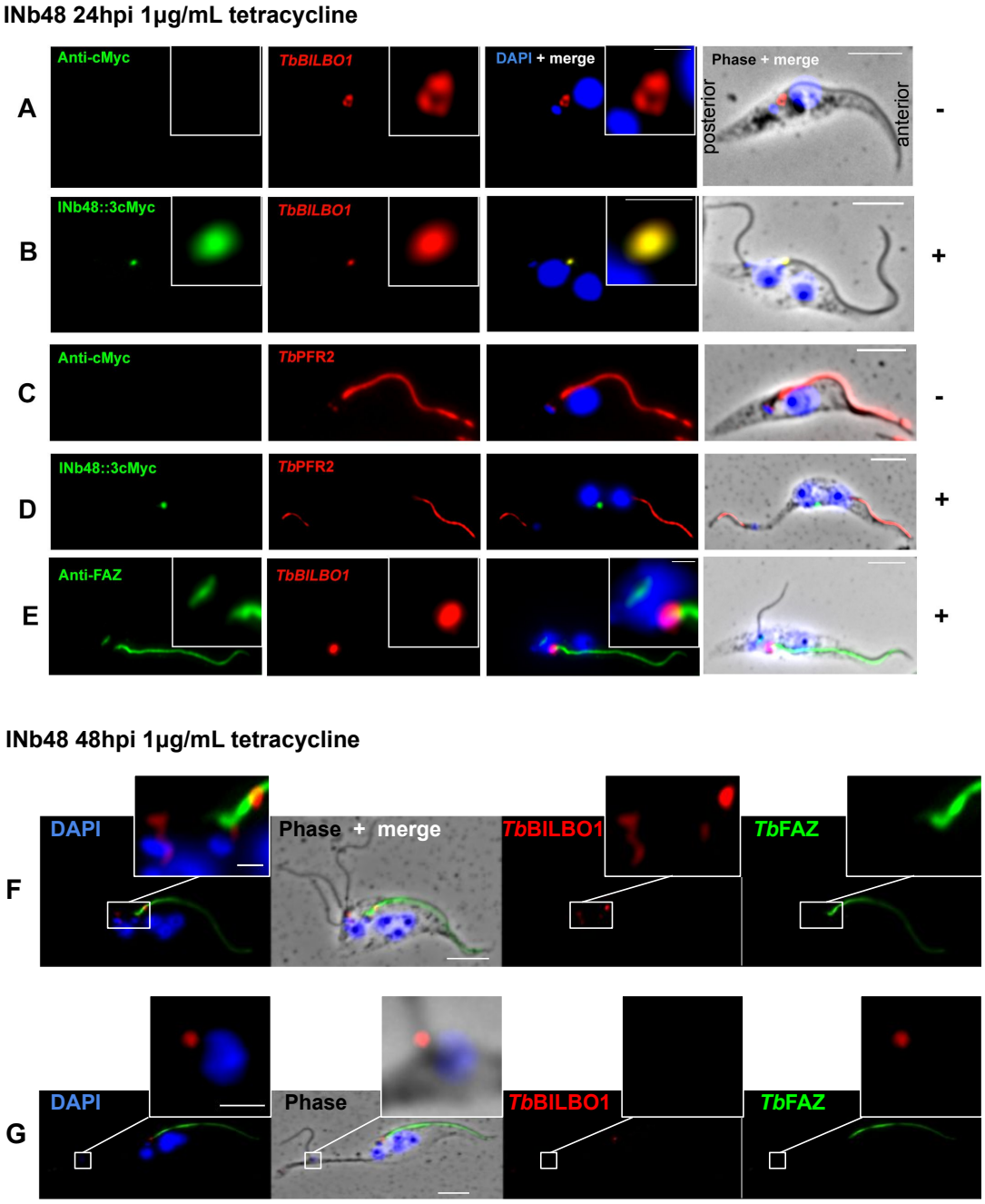

FIGURE 4.9: **INb48 expression resembled RNAi *TBBILBO1*.** **A** IFA of non-induced PCF *T. brucei*. **B** 24hpi showing co-localisation of INb48::3cMyc with *Tb*BILBO1 and a detached flagella (DF). **C** Non-induced trypanosome showing labelling of *Tb*PFR2. **D** 24hpi showing an extended posterior end of the cell with a DF labelled with *Tb*PFR2. **E** Flagellum attachment zone labelling (FAZ/L3B2) also seen at the base of the DF. **F** 48hpi multiple DF seen in a single trypanosome cell, with *Tb*BILBO1 labelling at the FPC location: at the old FPC and the base of the DF. **G** Extended posterior end with *Tb*BILBO1 labelling at the base of the detached flagella. Scale bar = 5μm, inset = 1μm.

At 48hpi cells with multiple nuclei, kinetoplast and detached flagella could be found, as seen in Figure 4.9.**F**. In this cell, a FAZ signal was not seen at the base of the detached flagella but a signal for *Tb*BILBO1 was seen. This cell has 3 kinetoplasts, 3 nuclei and 3 detached flagella, evidence that the cell had gone through the process of mitosis twice without division. It is known that *T. brucei* lacks certain cell cycle checkpoints (Ploubidou et al., 1999, Hammarton et al., 2003) and this result here adds to these known data, that *T. brucei* can replicate and segregate the kinetoplast without cytokinesis. The nuclei have divided but remain in close apposition to each other. Figure 4.9.**G**. shows a multi-nucleated trypanosome cell 48hpi, in this case the *T. brucei* cell exhibits an extended posterior end with a detached flagellum with a basal kinetoplast. In this cell, a signal is clearly seen for *Tb*BILBO1 at the base of the detached flagellum. These results are in contrast to those of RNAi *TBBILBO1* where the detached flagella were never accompanied with labelling of *Tb*BILBO1 at their base, neither were multiple detached flagella seen in the RNAi *TBBILBO1* phenotype (Bonhivers et al., 2008).

4.2.16 INb48 expression disrupts the flagellar pocket collar

These unusual phenotypes were observed in more detail by thin section transmission electron microscopy (TEM). Figure 4.10.**A**. shows a wild-type (WT) trypanosome cell with a single flagellum exiting the cell *via* the flagellar pocket (FP). In contrast to this, Figure 4.10.**B**. shows trypanosome cells 24 hours post induction of the expression of INb48 with 1μg/mL tetracycline. This image shows clearly a cell with an open flagellar pocket and a detached flagellum (DF; also in zoom). One finding that was not obvious previously on immunofluorescence was the accumulation of intracellular vesicles within induced trypanosomes. This lethal phenotype seen here was also seen with RNAi *Tb*BILBO1 (Bonhivers et al., 2008), in that a new flagellum was formed in the absence of a flagellar pocket indicating that *Tb*BILBO1 function was indeed hampered. The accumulation of intracellular vesicles was also seen when *Tb*BILBO1 protein was knocked-down in *T. brucei* indicating a disruption in endo-/exocytosis. Additional images of transmission electron microscopy from thin sections of PCF *T. brucei* cell lines expressing INb48 and INb9 can be found in Appendix B, Figure B.1. A population of trypanosomes can be observed containing intracellular vesicles as well as more examples of detached flagella. For INb9, *T. brucei* cells with some vacuoles can be observed as well as abnormal flagellar pocket collar and flagellum attachment zone with an abnormal flagellar pocket open on one side, see Appendix B, Figure B.2.

Isolated flagella, derived from cells that had expressed INb48 for 6, 12 or 24 hours were isolated, probed with a mouse anti-cMyc antibody, then 5nm gold conjugated anti-mouse beads and visualised by electron microscopy. Some flagella were double labelled by probing with anti-cMyc antibody as above and also anti-*Tb*BILBO1 (polyclonal 1-110aa) antibody followed by anti-rabbit 15nm, gold-conjugated beads. Figure 4.10.**C**. shows a WT PCF *T. brucei* flagellum probed with anti-*Tb*BILBO1 then 15nm gold beads; the distinctive annular shape of the FPC is outlined with

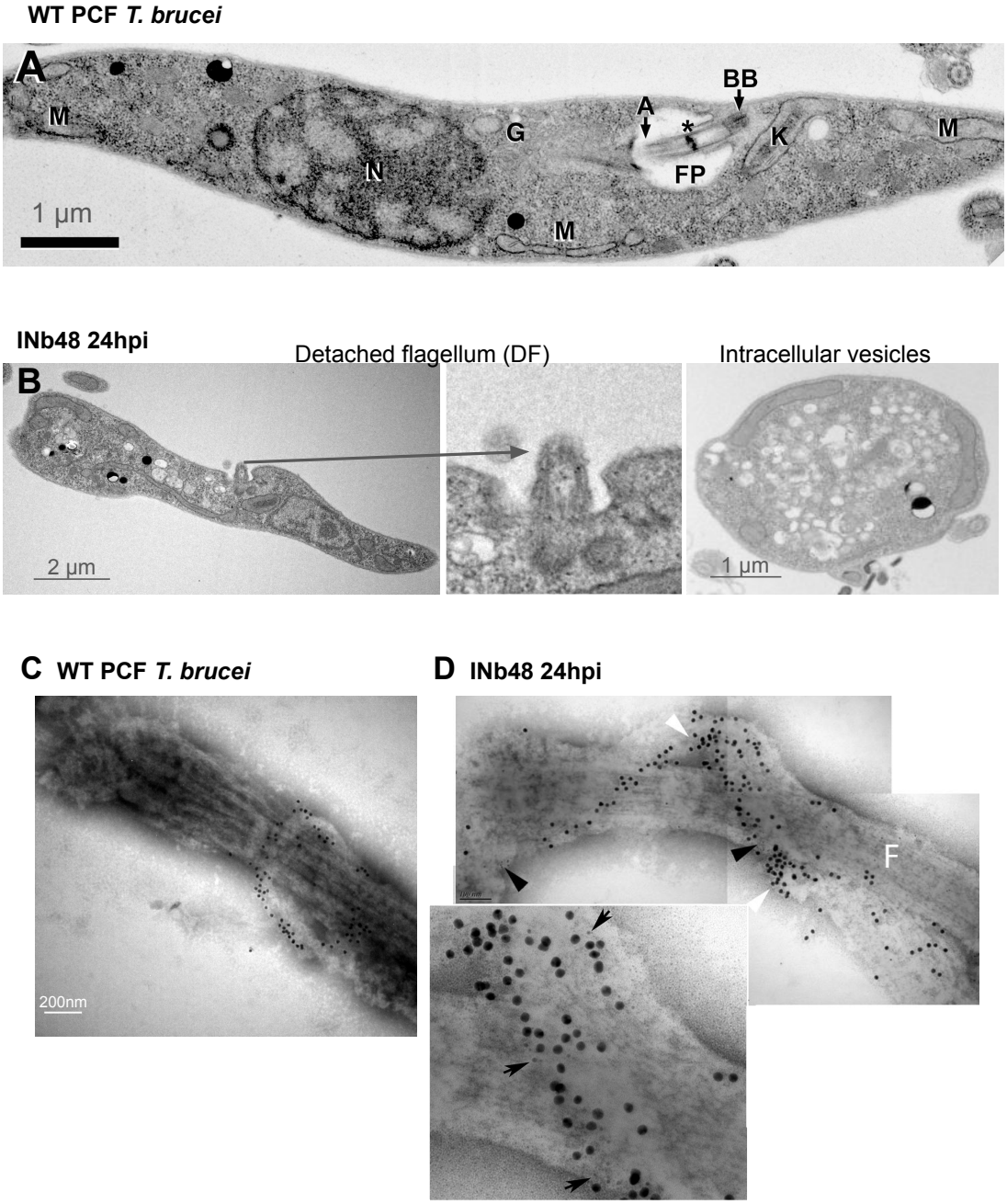

FIGURE 4.10: **INb48 expression disrupts FPC formation.** **A** Transmission electron micrograph of WT PCF *T. brucei* taken from Bonhivers et al., 2008. **B** INb48 24hpi showing a detached flagella and intracellular vesicles. **C** Immuno-electron micrograph of isolated flagella of WT PCF *T. brucei*. **D** INb48 24hpi showing co-localisation of INb48::3cMyc (5nm gold beads=black arrow heads) with *Tb*BILBO1 (15nm gold beads=white arrow heads) and disruption of the flagellar pocket collar (FPC). A=axoneme, BB=basal bodies, FP=flagellar pocket, G=Golgi, K=kinetoplast, M=mitochondrion and n=nucleus.

*Tb*BILBO1 protein labelling. The micrographs of trypanosomes expressing INb48 for 24 hours revealed that INb48::3cMyc (black arrow heads) was located from the basal bodies to the FPC in co-localisation with the gold labelling of anti-*Tb*BILBO1 (black arrow heads), Figure 4.10.**D**., indicating that INb48 was indeed targeting and binding to its epitope: *Tb*BILBO1. The anti-*Tb*BILBO1 signal was often present on the MTQ (see Introduction 1.4.2), a quartet of specialised FP-associated microtubules of unknown function, hypothesised to be the route for proteins to be trafficked to and from the FPC. Thus, the co-labelling of the MTQ with INb48 and anti-*Tb*BILBO1 could fit with this hypothesis. Disruption of the flagellar pocket collar (FPC) was seen with loss of the distinct annular structure and co-labelling of INb48::3cMyc (black arrow heads) with *Tb*BILBO1 (white arrow heads) along the same structure. To conclude, the targeting of *Tb*BILBO1 by INb48 was precise and led to a change in the structural conformation of the flagellar pocket collar, likely inhibiting its normal function, ability to replicate and therefore lack of a new FPC and hence a lack of a new FP and detached flagellum. Additional images of immuno-electron microscopy of isolated flagella from PCF expressing INb48 can be found in Appendix B, Figure B.3. INb9 (anti-cMyc) can also be seen co-localising with *Tb*BILBO1, as well as present between the basal bodies and the flagellar pocket collar, see Appendix B, Figure B.4. Disruption of the FPC can be seen 24hpi with *Tb*BILBO1 labelling seen extending in a linear form anteriorly along the flagellum.

4.2.17 INb48 expression induces to a structural change in *Tb*MORN1 of the hook complex

I also observed the fate of *Tb*MORN1 of the hook complex, when INb48 was expressed in PCF. *Tb*MORN1 is an essential structure positioned just distal to the FPC along the flagellum and involved in influencing the regulation of entry of molecules into the flagellar pocket (Morriswood and Schmidt, 2015; see Introduction Chapter 1.4.9). In Figure 4.11.**A** immunofluorescence images show in a non-induced (NI) trypanosome, the distinguishable hook-shape of the hook complex of which *Tb*MORN1 is a component. In trypanosomes expressing INb48 for 24 hours, the distinctive hook shape is elongated along the direction of the flagellum and the head of the hook is lost. A magnified view of this is seen in Figure 4.11.**B** where in the wild-type cells, the anti-*Tb*MORN1 gold beads are concentrated at the FPC and along a substantial arm of the shank of the hook curving distally along the flagellum (taken from Albisetti et al., 2017). A small amount of *Tb*MORN1 can be seen at the level of the basal bodies; a potential docking station for proteins destined for the FPC or further along the flagellum. Isolated flagella fixed 24 hours post induction of INb48 expression in PCF *T. brucei* are shown. The black arrow heads indicate INb48 and the white arrow heads indicate *Tb*MORN1. The labelling of *Tb*MORN1 and INb48 are both seen on the MTQ, however the labelling for *Tb*MORN1 has altered from the WT and there is no longer a concentration of 15nm gold beads at the FPC and the normal hook shape appears straight and extended along the flagellum, no longer displaying the characteristic hook-shape.

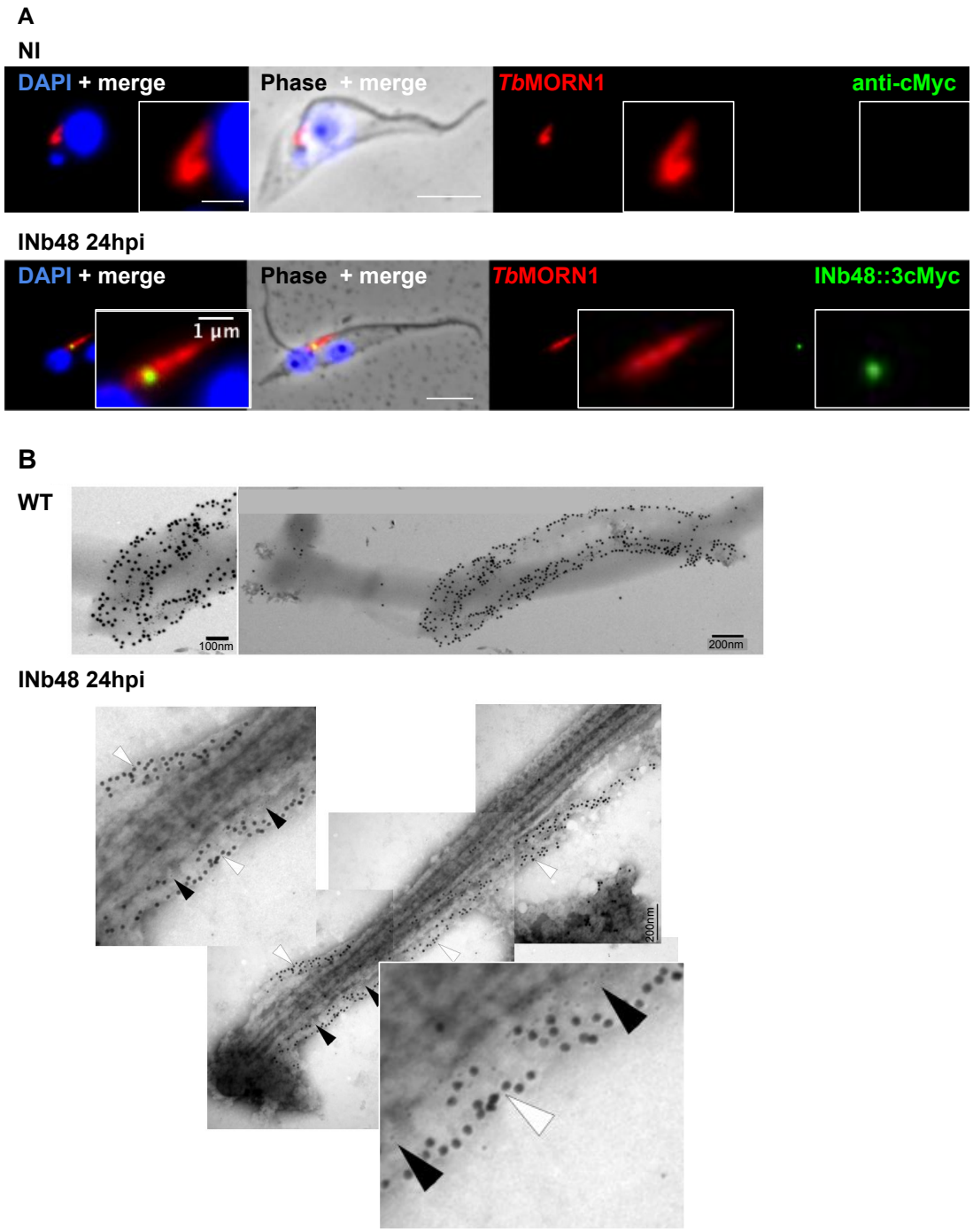

FIGURE 4.11: **INb48 expression disrupts *Tb*MORN1 of the hook complex. A NI** = non-induced: IFA of wild-type procyclic *T. brucei* showing the labelling for *Tb*MORN1 at the hook complex. **INb48 24hpi** expressing INb48 showing disruption of the hook-shape of *Tb*MORN1 protein complex and localisaton of INb48 at the FPC. Scale bar = 5μm, inset = 1μm. **B WT** Immuno-electron micrograph of isolated flagella of WT PCF *T. brucei* probed with anti-*Tb*MORN1 (Albisetti et al., 2017). **INb48 24hpi** showing co-localisation of INb48::3cMyc (5nm gold beads; black arrow heads) with *Tb*MORN1 (15nm gold beads; white arrow heads) and disruption of the FPC and hook complex.

4.2.18 INb48 expression in *T. brucei* leads to a block in cytokinesis

The linear organisation of the kinetoplast and nucleus was analysed and shown in Figure 4.12. I counted 200 cells for each cell condition and at each time-point for three independent inductions; the cell conditions were: PCF wild-type (WT), non-induced (NI) 12 hours and 24 hours of induction of the expression of intra-nanobody 48 at 1μg/mL tetracycline.

In order to understand the resulting abnormal phenotypes, a shall give a brief description of wild-type, procyclic culture form *T. brucei* cell morphology through the trypanosome cell cycle. In wild type G1 cells, when moving from the posterior to the anterior of the cell, the linear organisation of DNA containing organelles, the kinetoplast (or mitochondrial genome) and the nucleus is: kinteoplast (K), followed by the nucleus (N), which equates to the abbreviation 1K1N. As the cell passes through the cell cycle these organelles duplicate, firstly the kinetoplast to form 2K1N cells then the nucleus to form 2K2N cells, followed by cytokinesis, which returns the daughter cells to 1K1N. This means that wild-type cells never possess more than the 2K2N complement. For further description see Introduction Chapter 1.3, Figure 1.7 and Figure 4.12.B.

The results of cell cycle stage counting after expression of INb48 in *T. brucei* procyclics can be seen in bar graph **A** in Figure 4.12. For wild-type cells (blue bars), the majority, 78% of trypanosomes, were in 1K1N stage, followed by 14% in the 2K1N stage and 7% of cells in the 2K2N stage. The non-induced cells, followed the same pattern and number of cells in each cell cycle stage as for the wild-type (red bars). A distinct change was seen in trypanosomes expressing INb48 for 12 hours, with a reduction in 1K1N and 2K1N cells and an increase in 2K2N cells. There was also the appearance of abnormal K/N phenotypes and ratios, such as 1K2N, when the nucleus had divided before the kinetoplast. One prominent feature of induced cells was the appearance of trypanosomes with detached flagella (11%) and cells with abnormal and often multiple K/N ratios (5%; green bars). After 24 hours post induction, the profile seen for 12hpi continued to augment with a further reduction in 1K1N and 2K1N cells and a further increase in 2K2N cell stage trypanosomes (purple bars). At this stage of induction the number of abnormal 1K2N cells had greatly increased as had the number of trypanosomes with detached flagella, 45%. Over 3% of cells now had extended posterior ends and an increase in cells with abnormal ratios of K/N, including cells with more than 2K and/or 2N (15%). The normal PCF *T. brucei* cell cycle is shown in the schematic to the right, Figure 4.12.**B** (adapted from Ooi and Bastin, 2013).

I further investigated the cells in the 2K2N stage and categorised them according to linear organisation of K and N from posterior to anterior orientation in the cell for each trypanosome. I did this for 200 *T. brucei* cells from each cell condition and time-point post induction, over three independent inductions, as previously. Bar graph **C** in Figure 4.12 displays the results. For both wild-type (blue bars) and non-induced

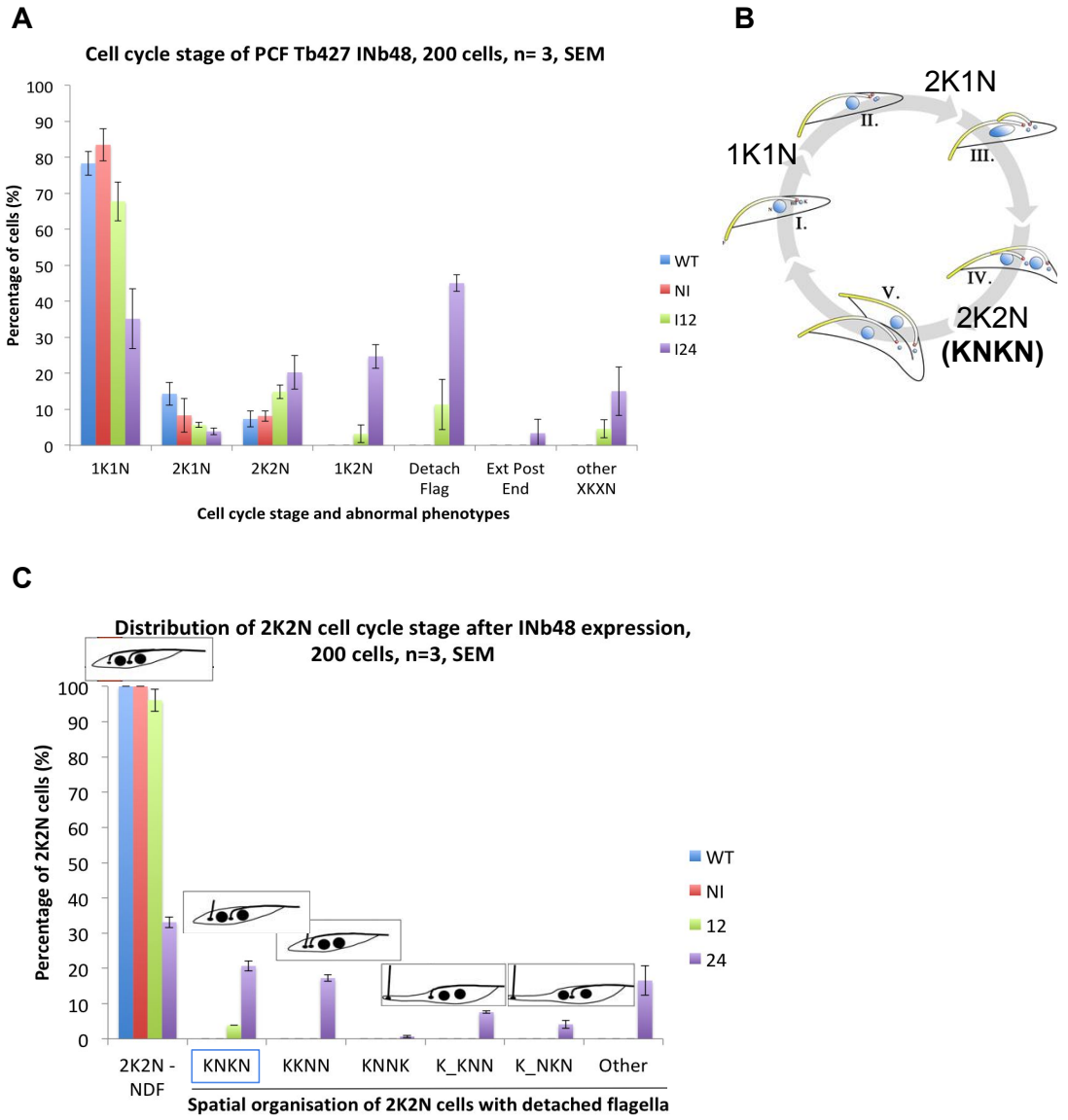

FIGURE 4.12: **INb48 expression disrupts cytokinesis in *T. brucei*** **A** Bar graph to show the percentage of trypanosomes counted at each stage of the cell cycle for *T. brucei* wild-type (WT), non-induced (NI), 12 and 24 hours post induction. **B** schematic of PCF *T. brucei* cell cycle indicating the order and number of kinetoplasts (K) and nuclei (N), adapted from Ooi and Bastin, 2013. **C** Distribution of the 2K2N cells. NDF = non-detached flagella, SEM = standard error of the mean.

cells (red bars) all trypanosomes possessing 2K2N are in the normal order of KNKN. At 12hpi the appearance of 2K2N cells with detached flagella started to appear (4%); these cells still had a normal linear organisation of KNKN (green bars). At 24 hpi, however, a drastic change was seen with almost 76% of 2K2N cells possessing a detached flagella (purple bars) distributed over a number of arrangements of order of K and N, with or without extended posterior ends. Figure 4.12**.C**. shows small line drawings (taken from Bonhivers et al., 2008) depicting the main possible phenotypes within the 2K2N arrangement.

These abnormal phenotypes are a clear indication of disruption in the cell division cycle. It appears that there is a general cell cycle arrest at the 2K2N stage, indicating the cells cannot undergo division. This is supported by the fact that multi-nucleated cells and those with greater than 2K were observed. Overall, this indicates that the DNA containing structures of the cell were able to divide and indeed separate, but the trypanosome cell itself was unable to undergo cytokinesis. Similar findings with regards to the cell cycle counts was seen with RNAi *TBBILBO1* (Bonhivers et al., 2008) suggesting that the crucial steps or structures required for cytokinesis were lost and thus cell death ensued. In the case of RNAi a simple reduction in *Tb*BILBO1 protein prevented a new FPC and FP being formed and this in turn led to a detached flagella. It then followed that trypanosomes with this phenotype were unable to divide. In the case of the intra-nanobody, the total amount of *Tb*BILBO1 had not been reduced, *per se*, but after INb48 targeted *Tb*BILBO1 protein *in vivo* the cytoskeletal structure of the FPC was disorganised and a new FP could not be formed leading to a detached flagellum. An accompanying disruption in endo-/exocytosis ensued due to disruption of the FP and the hook complex (*Tb*MORN1). The ultimate fate for the RNAi *TBBILBO1* and the cells expressing INb48 was the same.

Chapter 5

Discussion

5.1 Overview relative to aims and objectives

Overall, the aims and objectives of my thesis were met. I was able to make advances in the characterisation of a novel FPC/hook complex protein FPC6 as well as demonstrating the functionality of an scFv and nanobodies raised against *Tb*BILBO1 when used as an immuno-probe and when expressed in *T. brucei*. In this chapter, I shall discuss the findings of my results.

5.2 Discussion part one: FPC6 (Tb927.4.3120)

5.2.1 Summary of findings for FPC6

Here, I have shown that FPC6 is an essential protein in the bloodstream form of *T. brucei*. Depletion of FPC6 leads to rapid cell death, enlargement of the flagellar pocket accompanied with a block in endocytosis and the appearance of cells with a "BigEye" phenotype. I confirmed FPC6 as a partner of *Tb*BILBO1, showing its co-localisation *in vivo* in *T. brucei* by immunofluorescence on fixed trypanosomes. FPC6 is able to bind to the polymers formed by *Tb*BILBO1 when both proteins are co-expressed in U-2 OS mammalian cells. Specifically, the *Tb*BILBO1 binding domain (B1BD) of FPC6, previously identified by yeast 2-hybrid, was confirmed by expression of a truncated version of FPC6 protein in trypanosomes containing the B1BD and observing the co-localisation of this B1BD peptide with *Tb*BILBO1 *in vivo*. The N-terminus of FPC6 when expressed in *T. brucei* is cytoplasmic, whilst the B1BD + C-terminus truncated version is located to the FPC area but does not localise with the native FPC6 protein structure. I demonstrated that depletion of either *Tb*MORN1 or FPC6 protein by RNAi is sufficient for cell death with accompanying block in endocytosis; proving that neither protein is sufficient to rescue the other. These results taken together, confirm proteins of the hook complex as being essential in BSF *T. brucei* with a function in the regulation of molecules into the cell possibly by maintaining the functional structure of the neck of the flagellar pocket.

5.2.2 FPC6 is a trypanosomatid specific protein

The analyses that I carried out *in silico* of both nucleotide and amino acid sequences for FPC6 revealed that it was specific to trypanosomatids. It is not surprising that an early diverging eukaryote will possess specific genes and proteins adapted to its parasitic lifestyle. Another FPC cytoskeletal protein, FPC4 (Tb927.8.6370), is also trypanosomatid specific, with syntenic orthologues found only in trypanosomes and not in *Leishmania* spp. (Albisetti et al., 2017). Regarding *Tb*BILBO1, 20 orthologues exist in other kinetoplastid spp., including *Leishmania*, but not in mammalian spp. (Perdomo et al., 2016), confirming the specificity of the FPC proteins to trypanosomatids. Due to the uniqueness of FPC6 to the trypanosome genome, it is not surprising that information on the prediction of protein domains from present databases is not forth-coming. Data showed that FPC6 orthologue protein from *T. evansi* and *T. equiperdum* are over 99% identical to *T. brucei* spp. This is in-line with earlier evidence from Carnes et al., 2015 and others, that these three trypanosome species are extremely closely related and in fact "*petite mutants*" of each other.

5.2.3 Antibodies against FPC6 were not sufficiently specific

A total of five different antibodies produced against FPC6 were tested: one from chicken eggs and the others from four different rabbits. The fact that none of them were sufficiently precise enough or even able to detect FPC6 protein could be due to a number of reasons. Firstly, it could be possible that the amount of FPC6 protein in *T. brucei* is below the levels of detection, but this theory was later rejected after endogenously tagged FPC6 protein was easily identified by both IFA and WB. Secondly, it is possible that FPC6 is not immunogenic enough as a purified protein to select for antibodies specific enough for use on IFA or WB. An inherent lack of immunogenicity has been shown in the development of peptide vaccines, when these "aseptic" peptides are largely ignored by the immune system, either rapidly degraded by proteases or due to an induction of tolerance to these non-threatening antigens (Celis, 2002) the immune system is not stimulated. To enhance the immunogenicity of small peptides it is possible to use an adjuvant to provoke a stronger immune reaction, either as a depot effect by sustaining the antigen release at the injection site, or stimulating the innate immune system (Awate et al., 2013). Since the serendipitous discovery of adjuvants by the French veterinarian, Ramon, 1924 they have been widely used for over 90 years in vaccines. The most commonly used adjuvant is aluminium, but novel approaches such as virosomes are being adapted to increase the immunogenic response, for example, to *Leishmania* antigens (Liu et al., 2006). With regards to FPC6, an adjuvant was used: Freund's incomplete adjuvant. Freund and MacDermott, 1942 observed that the addition of paraffin oil and tubercle bacilli increases sensitization to the injected antigen. Complete Freund's adjuvant, an oil-in-water emulsion contains inactivated *Mycobacterium tuberculosis*; incomplete Freund's adjuvant lacks the mycobacteria. It might be possible to stimulate a stronger immune response against FPC6 by the addition of a complete adjuvant.

5.2.4 FPC6 is located within the hook complex in *T. brucei*

My results confirm the initial findings of the location of FPC6 protein in *T. brucei* published by Morriswood et al., 2013. In both in procyclic and bloodstream forms, FPC6 is a part of the multi-protein hook-shaped complex at the flagellar pocket neck, alongside *Tb*MORN1, *Tb*FPC4 (Albisetti et al., 2017) and *Tb*Smee1 (Perry et al., 2018). The hook complex is located in close proximity to the flagellar pocket collar. FPC6 co-localised partially with *Tb*BILBO1 of the flagellar pocket collar and completely with *Tb*MORN1 particularly concentrated at the head of the hook, tapering off into the shank of the hook complex, therefore FPC6 could be a linking protein between the FPC and the hook complex. Alternatively, the evidence for the BILBO1-binding domain of FPC6 could be explained if FPC6 interacts temporarily with *Tb*BILBO1 e*n route* to the hook complex. Later results of the potential function of FPC6 further suggest FPC6 is a part f the hook complex due to their similarity with the findings for *Tb*MORN1.

5.2.5 FPC6 binds to microtubules and to the MT organising centre in U-2 OS cells

The function of FPC6 protein in trypanosomes was previously unknown, with *in silico* domain analysis giving no further information. Expression of trypanosome-specific proteins in an heterologous mammalian system, in this case U-2 OS cells, can give some indication of its function. Intriguingly, FPC6 was identified at the centrosome in two separate experiments. In earlier experiments FPC6 was also seen at the base of the primary cilia in RPE-1 cells (Dr Celia Florimond, PhD thesis). The centrosome is the main microtubule nucleating centre of animal cells, first described in 1887 by Edouard van Beneden from Liège in Belgium and named "centrosomen" by Theodor Boveri in 1990 (Scheer, 2014). In animal cells, within the core of the centrosome is a pair of centrioles which nucleate microtubules. In unicellular ancestors of eukaryotes, the basal body (centriole) nucleates the flagellum, such as in *T. brucei* (Hu et al., 2015). The emergence of the centrosome as an independent cytoplasmic organelle no longer attached to the axoneme, may have led to the loss of certain anchoring proteins such as FPC6, over the course of evolution. FPC6 is located within close proximity (500nm) of the kinetoplast in *T. brucei*, and therefore the basal bodies (Robinson and Gull, 1991).

An additional finding from the expression of FPC6 protein in U-2 OS cells, was that when FPC6 was expressed alone it was seen throughout the whole cell, possibly tending to be extracted in detergent-extracted cells, however when co-expressed with *Tb*BILBO1 it was seen exclusively on the polymers formed by *Tb*BILBO1 and even influencing their morphology. This result confirms that FPC6 binds to *Tb*BILBO1, as was seen in earlier yeast 2-hybrid studies, in preference to the MT or centrosome and globular heads were formed, suggesting that FPC6 is a true binding partner of *Tb*BILBO1 and has a propensity to form hook-like structures even without the framework of the trypanosome axoneme and associated trypanosome-specific

proteins of the hook complex. In continuation of this study, truncated versions of FPC6 protein were co-expressed alone and with full-length *Tb*BILBO1. It was observed that the N-terminus alone (truncation 1) is present throughout the cell, in a similar expression pattern to the full-length FPC6, regardless of whether *Tb*BILBO1 was present or not. This needs to be repeated with detergent-extracted cells to determine of the N-ter is in fact cytoplasmic or on the microtubules. The B1BD of FPC6 (truncation 2) when expressed alone in U-2 OS cells is observed as small rounded aggregates of around 2μm in diameter; when co-expressed with *Tb*BILBO1, larger annular structures are formed of up to 5μm in diameter. Truncation 3, the B1BD + C-terminus gave a less uniform pattern of labelling either with or without *Tb*BILBO1: alone some cells displayed aggregates with globular heads and with *Tb*BILBO1 T3 was seen in ribbon-like polymers. However, all these co-expressions need to be redone with detergent-extracted cells to remove overlying membrane and determine precisely the location and MT/polymer binding properties of these truncations of FPC6. It would also be interesting to co-express the full-length and truncated versions of FPC6 with *Tb*MORN1 to determine any interaction in this heterologous system (Figures 3.5 and 3.6). Previously, when Florimond et al., 2015 expressed truncations of *Tb*BILBO1 in U-2 OS cells, the N-terminus was also cytoplasmic and only the coiled coil region was able to form polymers. therefore, this mammalian expression system remains an interesting tool to ascertain protein function and properties of individual domains.

5.2.6 RNAi *FPC6* is not lethal in procyclic forms of *T. brucei*

The phenotype observed after depletion of FPC6 protein in the PCF resembled that found by Morriswood et al., 2009 after RNAi of *TBMORN1* in PCF. In both instances there was a delay in cytokinesis seen with an accumulation of trypanosomes in the 2K2N cell cycle stage. For FPC6, I also recorded an accumulation of cells in the 2K1N cell cycle stage (3.7), which indicates a delay in kinetoplast replication or segregation. This delay in cell division, although not lethal, could indicate the importance of faithful replication and division of the hook complex which is physically connected to the kinetoplast *via* the axoneme and the basal bodies (Robinson and Gull, 1991). The timing of replication of the kinetoplast itself could then in turn influence the timing nuclear division. It is known that *T. brucei* lacks many common eukaryotic check-points, such as the mitosis to cytokinesis check point, meaning that in trypanosomes anucleated cells (zoids) can be produced (Ploubidou et al., 1999). In my study, despite a delay in cytokinesis, cells continued to replicate as a similar rate as wild-type cells, indicating an ability to cope with changes in kinetoplast segregation by continuing to divide regardless, or alternatively, the kinetoplast divided more rapidly and cells appeared to accumulate in 2K1N stage.

In the findings by Morriswood et al., 2009, the PCF *T. brucei* cells continued to grow, but at a slower rate, this contrasted somewhat with my findings, where PCF continued to grow at the same rate as the wild-type and non-induced trypanosomes (graph **B** in Figure 3.7). One explanation might be that different PCF parental cell

lines were used in the two separate studies: Tb427 SmOx for the FPC6 experiments and Tb427.29.13 in the case of *Tb*MORN1; or simply that it is a different protein of the multi-protein hook complex that was being depleted. The system for RNA interference may also play a part. In trypanosomes, gene regulation is primarily post-transcriptional and RNA interference (RNAi) is a mechanism through which genes can be silenced by degradation of homologous messenger RNA (mRNA). *T. brucei* has an intrinsic RNAi system that can be exploited for protein knockdown. The two different constructions available for RNAi in *T. brucei* were both employed in my study of FPC6: stem loop (Shi et al., 2000 and Bastin et al., 2000) and twin promoter (LaCount et al., 2000) making use of the inducible expression system developed by Wirtz et al., 1999. In the case of FPC6, neither the stem-loop nor the twin promoter system of RNAi (p2T7$^{Ti:TAblue}$; Alibu et al., 2005) were able to reduce the final amount of FPC6 protein in the trypanosomes to less than 26% of non-induced levels. In the case of *Tb*MORN1, in PCF RNAi silencing was able to reduce the level of protein to 20% of that of non-induced trypanosome cells. The inability to reduce the level of these proteins beyond this level, or the fact that cells grew regardless of this level of reduction of protein could be due to tight control of the levels of FPC6 (and *Tb*MORN1) protein by the trypanosomes, whereby the parasite can manage due to up-regulation of other neighbouring proteins to compensate for the loss of an important protein. Alternatively, cells inefficient in RNAi knock-down were selected for after transfection; this self-selection may indicate the RNAi phenotype is unstable. Resistance to RNAi in mammalian cells has been reported by Zheng et al., 2005, so theoretically a similar mechanism could develop in trypanosomes to enable the cells to continue expressing an essential gene.

5.2.7 RNAi *FPC6* is rapidly lethal in *T. brucei* bloodstream forms

The FPC6 RNAi construct (p2T7$^{Ti:TAblue}$; Alibu et al., 2005) used in PCF was also used to transfect BSF. *T. brucei* induction of RNAi *FPC6* in BSF has a strikingly different effect than in PCF. *T. brucei* BSF die rapidly from 24 hours post induction of RNA silencing of *FPC6*, see Figure 3.8. This finding also fits with that of Morriswood and Schmidt, 2015 when RNAi knock-down of another hook complex protein *Tb*MORN1 was induced in BSF *T. brucei*, cells died from 18 hours post induction. The fact that both of these proteins showed such a marked affect on cell growth followed rapidly by cell death after their depletion, indicates the importance of these proteins and indeed of the hook complex itself, in trypanosome cell survival. In the case of RNAi silencing of *FPC6* in bloodstream forms, the level of protein was reduced to 16% of non-induced; a greater reduction than for PCF. This extra reduction in protein might have been the tipping-point that led to cell death or simply that FPC6 is more important and essential in the BSF. The difference might also relate to the stability of the hook complex in BSF and even the half-life of the protein, which could be longer in the PCF *T. brucei*.

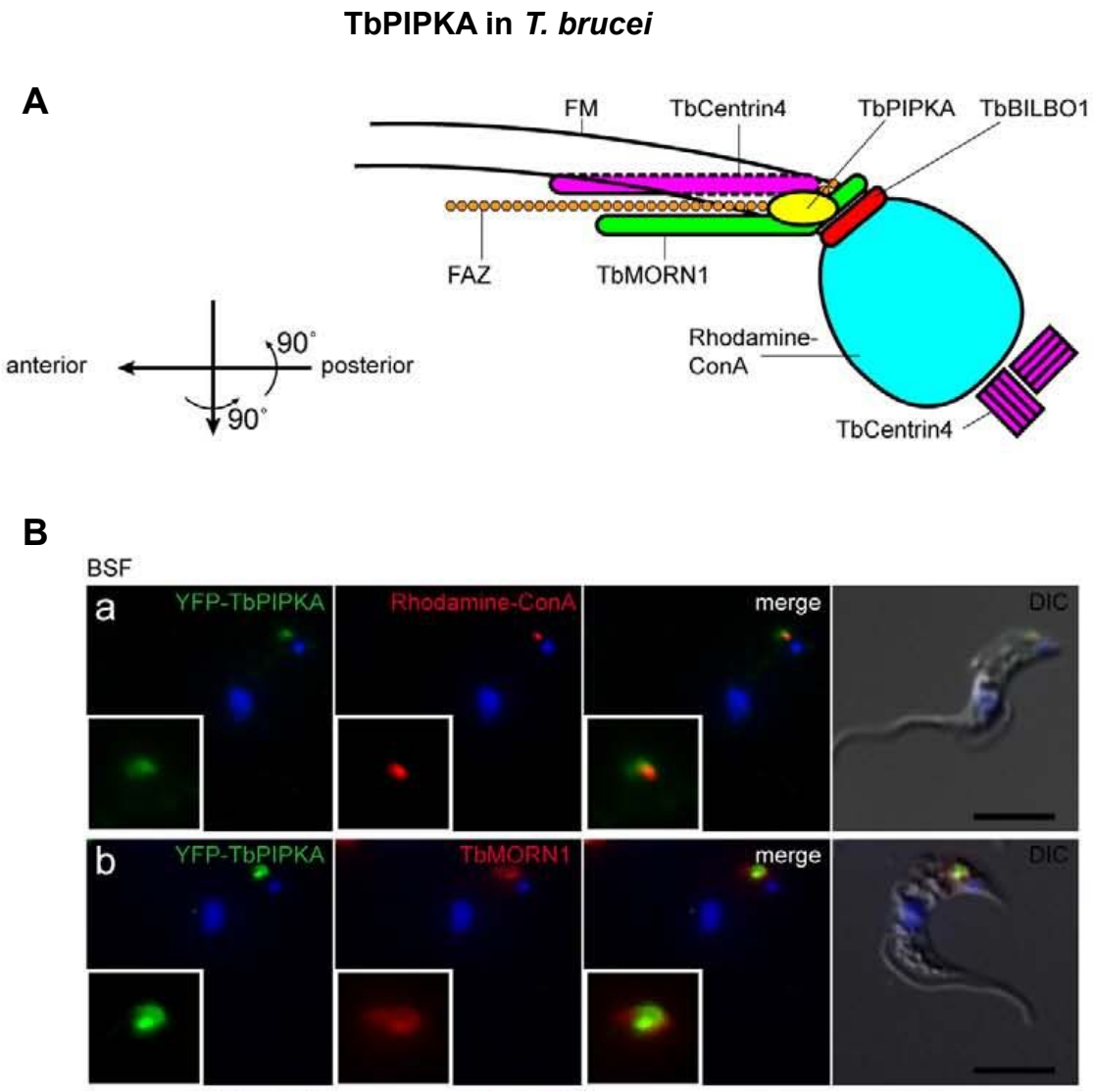

FIGURE 5.1: ***T. brucei* phosphatidylinositol phosphate kinase: *Tb*PIPKA. A** Schematic of the flagellar pocket, the FPC and hook complex and associated structures; **B a** IFA showing the location of YFP::*Tb*PIPKA at the neck of the flagellar pocket as seen by co-localisation with Rhodamine-ConA which fills the FP, and **B b** with *Tb*MORN1, in bloodstream forms. Taken from Demmel et al., 2016. Scale bar = 5μm

5.2.8 RNAi *FPC6* in BSF led to a "BigEye" phenotype

A clue to the function of FPC6 can be gained from observation of the cell phenotype as the trypanosomes die. A "BigEye" phenotype was seen whereby the flagellar pocket (FP) became grossly enlarged, causing the trypanosomes to become rounded and eventually the FP takes over the whole cell. This can be seen in the electron micrograph images in Figure 3.8.**E**, **B** and **C**. The phenotype, "BigEye" was first used by Allen et al., 2003 due to the characteristic appearance of cells after depletion, by RNAi, of the clathrin heavy chain involved in endocytosis, which in *T. brucei* occurs solely at the FP and is entirely clathrin-dependent.

The fact that knock-down of a cytoskeletal protein of the hook complex, leads to a defect in a membranous process was at first puzzling. An answer seemed to present itself by Demmel et al., 2016 who described an enzyme, *Tb*PIPKA (Tb927.10.1620) located at the neck of the flagellar pocket in *T. brucei*, overlying the area where FPC6 and *Tb*MORN1 are found, i.e. at the hook complex. In their investigation, Demmel et al., 2016 found that depletion of *Tb*PIPKA led to a reduction in phosphatidylinositol 4,5 biphosphate (PI(4,5)P_2) in the trypanosome cells accompanied with an enlargement in the flagellar pocket and impaired endocytosis. PI(4,5)P_2 is crucial for endocytosis in mammalian cells and is concentrated at the flagellar pocket membrane in *T. brucei*. If disruption of the hook complex (by depletion of FPC6 protein) has an effect on *Tb*PIPKA location and/or function then the crucial step of phosphorylation of phosphatydlinositol phosphate (PIP) and production of PI(4,5)P_2 might be blocked. This could explain the "BigEye" phenotype seen in my study of RNAi *FPC6* BSF in *T. brucei*. To explore this hypothesis it will be necessary to tag *Tb*PIPKA and study the location and amount of *Tb*PIPKA remaining in the cells after induction of RNAi *FPC*6. Unfortunately, after two transfection attempts, no positive clones for endogenously tagged *Tb*PIPKA have yet been obtained. Experiments are still on-going and this remains an interesting avenue to explore.

5.2.9 FPC6 is involved in influencing of protein entry into the FP

The location of FPC6 within the hook complex (HC) can give a clue to its function. The HC is a multi-protein complex located at the neck of the flagellar pocket and one of its components *Tb*MORN1 has been shown to be regulate protein entry into the flagellar pocket in *T. brucei* trypanosomes (Morriswood and Schmidt, 2015). To explore this hypothesis as an explanation for the resulting phenotype after RNAi *FPC6*, I carried out functional studies in RNAi *FPC6* depleted cells. These experiments involved evaluating endocytotic uptake assays in wild-type cells as well as before and after RNAi silencing of *FPC6* in BSF *T. brucei*, replicating those experiments carried out with *Tb*MORN1 knock-down. I obtained the same result with RNAi *FPC6* as Morriswood and Schmidt, 2015 had obtained with *Tb*MORN1, principally that depletion of FPC6 led to a size exclusion effect on molecule entry into the FP. These data suggest that FPC6 is also involved in the same pathways and function as *Tb*MORN1. However, it would be interesting to explore further uptake

assays to determine if it really is a size-exclusion effect, due to the smaller sized dextran being able to enter the pocket and the larger Concanavalin A (ConA) no longer having access after RNAi of *FPC6*, or whether it is due to the inability to gain access to a specific sub-set of glycoproteins to which ConA binds near the neck of the flagellar pocket before entering the FP (Gadelha et al., 2009). This question could be explored by reversing the sizes of the dextran and ConA. Dextran enters the FP in the fluid phase, therefore if two larger sizes of dextran are used (e.g. Dextran Texas red 70,000 neutral, ref. D1830 and Dextran Texas red 40,000 neutral, ref. D1829) and the endocytotic uptake assays are repeated, this could shed light onto whether it is simply a closing off of the neck channel and therefore a smaller or closed off entry point that leads to an enlarged FP in these cells. Likewise, ConA of a smaller size could be used (e.g. Concanavalin A succinylated Alexa Fluor^{TM}488 conjugate, ref. C21401) to determine if it is the process of entry i.e. binding to a location specific glycoprotein that inhibits entry into the FP post-RNAi *FPC6*, or simply the size of the molecule that matters.

5.2.10 Full-length recoded *FPC6* rescues the lethal RNAi phenotype in BSF *T. brucei*

It has been shown by Sinclair-Davis et al., 2017 that a recoded segment of the DNA sequence of one allele of *TOEFAZ1* rendered it resistant to RNAi in a complementation experiment. The codons were changed from the native allele gene sequence but the amino acids coded for were retained. In my study of FPC6, I replaced one allele of *FPC6* with a recoded version with a different tag to the tagged native allele. I was able to see that the location of the protein from the recoded allele was the same as the protein from the native allele, by co-localisation of their tags using different coloured fluorescent antibodies by immunofluorescence. After induction of RNAi *FPC6*, the trypanosomes did not die and the recoded allele was fully functional acting to rescue the loss of the native protein, see Figure 3.11. The complementation assay also determined that the RNAi sequence used targeted specifically the native FPC6 protein and not the recoded version.

By contrast, the truncated Δ*Nter FPC6* recoded sequence alone was not able to rescue the RNAi phenotype in BSF. IFA showed that this truncated protein (T3) is located in the region of the FPC but does not take on the conformation of the native hook-like shape of FPC6, see Figure 3.14. Therefore, although this truncated protein was able to target to the desired region of the trypanosome cell, it was not able to functional fully as the native FPC6 protein. Unexpectedly, this recoded protein disappeared instantly (and completely, see Figure 3.14.**C**.**i**.and **ii**.) upon RNAi *FPC6*. This lack of T3 now detected in the trypanosome cells might lakes it difficult to confirm that this trunction did not rescue the lethal phenotype.

5.2.11 The BIBD of FPC6 is necessary for targeting to the FPC

The truncated versions of FPC6 were the same as those expressed in U-2 OS cells (Figure 3.10). Two out of the three truncated versions of FPC6 localised precisely to the FPC region: T2, the B1BD of FPC6 and T3, the ΔNter of FPC6. Truncation 2 consisted of the predicted BILBO1-binding domain (B1BD) of FPC6 alone (plus globular domain - included to allow proper protein folding) and co-localised exactly with *Tb*BILBO1 by IFA in trypanosomes. No labelling was seen elsewhere in the cells, confirming this B1BD domain, indeed, as the BILBO1 binding domain. Figure 3.13.

Truncation 3, contained the B1BD (+ globular domain) plus the C-terminus and was also able to locate to the FPC. T3 however, did not take on the shape of native FPC6 (Figure 3.14), suggesting that the Nter is important in the final positioning of FPC6 to the hook complex, specifically to the shank, and possibly interacting with FPC6 itself or with other proteins of the hook complex, such as *Tb*MORN1. Truncation 1, the ΔB1BD/Cter, i.e. the N-terminus alone, was cytoplasmic in *T. brucei* (Figure 3.12), signifying that the N-terminus alone was not sufficient to target to the FPC, or other cytoskeletal structures. The location properties of these truncations in *T. brucei* are similar to those found in U-S O2 cells (Figure 3.6), where the N-terminus also gave a whole cell signal, the B1BD only being seen in conjunction with *Tb*BILBO1 (when co-expressed) and the B1BD + Cter having some *Tb*BILBO1 binding properties but of variable location in the cells. It will be interesting to see the results of future studies involving the expression of truncated versions of both FPC6 and *Tb*MORN1 in U2-OS and yeast 2-hybrid assays, to determine which domains of each protein are responsible for binding (to each other) and polymer forming properties.

5.2.12 Small truncated FPC6 peptide fragments are degraded after RNAi of native *FPC6*

Truncations 2 and 3 disappeared from detection by IFA and WB after induction of RNAi *FPC6*, see Figures 3.13 and 3.14. Confirmation that the recoded version of the FPC6 was not targeted by the RNAi system was seen in the earlier result with the full-length recoded *FPC6*. The full-length recoded allele was not targeted by the RNAi system, therefore another explanation was needed for the loss of these small peptides. T2 and T3 localised to the FPC area but did not co-localise fully with the native FPC6, indicating that although they could bind to cytoskeletal structures in the trypanosomes, they were not fully integrated into the native FPC6 structure at the hook complex, particularly the shank. When RNAi silencing of *FPC6* was induced, regardless of the fact that the protein knock-down was not complete, the reduction of FPC6 native protein, was enough to destabilise the small truncated fragments and induce their degradation. Interestingly, T2 was obtained only in the PCF and the disappearance of this protein was greater than the RNAi effect on the native FPC6. Even more remarkable was T3, which was only obtained in the BSF,

with complete loss of this truncated protein after 24 hours post induction of the native FPC6. Both of these small truncations of recoded FPC6 were degraded upon induction of RNAi ostensibly due to a paucity of FPC6 full-length protein, causing these abnormal proteins to become unstable and degraded. A plausible explanation for such a rapid loss of these peptides is degradation by the proteasome. One of the main roles of the proteasome is "proteolysis of abnormal, mis-folded or improperly folded proteins" (Paugam et al., 2003). To test this theory proteasome inhibitors such as lactacystin or MG132 could be used by incubation with *T. brucei*. Limitations of the use of these inhibitors has been reported, such as the previously long incubation time of 10 hours (roughly the time of a full cell cycle in *T. brucei*), leading to uncertainty over the cause and effect of the use of such inhibitors which have been shown to block cell cycle progression (Mutomba and Wang, 1997). Recently, Moura et al., 2019 described a *T. brucei* reporter cell line where activity of protease inhibitors, 5μM lactacystin or 10μM MG132, could be detected *in vivo* with GFP accumulation in cells detected by fluorescence microscopy or flow cytometry from just 2 hours post incubation. This reported cell line is open to the community and could be used in assessing proteasome inhibition after RNAi in the FPC6 recoded truncations cell lines.

5.2.13 Neither FPC6 nor *Tb*MORN1 is sufficient alone to prevent cell death

One interesting observation was the reciprocal effect of RNAi of either *FPC6* or *TBMORN1* in the bloodstream form. Both of these proteins are a part of the multi-protein hook-shaped complex at the flagellar pocket neck. When either of these proteins were knocked-down by RNAi cell death follows by 24 hours. The slightly faster rate for RNAi *TBMORN1* (see Figure 3.15) could be due to differences in turnover of these two proteins within the cell. The difference could also be explained by the difference in trypanosome parental cell lines: Tb427 SmOx (puromycin resistance marker) was used for FPC6 and Tb427.1313.514 (Alibu et al., 2005) was used for *Tb*MORN1 RNAi. The findings by IFA after RNAi of either protein separately were as expected, i.e. when one protein was knock-down its signal was reduced or disappeared, whilst the signal for the other protein remained. However, the findings of western blot were surprising and not easily explained. The same profile was seen for either knock-down. However, this preliminary result was only carried out on a single occasion due to time constraints, therefore it needs to be repeated.

5.2.14 Trouble-shooting FPC6

Over the course of my studies on FPC6, I encountered some hindrance to transfection of the bloodstream forms of *T. brucei*. Initial attempts to endogenously tag FPC6 were unsuccessful. I was following the protocol from Dean et al., 2015a where preparation of the DNA for transfection was firstly purified by a nucleic acid purification step using chloroform (see Methods Chapter 2.5.17) followed by ethanol

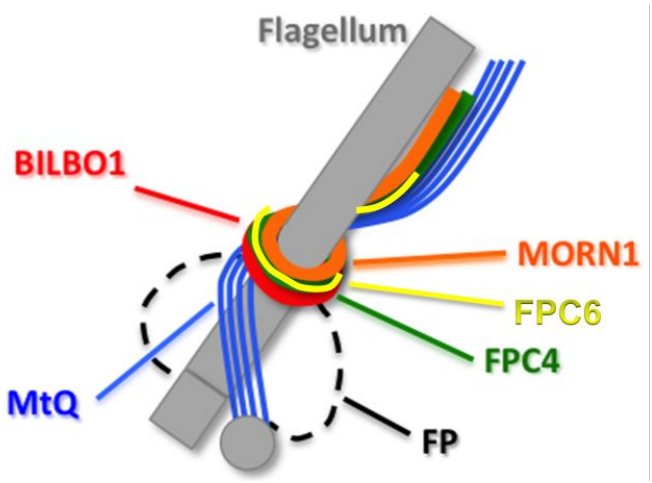

FIGURE 5.2: **The location of FPC6 in *T. brucei*.** Schematic to show the location of FPC6 (yellow) in relation to *Tb*BILBO1 (red) and *Tb*MORN1 (orange) at the neck of the flagellar pocket. Adapted, with permission, from Dr Anna Albisetti's PhD. FP=flagellar pocket and MtQ=microtubule quartet.

precipitation of the DNA (see Methods Chapter 2.5.18). I achieved successful transfections only after I stopped the chloroform step, possibly indicating that the final DNA sample still contained traces of chloroform. For some later transfections, when I was selecting under four different antibiotic selection markers, I added a further 10% foetal bovine serum and conditioned medium (medium used to grow the parental trypanosome cell line in for 24 hours, centrifuged and filtered), as well as increasing the amount of DNA per transfection from a combined 4 PCR reactions to 6, to increase the opportunity for transformant trypanosomes to grow.

An additional point relating to transfection of *T. brucei* that stalled progression, was that on some occasions, there was growth of trypanosomes in the selection antibiotic and yet these same cells were negative for the transected tag/construct. This happened on a number of occasions with both PCF and BSF. In these cases a cMyc tag construct was destined to endogenously tag a gene/or a recoded replacement, with a neomycin antibiotic selection marker. Despite the trypanosomes growing in the recommended concentration of neomycin (10μg/mL for PCF and 2.5μg/mL for BSF; see Table 2.1), the tag was undetectable by either IFA or WB. This could mean that cells were selected for that were able to grow in the presence of neomycin and had integrated the G148 gene for neomycin antibiotic resistance but had not integrated or had lost the endogenous tag.

5.2.15 Conclusion for FPC6

The initial research question was met and confirmation was shown that FPC6 is an essential cytoskeletal protein in the bloodstream form of *T. brucei*. Characterisation was accomplished with regard to the location of FPC6 in *T. brucei* at the flagellar pocket neck, co-localising with *Tb*BILBO1 and *Tb*MORN1, occupying a position similar to *Tb*FPC4, located partly at the flagellar pocket collar and within the multiprotein hook complex extending distally along the flagellum. A summary schematic of the location of FPC6 in *T. brucei* is given in Figure 5.2. The presence of FPC6 was observed throughout the trypanosome cell cycle in both PCF and BSF. A detailed description of the effect of knock-down of the protein in both procyclic and bloodstream forms showed an alteration in cell cycle timing (a delay in cytokinesis) in PCF and rapid cell death from 24hpi in BSF. Trypanosome cell death due to depletion of FPC6 was confirmed by the complementation experiment replacing one allele of *FPC6* with a recoded version resistant to RNAi that rescued the lethal phenotype. In depth exploration of the function of FPC6 and its constitutive domains was completed in trypanosomes and U-2 OS cells, confirming the BILBO1 binding domain and the cytoplasmic N-terminus when alone. The role of FPC6 in influencing entry of molecules into the flagellar pocket and upholding the local environment to allow the essential process of endocytosis at the FP membrane to occur and therefore the essential role of FPC6 in cell survival is clearly defined.

5.3 Discussion part two: scFv and Nanobodies

5.3.1 Summary of findings for scFv and nanobodies against *T. brucei*

I have demonstrated that a single-chain variable fragment (scFv) antibody fragment produced from a monoclonal antibody against *T. brucei* can be expressed intracellularly in *T. brucei* in both procyclic and bloodstream forms. The resultant scFv protein is soluble inside the trypanosome cytoplasm, has no detrimental effects on trypanosome cell growth and does not localise with *Tb*BILBO1 *in vivo*.

A total of seven nanobodies against *Tb*BILBO1 were initially selected by their ability to bind to *Tb*BILBO1 protein *in vitro*. These seven nanobodies differ in their amino acid sequence, notably in the CDR3 region, leading to the classification into three groups. I have shown that nanobodies produced against *Tb*BILBO1 protein in Alpaca can be expressed in and purified from the periplasmic extract of *E. coli* and can recognise purified *Tb*BILBO1 protein *in vitro* and endogenous protein *in vivo* in fixed trypanosomes by immunofluorescence and from whole trypanosome cell samples by western blot. I have described the successful transfection of procyclic forms of *T. brucei* with three nanobodies which are expressed within the trypanosomes and one nanobody in BSF. When one nanobody from each group was expressed as intra-nanobodies in trypanosomes, the results were strikingly different. Nanobody 48 (Nb48; group 1) expressed intracellularly, leads to rapid trypanosome cell death within 24 hours of induction. Death is accompanied with detached flagella and accumulation of intracellular vesicles, indicating perturbation of the biogenesis of a new flagellar pocket and disruption of the normal endo-/exocytotic pathways. Nanobody 9 (Nb9; group 2) expressed intracellularly leads to cell death but at a more reduced rate than nanobody 48. Nanobody 73 (Nb73; group 3) had no effect on growth rate of *T. brucei* when expressed intracellularly in either procyclic or bloodstream forms. Nb73 was the only nanobody for which I was able to obtain transformants in the BSF, possibly due to a small leak with the tetracycline induction system which was not lethal in the case of Nb73, but for Nb48 and Nb9 was sufficient to prevent BSF transfected cells from growing up.

5.3.2 Models of scFv and Nbs *in silico* were obtained with 100% confidence

Analyses *in silico* using Phyre^2 (Kelley et al., 2015) were able to predict the structure of both the scFv-*Tb*BILBO1 (Figure 4.1) and the nanobodies (as exemplified by Nb48, Figure 4.3). This is due to similarity in the framework sequences of all scFv and nanobody fragments, with differences in CDR regions being predicted from the large data-bases now available gathered over almost 50 years since their inception by Wu and Kabat, 1970.

5.3.3 Expression of nanobodies and purification from *E. coli* was more successful than for scFv

I was able to successfully express and purify nanobodies from the periplasmic extract of *E. coli*, however, multiple attempts to do the same for scFv-*Tb*BILBO1 were unsuccessful. Nanobodies are half the size of an scFv and are more soluble than conventional antibodies due to two characteristics. Firstly, amino acid mutations in key positions usually involved in interaction with the light chain variable region, as shown in Figure 1.18.**B**. This was proved by Davies and Riechmann, 1994 when they "camelised" human antibody VH fragments to create more soluble antibody fragments by mutating these exact same amino acid substitutions to match that of VHH (G44E, L45R and W47G). The second factor adding to the solubility of nanobodies is the structure of the CDR3. The CDR3 has important properties for both heavy chain stability and solubility of the VHH (Bond et al., 2003), as it partially covers the previous VH-VL interface preventing dimerization of the Nb fragment (Kunz et al., 2018). With regards to the scFv fragment there are, in fact, two possible versions: either VH-linker-VL or VL-linker-VH. In the case of scFv-*Tb*BILBO1, it is the latter (see Figure 4.1). The very first engineered scFv recombinant antibody single-chain variable fragment by Bird et al., 1988 was VL-linker-VH, however in more recent times the VH-linker-VL has been favoured (Ahmad et al., 2012). Therefore, it is possible that if scFv-*Tb*BILBO1 was re-engineered to be VH-Linker-VL the physical properties could be changed.

These recombinant antibody fragments were expressed in the periplasmic space of *E. coli* bacteria, the location of disulfide oxidoreductases and isomerases, which catalyze the formation of disulfide bonds enabling the accumulation of properly folded, soluble protein (Berkmen, 2014). However attempts to purify scFv in this system was less than fruitful and scFv protein was seen in minimal amounts in the periplasmic extract (Figure 4.1.**C**) and was undesirably present in the supernatant. It was reported by Dewi et al., 2016 that accumulation of scFv in the periplasmic space can cause swelling and leakage of the membrane, which could have been the case in these experiments, resulting in observation of scFv in the supernatant. In the future, it might be worth using a yeast system such as *Pichia pastoris* which has been cited as providing higher yields of scFv (Vallet-Courbin et al., 2017). An scFv against *Tb*BILBO1 still remains an interesting avenue to pursue and scFvs are being developed against *T. cruzi* ribosomal proteins (Ayub et al., 2012) and as diagnostics for hydatid cysts (*Echinococcus granulosus*; Xu et al., 2017).

During expression and purification of the nanobodies, it was noted that the HIS tag was being lost (low yield and double-band seen on western blot; Figure 4.4.**B** and **D**. This might be due to C-terminal proteolysis which could be reduced by the addition of protease inhibitors. However, in the case of nanobody production here, it appeared that the cleavage was occurring before the extraction and purification process, therefore inside the *E.coli*. It is be worth trying different strains of *E. coli*,

although WK6 is the strain of choice for expressing nanobodies (Pardon, 2014). Preliminary attempts to express Nb48 in a number of *E. coli* strains: SHuffle®T7 Competent (Biolabs), BL21 (DE3) Star^{TM}(Invitrogen), origami (DE3) and Rosetta (DE3) found minor differences between them, with BL21 observed to produce the highest amount of Nb. However, WK6 *E. coli* was chosen for continuation of expression of the nanobodies because this is the strain recommended by Pardon, 2014 despite the relatively low yield of nanobody, e.g. Nb48 = 0.255mg/mL.

Codon optimisation of recombinant protein gene sequences was explored by Fridy et al., 2014 to allow efficient expression in *E. coli*. Yeast systems, such as *Pichia pastoris* have also been used for expressing nanobodies (Ezzine et al., 2012). A potential novel mode of expression could be the LEXSY system. *Leishmania tarentolae*, first isolated from the blood of the Moorish gecko, *Tarentola mauritanica* (Wallbanks et al., 1985) has been established as a recombinant protein production system. The advantages of the LEXSY system is that the eukaryotic gene expression system allows disulphide bond formation and the choice of intracellular or secretory expression of the recombinant protein. *L. tarentolae* are non-pathogenic to mammals, have a fast rate of growth and are easy to culture in the lab. The only potential limiting factor, in relation to nanobodies raised against *T. brucei*, is the presence of a hyopthetical syntenic orthologue of *Tb*BILBO1 (Tb11.01.3960) in *L. tarentolae*. Therefore, preliminary tests would have to be carried out to determine if production of these nanobodies, in this system, had any detrimental effects *in vivo* on growth of *L. tarentolae*.

5.3.4 There are differences in the ability of nanobodies from different groups to bind *Tb*BILBO1

Despite the fact that all seven of the original nanobodies (listed in Chapter 4.3) were identified by ELISA using *Tb*BILBO1 purified protein, the results from testing the purified recombinant antibody fragments (Nbs) in my experiments were contrastingly different. Initial testing of the first two nanobodies to be purified, Nb9 (group 2) and Nb73 (group 3), by ELISA showed an ideal dose concentration dependent curve for Nb9, as seen in the bar graph in Figure 4.4.**E**. However, Nb73 was negative in this assay, with similar results to the two negative controls used (periplasmic extract without nanobody expression and BSA). An explanation for this could be that Nb73 recognises a mis-folded epitope of *Tb*BILBO1 protein presented and selected for at the initial ELISA selection stage. It is possible that the folding of the protein *in vitro* was different in the initial selection ELISA and Nb73 was chosen for an epitope not exposed in the later ELISA assay. The fact that Nb73 was also negative when used as a probe on western blot (Figure 4.5.**A**.) could be explained by the fact that *Tb*BILBO1 protein was not entirely denatured and thus the linear sequence (epitope) recognised by Nb73 was not available. Nb73 was also not able to recognise native *Tb*BILBO1 by IFA in fixed trypanosomes, indicating that in this form the epitope selected for was still not available. Expression of Nb73 intracellularly in trypanosomes had no effect on growth rate possibly because the

intra-nanobody was not able to bind to its epitope which was hidden in the native form, or that binding was very weak and had no effect on *Tb*BILBO1 function. Nb73 was classified in group 3 and was the only nanobody in this group, having a CDR3 (complementarity-determining region 3) particularly unique (varying greatly) from the other six nanobodies, as well as the highest number of differing amino acids in the CDR1 and CDR2 compared with the other groups. Since the CDR3 of nanobodies is unique and confers much of the epitope binding properties (Wesolowski et al., 2009) it fits that the functional properties will also be different, as was the case here.

5.3.5 The difference in affinity between Nb48 and Nb9 for *Tb*BILBO1 correlates to intra-nanobody activity

Once Nb48 was purified, a superior assay to test binding affinity (than ELISA) was desired. Surface Plasmon Resonance (SPR) measures the binding affinity of two proteins in real-time and is label-free. Here, SPR demonstrated that Nb48 had the highest binding affinity for *Tb*BILBO1, following near perfectly the theoretical curve (see Figure 4.4.**F**.). This result was confirmed when purified Nb48 was used as a probe on fixed trypanosomes by IFA, where Nb48 was able to detect native *Tb*BILBO1 in precise co-localisation with an anti-*Tb*BILBO1 antibody, see Figure 4.5.**D**. This compares to Nb9 which could only detect *Tb*BILBO1 in trypanosomes over-expressing *Tb*BILBO1, by both IFA and western blot. Both Nb48 and Nb9 are able to bind to *Tb*BILBO1 *in vitro*, as seen by SPR, with k_Ds in the nanomolar range, 8.8nM for Nb48 and 15.5nM for Nb9; the smaller the number indicating a higher affinity of Nb for its epitope. The difference in these results could again be the result of differences in the amino acid sequences, particularly of the CDR3. It would be interesting to probe different species of trypanosomes such as *T. congolense, T. cruzi, T. evansi* and *T. vivax* as well as *Leishmania* by IFA and western blot to determine if these purified nanobodies can detect *Tb*BILBO1 orthologues in other kinetoplastid species.

5.3.6 Nb48 has no effect on *T. brucei* growth when added to the culture medium

Preliminary studies of the incubation of Nb48 with bloodstream form *T. brucei* were made. No effect was seen, either because the Nb was unable to enter the parasites (it was not detected in the flagellar pocket or in the cells by IFA) or the Nb did enter but was rapidly degraded so was undetectable and unable to have any effect. This result also implies that *Tb*BILBO1 does not have epitopes accessible to the Nb, exposed on the inside of the pocket membrane.

5.3.7 The same difference in affinity of Nb48 and Nb9 when assessed as purified nanobodies was observed when they were expressed as intra-nanobodies.

Intra-nanobody 48 (INb48) expression causes rapid cell death from less than 24hpi, whilst INb9 causes cell death but over a more protracted time period (see growth curves Figure 4.6). The higher binding affinity of INb48 to *Tb*BILBO1 means that it is not displaced *in vivo* as INb9 is from its target *Tb*BILBO1. INb48 binds tightly to *Tb*BIL1BO1 (as seen by perfect co-localisation with *Tb*BILBO1 in IFA from early time points of expression; Figures 4.7 and 4.9) producing an irreversible disruption of *Tb*BILBO1 function and rapid cell death, whilst INb9 binds more weakly and is displaced, being seen elsewhere in the cell (Figure 4.8), bringing about a slower rate of death.

Nanobodies have been expressed in mammalian cells to assess protein function intracellularly, explore protein-protein interactions and as protein inhibitors. Van Audenhove et al., 2013 described the use of nanobodies to map cytoskeletal proteins, the actin binding proteins, gelsolin and CapG, in mammalian cells. Van Den Abbeele et al., 2010 demonstrated how a VHH (Nb) could block the interaction of the structural proteins, gelosolin-G-actin *in vivo*, providing novel information on their functional properties as well an intracellular location. In my observations, it was possible to see disruption of the cytoskeletal protein *Tb*BILBO1 caused by binding of a nanobody *in vivo*.

5.3.8 Nanobodies as an alternative to RNAi

RNA interference (RNAi) has been used to greatly enhance knowledge of gene and consequently protein function in living cells. However, RNAi can have several limitations, such as incomplete knock-down of the target protein, incomplete mRNA cleavage, potential inaccessibility of RNA and difficulty with proteins possessing a long half-life (which could be the case with *Tb*BILBO1). The double-stranded RNA produced during RNAi has a short half-life compared to an intra-nanobody, the Nbs also act at a post-translation stage, therefore can be more specific for tarting proteins of one specific post-translational form (Cao and Heng, 2005). In this regard, VHH (nanobodies) also have advantages over conventional antibodies for use as intrabodies, due to their smaller size, increased solubility, ability to cross the blood-brain barrier (Liu et al., 2006) which is a prerequisite for a potential treatment for the cerebral form of trypanosomiasis) and more elaborate CDR3 regions able to access cryptic epitopes. Conventional antibodies have a further disadvantageous of multi-epitope cross-reaction, a phenomenon exemplified by IgE in allergen cross-reaction (Negi and Braun, 2017), whereas, VHH are single epitope specific.

In my study, I have shown that the phenotype observed in trypanosomes expressing Nb48 and those of RNAi *TBBILBO1* are the same: rapid cell death, lack of biogenesis

of a new flagellar pocket, a new flagellum produced which is detached from the cell body, extended posterior ends, disruption in cytokinesis and accumulation of intracellular vesicles (Bonhivers et al., 2008). Nb48 was only ever seen intracellularly at the flagellar pocket collar (FPC), even at the earliest time points after induction (Figure 4.7) suggesting that either Nb48 bound to *Tb*BILBO1 before it arrived at the FPC, but at this stage was covered in chaperones, therefore inaccessible to antibody probes used by IFA, or that Nb48 specifically bound to *Tb*BILBO1 at the FPC alone and was only detected there. The consequence of INb48 expression in *T. brucei* being the same phenotype as that seen with RNAi *TBBILBO1*, also allows verification that indeed INb48 is targeting *Tb*BILBO1.

To try to determine the pathway that Nb48 takes from translation at the ribosome to the FPC and at which stage they bind to *Tb*BILBO1, fractionisation of whole cell trypanosomes could be explored, such as that described by Rovis and Baekkeskov, 1980. Probing of fractions obtained from early induction times of INb48 expression, with antibodies specific for the Nb (tag) and *Tb*BILBO1 could identify the time-point and location in the trypanosome cell where the two first bind together. Another question, is whether INb48 binding to *Tb*BILBO1 causes *Tb*BILBO1 degradation. This theory could be tested using proteasome inhibitors, as alluded to earlier in the section on FPC6 above (Section 5.2.12).

5.3.9 Nb48 interferes with *Tb*BILBO1 dimerisation and polymer formation *in vivo*

Preliminary results show that the functional nanobodies selected against *Tb*BILBO1 recognise the coiled-coil region. As described in the Introduction (Figure 1.13.**B**.), Vidilaseris et al., 2014b showed that the coiled-coil region of *Tb*BILBO1 forms anti-parallel dimers. Binding of the nanobody to this region could disrupt dimer formation and hence the structural polymers formed by *Tb*BILBO1 protein would be disrupted. Electron micrographs of *T. brucei* post induction with INb48 expression show disruption and loss of the flagellar pocket collar annular structure Figure 4.10. To further explore this hypothesis, experiments are planned to express Nb48 in U-2 OS cells with full-length and truncated versions of *Tb*BILBO1. Earlier work by Florimond et al., 2015 showed that only truncated versions of *Tb*BILBO1 containing the coiled-coil region were able to form polymers in U-2 OS cells. It will be interesting to see if Nb48 is able to bind to, and/or alter the shapes of polymers formed by *Tb*BILBO1 in this heterologous system, specifically when co-expressed with the truncation of *Tb*BILBO1 containing the coiled-coil alone. An alternative system to determine which domain of *Tb*BILBO1 to which the Nb48 binds, could be to use yeast 2-hybrid assays with full-length and truncated versions of *Tb*BILBO1 and Nb48 as both bait and prey.

5.3.10 INb48 expression affects the hook complex and endo-/exocytosis

The effect of INb48 expression in *T. brucei* led to perturbation of the structure of the hook complex, as seen by altered *Tb*MORN1 labelling by IFA and electron microscopy (Figure 4.11). This might be a knock-on effect from disturbance of the flagellar pocket collar. The accumulation of intracellular vesicles following INb48 expression indicates a disruption in endo-/exocytosis and could be a consequence of the disturbance of the flagellar pocket and the hook complex, with *Tb*MORN1, and now FPC6, implicated in influencing molecule entry into the flagellar pocket and protein knock-down (FPC6 or *Tb*MORN1) leading to a block in endocytosis (Morriswood and Schmidt, 2015).

5.3.11 Conclusions on scFv and nanobodies

Nb48 is a potential tool for use in the laboratory to further characterise *Tb*BILBO1. Using this nanobody in high-resolution microscopy such as stimulated emission depletion microscopy (STED) with an appropriate tag, such as HaloTag®, mNG or mEos 3.2, to determine more precisely the location of *Tb*BILBO1 in relation to nearby structures. The use of Nb48 which can directly bind *Tb*BILBO1 can bring the fluorophore into much closer relation with *Tb*BILBO1, around 2nm, compared with the traditional combination of two conventional antibodies: a primary against the protein of interest, followed by a secondary fluorophore conjugated against the primary which results in a localisation bias of 10-20nm. This idea was taken up by Cramer et al., 2019 using a nanobody fused to a fluorescent dye for STED microscopy. Alternatively, intracellular fluorescently labelled nanobodies, or chromobodies, have become versatile nanoprobes in imaging endogenous protein targets, for example, to trace actin in zebra-fish (Panza et al., 2015) and the generation of stable transgenic cell lines to to quantify changes in endogenous protein *in vivo* (Keller et al., 2019). In the case of Nb48 the idea is to use it as an external probe, since intracellular binding of its target *Tb*BILBO1 is lethal. With regards to the potential for Nb48 to be used as a nano-drug against trypanosomiasis in the field, the main challenge would be in gaining access to the inside of the trypanosome with a functional nanobody circulating in the host; to this end the Nb could be fused to a known molecule that is endocytosed into trypanosomes to aid its uptake. Nanobodies are growing in use and development as research tools, but also as disease diagnostics, imaging and therapeutics. With over ten single domain antibodies, from both camelid and shark origin, in either clinical or preclinical trials at present (Morrison, 2019) for treatment of a variety of conditions such as rheumatoid arthritis, solid tumours and renal disease.

The possibilities for future use of nanobodies are endless and who knows what other serendipitous discoveries are to be unearthed that could further revolutionise our understanding of the living world.

Appendix A

Electron microspcopy: FPC6

A.1 IEM showing the location of FPC6 in PCF *T. brucei*: cytoskeleton preparations

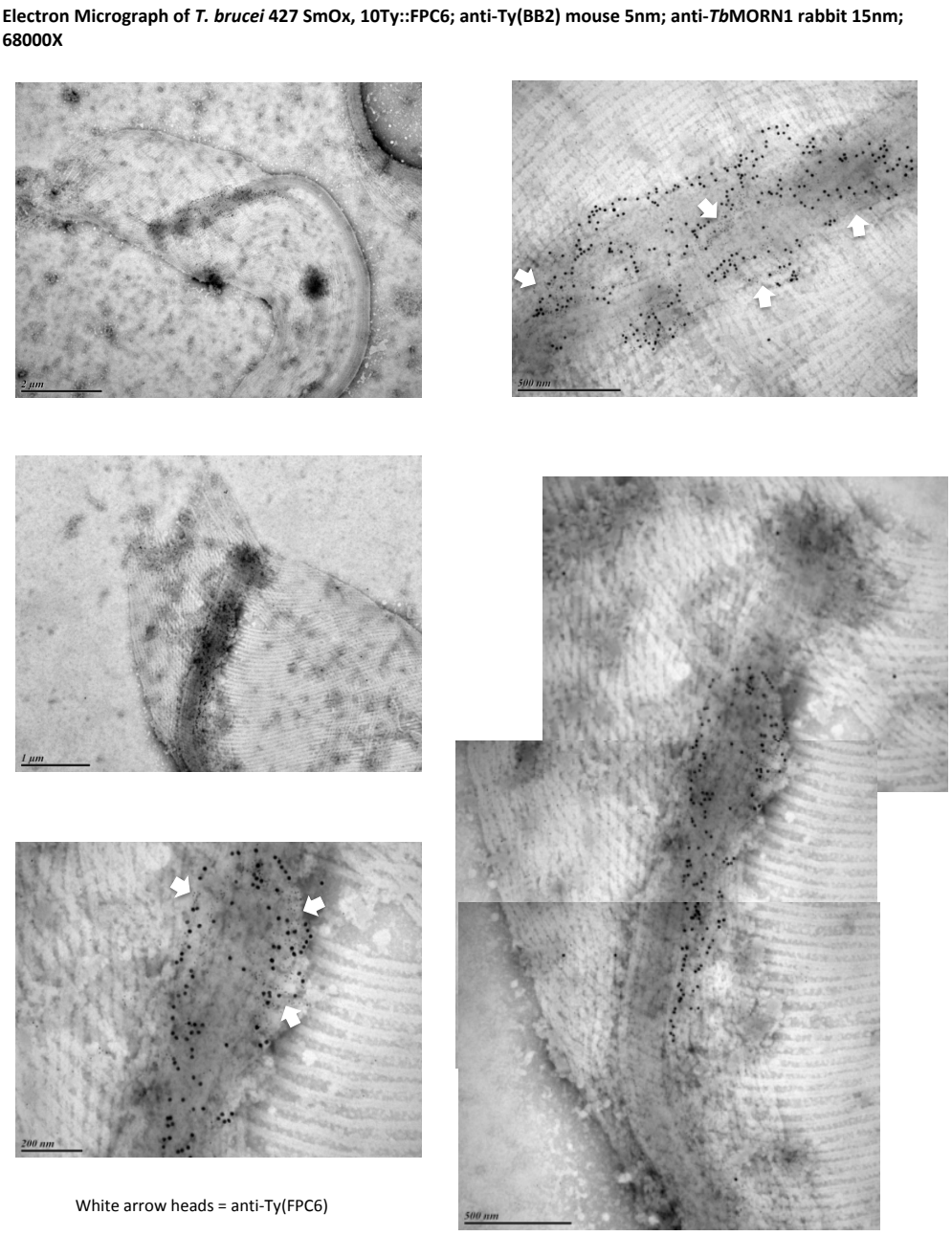

FIGURE A.1: **Immuno-electron microscopy of PCF *T. brucei* showing co-localisation of 10Ty1::FPC6 and *Tb*MORN1.** Cytoskeleton preparations of trypanosomes showing the location of FPC6 protein, observed as a hook-shaped structure curving around the flagellum in the location of the flagellar pocket collar and then extending anteriorly along the flagellum. White arrow heads=10Ty1::FPC6 (5nm gold beads). anti-*Tb*MORN1 (15nm gold beads).

A.2 IEM showing the location of FPC6 in PCF *T. brucei*: isolated flagella

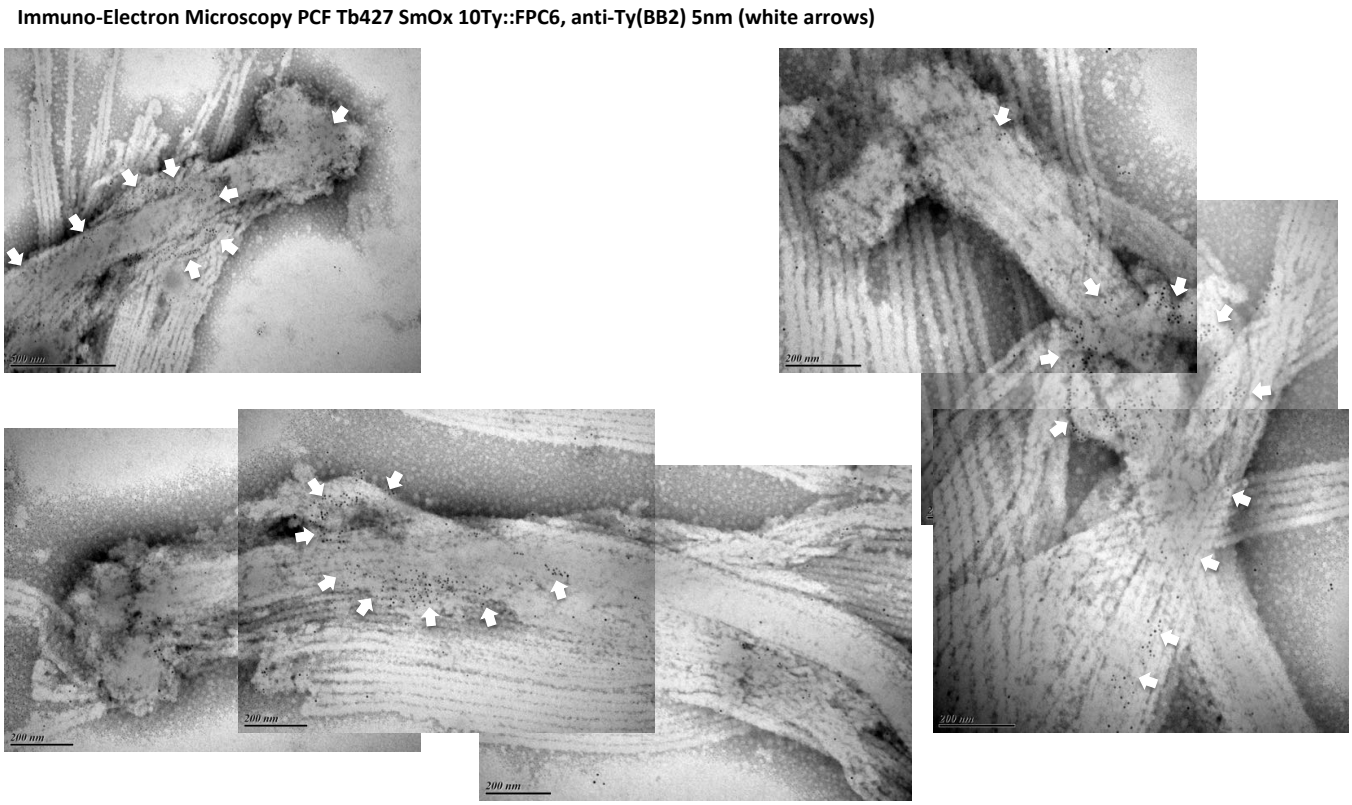

FIGURE A.2: **Immuno-electron microscopy of PCF*T. brucei* showing localisation of FPC6.** The typical hook shape of the structure formed by FPC6 protein is indicated by the white arrows=10Ty1::FPC6 (5nm gold beads).

A.3 IEM showing co-localisation of FPC6 and *Tb*MORN1 in PCF *T. brucei*

FIGURE A.3: **Immuno-electron microscopy of PCF *T. brucei* isolated flagella showing co-localisation of FPC6 with *Tb*MORN1.** White arrows=10Ty1::FPC6 (5nm gold beads) indicating the typical hook-shape structure, co-localising with *Tb*MORN1 (15nm gold beads).

A.4 IEM to show the co-localisation of FPC6 and *Tb*BILBO1 in PCF *T. brucei*

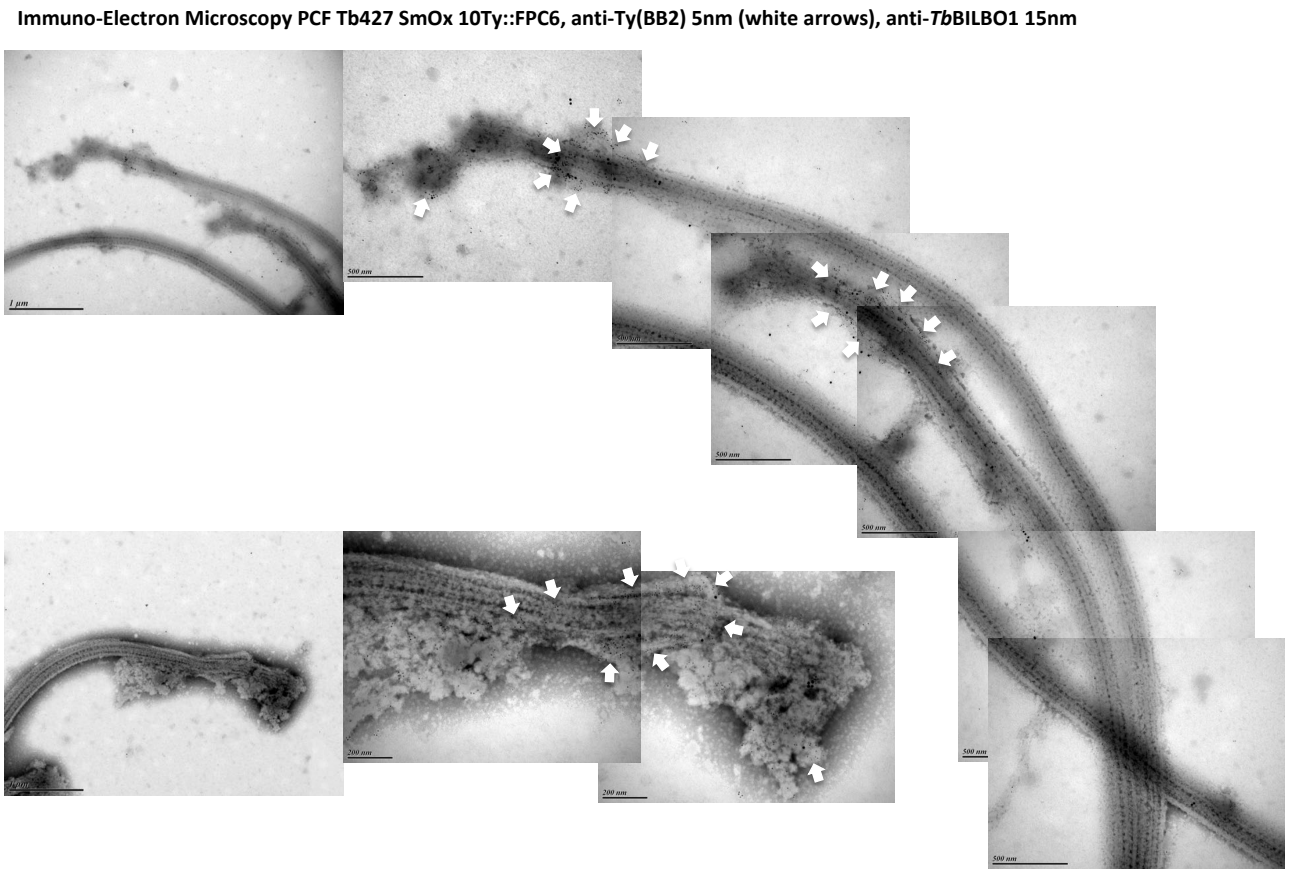

FIGURE A.4: **Immuno-electron microscopy of isolated flagella of *T. brucei* procyclic forms showing co-localisation of FPC6 and *Tb*BILBO1.** White arrows indicate 10Ty1::FPC6 (5nm gold beads) co-localising with *Tb*BILBO1 (15nm gold beads) as the hook-shape structure formed by FPC6 protein curves around the flagellar pocket collar and then extends anteriorly along the flagellum.

A.5 TEM after RNAi *FPC6* in BSF *T. brucei*

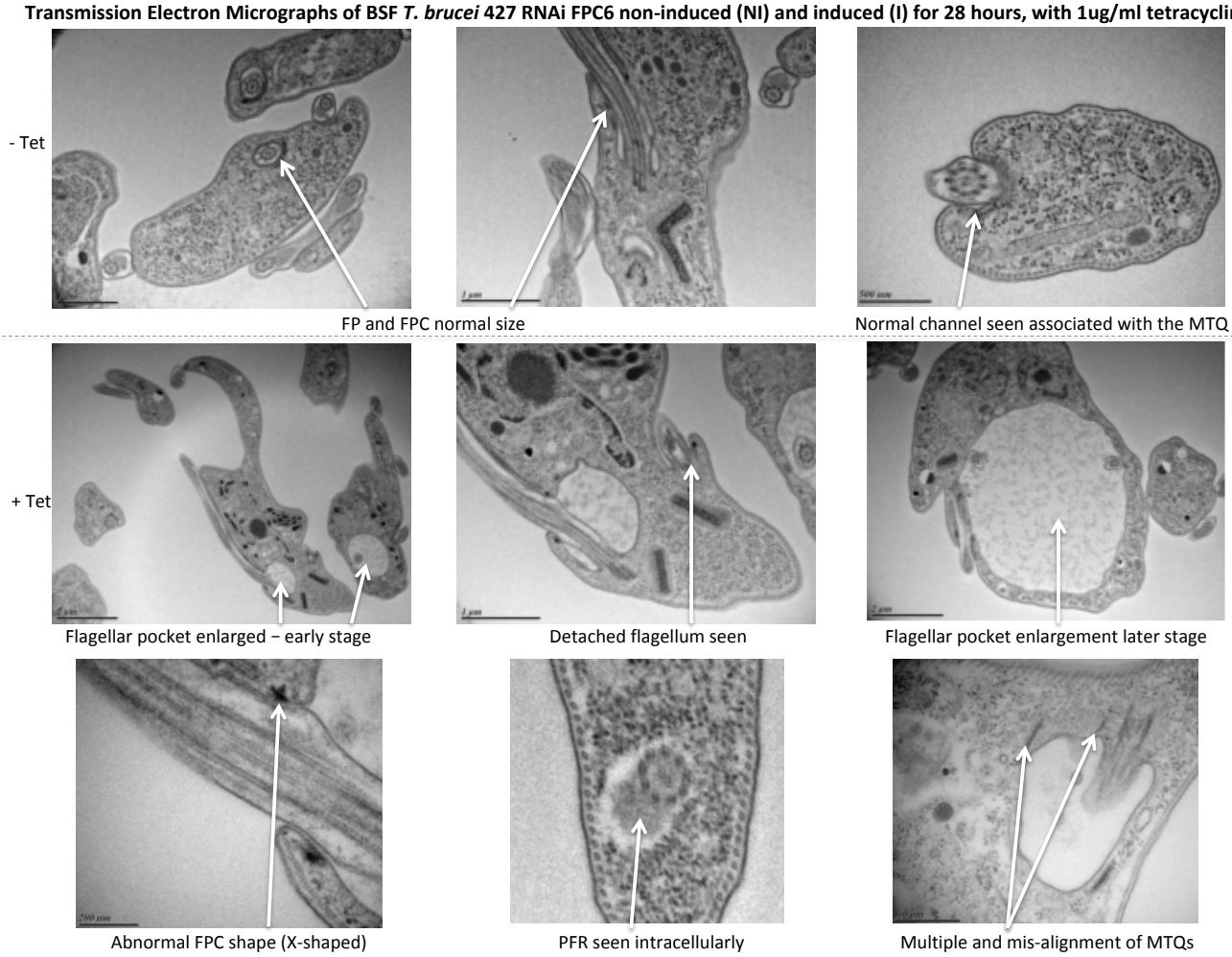

FIGURE A.5: **Transmission electron microscopy of BSF *T. brucei* thin sections after RNAi FPC6.** Images of thin sections of trypanosomes non-induced (- Tet) and induced (+ Tet) for 24 hours with 1μg/mL tetracycline. Induced cells have an enlarged flagellar pocket, unusual features of the flagellar pocket collar (FPC), intracellular para-flagellar rod (PFR) and multiple/mis-aligned microtubule quartets (MTQ).

A.6 TEM after RNAi *FPC6* in BSF *T. brucei*

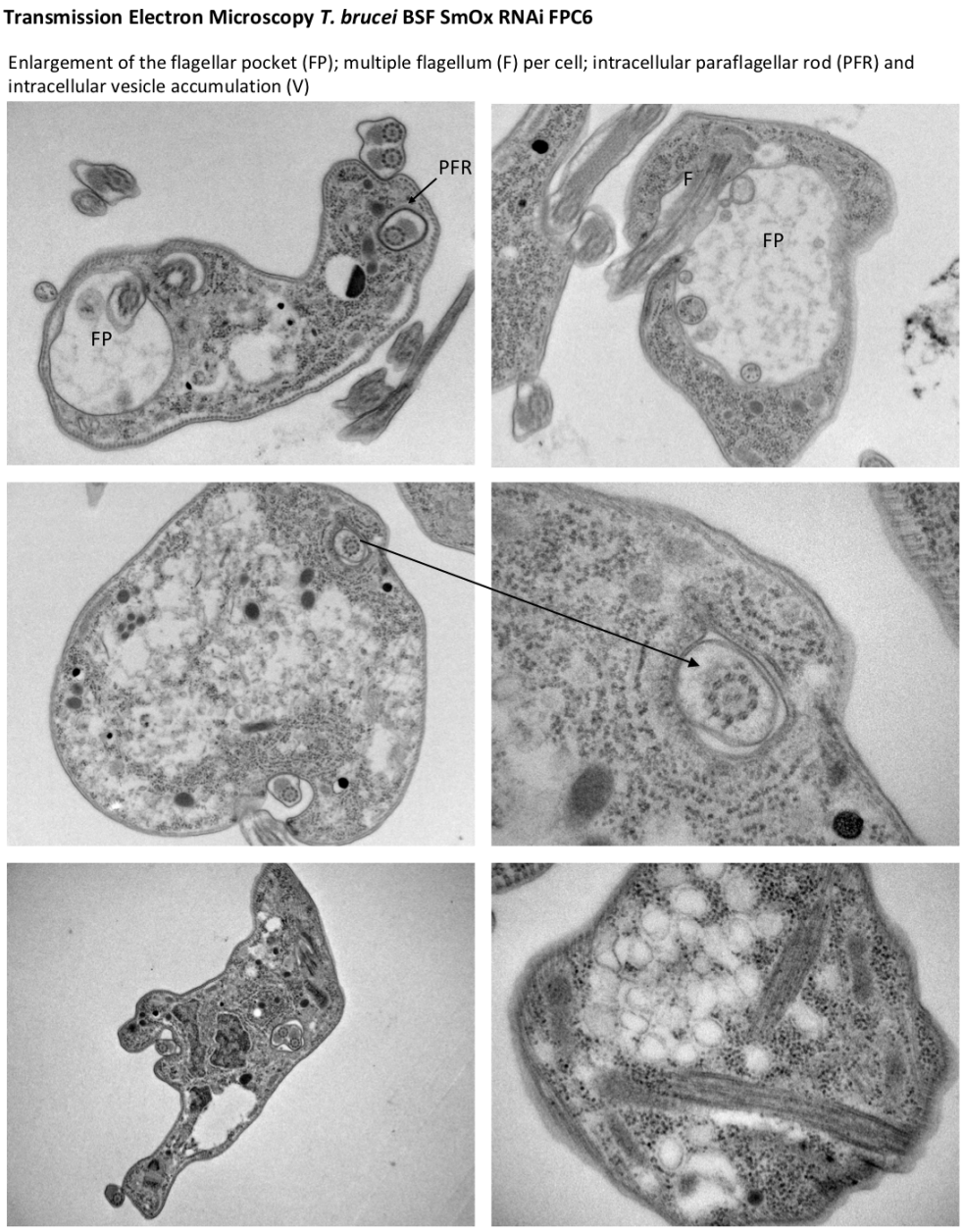

FIGURE A.6: **Transmission electron microscopy of BSF *T. brucei* thin sections after RNAi FPC6.** Images of thin sections of trypanosomes induced (+ Tet) for 24 hours with 1μg/mL tetracycline. Induced cells have an enlarged flagellar pocket (FP), intracellular para-flagellar rod (PFR) intracellular vesicle accumulation (V).

Appendix B

Electron microscopy: nanobodies

B.1 Transmission electron microscopy of INb48 in *T. brucei*

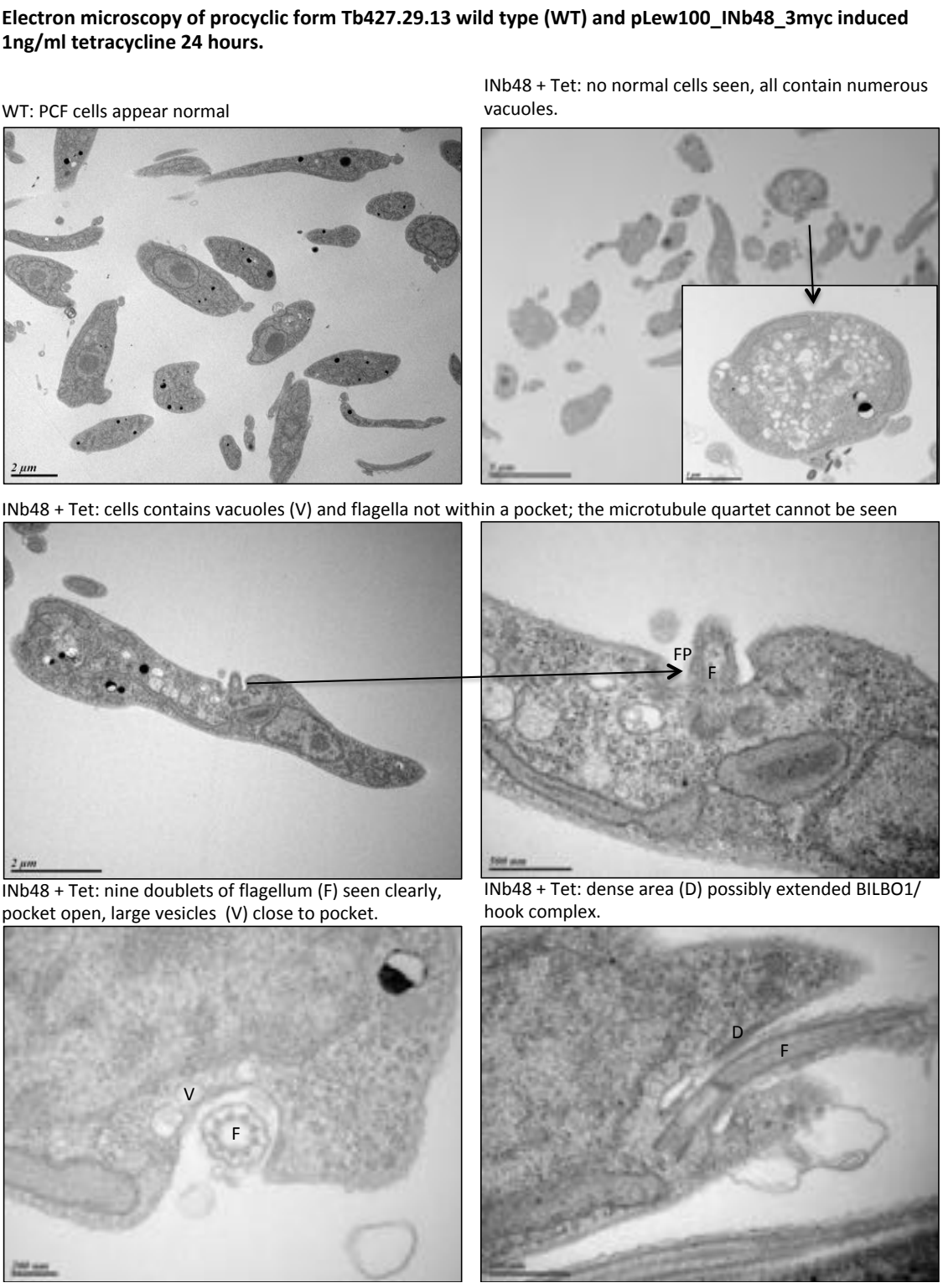

FIGURE B.1: **TEM of *T. brucei* thin sections expressing INb48.** Transmission electron microscopy (TEM) of thin sections of wild-type (WT) trypanosomes and cell lines expressing INb48, 24hpi, showing accumulation of intracellular vesicles and detached flagella. BB=basal bodies, F=flagellum, FP=flagellar pocket and V=vesicle.

B.2 Transmission electron microscopy of INb9 in PCF *T. brucei*

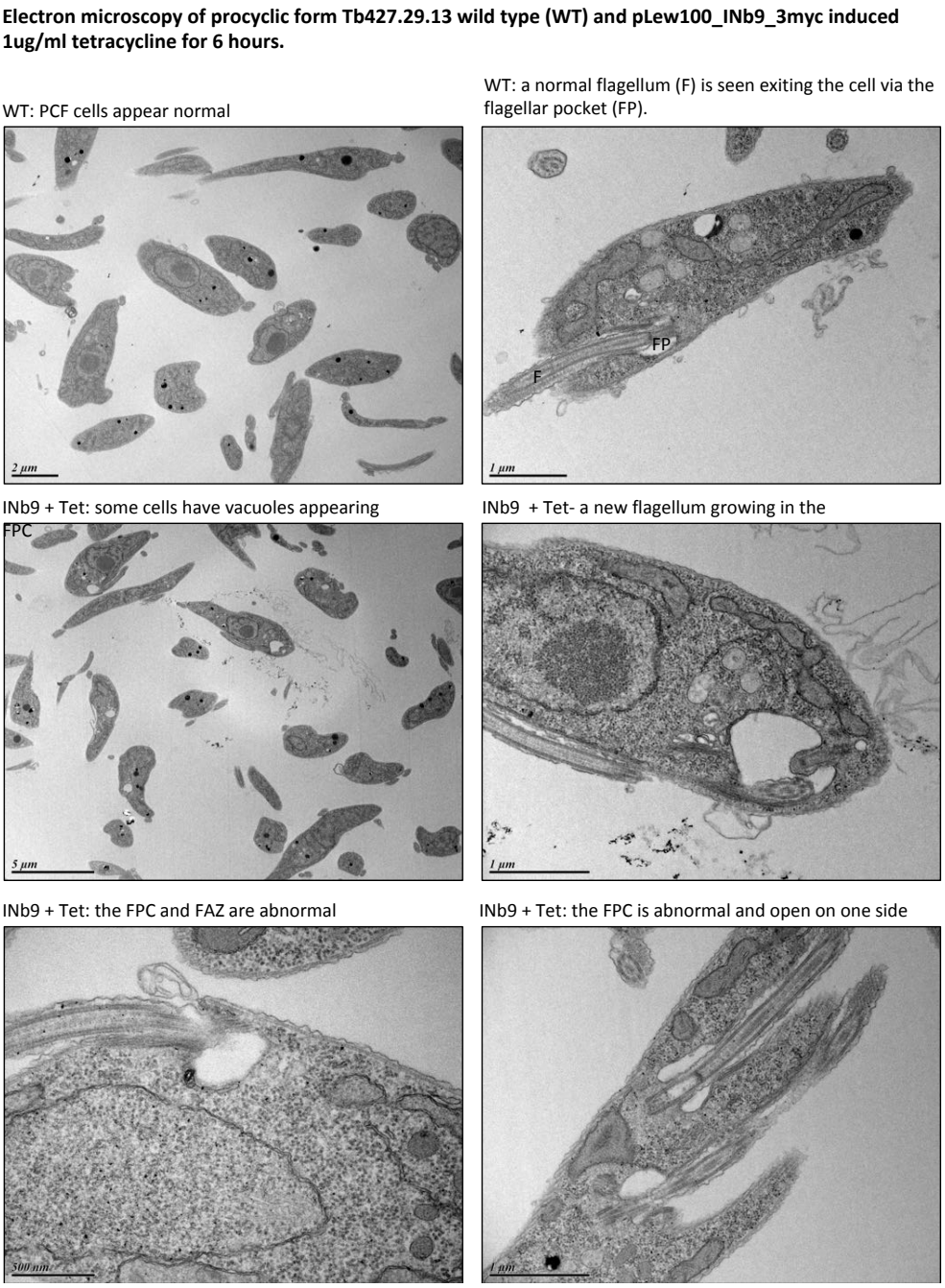

FIGURE B.2: **TEM of *T. brucei* thin sections expressing INb9.** TEM of thin sections of wild-type (WT) trypanosomes and cell lines expressing INb9, 6hpi, showing some intracellular vesicles, abnormal FPC, FAZ and a partially open flagellar pocket. FP=flagellar pocket.

B.3 IEM of isolated flagella showing co-localisation of INb48 and *Tb*BILBO1

Immuno-Electron Microscopy on isolated flagella, PCF Tb427.29.13 pLew100_INb48_3cMyc, induced for 24 hours with 1ug/ml tetracycline.

INb48_3cMyc 5nm gold beads – Nb48_3cMyc seen between the basal bodies and the area where the FPC is formed.

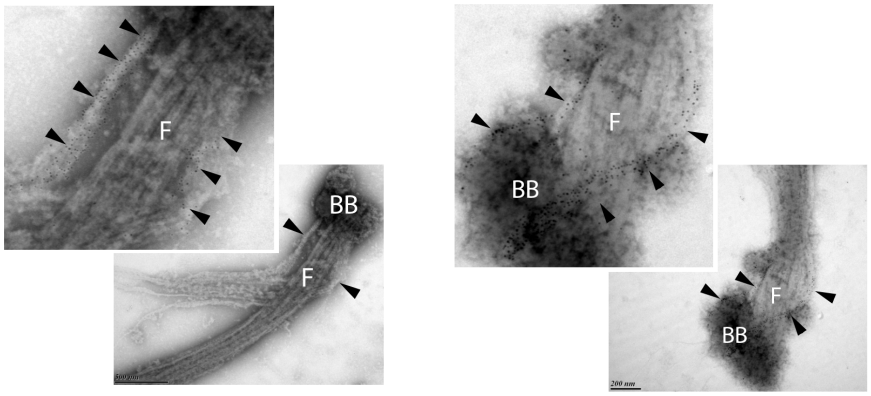

INb48_3cMyc 5nm, *Tb*BILBO1 15nm gold beads – Nb48_3cMyc seen co-localising with *Tb*BILBO1 from the basal bodies anteriorly along the flagellum without the formation of a proper FPC.

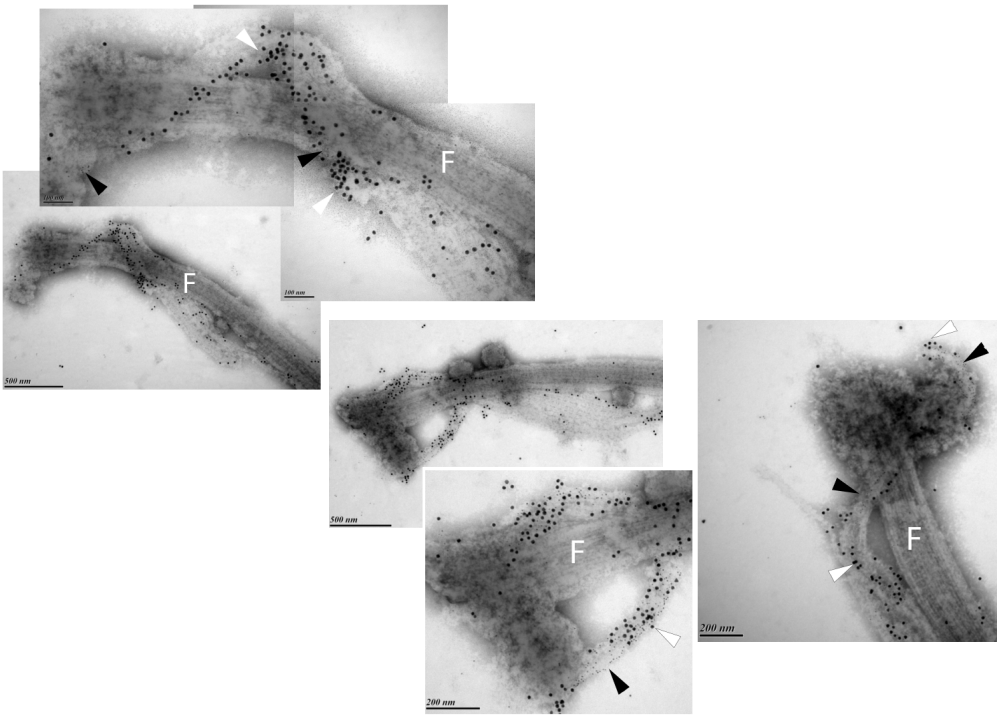

Key: F = flagellum, BB = basal bodies, black arrow heads = anti-cMyc 5nm gold beads (INb48); white arrowheads = anti-*Tb*BILBO1 15nm gold beads

FIGURE B.3: **INb48 and *Tb*BILBO1 on isolated flagella.** Immuno-electron microscopy of isolated flagella of PCF *T. brucei*, showing INb48::3cMyc (5nm gold beads=black arrow heads) alone, in the region between the basal bodies and the FPC. INb48 co-localising with *Tb*BILBO1 (15nm gold beads=white arrow heads) from the area between the basal bodies to the FPC, with disruption of the FPC. BB=basal bodies, F=flagellum.

B.4 IEM of isolated flagella of PCF *T. brucei* after INb48 and INb9 expression

Immuno-Electron Microscopy on isolated flagella, PCF Tb.427.29.13 pLew100_INb9_3cMyc and pLew100_INb48_3cMyc, induced 24 hours with 1ug/ml tetracycline.

INb48_3cMyc 5nm, *Tb*MORN1 15nm gold beads: INb48_3cMyc seen between the basal bodies and the area where the FPC would be formed; the normal hook-shape of *Tb*MORN1 is disrupted and *Tb*MORN1 is elongated in a linear form along the flagellum from the basal bodies anteriorly.

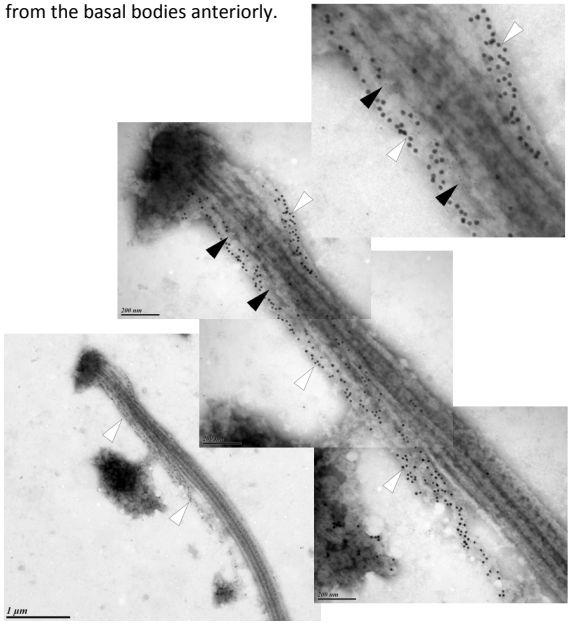

INb9_3cMyc 5nm, *Tb*BILBO1 15nm gold beads: INb9_3cMyc seen between the basal bodies and the FPC. **A** shows normal architecture of the FPC, **B** and **C** show some disruption in the normal shape of the FPC, with *Tb*BILBO1 seen extending anteriorly along the flagellum.

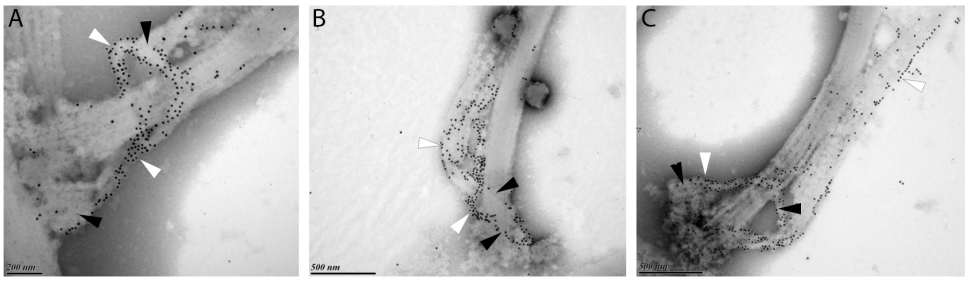

Key: Black arrow heads = anti-cMyc 5nm gold beads (INb48 or INb9); white arrowheads = anti-*Tb*BILBO1/anti-*Tb*MORN1 15nm gold beads.

FIGURE B.4: **IEM: INb48 with *Tb*MORN1 and INb9 with *Tb*BILBO1 on isolated flagella.** Immuno-electron micrograph of isolated flagella of PCF *T. brucei* showing co-labelling of INb48::3cMyc and *Tb*MORN1, with disruption of the hook-shaped complex normally formed by *Tb*MORN1. INb48::3cMyc (5nm gold beads=black arrow heads) co-localising with *Tb*BILBO1 (15nm gold beads=white arrow heads) showing disruption of the flagellar pocket collar (FPC). **A** Shows the normal architecture of the FPC. **B** and **C** show some disruption of the normal shape of the FPC at 24hpi with *Tb*BILBO1 extending anteriorly along the flagellum.

Appendix C

CV and publications

C.1 CV for Christine Reix, née Broster

Christine E REIX

Veterinarian and Scientific Researcher

Education

2016–present day **PhD**, *University of Bordeaux*, France, *Supervisor:* Derrick R. Robinson.
Characterisation and nanobody targeting of essential cytoskeletal proteins of *Trypanosoma brucei*.

2015–2016 **Master 2 in Microbiology-Immunology**, *University of Bordeaux*, France.
Research in Cytoskeletal Biogenesis of Trypanosomes, Robinson Laboratory.

1995–2001 **Bachelor Degree in Veterinary Science, BVSc**, *University of Liverpool*, UK.
Commendation. Gill and Jonathon Pycock Prize in Equine Studies.
Research study into the behaviour change in sheep infested with *Psoroptes ovis*.

1998–1999 **Bachelor Honours Degree in Science, BSc HONS**, *University of Liverpool*, UK.
First class. School of Anatomy and Human Biology.
Research dissertation: Study of hoof conformation of Welsh ponies.

Professional Research Experience

2014 **Reviewer for Veterinary Record Open**, UK.

2005–2009 **Clinical Researcher in Working Equine Lameness**, University of Bristol, UK.
Funded by Brooke. Development of research study methodology into working equine lameness; management, planning and collection of data in the field, in India (1 year) and Pakistan (6 months). Analysis, publication and oral presentation of results. Training of veterinarians and veterinary students.

1999 **The Cornell Leadership Program for Veterinary Students**, *Cornell University*, USA.
Epidemiological study of antibiotic resistance in bacterial samples from cattle in New York State.

International Development Work

2009–2014 **Veterinary Adviser (Resources/Training)**, *Brooke*, London, UK.
Trainer of veterinarians from Africa, Asia, Middle East and Central America. Organisation of international vet training workshops. Co-editor of "The Working Equid Veterinary Manual". Development and management of "Vetwiki" and on-line Formulary. Producer of training resources. Member of research ethics committee.

Veterinary Employment

2001–2005 **Equine Veterinarian**, Ashbrook Equine Clinic, Cheshire, UK.
Full-time ambulatory and hospital work including general anaesthesia of equine patients.

2001–2016 **Small Animal Veterinarian**, UK and France.
Full-time and locum work in clinics in NW, SW England and Bordeaux.

Additional Qualifications

2011 Certificate To Teach in the Life-long Learning Sector (CTLLS), City&Guilds, London, UK.

2009 Certificate in International Development (Merit), Open University, UK.

Languages

English Mothertongue

French Professional

C.2 Publications for Christine Reix, née Broster

Publications for Christine Reix née Broster

2019 **Reix, C.E.**, Ramanantsalama, M.R., Di Primo, C., Minder, L., Landrein, N., Bonhivers, M., Dacheux, D., and Robinson, D.R. Nanobodies and intrabodies as tools and killing agents against *Trypanosoma brucei*. *PLoS Biol. Under review*.

2019 Courtois, P., Nabos, P., Nzoumbou-Boko, R., **Reix, C.E.**, Dauchy, F. A., Daulouede, S., Bringaud, F., Robinson, D.R., and Vincendeau, P. Purification of Extracellular Trypanosomes, Including African, from Blood by Anion-Exchangers (Diethylaminoethyl-cellulose Columns). *J. Vis. Exp.* (146), e58415, doi:10.3791/58415.

2015 Whay, H.R., Dikshit, A.K., Hockenhull, J., Parker, R.M.A., Banerjee, A., Hughes, S.I., Pritchard, J.C. and **Reix, C.E.** Evaluation of changes in equine care and limb-related abnormalities in working horses in Jaipur, India, as part of a two year participatory intervention study. *PLoS ONE* 10 (5): doi:10.1371/journal.pone.0126160.

2015 **Reix, C.E.**, Dixit, A.K., Hockenhull, J., Parker, R.M.A., Banerjee, A., Burn, C.C., Pritchard, J.C., and Whay, H.R. A two-year participatory intervention project with owners to reduce lameness and limb abnormalities in working horses in Jaipur, India. *PLoS ONE* 10 (4): doi:10.1371/journal.pone.0124342.

2014 **Reix (née Broster), C.E.**, Burn, C.C., Pritchard, J.C., Barr, A.R.S. and Whay, H.R. The range and prevalence of clinical signs and conformation associated with lameness in working draught donkeys in Pakistan. *Equine Vet J.* 46 (6) 771-777. doi: 10.1111/evj.12231.

2013 Eds: **Reix, C.E.**, Saville, K. and Hirson, T. The Working Equid Veterinary Manual. The Brooke. Whittet Books Ltd, Essex, UK.

2009 **Broster, C.E.**, Burn, C.C., Barr, A.R.S. and Whay, H.R. The range and prevalence of pathological abnormalities associated with lameness in working horses from developing countries. *Equine Vet. J.* 41 (5) 474-481. doi.org/10.2746/042516409X373907.

2006 **Broster, C.** and Chan, C. Self-assessment case study, degenerative joint disease. *UK Vet*, 11, 9-11.

2001 Berriatua, E., French, N.P., **Broster, C.E.**, Morgan, K.L. and Wall, R. Effect of infestation with *Psoroptes ovis* on the nocturnal rubbing and lying behaviour of housed sheep. *Appl. Anim. Behav. Sci.* 71, 43-55. 10.1016/S0168-1591(00)00166-0.

Bibliography

Absalon, S. et al. (2007). "Intraflagellar Transport and Functional Analysis of Genes Required for Flagellum Formation in Trypanosomes". In: *Molecular Biology of the Cell* 19.3, pp. 929–944. ISSN: 1059-1524. DOI: 10.1091/mbc.e07-08-0749.

Abulrob, Abedelnasser et al. (2005). "The blood-brain barrier transmigrating single domain antibody: Mechanisms of transport and antigenic epitopes in human brain endothelial cells". In: *Journal of Neurochemistry* 95.4, pp. 1201–1214. ISSN: 00223042. DOI: 10.1111/j.1471-4159.2005.03463.x.

Ahmad, Zuhaida Asra et al. (2012). "scFv antibody: principles and clinical application." In: *Clinical & developmental immunology* 2012, p. 980250. ISSN: 1740-2530. DOI: 10.1155/2012/980250. URL: http://www.pubmedcentral.nih.gov/articlerender.fcgi?artid=3312285&tool=pmcentrez&rendertype=abstract.

Aiyedun, B. A. and A. A. Amodu (1976). "Miscellanea : Mel B toxicity in human trypanosomiasis in the Gboko endemic area of Nigeria". In: *Acta Tropica* 33. DOI: 10.5169/seals-312221. URL: http://doi.org/10.5169/seals-312221.

Albisetti, Anna et al. (2017). "Interaction between the flagellar pocket collar and the hook complex via a novel microtubule-binding protein in Trypanosoma brucei". In: *PLoS pathogens* 13.11, e1006710. ISSN: 15537374. DOI: 10.1371/journal.ppat.1006710.

Alcantara, C. L. et al. (2017). "The cytostome–cytopharynx complex of Trypanosoma cruzi epimastigotes disassembles during cell division". In: *Journal of Cell Science* 130.1, pp. 164–176.

Alexander, A. et al. (1982). "gamma Heavy chain disease in man: cDNA sequence supports partial gene deletion model." In: *Proceedings of the National Academy of Sciences* 79.10, pp. 3260–3264. ISSN: 0027-8424. DOI: 10.1073/pnas.79.10.3260.

Alibu, Vincent P. et al. (2005). "A doubly inducible system for RNA interference and rapid RNAi plasmid construction in Trypanosoma brucei". In: *Molecular and Biochemical Parasitology* 139.1, pp. 75–82. ISSN: 01666851. DOI: 10.1016/j.molbiopara.2004.10.002.

Alirahimi, E. et al. (2017). "Intrabody targeting vascular endothelial growth factor receptor-2 mediates downregulation of surface localization". In: *Cancer Gene Therapy* 24.1, pp. 33–37. ISSN: 14765500. DOI: 10.1038/cgt.2016.76.

Allen, C.L., D Goulding, and M.C.. Field (2003). "Clathrinmediatedendocytosisessential Tbrucei". In: *The EMBO Journal* 22.19, pp. 4991–5002.

Alsford, Sam et al. (2012). "High-throughput decoding of antitrypanosomal drug efficacy and resistance". In: *Nature* 482.7384, pp. 232–236. ISSN: 00280836. DOI: 10.1038/nature10771.

Anene, B. M. et al. (2006). "A diminazene resistant strain of Trypanosoma brucei brucei isolated from a dog is cross-resistant to pentamidine in experimentally infected albino rats". In: *Parasitology* 132.1, pp. 127–133. DOI: 10.1017/s0031182005008760.

Antonescu, C. N. et al. (2011). "Phosphatidylinositol-(4,5)-bisphosphate regulates clathrin-coated pit initiation, stabilization, and size". In: *Molecular Biology of the Cell* 22.14, pp. 2588–2600. ISSN: 1059-1524. DOI: 10.1091/mbc.e11-04-0362.

Arbabi Ghahroudi, M. et al. (1997). "Selection and identification of single domain antibody fragments from camel heavy-chain antibodies". In: *FEBS Letters* 414.3, pp. 521–526. ISSN: 00145793. DOI: 10.1016/S0014-5793(97)01062-4. URL: http://dx.doi.org/10.1016/S0014-5793(97)01062-4.

Arias, Jose. L. et al. (2015). "Nanobody conjugated PLGA nanoparticles for active targeting of African Trypanosomiasis". In: *Journal of Controlled Release* 197, pp. 190–198. DOI: 10.1016/j.jconrel.2014.11.002. URL: http://dx.doi.org/10.1016/j.jconrel.2014.11.002.

Awate, Sunita, Lorne A. Babiuk, and George Mutwiri (2013). "Mechanisms of action of adjuvants". In: *Frontiers in Immunology* 4.MAY. DOI: 10.3389/fimmu.2013.00114.

Ayub, Maximiliano et al. (2012). "Selective blockade of trypanosomatid protein synthesis by a recombinant antibody anti-trypanosoma cruzi P2β protein". In: *PLoS ONE* 7.5. ISSN: 19326203. DOI: 10.1371/journal.pone.0036233.

Babokhov, Peter et al. (2013). "A current analysis of chemotherapy strategies for the treatment of human African trypanosomiasis". In: *Pathogens and Global Health* 107.5, pp. 242–252. ISSN: 2047-7724. DOI: 10.1179/2047773213y.0000000105.

Baker, Nicola et al. (2013). "Europe PMC Funders Group Drug resistance in African trypanosomiasis : the melarsoprol and pentamidine story Chemotherapy against African trypanosomiasis Europe PMC Funders Author Manuscripts The diamidines". In: 29.3. DOI: 10.1016/j.pt.2012.12.005.Drug.

Baral, Toya Nath et al. (2006). "Experimental therapy of African trypanosomiasis with a nanobody-conjugated human trypanolytic factor". In: *Nature Medicine* 12.5, pp. 580–584. ISSN: 10788956. DOI: 10.1038/nm1395.

Bastin, Philippe et al. (1996). "A novel epitope tag system to study protein targeting and organelle biogenesis in Trypanosoma brucei". In: *Molecular and Biochemical Parasitology* 77.2, pp. 235–239. ISSN: 01666851. DOI: 10.1016/0166-6851(96)02598-4.

Bastin, P. et al. (2000). "Flagellum ontogeny in trypanosomes studied via an inherited and regulated RNA interference system". In: *Journal of Cell Science* 113, pp. 3321–3328.

Bauer, Burkhard et al. (2011). "Managing tsetse transmitted trypanosomosis by insecticide treated nets - An affordable and sustainable method for resource poor pig farmers in Ghana". In: *PLoS Neglected Tropical Diseases* 5.10. ISSN: 19352727. DOI: 10.1371/journal.pntd.0001343.

Ben Amar, M F et al. (1988). "Structure and transcription of the actin gene of Trypanosoma brucei." In: *Molecular and cellular biology* 8.5, pp. 2166–76. ISSN: 0270-7306. URL: http://www.ncbi.nlm.nih.gov/pubmed/3386635%20http://www.pubmedcentral.nih.gov/articlerender.fcgi?artid=PMC363398.

Bennett, S. C. J. (1930). "Camel Trypanosomias in the Sudan". In: *In Proceedings of the 1929 Pan African Veterinary Conference, Pretoria, South Africa*, pp. 10–15.

Berberof, Magali, David Pérez-Morga, and Etienne Pays (2001). "A receptor-like flagellar pocket glycoprotein specific to Trypanosoma brucei gambiense". In: *Molecular and Biochemical Parasitology* 113.1, pp. 127–138. ISSN: 01666851. DOI: 10.1016/S0166-6851(01)00208-0.

Berkmen, Mehmet (2014). "Production of disulfide-bonded proteins in Escherichia coli". In: *Current Protocols in Molecular Biology* 82, pp. 240–251. DOI: 10.1002/0471142727.mb1601bs108.

Berriman, Matthew et al. (2005). "The genome of the African trypanosome Trypanosoma brucei". In: *Science*. ISSN: 00368075. DOI: 10.1126/science.1112642. arXiv: 9809069v1 [gr-qc].

Berthier, David et al. (2015). "A comparison of phenotypic traits related to trypanotolerance in five West African cattle breeds highlights the value of shorthorn taurine breeds". In: *PLoS ONE* 10.5. ISSN: 19326203. DOI: 10.1371/journal.pone.0126498.

Beyer, Hannes M. et al. (2015). "AQUA cloning: A versatile and simple enzyme-free cloning approach". In: *PLoS ONE* 10.9. ISSN: 19326203. DOI: 10.1371/journal.pone.0137652.

Bird, R. E. et al. (1988). "Single-chain antigen-binding proteins". In: *Science* 242.4977, pp. 423–426.

Black, S. J. et al. (2001). "Innate and acquired control of trypanosome parasitaemia in Cape buffalo". In: *International Journal for Parasitology* 31.5-6, pp. 562–565. DOI: 10.1016/S0020-7519(01)00160-6.

Bock, M., R. Gonnert, and A. Haberkorn (1969). "Studies with Bay 2502 onanimals". In: *Bol Chil Parasitol* 24, pp. 13–19.

Bond, Christopher J., James C. Marsters, and Sachdev S. Sidhu (2003). "Contributions of CDR3 to VHH domain stability and the design of monobody scaffolds for naive antibody libraries". In: *Journal of Molecular Biology* 332.3, pp. 643–655. ISSN: 00222836. DOI: 10.1016/S0022-2836(03)00967-7.

Bonhivers, Mélanie et al. (2008). "Biogenesis of the trypanosome endo-exocytotic organelle is cytoskeleton mediated". In: *PLoS Biology* 6.5, pp. 1033–1046. ISSN: 15457885. DOI: 10.1371/journal.pbio.0060105.

Bonnet, Julien, Clotilde Boudot, and Bertrand Courtioux (2015). "Overview of the Diagnostic Methods Used in the Field for Human African Trypanosomiasis: What Could Change in the Next Years?" In: *BioMed Research International* 2015, pp. 1–10. ISSN: 2314-6133. DOI: 10.1155/2015/583262.

Bornhorst, By Joshua A and Joseph J. Falke (2010). "Reprint of: Purification of Proteins Using Polyhistidine Affinity Tags". In: *Protein Expression and Purification*. ISSN: 10465928. DOI: 10.1016/j.pep.2011.08.022.

Borst, Piet and Jan H J Hoeijmakers (1979). "REVIEW Kinetoplast DNA". In: *Plasmid*, pp. 20–40.

Boulangé, Alain et al. (2017). "Development of a rapid antibody test for point-of-care diagnosis of animal African trypanosomosis". In: *Veterinary Parasitology* 233, pp. 32–38. ISSN: 18732550. DOI: 10.1016/j.vetpar.2016.11.017.

Brickman, M.J., J.M. Cook, and A.E. Balber (1995). "Low temperature inhibits transport from tubular endosomes to a perinuclear, acidic compartment in African trypanosomes". In: *Journal of Cell Science* 108, pp. 3611–3621.

Briggs, Laura J. et al. (2004). " The flagella connector of Trypanosoma brucei : an unusual mobile transmembrane junction ". In: *Journal of Cell Science* 117.9, pp. 1641–1651. ISSN: 0021-9533. DOI: 10.1242/jcs.00995.

Brookman, Jayne L. et al. (1995). "An Immunological Analysis of Ty1 Virus-like Particle Structure". In: *Virology* 207.1, pp. 59–67.

Brooks, C.L., M.L. Rossotti, and K.A. Henry (2018). "Immunological Functions and Evolutionary Emergence of Heavy-Chain Antibodies". In: *Trends in Immunology* 39.12, pp. 956–960. DOI: doi.org/10.1016/j.it.2018.09.008.

Brooks, Darren R. et al. (2000). "Stable transformation of trypanosomatids through targeted chromosomal integration of the selectable marker gene encoding blasticidin S deaminase". In: *FEMS Microbiology Letters* 186.2, pp. 287–291. DOI: 10.1016/S0378-1097(00)00159-2.

Brown, K. N., J. Hill, and A. E. Holland (1961). "Antitrypanosomal activity of certain phenyldiazoamino and phenylazoamino phenanthridium compunds". In: *British Journal of Pharmacology and Chemotherapy* 17.3, pp. 396–405. DOI: 10.1111/j.1476-5381.1961.tb01125.x.

Browning, C. H. et al. (1938). "The trypanocidal action of certain phenanthridium compounds". In: *The Journal of Pathology* 46.1.

Bruce, D., A. E. Hamerton, and F. P. Mackie (1909). "Trypanosoma ingens". In: *Proceedings of the Royal Society B* 81.549, pp. 323–325.

Brun, R. and M. Schonenberger (1979). "Cultivation and in vitro cloning of procyclic culture forms of "Trypanosoma brucei" in a semi-defined medium : short communication". In: *Acta Tropica* 36, pp. 289–292. DOI: 10.5169/seals-312533. URL: http://doi.org/10.5169/seals-312533.

Brun, Reto et al. (2010). "Human African trypanosomiasis." In: *Lancet* 375.9709, pp. 148–59. ISSN: 1474-547X. DOI: 10.1016/S0140-6736(09)60829-1. URL: http://www.ncbi.nlm.nih.gov/pubmed/19833383.

Budd, Graham E (2013). "Send Orders for Reprints to reprints@benthamscience.net At the Origin of Animals: The Revolutionary Cambrian Fossil Record". In: *Current Genomics* 14, pp. 344–354.

Büscher, Philippe et al. (2019). "Equine trypanosomosis: enigmas and diagnostic challenges". In: *Parasites & Vectors* 12.1, p. 234. ISSN: 1756-3305. DOI: 10.1186/s13071-019-3484-x. URL: https://parasitesandvectors.biomedcentral.com/articles/10.1186/s13071-019-3484-x.

Caljon, Guy et al. (2015). "Description of a Nanobody-based Competitive Immunoassay to Detect Tsetse Fly Exposure". In: *PLoS Neglected Tropical Diseases* 9.2. ISSN: 19352735. DOI: 10.1371/journal.pntd.0003456.

Cao, Tong and Boon Chin Heng (2005). "Commentary: Intracellular antibodies (intrabodies) versus RNA interference for therapeutic applications". In: *Annals of Clinical and Laboratory Science* 35.3, pp. 227–229.

Capewell, Paul et al. (2016). "The skin is a significant but overlooked anatomical reservoir for vector-borne African trypanosomes". In: *eLife* 5. DOI: 10.7554/elife.17716.

Carlson, John R (1988). "A New Means of Inducibly Inactivating a Cellular Protein". In: *Molecular and Cellular Biology* 8.6, pp. 2638–2646.

Carnes, Jason et al. (2015). "Genome and Phylogenetic Analyses of Trypanosoma evansi Reveal Extensive Similarity to T. brucei and Multiple Independent Origins for Dyskinetoplasty". In: *PLoS Neglected Tropical Diseases* 9.1. ISSN: 19352735. DOI: 10.1371/journal.pntd.0003404.

Cavalier-Smith, T (1993). "Kingdom protozoa and its 18 phyla." In: *Microbiological reviews* 57.4, pp. 953–94. ISSN: 0146-0749. URL: http://www.ncbi.nlm.nih.gov/pubmed/8302218%20http://www.pubmedcentral.nih.gov/articlerender.fcgi?artid=PMC372943.

Cayla, Mathieu et al. (2019). "African trypanosomes". In: *Parasites and Vectors* 12.1. ISSN: 17563305. DOI: 10.1186/s13071-019-3355-5.

Celis, Esteban (2002). "Getting peptide vaccines to work: just a matter of quality control?" In: *Journal of Clinical Investigation* 110.12, pp. 1765–1768. ISSN: 0021-9738. DOI: 10.1172/jci200217405.

Chandler, R. L. (1952). "Comparative Tolerance of West African N'dama Cattle to Trypanosomiasis". In: *Annals of Tropical Medicine & Parasitology* 46.2, pp. 127–134.

Chen, Yunching et al. (2010). "Nanoparticles modified with tumor-targeting scFv deliver siRNA and miRNA for cancer therapy". In: *Molecular Therapy* 18.9, pp. 1650–1656. ISSN: 15250024. DOI: 10.1038/mt.2010.136.

coherent market insights (2019). *https://www.coherentmarketinsights.com/market-insight/monoclonal-antibody-therapeutics-market-2403*. URL: https://www.coherentmarketinsights.com/market-insight/monoclonal-antibody-therapeutics-market-2403.

Conrath, Katja E et al. (2001). " -Lactamase Inhibitors Derived from Single-Domain Antibody Fragments Elicited in the Camelidae". In: 45.10, pp. 2807–2812. DOI: 10.1128/AAC.45.10.2807.

Courtois, P. et al. (2019). "Purification of Extracellular Trypanosomes, Including African, from Blood by Anion-Exchangers (Diethylaminoethyl-cellulose Columns)". In: *J. Vis. Exp.* 146. DOI: doi:10.3791/58415.

Coutton, Charles et al. (2018). "Mutations in CFAP43 and CFAP44 cause male infertility and flagellum defects in Trypanosoma and human". In: *Nature Communications*. ISSN: 20411723. DOI: 10.1038/s41467-017-02792-7.

Cramer, Kimberly et al. (2019). "Visualization of Bacterial Protein Complexes Labeled with Fluorescent Proteins and Nanobody Binders for STED Microscopy". In: *International Journal of Molecular Sciences* 20.14, p. 3376. ISSN: 1422-0067. DOI: 10.3390/ijms20143376. URL: https://www.mdpi.com/1422-0067/20/14/3376.

Crick, F.H.C. (1952). "Is alpha-keratin a coiled coil?" In: *Nature* 170, pp. 882–3.

Cross, G A (1975). "Identification, purification and properties of clone-specific glycoprotein antigens constituting the surface coat of Trypanosoma brucei." In: *Parasitology* 71.3, pp. 393–417. ISSN: 0031-1820. URL: http://www.ncbi.nlm.nih.gov/pubmed/645.

Cunningham, M P and K Vickerman (1962). "Antigenic analysis in the Trypanosoma brucei group, using the agglutination reaction". In: *Transactions of the Royal Society of Topical Medicine and Hygiene* 56.1, pp. 48–59. URL: https://academic.oup.com/trstmh/article-abstract/56/1/48/1925588.

Curd, F. H. S. and D. G. Davey (1949). "Antrycide: a new trypanocidal drug". In: *Nature* 4133, pp. 89–90.

Da Silva, Frederico Aires et al. (2004). "Camelized rabbit-derived VH single-domain intrabodies against Vif strongly neutralize HIV-1 infectivity". In: *Journal of Molecular Biology* 340.3, pp. 525–542. ISSN: 00222836. DOI: 10.1016/j.jmb.2004.04.062.

Dacheux, Denis et al. (2012). "A MAP6-Related protein is present in protozoa and is involved in flagellum motility". In: *PLoS ONE* 7.2. ISSN: 19326203. DOI: 10.1371/journal.pone.0031344.

Davaasuren, Batdorj et al. (2019). " Draft Genome Sequence of Trypanosoma equiperdum Strain IVM-t1 ". In: *Microbiology Resource Announcements* 8.9. DOI: 10.1128/mra.01119-18.

Davies, Julian and Lutz Riechmann (1994). "'Camelising' human antibody fragments: NMR studies on VH domains". In: *FEBS Letters* 339.3, pp. 285–290. ISSN: 00145793. DOI: 10.1016/0014-5793(94)80432-X.

D'avila-Levy, Claudia Masini et al. (2015). "Exploring the environmental diversity of kinetoplastid flagellates in the high-throughput DNA sequencing era". In: *Memorias do Instituto Oswaldo Cruz* 110.8, pp. 956–965. ISSN: 16788060. DOI: 10.1590/0074-02760150253.

Dawe, H. R., H. Farr, and K. Gull (2007). "Centriole/basal body morphogenesis and migration during ciliogenesis in animal cells". In: *Journal of Cell Science* 120.1, pp. 7–15.

De Koning, Harry P. and Simon M. Jarvis (2001). "Uptake of pentamidine in Trypanosoma brucei brucei is mediated by the P2 adenosine transporter and at least one novel, unrelated transporter". In: *Acta Tropica* 80.3, pp. 245–250. ISSN: 0001706X. DOI: 10.1016/S0001-706X(01)00177-2.

De Vooght, Linda et al. (2012). "Expression and extracellular release of a functional anti-trypanosome Nanobody® in Sodalis glossinidius, a bacterial symbiont of the tsetse fly." In: *Microbial cell factories* 11.1, p. 23. ISSN: 1475-2859. DOI: 10.1186/1475-2859-11-23. URL: http://www.pubmedcentral.nih.gov/articlerender.fcgi?artid=3311065&tool=pmcentrez&rendertype=abstract.

De Vooght, Linda et al. (2014). "Delivery of a functional anti-trypanosome nanobody in different tsetse fly tissues via a bacterial symbiont, sodalis glossinidius". In: *Microbial Cell Factories* 13.1. ISSN: 14752859. DOI: 10.1186/s12934-014-0156-6.

Dean, Samuel et al. (2015a). "A toolkit enabling efficient, scalable and reproducible gene tagging in trypanosomatids". In: *Open Biology* 5.1. ISSN: 20462441. DOI: 10.1098/rsob.140197.

– (2015b). "A toolkit enabling efficient, scalable and reproducible gene tagging in trypanosomatids". In: *Open Biology* 5.1. ISSN: 20462441. DOI: 10.1098/rsob.140197.

Demmel, Lars et al. (2016). " The endocytic activity of the flagellar pocket in Trypanosoma brucei is regulated by an adjacent phosphatidylinositol phosphate kinase ". In: *Journal of Cell Science* 129.11, pp. 2285–2285. ISSN: 0021-9533. DOI: 10.1242/jcs.191569.

Dereeper, Alexis et al. (2010). "BLAST-EXPLORER helps you building datasets for phylogenetic analysis". In: *BMC Evolutionary Biology* 10.1. ISSN: 14712148. DOI: 10.1186/1471-2148-10-8.

Dereeper, A et al. (2008). "Phylogeny.fr: robust phylogenetic analysis for the non-specialist." In: *Nucleic acids research* 36.Web Server issue, pp. 465–9. ISSN: 1362-4962. DOI: 10.1093/nar/gkn180. URL: http://www.ncbi.nlm.nih.gov/pubmed/18424797%20http://www.pubmedcentral.nih.gov/articlerender.fcgi?artid=PMC2447785.

Dewi, Kartika Sari et al. (2016). "Construction and periplasmic expression of the anti-EGFRvIII ScFv antibody gene in escherichia coli". In: *Scientia Pharmaceutica* 84.1, pp. 141–152. DOI: 10.3797/scipharm.ISP.2015.06.

Dorn, Patricia L et al. (2007). "Autochthonous Transmission of Trypanosoma cruzi, Louisiana". In: *Emerging Infectious Diseases* 13.4, pp. 605–607. URL: www.cdc.gov/eid.

Doshi, Rupak et al. (2014). "In vitro nanobody discovery for integral membrane protein targets". In: *Scientific Reports* 4. ISSN: 20452322. DOI: 10.1038/srep06760.

Duggan, Sean (2018). "Caplacizumab: First Global Approval". In: *Drugs* 78.15, pp. 1639–1642. ISSN: 11791950. DOI: 10.1007/s40265-018-0989-0.

Edwards, J. T. (1926). "The chemotherapy of surra (Trypanosoma evansi infections) of horses and cattle in India". In: *Transactions of the Royal Society of Tropical Medicine and Hygiene* 20.1-2, pp. 10–26.

EMBL-EBI (2019). *InterPro*. DOI: https://www.ebi.ac.uk/interpro/.

EMBL-EMI (2019). *RADAR*. DOI: https://www.ebi.ac.uk/Tools/pfa/radar/.

Engstler, M. (2004). "Kinetics of endocytosis and recycling of the GPI-anchored variant surface glycoprotein in Trypanosoma brucei". In: *Journal of Cell Science* 117.7, pp. 1105–1115. ISSN: 0021-9533. DOI: 10.1242/jcs.00938. URL: http://jcs.biologists.org/cgi/doi/10.1242/jcs.00938.

Engstler, Markus et al. (2007). "Hydrodynamic Flow-Mediated Protein Sorting on the Cell Surface of Trypanosomes". In: *Cell* 131.3, pp. 505–515. ISSN: 00928674. DOI: 10.1016/j.cell.2007.08.046.

Esson, H. J. et al. (2012). "Morphology of the Trypanosome Bilobe, a Novel Cytoskeletal Structure". In: *Eukaryotic Cell* 11.6, pp. 761–772. DOI: 10.1128/ec.05287-11.

Ezzine, Aymen et al. (2012). "Efficient expression of the anti-AahI' scorpion toxin nanobody under a new functional form in a Pichia pastoris system". In: *Biotechnology and Applied Biochemistry* 59.1, pp. 15–21. ISSN: 08854513. DOI: 10.1002/bab.67.

Fairlamb, A. H. et al. (1985). "Trypanothione: A novel Bis(glutathionyl)spermidine cofactor for glutathione reductase in trypanosomatids". In: *Science* 227, pp. 1485–1487.

FAO (2017). *FAOSTAT*. URL: http://www.fao.org/faostat/en/#data.

Fèvre, E. M. et al. (2001). "The origins of a new Trypanosoma brucei rhodesiense sleeping sickness outbreak in eastern Uganda". In: *Lancet* 358.9282, pp. 625–628. ISSN: 01406736. DOI: 10.1016/S0140-6736(01)05778-6.

Field, Mark C and Mark Carrington (2009). "The trypanosome flagellar pocket." In: *Nature reviews. Microbiology* 7.11, pp. 775–86. ISSN: 1740-1534. DOI: 10.1038/nrmicro2221. URL: http://www.ncbi.nlm.nih.gov/pubmed/19806154.

Fletcher, Daniel A. and R. Dyche Mullins (2010). "Cell mechanics and the cytoskeleton". In: *Nature* 463.7280, pp. 485–492. DOI: 10.1038/nature08908.

Florimond, Célia et al. (2015). "BILBO1 is a scaffold protein of the flagellar pocket collar in the pathogen Trypanosoma brucei." In: *PLoS pathogens* 11.3, e1004654. ISSN: 1553-7374. DOI: 10.1371/journal.ppat.1004654. URL: http://www.pubmedcentral.nih.gov/articlerender.fcgi?artid=4379179&tool=pmcentrez&rendertype=abstract.

Freund, J. and K. MacDermott (1942). "Sensitization to Horse Serum by Means of Adjuvants". In: *Proc. Soc. Exper. BIol & Med.* 49.548, p. 1942.

Fridy, Peter C. et al. (2014). "A robust pipeline for rapid production of versatile nanobody repertoires". In: *Nature Methods* 11.12, pp. 1253–1260. ISSN: 15487105. DOI: 10.1038/nmeth.3170.

Friedheim, E. A. H. (1949). "Mel B in the Treatment of Human Trypanosomiasis". In: *The American Journal of Tropical Medicine and Hygiene* 29.2, pp. 173–80.

Fuchs, E. and D. W Cleveland (1998). "A Structural Scaffolding of Intermediate Filaments in Health and Disease". In: *Science* 279.5350, pp. 514–519.

Fuge, H. (1969). "Electron Microscopic Studies on the Intra-flagellar Structures of Trypanosomes". In: *J. Protozool* 13.3, pp. 460–466. DOI: doi.org/10.1111/j.1550-7408.1969.tb02301.x.

Furue, M. et al. (2018). *Emerging role of interleukin-31 and interleukin-31 receptor in pruritus in atopic dermatitis*. DOI: 10.1111/all.13239.

Fyfe, Jenna et al. (2017). "Impact of mass chemotherapy in domestic livestock for control of zoonotic T. b. rhodesiense human African trypanosomiasis in Eastern Uganda". In: *Acta Tropica*. ISSN: 18736254. DOI: 10.1016/j.actatropica.2016.08.022.

Gadelha, C. et al. (2009). "Membrane domains and flagellar pocket boundaries are influenced by the cytoskeleton in African trypanosomes". In: *Proceedings of the National Academy of Sciences* 106.41, pp. 17425–17430. ISSN: 0027-8424. DOI: 10.1073/pnas.0909289106.

García-Salcedo, José A. et al. (2004). "A differential role for actin during the life cycle of Trypanosoma brucei". In: *EMBO Journal* 23.4, pp. 780–789. ISSN: 02614189. DOI: 10.1038/sj.emboj.7600094.

Genovese, Giulio et al. (2010). "Association of trypanolytic ApoL1 variants with kidney disease in African Americans". In: *Science* 329.5993, pp. 841–845. ISSN: 00368075. DOI: 10.1126/science.1193032.

Ghannam, Ahmed et al. (2015). "Camelid nanobodies with high affinity for broad bean mottle virus: a possible promising tool to immunomodulate plant resistance against viruses". In: *Plant Molecular Biology* 87.4-5, pp. 355–369. ISSN: 01674412. DOI: 10.1007/s11103-015-0282-5.

Gheiratmand, Ladan et al. (2013). "Biochemical characterization of the bi-lobe reveals a continuous structural network linking the bi-lobe to other single-copied organelles in Trypanosoma brucei". In: *Journal of Biological Chemistry* 288.5, pp. 3489–3499. ISSN: 00219258. DOI: 10.1074/jbc.M112.417428.

Gibson, Wendy C. et al. (1985). "Trypanosomes of subgenus trypanozoon are diploid for housekeeping genes". In: *Molecular and Biochemical Parasitology* 16.3, pp. 231–242. ISSN: 01666851. DOI: 10.1016/0166-6851(85)90066-0.

Gibson, Wendy, Lori Peacock, and Rachel Hutchinson (2017). "Microarchitecture of the tsetse fly proboscis". In: *Parasites and Vectors* 10.1. ISSN: 17563305. DOI: 10.1186/s13071-017-2367-2.

Giordani, F. et al. (2016). "The animal trypanosomiases and their chemotherapy: a review". In: *Parasitology* 143.14. DOI: 10.1017/S0031182016001268.

Glockshuber, Rudi and Thomas Schmidt (1992). "The Disulfide Bonds in Antibody Variable Domains : Effects on Stability, Folding in Vitro, and Functional Expression in Escherichia Coli". In: *Biochemistry* 31.5, pp. 1270–1279. ISSN: 15204995. DOI: 10.1021/bi00120a002.

Goadsby, Peter J. et al. (2017). "A Controlled Trial of Erenumab for Episodic Migraine". In: *New England Journal of Medicine* 377.22, pp. 2123–2132. ISSN: 0028-4793. DOI: 10.1056/NEJMoa1705848. URL: http://www.nejm.org/doi/10.1056/NEJMoa1705848.

Gonzalez-Sapienza, Gualberto, Martín A. Rossotti, and Sofía Tabares-da Rosa (2017). "Single-domain antibodies as versatile affinity reagents for analytical and diagnostic applications". In: *Frontiers in Immunology* 8.AUG. DOI: 10.3389/fimmu.2017.00977.

Gordon, Kenneth B. et al. (2003). "Efalizumab for Patients With Moderate to Severe Plaque Psoriasis". In: *JAMA* 290.23, p. 3073. ISSN: 0098-7484. DOI: 10.1001/jama.290.23.3073.

Griffiths, F.L. (1898). *The Petrie Papyri: Hieratic Papyri from Kahun and Gurob (Principally of the Middle Kingdom)*. Bernard Quaritch in London ., p. 40.

Gruby, M (1843). "Comptes Rendus Hebdomadaires des Seances de L'Academie des Sciences". In: *Comptes rendus hebdomadaires des séances de l'Académie des sciences.* 17, pp. 1134–1136. DOI: 10.1259/jrs.1912.0009.

Grunfelder, C. G. (2003). "Endocytosis of a Glycosylphosphatidylinositol-anchored Protein via Clathrin-coated Vesicles, Sorting by Default in Endosomes, and Exocytosis via RAB11-positive Carriers". In: *Molecular Biology of the Cell* 14.5, pp. 2029–2040. ISSN: 10591524. DOI: 10.1091/mbc.e02-10-0640.

Haag, Jochen, Colm O'hUigin, and Peter Overath (1998). "The molecular phylogeny of trypanosomes: evidence for an early divergence of the Salivaria". In: *Molecular and Biochemical Parasitology* 91.1. ISSN: 01666851. DOI: 10.1016/S0166-6851(97)00185-0.

Haendel, L. and K. Joetlen (1920). "Ubber chemotherapeutische Versuehe mit " Bayer 205 ' einem neuen trypanociden Mittel van besonderen Wirkung". In: *Berlin Klin. Woch.* 1.7, p. 821.

Hafner, Mark S and Steven A Nadler (1988). "Phylogenetic trees support the coevolution of parasites and their hosts". In: *Nature* 332, pp. 258–259.

Hager, Kristin M. et al. (1994). "Endocytosis of a cytotoxic human high density lipoprotein results in disruption of acidic intracellular vesicles and subsequent killing of African trypanosomes". In: *Journal of Cell Biology* 126.1, pp. 155–167. ISSN: 00219525. DOI: 10.1083/jcb.126.1.155.

Hagos, A. et al. (2010). "Efficacy of Cymelarsan® and Diminasan® against Trypanosoma equiperdum infections in mice and horses". In: *Veterinary Parasitology* 171.3-4, pp. 200–206. ISSN: 03044017. DOI: 10.1016/j.vetpar.2010.03.041.

Hamers-Casterman, C. et al. (1993). "Naturally occurring antibodies devoid of light chains". In: *Nature* 363, pp. 446–8. DOI: 10.1038/363446a0.

Hamill, Louise C. et al. (2013). "Domestic pigs as potential reservoirs of human and animal trypanosomiasis in Northern Tanzania". In: *Parasites and Vectors* 6.1. ISSN: 17563305. DOI: 10.1186/1756-3305-6-322.

Hamill, Louise et al. (2017). "Evaluating the impact of targeting livestock for the prevention of human and animal trypanosomiasis, at village level, in districts newly affected with T. b. rhodesiense in Uganda". In: *Infectious Diseases of Poverty* 6.1. ISSN: 20499957. DOI: 10.1186/s40249-016-0224-8.

Hamilton, Patrick B. et al. (2004). "Trypanosomes are monophyletic: Evidence from genes for glyceraldehyde phosphate dehydrogenase and small subunit ribosomal RNA". In: *International Journal for Parasitology* 34.12, pp. 1393–1404. ISSN: 00207519. DOI: 10.1016/j.ijpara.2004.08.011.

Hammarton, Tansy C., Séverine Monnerat, and Jeremy C. Mottram (2007). *Cytokinesis in trypanosomatids*. DOI: 10.1016/j.mib.2007.10.005.

Hammarton, Tansy C. et al. (2003). "Stage-specific differences in cell cycle control in Trypanosoma brucei revealed by RNA interference of a mitotic cyclin". In: *Journal of Biological Chemistry* 278.25, pp. 22877–22886. DOI: 10.1074/jbc.M300813200.

Hanahan, Douglas (1983). *Studies on Transformation of Escherichia coli with Plasmids*. Tech. rep., pp. 557–580.

Handman, E. (2001). "Leishmaniasis: Current status of vaccine development". In: *Clinical Microbiology Reviews* 14.2, pp. 229–243. ISSN: 08938512. DOI: 10.1128/CMR.14.2.229-243.2001.

Hassanzadeh-Ghassabeh, Gholamreza et al. (2013). "Nanobodies and their potential applications". In: *Nanomedicine* 8.6, pp. 1013–1026. DOI: 10.2217/nnm.13.86.

Hawking, F. and A. B. Sen (1960). "The trypanocidal action of homidium, quinapyramine and suramin". In: *British Journal of Pharmacology and Chemotherapy* 15.4, pp. 567–570. DOI: 10.1111/j.1476-5381.1960.tb00283.x.

Hayes, Polly M. et al. (2014). "Morphological and molecular characterization of a marine fish trypanosome from South Africa, including its development in a leech vector". In: *Parasites and Vectors* 7.1. ISSN: 17563305. DOI: 10.1186/1756-3305-7-50.

He, Cynthia Y, Marc Pypaert, and Graham Warren (2005). "Golgi Duplication in Trypanosoma brucei Requires Centrin2". In: *Science* 310.5751, pp. 1196–198. DOI: 10.1126/science. URL: www.sciencemag.org/cgi/content/full/1119969/DC1.

He, Cynthia Y. et al. (2004). "Golgi duplication in Trypanosoma brucei". In: *Journal of Cell Biology* 165.3, pp. 313–321. ISSN: 00219525. DOI: 10.1083/jcb.200311076.

Heddergott, N. et al. (2012). "Trypanosome Motion Represents an Adaptation to the Crowded Environment of the Vertebrate Bloodstream". In: *PLoS Pathogens* 8.11.

Hightower, R.C. and R.B. Meagher (1986). "The molecular evolution of Actin". In: *Genetics* 114, pp. 315–332.

Hirumi, H and K Hirumi (1989). "Continuous cultivation of Trypanosoma brucei blood stream forms in a medium containing a low concentration of serum protein without feeder cell layers." In: *The Journal of parasitology* 75.6, pp. 985–9. ISSN: 0022-3395. URL: http://www.ncbi.nlm.nih.gov/pubmed/2614608.

Hoare, C and F Wallace (1966). "Developmental stages of trypanosomatid flagellates: a new terminology". In: *Nature* 212, pp. 1385–1386.

Hoare, Cecil A. (1964). "Morphological and taxonomic studies on mammalian trypanosomes". In: *J. Protozool.* 11.2, pp. 200–207.

Hoeijmakers, J. H.J. and P. J. Weijers (1980). "The segregation of kinetoplast DNA networks in Trypanosoma brucei". In: *Topics in Catalysis* 4.1, pp. 97–116. ISSN: 0147619x. DOI: 10.1016/0147-619X(80)90086-4.

Horn, David (2014). "High-throughput decoding of drug targets and drug resistance mechanisms in African trypanosomes". In: *Parasitology* 141, pp. 77–82. ISSN: 14698161. DOI: 10.1017/S0031182013000243.

Hornby, H. E. (1941). "Immunization against bovine trypanosomiasis". In: *Transactions of the Royal Society of Tropical Medicine and Hygiene* 35.3, pp. 165–176. ISSN: 18783503. DOI: 10.1016/S0035-9203(41)90050-0.

Hu, Huiqing et al. (2015). "The Centriole Cartwheel Protein SAS-6 in Trypanosoma brucei Is Required for Probasal Body Biogenesis and Flagellum Assembly". In: *Eukaryotic Cell* 14.9, pp. 898–907. ISSN: 1535-9778. DOI: 10.1128/ec.00083-15.

Hu, Huiqing et al. (2017). "CRL4WDR1Controls Polo-like Kinase Protein Abundance to Promote Bilobe Duplication, Basal Body Segregation and Flagellum Attachment in Trypanosoma brucei". In: *PLoS Pathogens* 13.1. ISSN: 15537374. DOI: 10.1371/journal.ppat.1006146.

Hughes, Louise C. et al. (2012). "Three-dimensional structure of the trypanosome flagellum suggests that the paraflagellar rod functions as a biomechanical spring". In: *PLoS ONE* 7.1. ISSN: 19326203. DOI: 10.1371/journal.pone.0025700.

Hung, Chien-Hui et al. (2004). " Clathrin-Dependent Targeting of Receptors to the Flagellar Pocket of Procyclic-Form Trypanosoma brucei ". In: *Eukaryotic Cell* 3.4, pp. 1004–1014. ISSN: 1535-9778. DOI: 10.1128/ec.3.4.1004-1014.2004.

Hutchinson, Rachel and Wendy Gibson (2015). "Rediscovery of Trypanosoma (Pycnomonas) suis, a tsetse-transmitted trypanosome closely related to T. brucei". In: *Infection, Genetics and Evolution* 36, pp. 381–388. ISSN: 15677257. DOI: 10.1016/j.meegid.2015.10.018.

Iezzi, María Elena et al. (2018). *Single-domain antibodies and the promise of modular targeting in cancer imaging and treatment*. DOI: 10.3389/fimmu.2018.00273.

Jacobs, Robert T. et al. (2011). "Scyx-7158, an orally-active benzoxaborole for the treatment of stage 2 human african trypanosomiasis". In: *PLoS Neglected Tropical Diseases* 5.6. ISSN: 19352727. DOI: 10.1371/journal.pntd.0001151.

Jain, Rakesh K (1990). "Physiological barriers to delivery of monoclonal antibodies and other macromolecules in tumors." In: *Cancer Research* 50, pp. 814–819.

Jensch, H. (1955). "4, 4 Diamidino diazoaminobenzol, ein neues Mittel gegen Trypanosomen und Babesien Infektionen". In: *Arzneimittel Forschung* 5.11, pp. 634–5.

Joshi, P.P. et al. (2005). "Human Trypanosomiasis caused by Trypanosoma evansi in India: The first case report". In: *The American Journal of Tropical Medicine and Hygiene* 73.3, pp. 491–495. DOI: 10.4269/ajtmh.2005.73.491.

Julve Parreño, Jose Manuel et al. (2018). "A synthetic biology approach for consistent production of plant-made recombinant polyclonal antibodies against snake

venom toxins". In: *Plant Biotechnology Journal* 16.3, pp. 727–736. ISSN: 14677652. DOI: 10.1111/pbi.12823.

Kaksonen, Marko and Aurelien Roux (2018). *Mechanisms of clathrin-mediated endocytosis*. DOI: 10.1038/nrm.2017.132.

Kaplon, Hélène and Janice M. Reichert (2018). "Antibodies to watch in 2018". In: *mAbs*. ISSN: 19420870. DOI: 10.1080/19420862.2018.1415671.

Kazibwe, A. J N et al. (2009). "Genotypic status of the TbAT1/P2 adenosine transporter of Trypanosoma brucei gambiense isolates from Northwestern Uganda following melarsoprol withdrawal". In: *PLoS Neglected Tropical Diseases* 3.9. DOI: 10.1371/journal.pntd.0000523.

Keller, Bettina-Maria et al. (2019). "A Strategy to Optimize the Generation of Stable Chromobody Cell Lines for Visualization and Quantification of Endogenous Proteins in Living Cells". In: *Antibodies* 8.1, p. 10. DOI: 10.3390/antib8010010.

Kelley, Lawrence A et al. (2015). "The Phyre2 web portal for protein modeling, prediction and analysis." In: *Nature protocols* 10.6, pp. 845–58. ISSN: 1750-2799. DOI: 10.1038/nprot.2015.053. URL: http://www.ncbi.nlm.nih.gov/pubmed/25950237%20http://www.pubmedcentral.nih.gov/articlerender.fcgi?artid=PMC5298202.

Kelly, Steven et al. (2014). "A draft genome for the African crocodilian trypanosome Trypanosoma grayi". In: *Scientific Data* 1. ISSN: 20524463. DOI: 10.1038/sdata.2014.24.

Kennedy, Peter G.E. (2004). *Human African trypanosomiasis of the CNS: Current issues and challenges*. DOI: 10.1172/JCI200421052.

Köhler, G. and C. Milstein (1975). "Continuous cultures of fused cells secreting antibody of predefined specificity". In: *Nature* 256.5517, pp. 495–497. ISSN: 00280836. DOI: 10.1038/256495a0.

Koltzoff, Nikolai K. (1903). "Ûber formbestimmende elastiche Gebilde in Zellen". In: *Biol. Zbl.* 23, pp. 680–696.

Koyfman, A. Y. et al. (2011). "Structure of Trypanosoma brucei flagellum accounts for its bihelical motion". In: *Proceedings of the National Academy of Sciences* 108.27, pp. 11105–11108. ISSN: 0027-8424. DOI: 10.1073/pnas.1103634108.

Kristjanson, P M et al. (1999). "Measuring the costs of African animal trypanosomosis, the potential bene®ts of control and returns to research". In: *Agricultural systems* 59, pp. 79–98.

Kunz, Patrick et al. (2018). "The structural basis of nanobody unfolding reversibility and thermoresistance". In: *Scientific Reports* 8.1. ISSN: 20452322. DOI: 10.1038/s41598-018-26338-z.

Lacomble, Sylvain et al. (2009a). "Three-dimensional cellular architecture of the flagellar pocket and associated cytoskeleton in trypanosomes revealed by electron microscope tomography." In: *Journal of cell science* 122.Pt 8, pp. 1081–90. ISSN: 0021-9533. DOI: 10.1242/jcs.045740. URL: http://www.pubmedcentral.nih.gov/articlerender.fcgi?artid=2714436&tool=pmcentrez&rendertype=abstract.

Lacomble, S. et al. (2009b). "Three-dimensional cellular architecture of the flagellar pocket and associated cytoskeleton in trypanosomes revealed by electron microscope tomography". In: *Journal of Cell Science* 122.8, pp. 1081–1090. ISSN: 0021-9533. DOI: 10.1242/jcs.045740.

Lacomble, S. et al. (2010). "Basal body movements orchestrate membrane organelle division and cell morphogenesis in Trypanosoma brucei". In: *Journal of Cell Science* 123.17, pp. 2884–2891. ISSN: 0021-9533. DOI: 10.1242/jcs.074161.

LaCount, Douglas J. et al. (2000). "Double-stranded RNA interference in Trypanosoma brucei using head-to-head promoters". In: *Molecular and Biochemical Parasitology* 111.1, pp. 67–76. ISSN: 01666851. DOI: 10.1016/S0166-6851(00)00300-5.

Lai, D.-H. et al. (2008). "Adaptations of Trypanosoma brucei to gradual loss of kinetoplast DNA: Trypanosoma equiperdum and Trypanosoma evansi are petite mutants of T. brucei". In: *Proceedings of the National Academy of Sciences* 105.6, pp. 1999–2004. ISSN: 0027-8424. DOI: 10.1073/pnas.0711799105.

Langousis, Gerasimos and Kent L Hill (2014). "Motility and more: the flagellum of Trypanosoma brucei." In: *Nature reviews. Microbiology* 12.7, pp. 505–18. ISSN: 1740-1534. DOI: 10.1038/nrmicro3274. URL: http://www.ncbi.nlm.nih.gov/pubmed/24931043.

Lanham, S.M. (1968). "Separation of Trypanosomes from the Blood of Infected Rats and Mice by Anion-exchangers". In: *Nature* 218.5148, p. 1273.

Laviopierre, M.M.J. (1965). "FeedingBloodArthropods". In: *nATURE* 208, pp. 302–3.

Lei, S P et al. (1987). "Characterization of the Erwinia carotovora pelB gene and its product pectate lyase." In: *Journal of Bacteriology* 169.9, pp. 4379–4383. DOI: 10.1128/jb.169.9.4379-4383.1987.

Letunic, Ivica and Peer Bork (2018). "20 years of the SMART protein domain annotation resource". In: *Nucleic Acids Research* 46.D1, pp. D493–D496. ISSN: 13624962. DOI: 10.1093/nar/gkx922.

Liu, Xinyu et al. (2006). "Enhancement of the immunogenicity of synthetic carbohydrates by conjugation to virosomes: a leishmaniasis vaccine candidate." In: *ACS chemical biology* 1.3, pp. 161–164. DOI: 10.1021/cb600086b.

Luckins, A.G. (1992). *Trypanosomiasis - The clinical picture*. URL: http://www.fao.org/3/u6600T0a.htm#trypanosomiasis%20%20%20the%20clinical%20picture.

Lukeš, Julius et al. (2014). *Evolution of parasitism in kinetoplastid flagellates*. DOI: 10.1016/j.molbiopara.2014.05.007.

Lun, Z. R. et al. (1991). "Cymelarsan in the treatment of buffaloes naturally infected with Trypanosoma evansi in south China". In: *Acta Trop.* 49.3, pp. 233–6.

MacGregor, Paula et al. (2012). *Trypanosomal immune evasion, chronicity and transmission: An elegant balancing act*. DOI: 10.1038/nrmicro2779.

MacGregor, Paula et al. (2013). "Stable transformation of pleomorphic bloodstream form Trypanosoma brucei". In: *Molecular and Biochemical Parasitology* 190.2, pp. 60–62. ISSN: 18729428. DOI: 10.1016/j.molbiopara.2013.06.007.

MacGregor, Paula et al. (2019). "A single dose of antibody-drug conjugate cures a stage 1 model of African trypanosomiasis". In: *PLOS Neglected Tropical Diseases* 13.5. Ed. by Jayne Raper, e0007373. ISSN: 1935-2735. DOI: 10.1371/journal.pntd.0007373. URL: http://dx.plos.org/10.1371/journal.pntd.0007373.

Marschall Andrea, L. J., Stefan Dübel, and Thomas Böldicke (2015). "Specific in vivo knockdown of protein function by intrabodies". In: *mAbs* 7.6, pp. 1010–1035. DOI: 10.1080/19420862.2015.1076601org/10.1080/19420862.2015.1076601. URL:

http://www.tandfonline.com/action/journalInformation?journalCode=kmab20.

Matovu, Enock et al. (2003). " Mechanisms of Arsenical and Diamidine Uptake and Resistance in Trypanosoma brucei ". In: *Eukaryotic Cell* 2.5, pp. 1003–1008. ISSN: 1535-9778. DOI: 10.1128/ec.2.5.1003-1008.2003.

Matthews, K. R. (2005). "The developmental cell biology of Trypanosoma brucei". In: *Journal of Cell Science* 118.2, pp. 283–290. ISSN: 0021-9533. DOI: 10.1242/jcs.01649.

Matthews, Keith R (2009). "Europe PMC Funders Group The developmental cell biology of Trypanosoma brucei". In: *Cell* 118.Pt 2, pp. 283–290. DOI: 10.1242/jcs.01649.The.

Mazet, Muriel et al. (2013). "Revisiting the Central Metabolism of the Bloodstream Forms of Trypanosoma brucei: Production of Acetate in the Mitochondrion Is Essential for Parasite Viability". In: *PLoS Neglected Tropical Diseases* 7.12. ISSN: 19352735. DOI: 10.1371/journal.pntd.0002587.

McCulloch, Richard et al. (2017). "Emerging challenges in understanding trypanosome antigenic variation". In: *Emerging Topics in Life Sciences* 1.6, pp. 585–592. ISSN: 2397-8554. DOI: 10.1042/etls20170104.

McKean, Paul G. (2003). *Coordination of cell cycle and cytokinesis in Trypanosoma brucei*. DOI: 10.1016/j.mib.2003.10.010.

McMahon, Harvey T. and Emmanuel Boucrot (2011). "Molecular mechanism and physiological functions of clathrin-mediated endocytosis". In: *Nature Reviews Molecular Cell Biology* 12.8, pp. 517–533. DOI: 10.1038/nrm3151.

Meli, G. et al. (2013). "Intrabodies for protein interference in Alzheimer's disease Clinic for Endocrinology, Diabetes and Metabolic Diseases, Clinical . . . " In: *Journal of Biological Regulators & Homeoststic Agents* 27.2, pp. 89–105. URL: https://www.researchgate.net/publication/262178811.

Menzel, Stephan et al. (2018). *Nanobody-based biologics for modulating purinergic signaling in inflammation and immunity*. DOI: 10.3389/fphar.2018.00266.

Mesu, Victor Kande Betu Ku et al. (2018). "Oral fexinidazole for late-stage African Trypanosoma brucei gambiense trypanosomiasis: a pivotal multicentre, randomised, non-inferiority trial". In: *The Lancet* 391.10116, pp. 144–154. ISSN: 1474547X. DOI: 10.1016/S0140-6736(17)32758-7.

Migden, Michael R. et al. (2018). "PD-1 Blockade with Cemiplimab in Advanced Cutaneous Squamous-Cell Carcinoma". In: *New England Journal of Medicine* 379.4, pp. 341–351. ISSN: 0028-4793. DOI: 10.1056/NEJMoa1805131. URL: http://www.nejm.org/doi/10.1056/NEJMoa1805131.

Miller, Keith D et al. (2005). "Production, purification, and characterization of human scFv antibodies expressed in Saccharomyces cerevisiae, Pichia pastoris, and Escherichia coli." In: *Protein expression and purification* 42.2, pp. 255–67. ISSN: 1046-5928. DOI: 10.1016/j.pep.2005.04.015. URL: http://www.ncbi.nlm.nih.gov/pubmed/15946857.

Mkunza, Fred, William M. Olaho, and Curtis N. Powell (1995). "Partial protection against natural trypanosomiasis after vaccination with a flagellar pocket antigen from Trypanosoma brucei rhodesiense". In: *Vaccine* 13.2, pp. 151–154. ISSN: 0264410X. DOI: 10.1016/0264-410X(95)93128-V.

Molinari, Jesús and S. Andrea Moreno (2018). "Trypanosoma brucei Plimmer & Bradford, 1899 is a synonym of T. evansi (Steel, 1885) according to current knowledge and by application of nomenclature rules". In: *Systematic Parasitology* 95.2-3, pp. 249–256. ISSN: 15735192. DOI: 10.1007/s11230-018-9779-z.

Molla-Herman, A. et al. (2010). "The ciliary pocket: an endocytic membrane domain at the base of primary and motile cilia". In: *Journal of Cell Science* 123.10, pp. 1785–1795. ISSN: 0021-9533. DOI: 10.1242/jcs.059519.

Monnier, Philippe, Robin Vigouroux, and Nardos Tassew (2013). "In Vivo Applications of Single Chain Fv (Variable Domain) (scFv) Fragments". In: *Antibodies* 2.2, pp. 193–208. ISSN: 2073-4468. DOI: 10.3390/antib2020193. URL: http://www.mdpi.com/2073-4468/2/2/193/.

Morgan, G W et al. (2001). "Developmental and morphological regulation of clathrin-mediated endocytosis in Trypanosoma brucei." In: *Journal of cell science* 114.Pt 14, pp. 2605–15. ISSN: 0021-9533. URL: http://www.ncbi.nlm.nih.gov/pubmed/11683388.

Morrison, C. (2019). "Nanobody approval gives domain antibodies a boost". In: *Nature reviews: Drug discovery*.

Morriswood, Brooke (2015). "Form, Fabric, and Function of a Flagellum-Associated Cytoskeletal Structure". In: *Cells* 4.4, pp. 726–747. ISSN: 2073-4409. DOI: 10.3390/cells4040726.

Morriswood, Brooke and Katy Schmidt (2015). "A MORN Repeat Protein Facilitates Protein Entry into the Flagellar Pocket of Trypanosoma brucei". In: *Eukaryotic Cell* 14.11, pp. 1081–1093. ISSN: 1535-9778. DOI: 10.1128/ec.00094-15.

Morriswood, Brooke et al. (2009). "The bilobe structure of Trypanosoma brucei contains a MORN-repeat protein". In: *Molecular and Biochemical Parasitology* 167.2, pp. 95–103. ISSN: 01666851. DOI: 10.1016/j.molbiopara.2009.05.001.

Morriswood, Brooke et al. (2013). "Novel bilobe components in Trypanosoma brucei identified using proximity-dependent biotinylation". In: *Eukaryotic Cell*. ISSN: 15359778. DOI: 10.1128/EC.00326-12.

Moura, Danielle M.N., Osvaldo P. de Melo Neto, and Mark Carrington (2019). "A new reporter cell line for studies with proteasome inhibitors in Trypanosoma brucei". In: *Molecular and Biochemical Parasitology*. ISSN: 18729428. DOI: 10.1016/j.molbiopara.2018.11.001.

Movahedi, Kiavash et al. (2012). "Nanobody-based targeting of the macrophage mannose receptor for effective in vivo imaging of tumor-associated macrophages". In: *Cancer Research* 72.16, pp. 4165–4177. ISSN: 00085472. DOI: 10.1158/0008-5472.CAN-11-2994.

Muhanguzi, Dennis et al. (2017). "African animal trypanosomiasis as a constraint to livestock health and production in Karamoja region: A detailed qualitative and quantitative assessment". In: *BMC Veterinary Research*. ISSN: 17466148. DOI: 10.1186/s12917-017-1285-z.

Murray, M. (1979). "Pathogenicity of trypanosomes : proceedings of a workshop held at Nairobi, Kenya, 20-23 November 1978". In: *Pathogenicity of Trypanosomes. Proceedings of a workshop held at Nairobi, Kenya.* Pp. 121–127.

Mutomba, Martha C and Ching C Wang (1997). "The role of proteolysis during differentiation of Trypanosoma brucei from the bloodstream to the procyclic form". In: *Molecular and Biochemical Parasitology* 93, pp. 11–22.

Muyldermans, Serge (2001). "Single domain camel antibodies: Current status". In: *Reviews in Molecular Biotechnology* 74.4, pp. 277–302. ISSN: 13890352. DOI: 10.1016/S1389-0352(01)00021-6.

– (2013). "Nanobodies: Natural Single-Domain Antibodies". In: *Annual Review of Biochemistry* 82.1, pp. 775–797. ISSN: 0066-4154. DOI: 10.1146/annurev-biochem-063011-092449. URL: http://www.annualreviews.org/doi/abs/10.1146/annurev-biochem-063011-092449.

Muyldermans, S. et al. (1994). "Sequence and structure of VH domain from naturally occurring camel heavy chain immunoglobulins lacking light chains". In: *Protein Engineering* 7.9, pp. 29–1135. URL: https://www.researchgate.net/publication/15368506.

Natesan, S. K. A. et al. (2007). "Activation of Endocytosis as an Adaptation to the Mammalian Host by Trypanosomes". In: *Eukaryotic Cell* 6.11, pp. 2029–2037. DOI: 10.1128/ec.00213-07.

Navarro, M. et al. (2012). "Chagas Disease in Spain: Need for Further Public Health Measures". In: *PLoS Neglected Tropical Diseases* 6.12, e1962. DOI: 10.1371/journal.pntd.0001962.

NCBI (2019a). *BLASTn*. DOI: https://blast.ncbi.nlm.nih.gov/Blast.

– (2019b). *BLASTp*. DOI: https://blast.ncbi.nlm.nih.gov/Blast.

– (2019c). *Structure*. DOI: https://www.ncbi.nlm.nih.gov/structure.

Negi, Surendra S. and Werner Braun (2017). "Cross-React: A new structural bioinformatics method for predicting allergen cross-reactivity". In: *Bioinformatics* 33.7, pp. 1014–1020. ISSN: 14602059. DOI: 10.1093/bioinformatics/btw767.

Nelson, A.L. (2010). "Antibody Fragments Hope and Hype". In: *mAbs* 2.1, pp. 77–83. URL: www.landesbioscience.comwww.landesbioscience.com/journals/mabs/article/10786.

Nelson, M. R. et al. (2009). "The EF-hand domain: A globally cooperative structural unit". In: *Protein Science* 11.2, pp. 198–205. DOI: 10.1110/ps.33302.

Nett, I. R. E. et al. (2009). "The Phosphoproteome of Bloodstream Form Trypanosoma brucei , Causative Agent of African Sleeping Sickness". In: *Molecular & Cellular Proteomics* 8.7, pp. 1527–1538. DOI: 10.1074/mcp.m800556-mcp200.

Newton, B. A. (1958). "The action of antrycide on nucleic acid synthesis in a trypanosomid flagellate". In: *J. gen. Microbio.* 19, p. 2.

– (1962). "Inactivation of ribosomes by antrycide". In: *Biochemical Journal* 84, p. 109.

Ngô, H et al. (1998). "Double-stranded RNA induces mRNA degradation in Trypanosoma brucei." In: *Proceedings of the National Academy of Sciences of the United States of America* 95.25, pp. 14687–92. ISSN: 0027-8424. DOI: 10.1073/pnas.95.25.14687. URL: http://www.ncbi.nlm.nih.gov/pubmed/9843950%20http://www.pubmedcentral.nih.gov/articlerender.fcgi?artid=PMC24510.

Nussbaum, K. et al. (2010). "Trypanosomatid Parasites Causing Neglected Diseases". In: *Current Medicinal Chemistry* 17.15, pp. 1594–1617. ISSN: 09298673. DOI: 10.2174/092986710790979953. URL: http://www.eurekaselect.com/openurl/

content.php?genre=article&issn=0929-8673&volume=17&issue=15&spage=1594.

Obishakin, E. et al. (2014). "Generation of a nanobody targeting the paraflagellar rod protein of trypanosomes." In: *PloS one* 9.12, e115893. DOI: 10.1371/journal.pone.0115893. URL: http://www.pubmedcentral.nih.gov/articlerender.fcgi?artid=4281110&tool=pmcentrez&rendertype=abstract.

Odongo, S. et al. (2016). "An Anti-proteome Nanobody Library Approach Yields a Specific Immunoassay for Trypanosoma congolense Diagnosis Targeting Glycosomal Aldolase". In: *PLoS Neglected Tropical Diseases* 10.2. DOI: 10.1371/journal.pntd.0004420.

Ogbadoyi, E. O. (2003). "A High-Order Trans-Membrane Structural Linkage Is Responsible for Mitochondrial Genome Positioning and Segregation by Flagellar Basal Bodies in Trypanosomes". In: *Molecular Biology of the Cell* 14.5, pp. 1769–1779. ISSN: 10591524. DOI: 10.1091/mbc.e02-08-0525.

OIE (2019). *OIE Disease Cards*. URL: http://www.fao.org/ag/againfo/programmes/en/empres/gemp/avis/cards.html.

Okello, W. O. et al. (2015). "Contribution of draft cattle to rural livelihoods in a district of southeastern Uganda endemic for bovine parasitic diseases: An economic evaluation". In: *Parasites and Vectors* 8.1. DOI: 10.1186/s13071-015-1191-9.

Oli, Monika W. et al. (2006). "Serum resistance-associated protein blocks lysosomal targeting of trypanosome lytic factor in Trypanosoma brucei". In: *Eukaryotic Cell* 5.1, pp. 132–139. ISSN: 15359778. DOI: 10.1128/EC.5.1.132-139.2006.

Omeke, B C O (1994). "Pig trypanosomosis : prevalence and significance in the endemic Middle Belt zone of Southern Nigeria = Tripanosomosis porcina : prevalencia y significancia en la zona endémica de la faja media del sur de Nigeria= La trypanosomose porcine. Prévalence et incidence dans la zone endémique du Middle Belt au Sud-Nigeria". In: *Revue Elev. Med. vet. Pays trop* 47.3, pp. 381–386.

Ooi, C. and P. Bastin (2013). "More than meets the eye: understanding Trypanosoma brucei morphology in the tsetse". In: *Frontiers in Cellular and Infection Microbiology* 3. DOI: 10.3389/fcimb.2013.00071.

Ormerod, W. E. (1951). "The mode of action of antrycide". In: *British Journal of Pharmacology and Chemotherapy* 6.2, pp. 325–333. DOI: 10.1111/j.1476-5381.1951.tb00646.x.

O'Toole, E. T. et al. (2012). "Computer-assisted image analysis of human cilia and chlamydomonas flagella reveals both similarities and differences in axoneme structure". In: *Cytoskeleton* 69.8, pp. 577–590. DOI: 10.1002/cm.21035.

Panza, P. et al. (2015). "Live imaging of endogenous protein dynamics in zebrafish using chromobodies". In: *Development* 142.10, pp. 1879–1884. ISSN: 0950-1991. DOI: 10.1242/dev.118943.

Pardon, E. (2014). "A general protocol for the generation of Nanobodies for structural biology". In: *Nat Protoc.* 9.3, pp. 674–693.

Paugam, André et al. (2003). *Characterization and role of protozoan parasite proteasomes*. DOI: 10.1016/S1471-4922(02)00064-8.

Peacock, Lori et al. (2014). "Meiosis and haploid gametes in the pathogen Trypanosoma brucei". In: *Current Biology* 24.2, pp. 181–186. ISSN: 09609822. DOI: 10.1016/j.cub.2013.11.044.

Pearse, B M (1976). "Clathrin: a unique protein associated with intracellular transfer of membrane by coated vesicles." In: *Proceedings of the National Academy of Sciences of the United States of America* 73.4, pp. 1255–9. ISSN: 0027-8424. URL: http://www.ncbi.nlm.nih.gov/pubmed/1063406%20http://www.pubmedcentral.nih.gov/articlerender.fcgi?artid=PMC430241.

Perdomo, D., M. Bonhivers, and D. Robinson (2016). "The Trypanosome Flagellar Pocket Collar and Its Ring Forming Protein—TbBILBO1". In: *Cells* 5.1, p. 9. DOI: 10.3390/cells5010009. URL: http://www.mdpi.com/2073-4409/5/1/9.

Perry, Jenna A. et al. (2018). "TbSmee1 regulates hook complex morphology and the rate of flagellar pocket uptake in Trypanosoma brucei". In: *Molecular Microbiology* 107.3, pp. 344–362. ISSN: 13652958. DOI: 10.1111/mmi.13885.

Persechini, A., N. D. Moncrief, and R.H. Kretsinger (1989). "The EF-hand family of calcium-modulated proteins". In: *Trends Neurosci* 12.11, pp. 462–467.

Picco, Andrea et al. (2018). "The contributions of the actin machinery to endocytic membrane bending and vesicle formation". In: *Molecular Biology of the Cell* 29.11, pp. 1346–1358. ISSN: 1059-1524. DOI: 10.1091/mbc.e17-11-0688.

Pinger, Jason, Shanin Chowdhury, and F. Nina Papavasiliou (2017). "Variant surface glycoprotein density defines an immune evasion threshold for African trypanosomes undergoing antigenic variation". In: *Nature Communications*. ISSN: 20411723. DOI: 10.1038/s41467-017-00959-w.

Pinto Torres, Joar E. et al. (2018). "Development of a Nanobody-based lateral flow assay to detect active Trypanosoma congolense infections". In: *Scientific Reports* 8.1. ISSN: 20452322. DOI: 10.1038/s41598-018-26732-7.

Ploubidou, A. et al. (1999). "Evidence for novel cell cycle checkpoints in trypanosomes: kinetoplast segregation and cytokinesis in the absence of mitosis". In: *Journal of Cell Science* 112, pp. 4641–4650.

Poinar, George (2007). "Early Cretaceous trypanosomatids associated with fossil sand fly larvae in Burmese amber". In: *Memorias do Instituto Oswaldo Cruz* 102.5, pp. 635–637. ISSN: 00740276.

Polson, A., M. Barbara von Wechmar, and M. H.V. van Regenmortel (1980). "Isolation of viral igy antibodies from yolks of immunized hens". In: *Immunological Investigations* 9.5, pp. 475–493. ISSN: 08820139. DOI: 10.3109/08820138009066010.

Ponten, Jan and Eero Saksela (1967). "Two established in vitro cell lines from human mesenchymal tumours". In: *Int. J. Cancer* 2.5, pp. 434–447.

Poon, S. K. et al. (2012). "A modular and optimized single marker system for generating Trypanosoma brucei cell lines expressing T7 RNA polymerase and the tetracycline repressor". In: *Open Biology* 2. DOI: 10.1098/rsob.110037.

Pradel, L. C. (2006). "NIMA-related kinase TbNRKC is involved in basal body separation in Trypanosoma brucei". In: *Journal of Cell Science* 119.9, pp. 1852–1863. ISSN: 0021-9533. DOI: 10.1242/jcs.02900.

Price, H. P., M. Stark, and D. .F Smith (2007). "Trypanosoma brucei ARF1 Plays a Central Role in Endocytosis and Golgi-Lysosome Trafficking". In: *Molecular Biology of the Cell* 18, pp. 864–873.

Priotto, Gerardo et al. (2009). "Nifurtimox eflornithine combination therapy for second-stage African Trypanosoma brucei gambiense trypanosomiasis: a multicentre, randomised, phase III, non-inferiority trial". In: *The Lancet* 374. DOI: 10.1016/S0140. URL: www.thelancet.com.

Radwanska, Magdalena et al. (2018). *Salivarian trypanosomosis: A review of parasites involved, their global distribution and their interaction with the innate and adaptive mammalian host immune system*. DOI: 10.3389/fimmu.2018.02253.

Raina, A.K. et al. (1985). "Oral transmission of Trypanosoma evansi infection in dogs and mice". In: *Veterinary Parasitology* 18, pp. 67–69.

Rajão, M. A. et al. (2013). "Unveiling Benznidazole's mechanism of action through overexpression of DNA repair proteins in Trypanosoma cruzi". In: *Environ Mol Mutagen.* 55.4, pp. 309–21.

Ramaswami, N.S. (1994). "Draught animals and welfare". In: *Rev Sci Tech 'OIE* 13.1, pp. 195–216.

Ramon, Gaston (1924). "Sur la toxine et sur I'anatoxine diphtheriques". In: *Ann. Inst. Pasteur* 38, pp. 1–10.

Raper, Jayne et al. (1999). "Characterization of a novel trypanosome lytic factor from human serum". In: *Infection and Immunity* 67.4, pp. 1910–1916. ISSN: 00199567.

Reimer, Elisa et al. (2013). "Molecular cloning and characterization of a novel anti-TLR9 intrabody". In: *Cellular and Molecular Biology Letters*. ISSN: 16891392. DOI: 10.2478/s11658-013-0098-8.

Richle, R. (1973). "Chemotherapy of experimental acute Chagas disease inmice: beneficial effect of Ro-71051 on parasitemia and tissue parasitism". In: *Le Progres Medical* 101, p. 282.

Rifkin, M R (1978). "Identification of the trypanocidal factor in normal human serum: high density lipoprotein." In: *Proceedings of the National Academy of Sciences of the United States of America* 75.7, pp. 3450–4. ISSN: 0027-8424. URL: http://www.ncbi.nlm.nih.gov/pubmed/210461%20http://www.pubmedcentral.nih.gov/articlerender.fcgi?artid=PMC392795.

Rijo-Ferreira, Filipa et al. (2018). "Sleeping sickness is a circadian disorder". In: *Nature Communications* 9.1. ISSN: 20411723. DOI: 10.1038/s41467-017-02484-2.

Robinson, D. R. and K. Gull (1991). "Basal body movements as a mechanism for mitochondrial genome segregation in the trypanosome cell cycle". In: *Nature* 352.731-733.

Robinson, Derrick R et al. (1995). "Microtubule Polarity and Dynamics in the Control of Organelle Positioning, Segregation, and Cytokinesis in the Trypanosome Cell Cycle". In: *The Journal of Cell Biology* 128.6, pp. 1163–1172.

Rojas, Federico et al. (2019). "Oligopeptide Signaling through TbGPR89 Drives Trypanosome Quorum Sensing". In: *Cell* 176.1-2, pp. 306–317. ISSN: 10974172. DOI: 10.1016/j.cell.2018.10.041.

Ross, R. and D. Thomson (1910). "A Case o f Sleeping Sickness studied by Precise M ethods: Further Observations". In: *Roy Soc Proc B* 83, pp. 187–205.

Roux, K. H. et al. (1998). "Structural analysis of the nurse shark (new) antigen receptor (NAR): Molecular convergence of NAR and unusual mammalian immunoglobulins". In: *Proceedings of the National Academy of Sciences* 95.20, pp. 11804–11809. DOI: 10.1073/pnas.95.20.11804.

Rovis, Luciana and Steinunn Baekkeskov (1980). "Sub-cellular fractionation of Trypanosoma brucei. Isolation and characterization of plasma membranes". In: *Parasitology* 80.3, pp. 507–524. ISSN: 14698161. DOI: 10.1017/S0031182000000974.

Ruggiero, Michael A. et al. (2015). "A higher level classification of all living organisms". In: *PLoS ONE* 10.4. ISSN: 19326203. DOI: 10.1371/journal.pone.0119248.

Saerens, Dirk et al. (2004). "Single domain antibodies derived from dromedary lymph node and peripheral blood lymphocytes sensing conformational variants of prostate-specific antigen". In: *Journal of Biological Chemistry* 279.50, pp. 51965–51972. ISSN: 00219258. DOI: 10.1074/jbc.M409292200.

Salema, Valencio and Luis Ángel Fernández (2013). "High yield purification of nanobodies from the periplasm of E. coli as fusions with the maltose binding protein". In: *Protein Expression and Purification* 91.1, pp. 42–48. ISSN: 10465928. DOI: 10.1016/j.pep.2013.07.001.

Sánchez, E. et al. (2015). "Molecular characterization and classification of Trypanosoma spp. Venezuelan isolates based on microsatellite markers and kinetoplast maxicircle genes". In: *Parasites and Vectors* 8.1. ISSN: 17563305. DOI: 10.1186/s13071-015-1129-2.

Scheer, Ulrich (2014). *Historical roots of centrosome research: Discovery of Boveri's microscope slides in Würzburg*. DOI: 10.1098/rstb.2013.0469.

Schilling, C. (1935). "Immunization against Trypanosomes". In: *J. Trop. Med.* P. 159.

Schumann Burkard, Gabriela, Pascal Jutzi, and Isabel Roditi (2011). "Genome-wide RNAi screens in bloodstream form trypanosomes identify drug transporters". In: *Molecular and Biochemical Parasitology* 175.1, pp. 91–94. DOI: 10.1016/j.molbiopara.2010.09.002.

Schuster, Sarah et al. (2019). "A modification to the life cycle of the parasite Trypanosoma brucei". In: *bioRxiv*. DOI: 10.1101/717975. URL: http://dx.doi.org/10.1101/717975.

Scott, V., T. Sherwin, and K. Gull (1997). "γ-Tubulin in trypanosomes: molecular characterisation and localisation to multiple and diverse microtubule organising centres". In: *Journal of Cell Science* 110, pp. 157–168.

Sherwin, T. and K. Gull (1989). "The cell division cycle of Trypanosoma brucei brucei: timing of event markers and cytoskeletal modulations". In: *Phil. Trans. R. Soc. Lond.* 323, pp. 573–588.

Shi, Huafang et al. (2000). *Genetic interference in Trypanosoma brucei by heritable and inducible double-stranded RNA*. Tech. rep.

Shi, J. et al. (2008). "Centrin4 coordinates cell and nuclear division in T. brucei". In: *Journal of Cell Science* 121.18, pp. 3062–3070. ISSN: 0021-9533. DOI: 10.1242/jcs.030643.

SIB (2019a). *ExPASy PROSITE*. DOI: https://prosite.expasy.org/.

– (2019b). *MyHits*.

– (2019c). *SWISS-MODEL*. DOI: https://swissmodel.expasy.org/interactive.

Simpson, Alastair G.B., Jamie R. Stevens, and Julius Lukeš (2006). *The evolution and diversity of kinetoplastid flagellates*. DOI: 10.1016/j.pt.2006.02.006.

Sinclair-Davis, Amy N, Michael R McAllaster, and Christopher L de Graffenried (2017). "A functional analysis of TOEFAZ1 uncovers protein domains essential for cytokinesis in Trypanosoma brucei." In: *Journal of cell science* 130.22, pp. 3918–3932.

ISSN: 1477-9137. DOI: 10.1242/jcs.207209. URL: http://www.ncbi.nlm.nih.gov/pubmed/28993462%20http://www.pubmedcentral.nih.gov/articlerender.fcgi?artid=PMC5702046.

Siontorou, Christina G (2013). "Nanobodies as novel agents for disease diagnosis and therapy". In: pp. 4215–4227.

Smith, T. K. et al. (2017). "Metabolic reprogramming during the Trypanosoma brucei life cycle". In: *F1000Research* 6, p. 683. DOI: 10.12688/f1000research.10342.2. URL: https://f1000research.com/articles/6-683/v2.

Songa, E.B. and R. Hamers (1988). "1988BATTTevansi". In: *Ann Soc belge Med trop* 68, pp. 233–240.

Stevens, J., H. Noyes, and W. Gibson (1998). "The Evolution of Trypansomes Infecting Humans and Primates". In: *Mem Inst Oswaldo Cruz* 93.5, pp. 669–676.

Stevens, Jamie R and Wendy C Gibson (1999). "The evolution of pathogenic trypanosomes". In: *Cad. Saude Publica* 15.4, pp. 673–684.

Steverding, Dietmar (2008). "The history of African trypanosomiasis." In: *Parasites & vectors* 1.1, p. 3. ISSN: 1756-3305. DOI: 10.1186/1756-3305-1-3. URL: http://www.pubmedcentral.nih.gov/articlerender.fcgi?artid=2270819&tool=pmcentrez&rendertype=abstract.

Stijlemans, Benoit et al. (2004). "Efficient targeting of conserved cryptic epitopes of infectious agents by single domain antibodies. African trypanosomes as paradigm." In: *The Journal of biological chemistry* 279.2, pp. 1256–61. ISSN: 0021-9258. DOI: 10.1074/jbc.M307341200. URL: http://www.ncbi.nlm.nih.gov/pubmed/14527957.

Stijlemans, Benoît et al. (2011). "High affinity nanobodies against the Trypanosome brucei VSG are potent trypanolytic agents that block endocytosis." In: *PLoS pathogens* 7.6, e1002072. ISSN: 1553-7374. DOI: 10.1371/journal.ppat.1002072. URL: http://www.pubmedcentral.nih.gov/articlerender.fcgi?artid=3116811&tool=pmcentrez&rendertype=abstract.

Studier, F William (2005). "Protein production by auto-induction in high density shaking cultures." In: *Protein expression and purification* 41.1, pp. 207–234. ISSN: 1046-5928. DOI: 10.1016/j.pep.2005.01.016.

Sunter, J. D. et al. (2015). "Modulation of flagellum attachment zone protein FLAM3 and regulation of the cell shape in Trypanosoma brucei life cycle transitions". In: *Journal of Cell Science* 128.16, pp. 3117–3130. ISSN: 0021-9533. DOI: 10.1242/jcs.171645.

Sunter, Jack D. and Keith Gull (2016). *The Flagellum Attachment Zone: 'The Cellular Ruler' of Trypanosome Morphology*. DOI: 10.1016/j.pt.2015.12.010.

Szempruch, Anthony J. et al. (2016). "Extracellular Vesicles from Trypanosoma brucei Mediate Virulence Factor Transfer and Cause Host Anemia". In: *Cell* 164.1-2. ISSN: 10974172. DOI: 10.1016/j.cell.2015.11.051.

Takeet, M.I. et al. (2016). "Phylogeny of Trypanosoma brucei and Trypanosoma evansi in naturally infected cattle in Nigeria by analysis of repetitive and ribosomal DNA sequences". In: *Tropical Animal Health and Production* 48.6, pp. 1235–1240.

Taylor, A.E.R. and Godfrey D.G. (1969). "A New Organelle of Bloodstream Salivarian Trypanosomes". In: *J. Protozool.* 16.3, pp. 466–470.

Teixeira, Antonio R.L. et al. (2011). "Pathogenesis of chagas' disease: Parasite persistence and autoimmunity". In: *Clinical Microbiology Reviews* 24.3, pp. 592–630. ISSN: 08938512. DOI: 10.1128/CMR.00063-10.

The Chagas Disease Foundation (2019). *Life Cycle of The Chagas Disease*. URL: https://www.chagasfound.org/chagas-disease/life-cycle/.

Thomas, James et al. (2018). "Insights into antitrypanosomal drug mode-of-action from cytology-based profiling". In: *PLoS Neglected Tropical Diseases* 12.11. ISSN: 19352735. DOI: 10.1371/journal.pntd.0006980.

Thomson, Russell et al. (2014). "Evolution of the primate trypanolytic factor APOL1". In: *Proceedings of the National Academy of Sciences of the United States of America* 111.20. ISSN: 10916490. DOI: 10.1073/pnas.1400699111.

Torres-Guerrero, Edoardo et al. (2017). "Leishmaniasis: a review". In: *F1000Research* 6, p. 750. DOI: 10.12688/f1000research.11120.1.

Trindade, Sandra et al. (2016). "Trypanosoma brucei Parasites Occupy and Functionally Adapt to the Adipose Tissue in Mice". In: *Cell Host and Microbe* 19.6, pp. 837–848. ISSN: 19346069. DOI: 10.1016/j.chom.2016.05.002.

TriTrypDB (2019). *TriTrypDB*. URL: https://tritrypdb.org/tritrypdb/.

Truebestein, Linda and Thomas A. Leonard (2016). "Coiled-coils: The long and short of it". In: *BioEssays* 38.9, pp. 903–916. ISSN: 15211878. DOI: 10.1002/bies.201600062.

Upjohn, M. and D. Valette (2014). "The Relationship Between Working Equids and Women in Developing Countries". In: *Equine Veterinary Journal: Clinical Research Abstracts of the British Equine Veterinary Association Congress 2014* 46.47, p. 20.

Urbaniak, Michael D., David M.A. Martin, and Michael A.J. Ferguson (2013). "Global quantitative SILAC phosphoproteomics reveals differential phosphorylation is widespread between the procyclic and bloodstream form lifecycle stages of Trypanosoma brucei". In: *Journal of Proteome Research* 12.5, pp. 2233–2244. ISSN: 15353907. DOI: 10.1021/pr400086y.

Vallet-Courbin, Amelie et al. (2017). "A recombinant human anti-platelet SCFV antibody produced in pichia pastoris for atheroma targeting". In: *PLoS ONE* 12.1. ISSN: 19326203. DOI: 10.1371/journal.pone.0170305.

Van Audenhove, Isabel et al. (2013). "Mapping cytoskeletal protein function in cells by means of nanobodies". In: *Cytoskeleton* 70.10, pp. 604–622. ISSN: 19493584. DOI: 10.1002/cm.21122.

Van Den Abbeele, Anske et al. (2010). "A llama-derived gelsolin single-domain antibody blocks gelsolin-G-actin interaction". In: *Cellular and Molecular Life Sciences* 67.9, pp. 1519–1535. ISSN: 1420682X. DOI: 10.1007/s00018-010-0266-1.

Van Impe, Katrien et al. (2013). "A nanobody targeting the F-actin capping protein CapG restrains breast cancer metastasis". In: *Breast Cancer Research*. ISSN: 14655411. DOI: 10.1186/bcr3585.

Van Nieuwenhove, S. et al. (1985). "Treatment of gambiense sleeping sickness in the sudan with oral dfmo (dldifluoromethylornithine), an inhibitor of ornithine decarboxylase; first field trial". In: *Transactions of the Royal Society of Tropical Medicine and Hygiene* 79.5, pp. 692–698. ISSN: 18783503. DOI: 10.1016/0035-9203(85)90195-6.

Van Vinh Chau, Nguyen et al. (2016). "A Clinical and Epidemiological Investigation of the First Reported Human Infection With the Zoonotic Parasite Trypanosoma evansi in Southeast Asia". In: *Clinical Infectious Diseases* 62.8, pp. 1002–1008. ISSN: 15376591. DOI: 10.1093/cid/ciw052.

Van Xong, Hoang et al. (1998). "A VSG Expression Site-Associated Gene Confers Resistance to Human Serum in Trypanosoma rhodesiense". In: *Cell* 95, pp. 839–846.

Vassella, E. et al. (1997). "Differentiation of African trypanosomes is controlled by a density sensingmechanism which signals cell cycle arrest via the cAMP pathway". In: *Journal of Cell Science* 110, pp. 2661–2671.

Vaughan, Sue and Keith Gull (2008). " The structural mechanics of cell division in Trypanosoma brucei ". In: *Biochemical Society Transactions* 36.3, pp. 421–424. ISSN: 0300-5127. DOI: 10.1042/bst0360421.

– (2016). *Basal body structure and cell cycle-dependent biogenesis in Trypanosoma brucei*. DOI: 10.1186/s13630-016-0023-7.

Vaughan, Susan et al. (2000). "New tubulins in protozoal parasites". In: *Current Biology* 10.7, R258–R259. ISSN: 09609822. DOI: 10.1016/s0960-9822(00)00414-0.

Vickerman, K (1969). "On the surface coat and flagellar adhesion in trypanosomes." In: *Journal of cell science* 5.1, pp. 163–93. ISSN: 0021-9533. URL: http://www.ncbi.nlm.nih.gov/pubmed/5353653.

Vidilaseris, Keni et al. (2014a). "Assembly mechanism of Trypanosoma brucei BILBO1, a multidomain cytoskeletal protein". In: *Journal of Biological Chemistry* 289.34, pp. 23870–23881. ISSN: 1083351X. DOI: 10.1074/jbc.M114.554659.

Vidilaseris, Keni et al. (2014b). "Structure of the TbBILBO1 Protein N-terminal domain from Trypanosoma brucei reveals an essential requirement for a Conserved surface patch". In: *Journal of Biological Chemistry* 289.6, pp. 3724–3735. ISSN: 00219258. DOI: 10.1074/jbc.M113.529032.

Wallbanks, K. R. et al. (1985). "The identity of Leishmania tarentolae Wenyon 1921". In: *Parasitology* 90.1, pp. 67–78. ISSN: 14698161. DOI: 10.1017/S0031182000049027.

Webster, P. and D. G. Russell (1993). "The flagellar pocket of trypanosomatids". In: *Parasitology Today* 9.6, pp. 201–206. DOI: 10.1016/0169-4758(93)90008-4.

Wellcome Sanger institute (2019). *Trypanosoma brucei*. URL: https://www.sanger.ac.uk/resources/downloads/protozoa/trypanosoma-brucei.html.

Wellde, B. T. et al. (2016). " Experimental infection of cattle with Trypanosoma brucei rhodesiense ". In: *Annals of Tropical Medicine & Parasitology* 83.sup1, pp. 133–150. ISSN: 0003-4983. DOI: 10.1080/00034983.1989.11812418.

Wesolowski, Janusz et al. (2009). "Single domain antibodies: Promising experimental and therapeutic tools in infection and immunity". In: *Medical Microbiology and Immunology* 198.3, pp. 157–174. DOI: 10.1007/s00430-009-0116-7.

Wheeler, Richard J. et al. (2013). "Cytokinesis in trypanosoma brucei differs between bloodstream and tsetse trypomastigote forms: Implications for microtubule-based morphogenesis and mutant analysis". In: *Molecular Microbiology* 90.6, pp. 1339–1355. ISSN: 0950382X. DOI: 10.1111/mmi.12436.

Whiteside, E. F. (1963). "A strain of Trypanosoma congolense directly resistant to Berenil". In: 73, pp. 167–175.

WHO (2018). *Human African trypanosomiasis*. URL: Human % 20African % 20trypanosomiasis.

Wiedemar, Natalie et al. (2018). "Beyond immune escape: a variant surface glycoprotein causes suramin resistance in Trypanosoma brucei". In: *Molecular Microbiology* 107.1. ISSN: 13652958. DOI: 10.1111/mmi.13854.

Wilson, S.G. (1948). "Further Observations on the Curative Value of Dimidium Bromide (Phenanthridinium 1553) in Trypanosoma Congolense Infections in Bovines in Uganda". In: *Journal of Comparative Pathology and Therapeutics* 58, pp. 94–106. DOI: 10.1016/s0368-1742(48)80008-1.

Wirtz, Elizabeth et al. (1999). "A tightly regulated inducible expression system for conditional gene knock-outs and dominant-negative genetics in Trypanosoma brucei". In: *Molecular and Biochemical Parasitology* 99, pp. 89–101. URL: www.rockefeller.edu/labheads/cross/cross-.

Wolbach, S B and C A L Binger (1912). "A Contribution to the Parasitology of Trypanosomiasis". In: *J Med Res* 27.1, pp. 83–108.

Woodward, R and K Gull (1990). "Timing of nuclear and kinetoplast DNA replication and early morphological events in the cell cycle of Trypanosoma brucei." In: *Journal of cell science* 95 (Pt 1), pp. 49–57. ISSN: 0021-9533. URL: http://www.ncbi.nlm.nih.gov/pubmed/2190996.

Wu, T. T. and E. A. Kabat (1970). "An Analysis of the sequences of the variable regions of Bence Jones proteins and myeloma light chains and their implications for antibody complementarity". In: *J. Exp. Med.* 132, pp. 211–250.

Xu, Xiaobo, Ruiqing Zhang, and Xinhua Chen (2017). "Application of a single-chain fragment variable (scFv) antibody for the confirmatory diagnosis of hydatid disease in non-endemic areas". In: *Electronic Journal of Biotechnology* 29, pp. 57–62. ISSN: 07173458. DOI: 10.1016/j.ejbt.2017.07.003.

Yorke, W. (1940). "Recent work on the chemotherapy of protozoal infections". In: *Transactions of the Royal Society of Tropical Medicine and Hygiene* 33.5, pp. 463–476.

Zheng, Zhi Ming, Shuang Tang, and Mingfang Tao (2005). *Development of resistance to RNAi in mammalian cells.* DOI: 10.1196/annals.1359.019.

Zhou, Jinlin et al. (2004). "Resistance to drug by different isolates Trypanosoma evansi in China". In: *Acta Tropica* 90.3, pp. 271–275. ISSN: 0001706X. DOI: 10.1016/j.actatropica.2004.02.002.

Zhou, Qing et al. (2010). "A comparative proteomic analysis reveals a new bi-lobe protein required for bi-lobe duplication and cell division in Trypanosoma brucei". In: *PLoS ONE* 5.3. ISSN: 19326203. DOI: 10.1371/journal.pone.0009660.

Zielonka, Stefan et al. (2015). "Structural insights and biomedical potential of IgNAR scaffolds from sharks". In: *mAbs* 7.1, pp. 15–25. DOI: 10.4161/19420862.2015.989032.